Progressive Failure Analysis of Laminated Composite Structures

Arafat Islam Khan

Dissertation submitted to the Faculty of the
Virginia Polytechnic Institute and State University
in partial fulfillment of the requirements for the degree of

Doctor of Philosophy
in
Aerospace Engineering

Rakesh K. Kapania, Chair
Romesh C. Batra, Co-Chair
Eric R. Johnson
Gary D. Seidel

January 20, 2015

Blacksburg, Virginia

Keywords: Composites, Progressive Failure, Puck and Schürmann Failure Criteria, USDFLD, Laminated Structure

Progressive Failure Analysis of Laminated Composite Structures

Arafat Islam Khan

ABSTRACT

Laminated composite structures have started to play a very significant role in today's aircraft industry. The application of composite materials has now gone beyond the borders of aircraft design and has entered into such fields as automotive, athletics and recreational equipment, etc. The light weight and high specific strength of composite material helps design vehicles with higher fuel efficiency and longevity. In order to understand the influence of design parameters related to the use of composite materials in these applications, a proper study of the laminated composite structures requires a complete failure analysis, which includes both initiation and propagation of damage. In this work a progressive failure methodology is developed and implemented in the commercial Finite Element software package, Abaqus. Out of the numerous failure criteria available in the literature to study damage initiation and propagation in unidirectional fiber reinforced composites, Puck and Schürmann's failure criteria have been chosen due to their ability to predict results close to those observed experimentally. Key features of the Puck and Schürmann's failure criteria for three-dimensional deformations of unidirectional fiber reinforced composites have been summarized. Failure modes in the matrix and the fiber are considered separately. The failure criteria are simplified for plane stress deformations. Whereas the failure plane can be analytically identified for plane stress deformations, a numerical search algorithm is needed for three-dimensional problems. Subsequent to the initiation of matrix failure, elastic moduli are degraded and values of these degradation parameters and fracture plane angles are found by using a Continuum Damage Mechanics (CDM) approach. It is found that the assumption that the material response remains transversely isotropic even after the matrix failure has initiated requires the degradation of the transverse Poisson's ratio. The Puck and Schürmann's failure criteria and the material degradation process have been implemented as a User Defined Field (USDFLD) subroutine in Abaqus. The implementation has been verified by analytically computing results for simple loadings and comparing them with predictions from using the

USDFLD in Abaqus. Subsequently, both two- and three-dimensional problems of more realistic geometries and loadings have been analyzed and computed results compared with either experimental findings or results available in the literature. Major contributions of the work include identifying the degradation parameter for the transverse Poisson's ratio in terms of the matrix degradation parameter for the matrix failure in compression, development of the USDFLD based on Puck and Schürmann's failure criteria, implementing the USDFLD in the commercial finite element software, Abaqus, and verifying that results computing using the USDFLD for various laminates and loadings agree with those from either the analytical solution of the problem or those available in the literature.

DEDICATION

Dedicated

to

My Family

ACKNOWLEDGEMENTS

I would like to express my deepest gratitude to my advisors Dr. Rakesh K. Kapania and Dr. Romesh C. Batra, for their excellent suggestions, invaluable advice and support. They met with me on a regular basis throughout this research to discuss and refine the theoretical and computational aspects of this work. I would especially like thank Dr. Eric R. Johnson for his constant advice and for patiently explaining to me many intricacies of composite structures for the current research. I would also like to thank Dr. Gary D. Seidel for serving on the advisory committee, and for the technical suggestions to this dissertation.

This research is sponsored by The AIRBUS Group, France. The financial support provided by AIRBUS is gratefully acknowledged. I also wish to thank Dr. Jean-Mathieu Guimard, the technical monitor of this research, for sharing his deep insight into behavior of laminated composites. In addition I would like to thank Mr. Qian Li for his suggestions throughout my research.

The author is responsible for errors, if any, in the dissertation.

TABLE OF CONTENTS

LIST OF FIGURES

LIST OF TABLES

ABBREVIATION

C-M	Coulomb-Mohr
CLPT	Classical Lamination Plate Theory
CDM	Continuum Damage Mechanics
CFRP	Carbon Fiber Reinforced Polymer
D/L	Delamination or local buckling
IFF	Inter fiber failure
FF_T	Fiber failure index in tension
FF_C	Fiber failure index in compression
FRC	Fiber reinforced composite
FV	Field Variable
GFRP	Glass Fiber Reinforced Polymer
PFA	Progressive failure analysis
OHT	Open Hole Tension
USDFLD	User defined field
UEL	User Defined Element
WWFE	World Wide Failure Exercise
LEFM	Linear elastic fracture mechanics
RVE	Representative volume element
VCCT	Virtual crack closure technique
SDV	Solution Dependent Variable

SYMBOLS

English characters

A	Tensile mode of failure in the matrix
B, C	Compressive modes of failure in the matrix
$A^{(R)}$	Reduced stiffness parameter, N^2/mm^2
$B^{(R)}$	Reduced stiffness parameter, N^2/mm
$C^{(R)}$	Reduced stiffness parameter, N^2/mm
$D^{(R)}$	Reduced stiffness parameter, N^3/mm
E_1, E_2	Elastic moduli in the longitudinal and the transverse directions, respectively, within a ply, GPa
FI	Dimensionless failure index; for no failure $0 \leq FI < 1$ and FI=1 at failure initiation
G_{12}	Shear modulus in the x_1-x_2 plane, GPa
H	Laminate thickness, mm
M	Applied moment about y-axis per unit length, N-mm/mm
M_0	Applied moment about y-axis per unit length, N-mm/mm
$p_{n\psi}^{(+)}$ $p_{nt}^{(+)}$	Dimensionless inclination parameters, slopes of the failure surface in stress space at $\sigma_{nn} = 0$ for mode A
$p_{nt}^{(-)}$	Dimensionless inclination parameters, slopes of the failure surface in stress space at $\sigma_{nn} = 0$ for modes B and C
N_x	In-plane force resultant per unit length in x-direction, N/mm
N_{xy}	In-plane force resultant per unit length in x-y plane, N/mm
S	Compliance matrix, $(MPa)^{-1}$

S_L	In-plane shear strength, MPa
S_T	Shear strength transverse to the fibers in the failure plane, MPa
$\bar{S}_T$	Shear strength ST written as a function of the normal stress when $\sigma_{22} = 0$, MPa
S_ψ	Shear strength resultant in the failure plane for $\sigma_{22} = 0$ or $\sigma_{nn} = 0$, MPa
$\bar{S}_\psi$	Shear strength resultant S_ψ as a function of the normal stress σ_{22} or σ_{nn}, MPa
T	Transformation matrix for transforming vectors from global to local coordinate system
$T_{\sigma i}$	Transformation matrix for transforming stresses from global to local coordinate system
$\bar{Q}$	Transformed reduced stiffness matrix
X_C	Absolute value of the compressive strength in the fiber direction, MPa
X_T	Absolute value of the tensile strength in the fiber direction, MPa
Y_C	Absolute value of the compressive strength in the transverse or x_2-direction, MPa
Y_T	Absolute value of the tensile strength in the transverse or x_2- direction, MPa
x_1, x_2, x_3	Material principal coordinates; x_1 parallel to the fiber and x_3 along the ply thickness, mm
x_n, x_t	Coordinates in the x_2, x_3 plane obtained by a rotation α about the x_1-axis; x_1-x_t is the failure plane
d_F, d_M, d_S	Damage variables for the fiber, matrix, and fiber-matrix debonding in shear, respectively, dimensionless. *d = 0* for no damage and *d = 1* at failure.
G_{12}, G_{13}, G_{23}	Shear moduli in the x_1-x_2, x_1-x_3, and the x_2-x_3 planes, respectively, for linear material behavior, GPa
I_1, I_2, I_3, I_4	Stress invariants associated with the any rotation of the x_2, x_3 -axes about x_1-axis
$m_{\sigma f}$	Stress magnification factor, dimensionless

Greek characters

α	Rotation angle about the x_1-axis in the coordinate transformation (x_1, x_2, x_3) to (x_1, x_n, x_t), radians
ε_x	Axial strain in x-direction
ε_y	Axial strain in y-direction
γ_{xy}	Shear strain in *x*-*y* plane
κ_x	Curvature of the laminate under cylindrical bending, $(mm)^{-1}$
η_a	Degradation factors in Modes A
$\eta^{(-)}$	Degradation factors in Modes B and C
η_T	Degradation factor in 3D for $\sigma_{nn} \geq 0$
η_C	Degradation factor in 3D for $\sigma_{nn} < 0$
σ_{11}	Normal stress in the fiber direction, MPa
σ_{22}	Normal stress transverse to the fiber direction, MPa
σ_{21}	Shear stress acting in the x_1-x_2 plane, MPa
σ_{nn}	Normal stress on the failure plane for matrix failure in compression, MPa
σ_{n1}	Shear stress in the x_1-direction on the failure plane for matrix failure in compression, MPa
σ_{nt}	Shear stress in the x_t-direction on the failure plane for matrix failure in compression, MPa
γ_{12}	Engineering shear strain in the x_1-x_2 plane
ε_{11}	Normal strain in the fiber direction, respectively.
ε_{22}	Normal strain in the transverse direction, respectively.
ν_{12}	Major, in-plane Poisson's ratio, dimensionless

$\sigma_{n\psi}$	Resultant shear stress on the fracture plane equal to $\sqrt{\sigma_{n1}^2 + \sigma_{nt}^2}$, MPa

Subscripts

F	Fiber failure mode in tension or compression
i,j	Free indices that can take on the values 1, 2, or 3
M	Matrix failure mode in tension or compression

Chapter 1

Introduction

1.1 Overview of Failure in Composites

Composite materials are increasingly being used in aerospace, automobile and marine structures due to their high specific strength, light weight, resistance to fatigue and corrosion, and their ability to be tailored for various designs. This trend, with considerable resulting improvement in fuel economy and passenger comfort level among other benefits, is anticipated to continue well into the future. In Boeing's 787 Dreamliner major structural elements are made of composite materials rather than aluminum alloys. Airbus has also extensively used composites on large transport commercial aircraft [1], [2].

The A310 was the first aircraft in production to have a composite fin box. The A320 was the first aircraft to go into production with an all-composite tail. About 13 percent by weight of the wing of the A340 is made of composite materials, and the A340/500-600 was the first airliner with a carbon fiber reinforced polymer (CFRP) keel beam and rear pressure bulkhead [1]. The A380 is the first large commercial aircraft with a center wing box produced largely from CFRP, representing a weight saving of up to 1.5 tons compared with the most advanced aluminum alloy [2]. The A380 also incorporates world's largest composite rear fuselage section to date.

The increasingly high demand placed upon the performance of laminated structures means that the design envelopes for composite structures should be carefully developed. There is a need for more reliable failure theories and damage propagation methodologies that will accurately predict the complex failure mechanisms in composite structures. Predictive tools are becoming more important, driven by the observation that extensive tests on composite structures are extremely expensive. It would be very desirable to have accurate predictive tools that complement a reduced number of essential tests. This rather ambitious goal can be achieved through computational modelling and methodologies whose predictions have been validated against experimental data. However, anisotropy, non-linear stress-strain response, especially in shear, and complexity of failure processes contribute to the complexity of modeling the structural behavior

of composites, especially the initiation and propagation of failure. One of the most significant barriers to more extensive use of laminate composites is the difficulty to capture structural failure phenomena. Predictions of composite behavior are challenging because matrix (resin) dominated failure mechanisms such as matrix cracking contribute to structural failures in addition to fiber-dominated failures.

1.2 Motivation from the World Wide Failure Exercise

The World Wide Failure Exercise (WWFE) was an "experts meeting" held in St Albans (UK) in 1991 to investigate the status of polymer composite failure theories [3]. The WWFE was divided into three main phases. First, to establish the framework, the organizers selected participants through detailed selection criteria as mentioned by Soden and Hinton [3] and supplied them with test cases, materials definitions, geometries and loads as described in Ref. [4]. Second, technical papers were collected from each of the participants detailing their failure theories and predictions for the specified test cases. This phase was referred to as Part A of the WWFE [5]. The organizers presented results from a direct comparison of the predictive capabilities of various failure theories, and collected their findings in a special issue of the journal Composites Science and Technology (Volume 58, 1998) [6–8]. This was the first time that the composite researchers compared failure prediction using different models/theories for the same set of geometry, loading and material property values.

In Part B of the WWFE as mentioned in Ref. [9], the third phase of the exercise, experimental details were provided for all test cases, including how the tests were conducted. Technical papers were collected from all the participants who compared predictions of their theories with the test results. Shortfalls in the various theories and experiments were also highlighted. The WWFE was further extended to Part C mentioned in Refs. [10-12]. Here the authors widened the scope of the investigation by incorporating five failure theories that emerged as winners since the inception of the study, and included predictions from modifications to the original theories. They provided a wide-ranging discussion on strengths and weaknesses of the failure theories. They also presented guidelines to composite structural designers on choosing appropriate failure theories, and recommendations were made to the research community on how to advance the current state-of-the art of composite material failure predictions. Based on results

of the experiments conducted in the WWFE as mentioned in Ref. [4], one of the five failure theories producing the highest number of predictions consistent with and capturing more general features of the experimental results was developed by Puck and Schürmann [13, 14].

1.3 Failure Analysis of Laminated Composite Structures

The main failure modes of FRP composites are: matrix compression, matrix tension, fiber compression, fiber tension, and delamination between adjacent plies. The fiber and the matrix failure modes are intralaminar, meaning these failures occur within a ply. Intralaminar modes include fractures of the fiber and/or matrix, and fiber kinking or buckling in compression. The intralaminar failure modes in this dissertation are described by phenomenological theories based on stress levels initiating damage or fracture. These phenomenological failure models can be easily delineated through finite element analyses of structural problems.

The stiffness of reinforcing fibers being significantly larger than that of the matrix material, substantial strain magnification occurs in the matrix when a ply is loaded in the transverse direction [14]. In cross ply laminates, the strain at which failure occurs in off-axis plies can be quite different from that in plies aligned in the loading direction. In a laminate under tension, cracks develop in the off-axis plies as illustrated in Fig. **1.1a**. Transverse matrix cracking can be followed by delamination between the 0^o and the 90^o interfaces (Fig. **1.1b**). Because of a mismatch in the in-plane Poisson's ratios of the longitudinal and transverse plies, matrix cracks can also appear in longitudinal plies (Fig. **1.1c**). A similar type of damage also occurs in laminates subjected to fatigue, thermal cycling and other loadings.

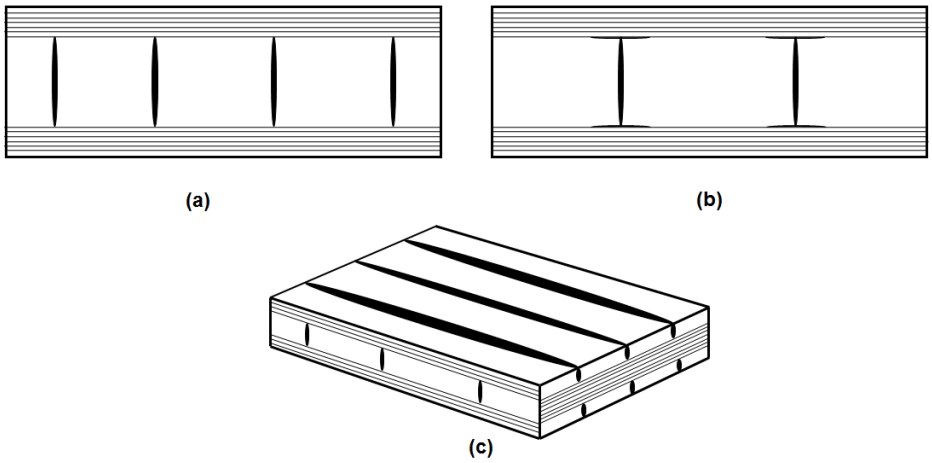

Figure 1.1: Failure modes in cross-ply laminates under tension. (a) Transverse matrix cracking; (b) transverse matrix crack and interface delamination; (c) matrix splitting of 0^o plies, Ref. [15]

In uni-directional laminates the intralaminar failure predictions are made by analyzing strains and stresses in each lamina, with failure criteria evaluated in each lamina. A failure initiated in one lamina predicts the onset of damage that is usually not the ultimate failure of the laminate. To model damage propagation, material degradation models are needed. These are empirical generally employ concepts of continuum damage mechanics (CDM). In general CDM approach is helpful for describing coupling between different failure processes and the stress-strain behavior of the structure [15, 16]. In CDM cracks are smeared out continuously over a failure zone where displacements are continuous and strains may be very large.

Delamination is an interlaminar failure mode, and it refers to the formation of an interfacial crack, or a debond between adjacent lamina. Delamination has been modeled with concepts of fracture mechanics where displacements are discontinuous across the interfacial crack faces. An initial delamination crack is postulated and fracture mechanics principles are used to determine if the crack will propagate. Alternatively, cohesive zone models (CZM) have been successfully used to simulate the delamination process.

1.3.1 Length Scales for Different Analysis

Continuous glass fibers are 3-20 μm in diameter, with most about 12 μm. The diameter of carbon and graphite fibers is about 8 μm. Ply thickness is about 125 μm for carbon FRP composites with a typical fiber volume fraction of 0.7, and also for glass FRP composites with

a typical fiber volume fraction of 0.45. In mechanics and materials engineering the physical scale at micro-level modeling is 10 μm, and the physical scale of meso-level modeling is 1 mm. Micro-level modeling treats the lamina as a heterogeneous continuum with distinct fiber and matrix material properties. Meso-level modeling treats the lamina as a homogeneous continuum with effective material properties. Typically micro-level modeling is used to develop homogenization rules to predict meso-level effective material properties. For example, the rule of mixtures links the constituent fiber and matrix properties to the effective properties of the lamina. The macro scale analysis is of order 10^0 m which includes structural elements such as beams, columns and plates. Finally, system level analysis is of order 10^3 m which is the scale of an airplane or a bridge, for example. In this dissertation, we focus on mesoscale modeling of the response and failure of a lamina with the goal of predicting laminate progressive failure. The meso-level material properties are assumed to be given.

1.3.2 Modelling of Intralaminar Behavior

Important contributions to intralaminar failure initiation criteria based on the mechanics of materials approach are, among others, by Hashin and Rotem [17], Hashin [18], Puck and Schürmann [13, 14], Dávila *et al.* [19], and Pinho *et al.* [20]. The failure initiation criteria proposed by Hashin [18], Puck and Schürmann [13, 14], and Pinho *et al.* [20] are reviewed. Each criterion is expressed in terms of a dimensionless failure index for a matrix by FI_M and a fiber by FI_F. The range of the failure indices are $0 \leq FI < 1$ for no failure, and $FI = 1$ at failure initiation.

The material principal coordinate axes and the global coordinate axes are shown in Fig. 1.2. Stresses with respect to the material principal coordinates are generally used to describe a failure criterion. The material principal directions 1 and 3 are along the fiber and the thickness directions, respectively.

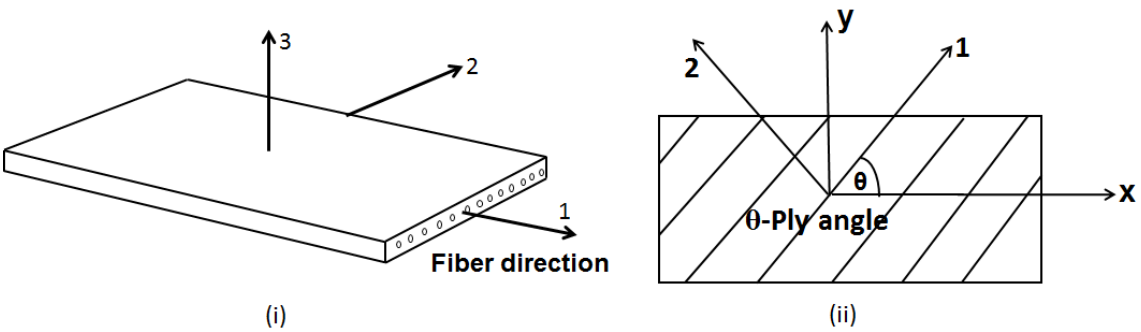

Figure 1.2: Material principal coordinate system used in current work; (ii) Fiber direction considered in the current work.

1.4 Hashin's Failure Initiation Criteria

Hashin [18] assumed matrix failure to be brittle and in a plane parallel to the fibers caused by stress components acting on this plane. Let (x_1, x_n, x_t) denote Cartesian coordinate directions on the fracture plane obtained by the transformation:

$$\begin{bmatrix} x_1 \\ x_n \\ x_t \end{bmatrix} = \begin{bmatrix} 1 & 0 & 0 \\ 0 & \cos\alpha & \sin\alpha \\ 0 & -\sin\alpha & \cos\alpha \end{bmatrix} \begin{bmatrix} x_1 \\ x_2 \\ x_3 \end{bmatrix} \tag{1.1}$$

The stresses in the (x_1, x_n, x_t) system are denoted by σ_{11}, σ_{nn}, σ_{tt}, σ_{nt}, σ_{t1}, and σ_{1n}, and they are related to the stresses in the material principal directions σ_{ij}, $i, j = 1, 2, 3$, by the stress transformation equations:

$$\begin{bmatrix} \sigma_{11} \\ \sigma_{nn} \\ \sigma_{tt} \\ \sigma_{nt} \\ \sigma_{t1} \\ \sigma_{1n} \end{bmatrix} = \begin{bmatrix} 1 & 0 & 0 & 0 & 0 & 0 \\ 0 & \cos^2\alpha & \sin^2\alpha & 2\sin\alpha\cos\alpha & 0 & 0 \\ 0 & \sin^2\alpha & \cos^2\alpha & -2\sin\alpha\cos\alpha & 0 & 0 \\ 0 & -\sin\alpha\cos\alpha & \sin\alpha\cos\alpha & \cos^2\alpha - \sin^2\alpha & 0 & 0 \\ 0 & 0 & 0 & 0 & \cos\alpha & -\sin\alpha \\ 0 & 0 & 0 & 0 & \sin\alpha & \cos\alpha \end{bmatrix} \begin{bmatrix} \sigma_{11} \\ \sigma_{22} \\ \sigma_{33} \\ \sigma_{23} \\ \sigma_{31} \\ \sigma_{12} \end{bmatrix} \tag{1.2}$$

The plane of fracture is the x_1-x_t plane with direction x_n normal to the plane. The stress components acting on the fracture plane obtained from Eq. (1.2) are

$$\sigma_{n1} = \sigma_{21}\cos\alpha + \sigma_{31}\sin\alpha \tag{1.3a}$$

$$\sigma_{nn} = \frac{(\sigma_{22} + \sigma_{33})}{2} + \frac{(\sigma_{22} - \sigma_{33})}{2} cos\ 2\alpha + \sigma_{23} sin\ 2\alpha \tag{1.3b}$$

$$\sigma_{nt} = \frac{-(\sigma_{22} - \sigma_{33})}{2} \sin 2\alpha + \sigma_{23} \cos 2\alpha \tag{1.3c}$$

The stresses acting on the fracture plane are shown in Fig. **1.3**.

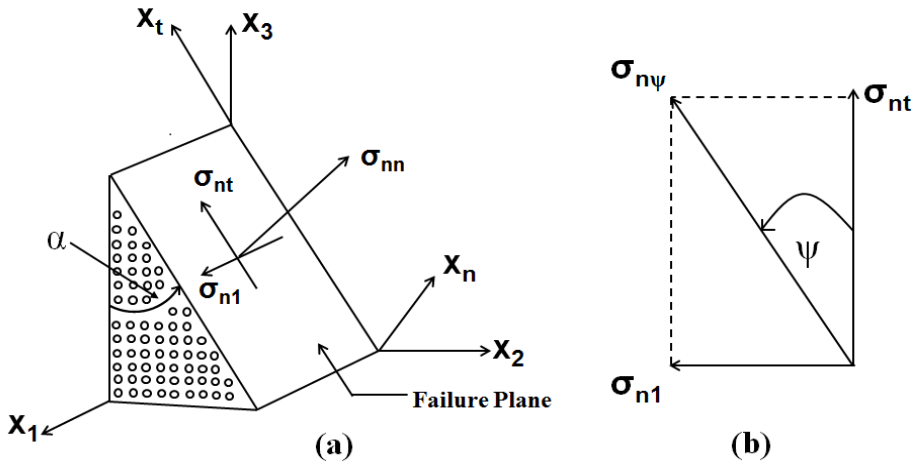

Figure 1.3: (a) Stresses acting on the failure plane, (b) resultant shear stress on the failure plane.

Note that the stress component σ_{11} does not appear in a criterion formulated from the stress components on the fracture plane given by Eq. (1.3). Hashin proposed a quadratic form in three of the five stress invariants associated with a rotation of the x_2, x_3-axes around the x_1-axis. Terms in the first stress invariant $I_1 = \sigma_{11}$ are omitted from the criterion, and the fifth invariant is cubic in stresses so it is not included in a quadratic criterion with integer powers of the invariants. The failure criterion is written as

$$A_2 I_2 + B_2 I_2^2 + A_3 I_3 + A_4 I_4 = 1 \tag{1.4}$$

where coefficients A_2, B_2, A_3, and A_4 are to be determined from test data and the three stress invariants are

$$I_2 = \sigma_{22} + \sigma_{33}; \quad I_3 = \sigma_{23}^2 - \sigma_{22}\sigma_{33}; \quad I_4 = \sigma_{12}^2 + \sigma_{13}^2 \tag{1.5}$$

From the pure transverse shear test in which at failure $\sigma_{nt} = S_T$, and the pure axial shear test in which $\sigma_{n1} = S_L$ at failure, we get $A_3 = 1/S_T^2$ and $A_4 = 1/S_L^2$. Thus, two coefficients in the quadratic form remain unknown. These two coefficients are different for the matrix failure in tension (i.e,

$\sigma_{nn} \geq 0$) and the matrix failure in compression (i.e, $\sigma_{nn} < 0$).

Hashin pointed out that it is difficult to experimentally measure the shear strength S_T in the fracture plane parallel to the fibers. Perhaps no test exists. For the in-plane shear test in which all stresses in the (x_1, x_2, x_3) coordinate system vanish except σ_{12}, the ultimate value of σ_{12} is equal to the longitudinal shear strength S_L.

1.4.1 Matrix Compression Mode

From the transverse compression test σ_{22}=-Y_C at failure and all other stress components in the (x_1, x_2, x_3) system vanish. Additional information is required to determine the two unknown coefficients in the quadratic criterion. Hashin argues that if the material fails under a transversely isotropic pressure $\sigma_{22} = -p_h$, then the hydrostatic pressure at failure is much larger than the compressive strength Y_C in transverse compression; i.e., $p_h >> Y_C$. The quadratic criterion is formulated in terms of Y_C and the ratio Y_C/p_h, and the lowest order terms in a series expansion of the quadratic criterion in Y_C/p_h are retained. On this basis the quadratic criterion for the matrix failure in compression is

$$FI_M = \frac{1}{Y_C}\left[\frac{Y_C}{2S_T} - 1\right](\sigma_{22} + \sigma_{33}) + \frac{1}{4S_T^2}(\sigma_{22} + \sigma_{33})^2 + \frac{1}{4S_T^2}(\sigma_{23}^2 - \sigma_{22}\sigma_{33}) + \frac{1}{4S_L^2}(\sigma_{21}^2 + \sigma_{31}^2) = 1, \quad \sigma_{nn} < 0 \tag{1.6}$$

Hashin showed that $\sigma_{nn} < 0$ if the invariant $I_2 = \sigma_{22} + \sigma_{33} < 0$.

1.4.2 Matrix Failure in Tension

To determine the two unknown coefficients in the quadratic form for the matrix failure in tension results of two tests are needed. From the transverse tension test $\sigma_{22} = Y_T$. It is assumed that coefficient A_2 associated with invariant I_2 in Eq. (1.4) equals zero to obtain a convex failure locus. Hashin's criterion for tensile matrix mode failure is:

$$FI_M = \left(\frac{\sigma_{22} + \sigma_{33}}{Y_T}\right)^2 + \frac{\sigma_{23}^2 - \sigma_{22}\sigma_{33}}{S_T^2} + \frac{\sigma_{12}^2 + \sigma_{13}^2}{S_T^2} = 1, \quad \sigma_{nn} > 0 \tag{1.7}$$

Also $\sigma_{nn} > 0$ if the invariant $I_2 = \sigma_{22} + \sigma_{33} > 0$. Note that in the σ_{22}-σ_{33} stress plane $Y_T < 2S_T$

for the failure locus $FI_M = I$ to be convex (an ellipse).

1.4.3 Hashin's compression fiber failure mode

Citing that the influence of shear on compressive fiber mode was not well understood at the time Ref. [18] was written, Hashin's criterion is a non-interacting maximum allowable compressive stress criterion. Hence, the failure index is simply

$$FI_F = \frac{-\sigma_{11}}{X_C} \ , \quad \sigma_{11} < 0 \tag{1.8}$$

1.4.4 Hashin's tension fiber failure mode

The plane of failure is the x_1-x_3 plane in uniaxial tension tests. Hashin formulated a quadratic stress criterion in terms of the stress invariant $I_1 = \sigma_{11}$ and invariant I_4 given in Eq. (1.5). For a convex failure locus in the σ_{11}, σ_{12}, and σ_{13} stress space, the linear term in the invariant I_1 is omitted in the failure criterion. The tensile fiber mode failure index is

$$FI_F = \left(\frac{\sigma_{11}}{X_T}\right)^2 + \left(\frac{\sigma_{12}^2 + \sigma_{13}^2}{S_L^2}\right)^2, \quad \sigma_{11} < 0 \tag{1.9}$$

Hashin also gave the approximation

$$FI_F = \frac{\sigma_{11}}{X_T} \ , \quad \sigma_{11} > 0 \tag{1.10}$$

in which influences of the longitudinal shear stresses σ_{12} and σ_{13} on fracture are neglected.

1.5 Discussion of Hashin's Intralaminar Failure Criteria

A fracture plane parallel to fibers to model the matrix failure modes was introduced by Hashin, and although he discussed the procedure to find the orientation of the fracture plane it was abandoned because of the computational complexity involved to locate it in a three-dimensional stress state. Instead Hashin continued with the logical development of the fracture criteria based on the quadratic approximation in terms of stress invariants. As a result, the intersection of the tensile and the compression matrix failure modes occurs when the invariant $I_2 = \sigma_{22} + \sigma_{33} = 0$. Invariant I_2 is also equal to the sum of the principal stresses. For $\sigma_{22} + \sigma_{33} = 0$, the fracture plane is at $\alpha = \pm 45^o$ on which the normal stress $\sigma_{nn} = 0$ and the shear stress σ_{nt}

is a maximum and equal to $(\sigma_{22}-\sigma_{33})/2$. Hashin recognized that fracture occurs on the plane where the transverse shear stress σ_{nt} is the maximum was difficult to accept as a general conclusion, but it is a consequence of the quadratic approximation. Also, the shear strength S_T transverse to fibers in the fracture plane that appears in the matrix mode criteria is not available from standard tests. Because of no direct test method to measure S_T, researchers using Hashin's criteria have taken the value of S_T equal to the longitudinal shear strength S_L, or have taken S_T equal to the apparent interlaminar shear strength; e.g., see the review of existing composite failure criteria by Paris [21]. Also, Paris pointed out that for a plane stress state the out-of-plane allowable strength S_T appearing in the matrix compression criterion, Eq. (1.6), is not accompanied by the corresponding shear stress σ_{23}.

1.6 Puck and Schürmann's Failure Criteria

Puck and Schürmann's [13, 14] proposed phenomenological models to analyze failure of unidirectional FRP composites. The failure criterion depends upon the failure mode in a unidirectional ply and is expressed in terms of stresses on material principal planes. Following Hashin's [18] work, the matrix failure is assumed to be brittle and to occur on a plane parallel to the fibers. Fiber failure modes in tension and compression are considered separately. However, contrary to Hashin's work in which matrix failure at a point is assumed to be instantaneous, Puck and Schürmann distinguish between failure initiation and completion. Subsequent to failure initiation at a point, the matrix elastic moduli are assumed to degrade due to weakening of the matrix due to cracks. It is modeled using the CDM approach in which cracks are smeared-out over an infinitesimal volume that is assigned degraded material properties.

Following Hashin's [18] work, in which it is postulated that there is a brittle failure plane parallel to the x_1-axis, Puck and Schürmann [14] developed an inter fiber failure (IFF) criterion similar to the modified Coulomb-Mohr (C-M) criterion, in which the limiting shear stress acting on the failure plane increases as the magnitude of the normal compressive stress σ_{nn} increases. In the Puck and Schürmann criteria, a different expression for stresses at failure initiation is specified for the tensile and the compressive normal stresses on the failure plane. The IFF refers to cracks

that either extend through the thickness of the unidirectional lamina and can be initiated by a cohesive failure of the matrix or by adhesive failure at the fiber-matrix interface.

We assume that the normal to the matrix failure plane is at a counterclockwise angle α with the x_1 –axis, and the direction of the normal is denoted by x_n as shown in Figure **1.3(a)**. The stress components acting on the failure plane are given by Eq. (1.3). Puck and Schürmann [13, 14] hypothesize that the brittle failure on a plane parallel to the fibers is promoted by a tensile normal stress $\sigma_{nn} \geq 0$, and impeded by a compressive normal stress $\sigma_{nn} < 0$. Hence two separate criteria are formulated, one for tension failure and the other for compression failure.

1.6.1 Tensile Failure Criterion, $\sigma_{nn} \geq 0$

The Puck and Schürmann [13, 14] matrix failure criterion for $\sigma_{nn} \geq 0$, classified as Mode A failure, is described first. In the uni-axial transverse tension test (along the x_2- direction) and in the in-plane (x_1-x_2) simple shear test, the failure plane is normal to the x_2-direction and $\alpha = 0$. From Eqs. (1.3) $\sigma_{n1} = \sigma_{21}$, $\sigma_{nn} = \sigma_{22}$, and $\sigma_{nt} = \sigma_{23}$. In the uniaxial transverse tension test, $\sigma_{22} = Y_T$ at failure initiation, and all other stresses in the x_1, x_2, x_3 coordinate system vanish. In the x_1-x_2 plane shear test, $\sigma_{21} = S_L$ at failure initiation, and all other stresses in the x_1, x_2, x_3 system vanish. The Puck and Schürmann failure initiation criterion is at most quadratic in stress components acting on the failure plane, and is expressed as

$$(1 - c_1)\left(\frac{\sigma_{nn}}{Y_T}\right)^2 + c_1\left(\frac{\sigma_{nn}}{Y_T}\right) + \left(\frac{\sigma_{nt}}{S_T}\right)^2 + \left(\frac{\sigma_{n1}}{S_L}\right)^2 = 1, \qquad \sigma_{nn} > 0 \tag{1.11}$$

The strength parameter S_T in Eq. (1.11) denotes the shear strength transverse to fibers in the x_1-x_2 failure plane. There is no simple test available to determine S_T. For the constant $c_1 < 1$, Eq. (1.11) defines an ellipsoidal surface in the stress space with axes σ_{nn}, σ_{nt} and σ_{n1}. On the failure plane, the resultant shear stress is denoted by $\sigma_{n\psi}$ where, $\sigma_{n\psi} = \sqrt{\sigma_{nt}^2 + \sigma_{n1}^2}$, and the direction of $\sigma_{n\psi}$ on the failure plane is denoted by the angle ψ shown in Fig. **1.3(b)**. Substituting $\sigma_{nt} = \sigma_{n\psi}\cos\psi$ and $\sigma_{n1} = \sigma_{n\psi}\sin\psi$ in Eq. (1.11) yields

$$(1 - c_1)\left(\frac{\sigma_{nn}}{Y_T}\right)^2 + c_1\left(\frac{\sigma_{nn}}{Y_T}\right) + \left(\frac{\sigma_{n\psi}}{S_\psi}\right)^2 = 1\,, \qquad \sigma_{nn} > 0 \tag{1.12}$$

where the shear strength S_ψ is defined by

$$\frac{1}{S_\psi^2} = \left(\frac{Cos^2\psi}{S_T^2} + \frac{Sin^2\psi}{S_L^2}\right) \tag{1.13}$$

The constant c_1 is related to the negative of the slope of $\sigma_{n\psi}$ with respect to σ_{nn} along the contour ψ = constant on the ellipsoidal surface evaluated at $\sigma_{nn} = 0$. We denote the negative of this slope by $p_{n\psi}^{(+)}$; i.e.,

$$p_{n\psi}^{(+)} = -\left.\frac{d\sigma_{n\psi}}{d\sigma_{nn}}\right|_{\sigma_{nn}=0} = 0; \quad \psi = \text{constant} \tag{1.14}$$

For a fixed value of ψ, differentiating Eq. (1.12) with respect to σ_{nn} followed by setting $\sigma_{nn}= 0$, and noting that at failure initiation, $\sigma_{n\psi} = S_\psi$, we get

$$c_1 = \frac{2Y_T}{S_\psi}\, p_{n\psi}^{(+)}, \quad \psi = \text{constant} \tag{1.15}$$

Substitute the value of c_1 from Eq. (1.15) into Eq. (1.12), we obtain

$$\left(1 - 2p_{n\psi}^{(+)}\frac{Y_T}{S_\psi}\right)\left(\frac{\sigma_{nn}}{Y_T}\right)^2 + 2p_{n\psi}^{(+)}\frac{Y_T}{S_\psi}\left(\frac{\sigma_{nn}}{Y_T}\right) + \left(\frac{\sigma_{n\psi}}{S_\psi}\right)^2 = 1\,, \qquad \sigma_{nn} > 0 \tag{1.16}$$

To get the final form of the tension failure criterion listed as Eq. (16) in Puck and Schürmann [14], we add the term $\left[p_{n\psi}^{(+)}\frac{Y_T}{S_\psi}\left(\frac{\sigma_{nn}}{Y_T}\right)\right]^2$ to both sides of Eq. (1.16), and rearrange the result to get

$$\left[1 - p_{n\psi}^{(+)}\frac{Y_T}{S_\psi}\right]^2\left(\frac{\sigma_{nn}}{Y_T}\right)^2 + \left(\frac{\sigma_{n\psi}}{S_\psi}\right)^2 = \left[1 - p_{n\psi}^{(+)}\frac{Y_T}{S_\psi}\right]^2\,, \qquad \sigma_{nn} > 0 \tag{1.17}$$

Taking the positive square root of each side of Eq. (1.17), and using $\left(\frac{\sigma_{n\psi}}{S_\psi}\right)^2 = \left(\frac{\sigma_{nt}}{S_T}\right)^2 + \left(\frac{\sigma_{n1}}{S_L}\right)^2$, we define the index for the matrix failure initiation in tension as

$$FI_M = \sqrt{\left[1 - p_{n\psi}^{(+)}\frac{Y_T}{S_\psi}\right]^2\left(\frac{\sigma_{nn}}{Y_T}\right)^2 + \left(\frac{\sigma_{nt}}{S_T}\right)^2 + \left(\frac{\sigma_{n1}}{S_L}\right)^2} + \frac{p_{n\psi}^{(+)}\sigma_{nn}}{S_\psi}\,, \qquad \sigma_{nn} > 0 \tag{1.18}$$

Projections of the failure initiation surface, $FI_M = 1$, on the σ_{n1}- σ_{nt} plane $\sigma_{nn} = 0$, and on the σ_{n1} - $\sigma_{n\psi}$ plane for $\sigma_{nn} > 0$ are shown in Figs. **1.4(a)** and **1.4 (b)**, respectively.

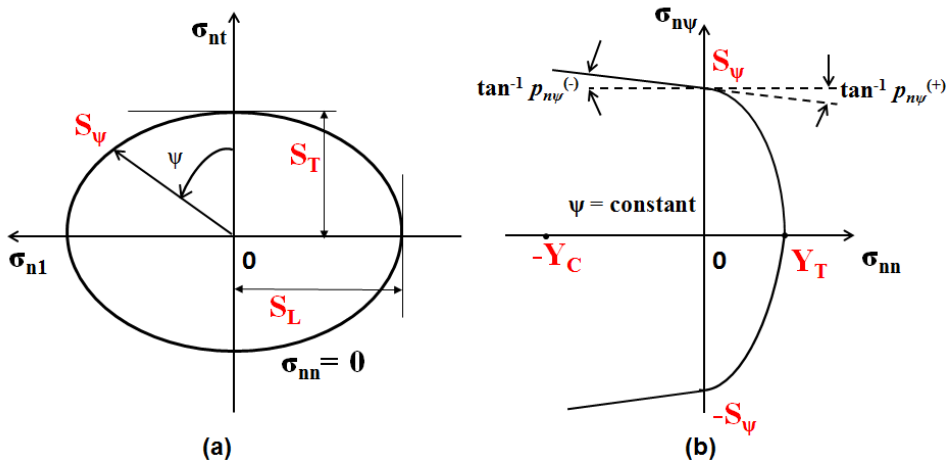

Figure 1.4: Projection of the failure initiation surface on the (a) σ_{n1}-σ_{nt} plane, $\sigma_{nn} = 0$, and (b) σ_{nn}-$\sigma_{n\psi}$ plane for $\sigma_{nn} \geq 0$

For $\psi = 0$ and $\psi = \frac{\pi}{2}$, we write Eq. (1.14) as

$$p_{nt}^{(+)} = -\frac{d\sigma_{nt}}{d\sigma_{nn}}\bigg|_{\sigma_{nn}=0}, \psi = 0; \quad p_{n1}^{(+)} = -\frac{d\sigma_{n1}}{d\sigma_{nn}}\bigg|_{\sigma_{nn}=0}, \psi = \frac{\pi}{2} \tag{1.19}$$

The contour line of the failure initiation surface for $\psi = 0$ is defined by setting $\sigma_{n1} = 0$ in Eq. (1.11). For the $\psi = 0$ contour, we set $\sigma_{n1} = 0$ in Eq. (1.11), differentiate the resulting equation with respect to σ_{nn} and set $\sigma_{nn} = 0$ to get

$$\frac{c_1}{Y_T} = \frac{2}{S_T} p_{nt}^{(+)} \tag{1.20}$$

Following the same procedure for the $\psi = \frac{\pi}{2}$ contour for which $\sigma_{nt} = 0$, we get

$$\frac{c_1}{Y_T} = \frac{2}{S_L} p_{n1}^{(+)} \tag{1.21}$$

After multiplying both sides of Eq. (1.20) by $\cos^2\psi$ and of Eq. (1.21) by $\sin^2\psi$, adding respective sides of the resulting equations, and substituting for c_1 from Eq. (1.15) we get

$$\frac{p_{n\psi}^{(+)}}{S_\psi} = \frac{p_{nt}^{(+)}}{S_T} Cos^2\psi + \frac{p_{n1}^{(+)}}{S_L} Sin^2\psi \tag{1.22}$$

Equation (1.22) is listed as Eq. (18) in Puck and Schürmann [14]. It follows from Eqs. (1.20) and (1.21) that $\frac{p_{n1}^{(+)}}{S_L} = \frac{p_{nt}^{(+)}}{S_T}$.

We note that FI_M cannot exceed 1. For $FI_M < 1$, no failure initiates. For shear stress $\sigma_{nt} = 0$, we have plotted the failure surface in the σ_{nn}-σ_{n1} plane for $\sigma_{nn} \geq 0$ in Figure **1.5**.

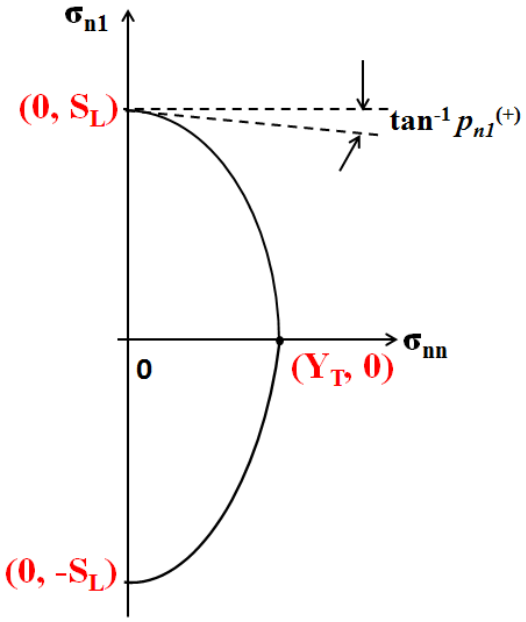

Figure 1.5: Projection of the failure initiation surface on the σ_{nn}-σ_{n1} stress plane; $\sigma_{nt} = 0$.

The tension failure index FI_M given by Eq. (1.18) is a function of the failure plane angle α. The value of α that maximizes FI_M defines the failure plane.

1.6.2 Compression Matrix Failure Initiation Criterion, $\sigma_{nn} < 0$.

As in the C-M criterion a compressive normal stress, $\sigma_{nn} < 0$, is assumed to resist failure caused by the shear stresses σ_{nt} and σ_{n1} . In the σ_{nn}- σ_{nt} and the σ_{nn}- σ_{n1} planes, the C-M criterion can be written, respectively, as $|\sigma_{nt}| - \mu|\sigma_{nn}| = S_T$ and $|\sigma_{n1}| - \mu|\sigma_{nn}| = S_L$, where μ is the coefficient of friction. Motivated by the C-M failure criterion, Puck and Schürmann [14] proposed that there is no matrix failure under pure normal compressive stress on a plane and the following criterion for initiation of matrix failure with $\sigma_{nn} < 0$ but non-zero shear stresses:

$$\left(\frac{\sigma_{nt}}{S_T - p_{nt}^{(-)}\sigma_{nn}}\right)^2 + \left(\frac{\sigma_{n1}}{S_L - p_{n1}^{(-)}\sigma_{nn}}\right)^2 = 1\,, \quad \sigma_{nn} < 0 \tag{1.23}$$

In Eq. (1.23) strengths in the denominators are increased by the compressive normal stress, and ($p_{nt}^{(-)}$, $p_{n1}^{(-)}$) are the inclination parameters in compression. For the stress state having $\sigma_{n1} = 0$, Eq. (1.23) reduces to $\sigma_{nt} = S_T - p_{nt}^{(-)}\sigma_{nn}$, and from this expression the inclination parameter is interpreted as the negative slope of σ_{nt} with respect to σ_{nn}.. That is,

$$p_{nt}^{(-)} = -\left(\frac{d\sigma_{nt}}{d\sigma_{nn}}\right), \quad \sigma_{n1} = 0 \tag{1.24}$$

Similarly for the stress state in which $\sigma_{nt} = 0$, Eq. (1.23) simplifies to $\sigma_{n1} = S_L - p_{n1}^{(-)}\sigma_{nn}$, and from this expression the inclination parameter $p_{nt}^{(-)}$ is interpreted as the negative slope of σ_{n1} with respect to σ_{nn}, or

$$p_{n1}^{(-)} = -\left(\frac{d\sigma_{n1}}{d\sigma_{nn}}\right), \sigma_{nt} = 0 \tag{1.25}$$

Citing better agreement with experimental results, Puck and Schürmann [14] neglected, in Eq. (1.23), the quadratic terms in σ_{nn} and wrote it as

$$\frac{\sigma_{nt}^2}{S_T^2 - 2p_{nt}^{(-)}S_T\sigma_{nn}} + \frac{\sigma_{n1}^2}{S_L^2 - 2p_{n1}^{(-)}S_L\sigma_{nn}} = 1, \quad \sigma_{nn} < 0\,. \tag{1.26}$$

For mathematical simplification, Puck and Schürmann [14] assumed that the inclination parameters are related as follows:

$$\frac{p_{nt}^{(-)}}{S_T} = \frac{p_{n1}^{(-)}}{S_L} = \frac{p}{R} \tag{1.27}$$

Variables *p* and *R* are defined by Eq. (1.27). With relations given in Eq. (1.27), Eq. (1.26) reduces to the simpler form:

$$\left(\frac{\sigma_{nt}}{S_T}\right)^2 + \left(\frac{\sigma_{n1}}{S_L}\right)^2 + 2\left(\frac{p}{R}\right)\sigma_{nn} = 1, \quad \sigma_{nn} < 0. \tag{1.28}$$

The failure initiation surface in the (σ_{nn}, σ_{nt}, σ_{n1}) stress space given by Eq. (1.28) is an elliptic paraboloid, and its intersection with the plane σ_{nn} = *constant* is an ellipse with the shear stresses as the axes. *Note that the failure initiation surface does not intersect the negative σ_{nn} axis because of the hypothesis that a compressive normal stress impedes shear failure.* Differentiating Eq. (1.28) with respect to σ_{nn} and using Eq. (1.27), the inclination parameters are related to the slopes of the failure initiation surface by

$$\frac{1}{S_T}\frac{d\sigma_{nt}}{d\sigma_{nn}} = -\left(\frac{p_{nt}^{(-)}}{S_T}\right) = -\left(\frac{p}{R}\right) \text{ in the } (\sigma_{nt}, \sigma_{nn}) \text{ plane at } (\sigma_{nt}, \sigma_{nn}) = (S_T, 0) \tag{1.29}$$

$$\frac{1}{S_L}\frac{d\sigma_{n1}}{d\sigma_{nn}} = -\left(\frac{p_{n1}^{(-)}}{S_L}\right) = -\left(\frac{p}{R}\right) \text{ in the } (\sigma_{n1}, \sigma_{nn}) \text{ plane at } (\sigma_{n1}, \sigma_{nn}) = (S_L, 0) \tag{1.30}$$

For the elliptic failure envelope in the plane σ_{nn} = *constant* let $\sigma_{nt} = \bar{S}_\psi \cos\psi$ and $\sigma_{n1} = \bar{S}_\psi \sin\psi$ where $\bar{S}_\psi = \sqrt{\sigma_{nt}^2 + \sigma_{n1}^2}$ at failure (Fig. **1.3(b)**). Then the failure ellipse, from Eq (1.28), reduces to

$$\bar{S}_\psi^2 \left[\left(\frac{\cos\psi}{S_T}\right)^2 + \left(\frac{\sin\psi}{S_L}\right)^2\right] = 1 - 2\left(\frac{p}{R}\right)\sigma_{nn} \tag{1.31}$$

For $\sigma_{nn} = 0$, let $S_\psi = \bar{S}_\psi$, where

$$\frac{1}{S_\psi^2} = \left(\frac{\cos\psi}{S_T}\right)^2 + \left(\frac{\sin\psi}{S_L}\right)^2 \tag{1.32}$$

Hence

$$\left(\frac{\bar{S}_\psi}{S_\psi}\right)^2 = 1 - 2\left(\frac{p}{R}\right)\sigma_{nn} \tag{1.33}$$

The derivative of $\bar{S}_\psi$ with respect to the normal stress σ_{nn} at $\sigma_{nn} = 0$ is given by

$$\frac{2\bar{S}_\psi}{S_\psi^2}\left(\frac{d\bar{S}_\psi}{d\sigma_{nn}}\right)\Bigg|_{\sigma_{nn}=0} = \frac{2}{S_\psi}\frac{d\bar{S}_\psi}{d\sigma_{nn}}\Bigg|_{\sigma_{nn}=0} = -2\left(\frac{p}{R}\right) \tag{1.34}$$

On the contour of the failure surface for ψ = *constant*, let $p_{n\psi}^{(-)}$ denote the negative of the slope of S_ψ with respect to σ_{nn} at $\sigma_{nn} = 0$. Hence Eq. (1.34) becomes

$$\frac{p_{n\psi}^{(-)}}{S_\psi} = \frac{p}{R} \tag{1.35}$$

Now multiply Eq. (1.29) by $cos^2\psi$ and add it to Eq. (1.30) multiplied by $sin^2\psi$ to get

$$\frac{p_{nt}^{(-)}}{S_T} cos^2\psi + \frac{p_{n1}^{(-)}}{S_L} sin^2\psi = \frac{p}{R} \tag{1.36}$$

Substitute for p / R from Eq. (2.28) in Eq. (2.29) to get

$$\frac{p_{n\psi}^{(-)}}{S_\psi} = \frac{p_{nt}^{(-)}}{S_T} cos^2\psi + \frac{p_{n1}^{(-)}}{S_L} sin^2\psi \tag{1.37}$$

Equation (1.37) is analogous to Eq. (1.22) for $\sigma_{nn} > 0$. Equation (1.28) is manipulated to a final form by the following algebraic steps: Substitute for p / R from Eq. (1.35) in Eq. (1.28), add the term $\left(p_{n\psi}^{(-)}\sigma_{nn}/S_\psi\right)^2$ to each side of Eq. (1.28) and rearrange the terms to get

$$\left(\frac{\sigma_{nt}}{S_T}\right)^2 + \left(\frac{\sigma_{n1}}{S_L}\right)^2 + \left(p_{n\psi}^{(-)}\sigma_{nn}/S_\psi\right)^2 = \left[1 - \frac{p_{n\psi}^{(-)}\sigma_{nn}}{S_\psi}\right]^2 \tag{1.38}$$

Take the positive square root of both sides of Eq. (1.38) to get

$$FI_M = \sqrt{\left(\frac{\sigma_{nt}}{S_T}\right)^2 + \left(\frac{\sigma_{n1}}{S_L}\right)^2 + \left(\frac{p_{n\psi}^{(-)}}{S_\psi}\sigma_{nn}\right)^2} + \left(\frac{p_{n\psi}^{(-)}}{S_\psi}\right)\sigma_{nn} \ , \qquad \sigma_{nn} < 0. \tag{1.39}$$

$FI_M = 1$ defines the failure initiation surface. Thus to check if a matrix failure has initiated or not, one needs to find the angle α that makes the failure index the maximum for a given stress state, and then check if $FI_M = 1$ for this value of α. The necessary condition for an extremum is $\left(\frac{\partial FI_M}{\partial \alpha}\right) = 0$ which can be numerically solved for the angle α.

1.6.3 Failure Criteria for Plane State of Stress

For a plane stress state in the x_1- x_2 plane, the failure plane is normal to the x_2-direction, and angle α = 0. From Eq. (1.3), $\sigma_{n1} = \sigma_{21}$, $\sigma_{nn} = \sigma_{22}$, $\sigma_{nt} = 0$. Thus, the angle ψ in Fig. **1.3(b)** equals π/2, and from Eq. (1.22) we get $\frac{p_{n\psi}^{(+)}}{S_\psi} = \frac{p_{n1}^{(+)}}{S_L}$. Hence, the failure index given by Eq. (1.18) reduces to

$$FI_M = \sqrt{\left[1 - p_{n1}^{(+)}\frac{Y_T}{S_L}\right]^2\left(\frac{\sigma_{22}}{Y_T}\right)^2 + \left(\frac{\sigma_{21}}{S_L}\right)^2} + \frac{p_{n1}^{(+)}\sigma_{22}}{S_L}, \qquad \sigma_{22} > 0 \tag{1.40}$$

Equation (1.40) is Puck and Schürmann's [14] Eq. (19).

The longitudinal shear strength, S_L, of a unidirectional ply is determined from in-plane shear tests in which failure is transverse matrix cracking parallel to fibers similar to the fracture in the transverse tension test. The shear strength, S_T, transverse to fibers in the failure plane, or what Puck and Schürmann [14] call the fracture resistance in the action plane, cannot be determined from simple tests. Instead S_T is derived from the uniaxial transverse compression test in which $\sigma_{22} = -Y_C$ at failure and all other stresses in the x_i-coordinate system vanish. To determine the relationship of S_T to Y_C, we first consider a plane stress state for which $\sigma_{n1} = \sigma_{21}\cos\alpha$, $\sigma_{nn} = \sigma_{22}\cos^2\alpha$, and $\sigma_{nt} = -\sigma_{22}\cos\alpha\ \sin\alpha$. Substitute these stresses in the left-hand side of Eq. (1.28) and write the result as

$$FI_M = \left(\frac{\sigma_{22}}{S_T}\right)^2 sin^2\alpha\ cos^2\alpha + \left(\frac{\sigma_{21}}{S_L}\right)^2 cos^2\alpha + 2\left(\frac{p}{R}\right)\sigma_{22}cos^2\alpha = 1;\ \sigma_{22} < 0 \tag{1.41}$$

The angle α of the fracture plane is determined when index FI_M has the maximum value with respect to α. Using trigonometric identities, Eq. (1.41) is rewritten in terms of $\cos^2\alpha$, and then the necessary condition for a maximum can be written as

$$\frac{dFI_M}{d\alpha} = \frac{dFI_M}{d(cos^2\alpha)}(-2\ \cos\alpha\ \sin\alpha) = 0 \tag{1.42}$$

One solution of Eq. (1.42) is α = 0, which is the mode B failure where the failure plane is normal to the x_2-direction. The other solution of Eq. (1.42) gives

$$cos^2\alpha = \frac{1}{2}\left[1 + \left(\frac{S_T}{S_L}\right)^2\left(\frac{\sigma_{21}}{\sigma_{22}}\right)^2\right] + \frac{S_T(p/R)}{\sigma_{22}} \tag{1.43}$$

where the assumption in Eq. (1.27) has been used. Substitute Eq. (1.43) for $\cos^2\alpha$ in Eq. (1.41) to get

$$FI_M = \left[p_{nt}^{(-)}\right]^2 + \frac{1}{2}\left(\frac{\sigma_{21}}{S_L}\right)^2 + \frac{1}{4}\left(\frac{S_T}{\sigma_{22}}\right)^2\left(\frac{\sigma_{21}}{S_L}\right)^4 + p_{nt}^{(-)}\left(\frac{S_T}{\sigma_{22}}\right)\left(\frac{\sigma_{21}}{S_L}\right)^2 + p_{nt}^{(-)}\left(\frac{S_T}{\sigma_{22}}\right) + \frac{1}{4}\left(\frac{\sigma_{22}}{S_T}\right)^2;\ \sigma_{22} < 0, \qquad \text{Mode C} \tag{1.44}$$

Equation (1.44) can be rewritten as

$$FI_M = \frac{1}{2\left(1 + p_{nt}^{(-)}\right)}\left[\left(\frac{\sigma_{22}}{S_T}\right)^2 + \left(\frac{\sigma_{21}}{S_L}\right)^2\right]\left(-\frac{S_T}{\sigma_{22}}\right); \quad \sigma_{22} < 0, \quad \text{Mode C} \tag{1.45}$$

which is the form given by Puck and Schürmann [14] as their Eq. (26) if the degradation term due to the longitudinal normal stress σ_{11} is neglected in their Eq. (26). In Eq. (1.45) set $FI_M = 1$, $\sigma_{21} = 0$, and $\sigma_{22} = -Y_C$ to evaluate the transverse shear strength S_T. The result is

$$S_T = \frac{Y_C}{2\left(1 + p_{nt}^{(-)}\right)} \tag{1.46}$$

Equation (1.46) is listed in Table 1 of Puck and Schürmann [14]. If we set $FI_M = 1$ in Eq. (1.44) or Eq. (1.45), then Eq. (1.43) can be simplified to

$$cos^2\alpha = \frac{S_T}{(-\sigma_{22})} \tag{1.47}$$

Since $\cos^2 \alpha \leq 1$, therefore for Mode C failure $\sigma_{22} \leq -S_T$. Equation (1.47) is Eq. (25) of Puck and Schürmann [14] if we set their weakening factor $f_w = 1$.

For mode B failure in plane stress, set $\alpha = 0$ and $FI_M = 1$ in Eq. (1.41) to get

$$1 = \left(\frac{\sigma_{21}}{S_L}\right)^2 + 2\, p_{n1}^{(-)}\left(\frac{\sigma_{22}}{S_L}\right), \quad \sigma_{22} < 0 \qquad Mode\ \text{B} \tag{1.48}$$

where we have substituted for p/R from Eq. (1.27). To find the transition values of stresses σ_{22} and σ_{21} between modes B and C, solve Eq. (1.48) for σ_{21} and substitute this result for σ_{21} in Eq. (1.44) with $FI_M = 1$. The results are:

$$\sigma_{22} = -S_T \ , \quad \sigma_{21} = S_L\sqrt{1 + 2p_{nt}^{(-)}} \tag{1.49}$$

In Fig. **1.6**, a schematic of the three matrix failure modes, known as A, B and C, is shown.

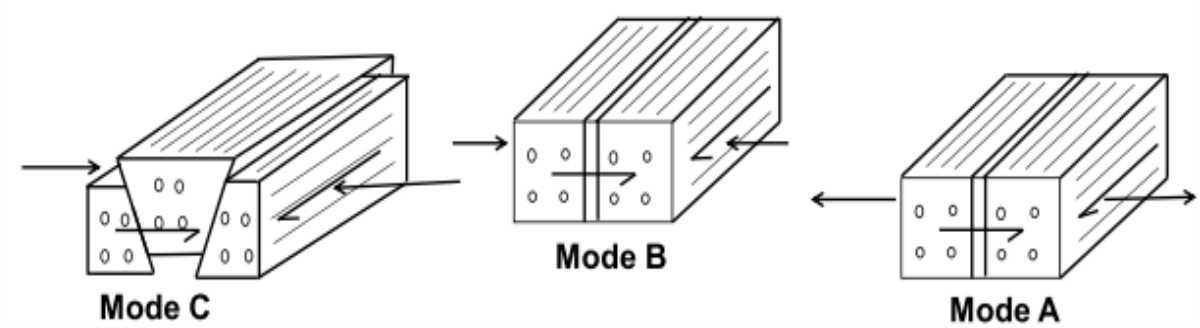

Figure 1.6: Schematics of the matrix failure modes in Puck and Schürmann's failure criteria in plane stress state of deformation

1.6.4 Summary of Matrix Failure Criteria

For plane stress the failure indices are given by

$$FI_M = \sqrt{\left[1 - p_{n1}^{(+)} \frac{Y_T}{S_L}\right]^2 \left(\frac{\sigma_{22}}{Y_T}\right)^2 + \left(\frac{\sigma_{21}}{S_L}\right)^2} + \frac{p_{n1}^{(+)} \sigma_{22}}{S_L} \quad , \qquad \sigma_{22} > 0, \qquad Mode\ \text{A} \tag{1.50}$$

$$FI_M = \left(\frac{\sigma_{21}}{S_L}\right)^2 + 2\, p_{nt}^{(-)} \left(\frac{\sigma_{22}}{S_T}\right) ; \quad -S_T \leq \sigma_{22} < 0;\ S_L < |\sigma_{21}| \leq S_L \sqrt{1 + 2p_{nt}^{(-)}}\,, Mode\ \text{B} \tag{1.51}$$

$$FI_M = \frac{1}{2\left(1 + p_{nt}^{(-)}\right)} \left[\left(\frac{\sigma_{22}}{S_T}\right)^2 + \left(\frac{\sigma_{21}}{S_L}\right)^2\right] \frac{S_T}{(-\sigma_{22})}; \quad -Y_C < \sigma_{22} < -S_T, Mode\ \text{C} \tag{1.52}$$

The location of the fracture plane parallel to fibers is explicitly determined for a plane stress state by Eq. (1.47), and a numerical search for the failure plane in a three dimensional state of stress is needed to solve for the maximum value of the failure index FI_M . The value of the shear strength S_T is explicitly determined from the uniaxial transverse compression test and is given by Eq. (1.46). Puck, Kopp and Knops [22] have proposed that one should take $p_{nt}^{(+)} = p_{nt}^{(-)}$ which makes the slope of the (σ_{nt}, σ_{nn}) failure curve continuous at the points of intersection with the σ_{nt} axis. The following relation between inclination parameters $p_{nt}^{(+)}$ and $p_{n1}^{(-)}$ is obtained by combining Eqs. (1.27) and (1.46):

$$p_{nt}^{(+)} = \frac{1}{2}\left[\sqrt{1 + \frac{2Y_C}{S_L} p_{n1}^{(-)}} - 1\right] \tag{1.53}$$

Recommended ranges of inclination parameters are listed in Table 1.1. The inclination parameters $p_{n1}^{(-)} = 0.25$ and $p_{n1}^{(+)} = 0.30$ with $p_{nt}^{(-)}$ calculated from Eq. (1.27) were used in Ref. [13] for the WWFE [14]. Puck, Kopp and Knops [22] state that measurement of the fracture angle from test coupons is very difficult and that there is considerable scatter in the data.

Table 1.1: Recommended range of values of the inclination parameters from Ref. [22]

Material Type	$p_{nt}^{(-)}$	$p_{nt}^{(+)}$
Glass-fiber/epoxy	0.20 to 0.25	0.20 to 0.25
Carbon-fiber/epoxy	0.25 to 0.30	0.25 to 0.30

1.6.5 Wedge Effect in Mode C

Matrix failure in Mode C may have significant effect on the laminate failure, especially when the value of σ_{22} is very large as compared to that of the shear stress, i.e., $|\sigma_{22}| >> \sigma_{21}$ [13]. The constantly acting large value of compressive σ_{22} and the inclined fracture plane cause an effect known as the wedge effect [13]. When transverse compressive strength Y_C on the failure plane is being overcome by the normal stress one side of the broken layer tends to push its way over the other part gliding on the fracture plane, so it moves upward in the thickness direction as shown in Fig. **1.7**. This may lead to local delaminations and subsequent buckling of neighboring layers upon further increase in the load. This delamination behavior depends on local parameters such as the layer thickness, the fiber direction, the affected layer being inside or on the surface of the laminate, etc. This behavior is later expressed in Chapter 2 as D/L, delamination or local buckling for the PFA of 2D problems.

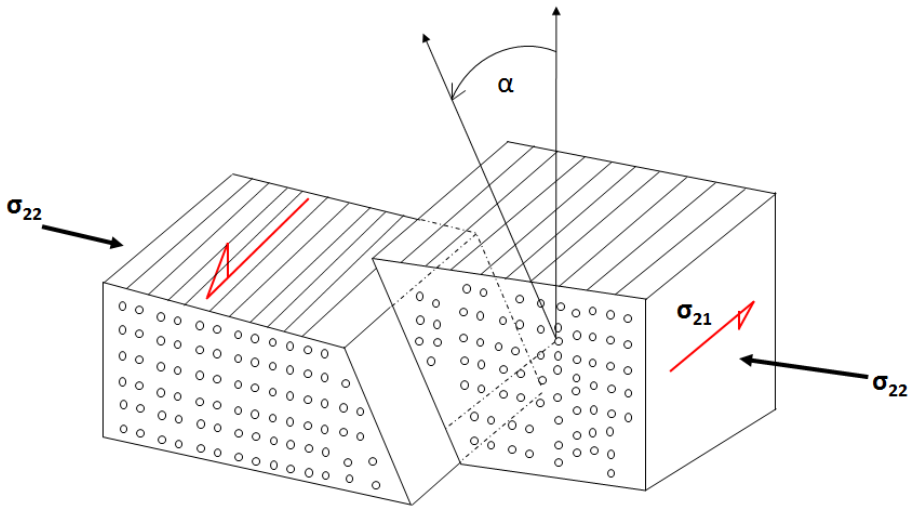

Figure 1.7: The wedge effect showing the fractured pieces gliding one against another in Mode C of matrix failure [13]

1.6.6 Fiber Failure Modes

Puck and Schürmann [14] hypothesize that the tensile failure of the fiber occurs in a general state of stress when the axial stress in the fiber equals its value at failure in a uniaxial tension test, X_T, and the compressive failure of the fiber occurs when the negative value of the axial stress equals the strength in the uniaxial compression test, X_C. The fiber failure indices in tension and compression are non-interactive maximum stress criteria, and are given by:

$$FF_T = \frac{\sigma_{11}}{X_T} \quad , \qquad \sigma_{11} > 0 \tag{1.54}$$

$$FF_C = \frac{(-\sigma_{11})}{X_C} \quad , \qquad \sigma_{11} < 0 \tag{1.55}$$

In Eqs. (1.54) and (1.55), FF_T and FF_C are the indices for the fiber failure modes in tension and compression, respectively, and the failure occurs when any one of them equals 1.

Under three dimensional loading conditions, the fiber failure index in tension ($\sigma_{11} > 0$) is given by

$$FF_T = \frac{1}{X_T}\left[\sigma_{11} - \left(\nu_{12} - \nu_{12f} m_{\sigma f} \frac{E_1}{E_{1f}}\right)(\sigma_{22} + \sigma_{33})\right] \tag{1.56}$$

and in compression ($\sigma_{11} < 0$) is given by

$$FF_C = \frac{1}{|X_C|}\left[\sigma_{11} - \left(\nu_{12} - \nu_{12f} m_{\sigma f} \frac{E_1}{E_{1f}}\right)(\sigma_{22} + \sigma_{33})\right] \tag{1.57}$$

Details of the fiber failure criteria in 3D are given in Chapter 4 of this dissertation.

1.7 Failure Progression through Material Degradation

Puck and Schürmann [14] account for material property degradation for IFF in Modes A, B and C in plane stress deformations by introducing a dimensionless degradation factor η. For no degradation, η = 1, and values of η less than one correspond to degraded material property values. The Mode A degradation factor is denoted by η_a and for both Modes B and C the degradation factor is denoted by $\eta^{(-)}$. The range of values of the matrix degradation factors are:

$$0 < \eta_a \leq 1 \qquad and \quad 0 < \eta^{(-)} \leq 1 \tag{1.58}$$

The onset of matrix cracking in Mode A (transverse tension) occurs when the failure index FI_M = 1 in Eq. (1.50), and at the crack location the moduli drop to zero. However, an increase in stresses σ_{22} and σ_{21}, within the cracked ply away from the crack, results from the action of the interlaminar shear stress from neighboring plies. The non-uniform distribution of stresses σ_{22} and σ_{21} in the cracked ply at the micro-level are represented as spatially uniform average stresses, or effective stresses, at the meso-level. Hence, for meso-level modelling of the cracked ply, the moduli for progressive cracking of the ply gradually decrease, i.e., the cracks are smeared over some length of the ply. This gradual decrease of the moduli in Mode A is represented by reduced moduli $\eta_a E_2$ and $\eta_a G_{12}$ and reduced Poisson's ratio, $\eta_a \nu_{12}$. The value of η_a is computed by enforcing the condition FI_M = 1 in Eq. (1.50) after the onset of the Mode A failure.

Modes B and C are shear failures impeded by a compressive normal stress under which the cracks do not open. In the compression case there is no degradation of the modulus E_2 and Poisson's ratio, ν_{12}, but the modulus G_{12} is degraded by the factor $\eta^{(-)}$. The failure index for Mode B in Eq. (1.51) is kept equal to unity to find the value of $\eta^{(-)}$. For an increasing load, the failure mode can change from B to C, and at the point of transition, the magnitude of the shear stress, σ_{21} is the maximum. For further increase in load, the failure index for Mode C in Eq. (1.52) is kept equal to unity to find the value of $\eta^{(-)}$ until σ_{21} = 0 and σ_{22} = -Y_C.

1.7.1 Matrix Damage Variable Determination in 2D

The damage variables or the material degradation factors are found once the failure has initiated in the matrix. The material degradation factors are found by determining the state of stress as functions of the material degradation factors. The symmetric compliance matrix as a function of the material degradation factors is given by

$$S\left[\eta_a, \eta^{(-)}\right] = \begin{bmatrix} \frac{1}{E_1} & -\frac{\eta_a \nu_{12}}{E_1} & 0 \\ -\frac{\eta_a \nu_{12}}{E_1} & \frac{1}{\eta_a E_2} & 0 \\ 0 & 0 & \frac{1}{\eta_a \eta^{(-)} G_{12}} \end{bmatrix} \tag{1.59}$$

where η_a is the degradation factor in Mode A and $\eta^{(-)}$ in Modes B and C. For an undamaged laminate, η_a = 1 and $\eta^{(-)}$= 1. Once failure has initiated, failure indices are found as functions of the material degradation factor η_a or $\eta^{(-)}$depending on the failure mode. The state of stress with respect to the material principal axes (x_1, x_2) is found using

$$\begin{bmatrix} \sigma_{11}\left(\eta_a, \eta^{(-)}\right) \\ \sigma_{22}\left(\eta_a, \eta^{(-)}\right) \\ \sigma_{21}\left(\eta_a, \eta^{(-)}\right) \end{bmatrix} = T_{\sigma i}\left[S^{-1}\left(\eta_a, \eta^{(-)}\right)\right] T_{\varepsilon i} \begin{bmatrix} \varepsilon_x \\ \varepsilon_y \\ \gamma_{xy} \end{bmatrix} \tag{1.60}$$

where $T_{\sigma i}$, and $T_{\varepsilon i}$ are the transformation matrices. These stresses are substituted in the expression for the appropriate failure mode, FI_M = 1, and the non-linear equations are solved for the degradation factors η_a and $\eta^{(-)}$. Further details regarding the computation of the material degradation factors are given in Chapter 2.

1.8 Modeling Interlaminar Behavior

1.8.1 Virtual Crack Closure Technique

Delamination in composite structures has been analyzed by linear elastic fracture mechanics (LEFM). One method to implement LEFM in finite element analyses is the virtual crack closure technique (VCCT). The VCCT is used for computing strain energy release rates that are compared to critical values of the energy release rates to advance the crack. The

VCCT was introduced by Rybicki and Kanninen [23], and an extensive review of the VCCT is given by Krueger [24]. The VCCT is based on Irwin's concept which states that the energy released by an incremental crack extension equals the work done to close the crack. In this method an initial delamination crack is assumed, the initial position of the delamination front needs to be known a priori, and the delamination growth is assumed to be self-similar. Glaessgen *et al.* [25] found that the correct total strain energy release rates were computed with the VCCT for delamination and debond configurations, but the mode mixity did not converge with the finite element mesh refinement.

1.8.2 Cohesive Zone Models

Cohesive zones are zero-thickness surfaces situated at the interface between the two adjoining lamina and feature combined strength and fracture criteria. The interlaminar tractions are continuous across the interface but displacements corresponding to the tractions are discontinuous. The tractions are related to the displacement jumps across the interface by a cohesive-decohesive law, or the CZM law, in which the traction is zero at no separation, increases to its interfacial strength with increasing separation, and then decreases to zero at complete separation. The area under the traction-separation curve is the fracture toughness. The decohesive portion, or the softening portion, of the CZM law corresponds to the separation of adjacent lamina in the process zone ahead of the crack tip. The process zone corresponds to the micromechanical fracture processes occurring in the volume of the material ahead of the crack tip such as void nucleation, void growth, and coalescence of micro-cavitities. The cohesive-decohesive law expunges the stress singularity of the idealized sharp crack tip in fracture mechanics. In effect, the traction-separation law represents a continuous distribution of disconnected non-linear springs within the surface of initially zero-thickness interface. The minimum number of material parameters in the CZM law are the interfacial strength and the fracture toughness. Various mathematical forms of the cohesive-decohesive law have been proposed; an initially rigid law followed by linear softening [26], a bilinear form [27], and an exponential form [28]. Some other mathematical forms have been reviewed by Chandra *et al.* [29]. As an example, consider a mode-I failure where T denotes the traction normal to the

interface positive in tension, T_C the interlaminar tensile normal strength, Δ the opening displacement jump, and Δ_C denotes the opening displacement jump at $T = T_C$. The bilinear and exponential mode I laws are shown in Fig. **1.8** for a T300/977-2 carbon fiber reinforced epoxy. The particular exponential law used to plot Fig. **1.8(c)** is taken from Goyal *et al*. [28], and is given by

$$\frac{T}{T_C} = \left(\frac{\Delta}{\Delta_c}\right) \exp\left[\frac{1-(\Delta-\Delta_c)^3}{3}\right] \tag{1.61}$$

The CZM laws shown in the figure are plotted such that the mode-I critical strain energy release rate, G_{Ic}, in each plot is equal to 0.352 N/mm, where

$$G_{IC} = \int_0^\infty T d\Delta \tag{1.62}$$

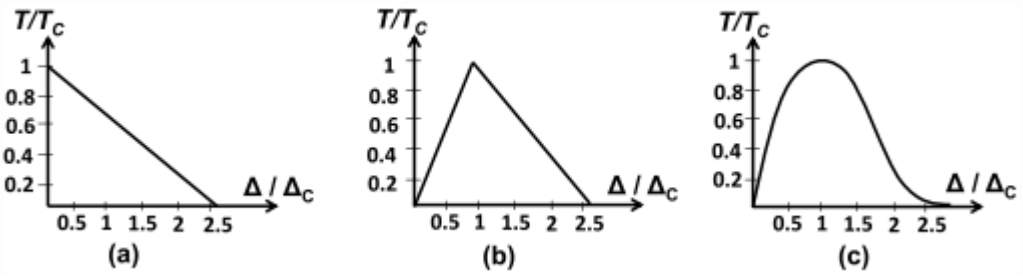

Figure 1.8: Mode-I traction-separation laws for a carbon-epoxy laminate: G_{I_C}= 0.352 N/m, T_C= 60 MPa, Δ_C = 4.48 μm. (a) Initially rigid with linear softening, (b) bilinear, and (c) exponential [28].

The initial cohesive portion can be rigid as depicted in Fig. **1.8 (a)** or linear or nonlinear as shown in parts (b) and (c) (In Fig. **1.8 (a)** Δ_C is actually equal to zero, but the abscissa is normalized using the value of Δ_C determined from Fig. **1.8 (c)**. The mathematical form of the CZM law has been found for some material systems to affect the crack growth behavior. In finite element simulations of dynamic fracture of an isotropic homogeneous solid containing an edge crack, Falk *et al*. [30] observed that the initially elastic CZM law produced spontaneous crack branching at high velocity, but the initially rigid CZM law did not. However, the initially elastic CZM law modifies the linear elastic properties of the body but the initially rigid CZM law does not. The fact that the crack speed is less than the limiting Rayleigh wave speed is attributed to branching instability in the vicinity of the crack tip. Chandra *et al*. [29]

found that the bilinear form of the CZM law correlates well with test data for a thin-slice push-out test of a metal matrix composite while the exponential form failed to do so. Goyal *et al.* [28] found good correlation with test data in modeling standard FRP composite fracture configurations using the exponential form of the CZM law.

References [28], [31], and [32] extend either the exponential or the bilinear CZM laws to include effects such as a mixed mode strength criterion for the onset of delamination, a mixed mode fracture criterion for the progression of delamination, irreversibility on unloading from the softening portion of the law to prevent restoration of the cohesive state, and prevention of interpenetration of the crack faces. Ortiz and Pandolfi [31] have considered the CZM with loading and reloading as well as normal and tangential tractions on the interface.

Implementation of CZM's in finite element simulations is accomplished by developing a zero-thickness interface element. Since the CZM law is nonlinear, an iterative solution procedure is necessary. Also, since interlaminar tractions are required, solid elements are usually required for the laminae encapsulating the interface element. Interface elements have been used to simulate initiation and progression of delamination by Allix and Ladevéze [33], Schellekens and de Borst [34], Cui and Wisnom [35], and Song and Waas [36] among others. Analysis of the interaction of delamination and buckling for a beam is discussed by Allix and Coriglinao [37]. The interaction of delamination and intralaminar material degradation in finite element analyses of post-buckled, AS4-3502 graphite-epoxy panels containing circular cut-outs is presented by Goyal *et al.* [38]. Dávila *et al.* [19] present a method for the construction of interface elements used with shell elements, which improves the efficiency of the finite element analysis relative to using solid elements in the laminae adjacent to the interface. Finite element simulations using interface elements to model delamination are susceptible to mesh sensitivity. Mi *et al.* [27] demonstrated that if a coarse mesh is used ahead of the crack tip, the softening portion of the CZM law causes an oscillatory load-deflection structural response. A coarse mesh cannot represent the large stress gradients that occur ahead of the crack tip. They [27] recommended that the mesh should be fine enough to contain at least two interface elements in the cohesive-decohesive zone ahead of the crack tip.

For numerical integration of continuum elements, the Gauss integration points are

commonly used because of their accuracy. Schellekens and de Borst [39] and Goncalves *et al*. [40] used eigenmode analysis of the element stiffness matrices to demonstrate that the application of the Gauss integration rule in evaluating the tangent stiffness matrix and the internal force vector of the interface elements leads to oscillatory traction profiles when large stress gradients are present over the interface element. The large stress gradients are a result of the initial large stiffness of the CZM law. For linear interface elements, the Newton-Cotes and the Lobatto integration schemes produced smooth profiles. For the full Newton-Raphson nonlinear solution procedure, the consistent tangent stiffness matrix is used in the finite element analysis. However, when softening CZM laws with the consistent tangent stiffness are employed, the tangent stiffness is often ill-conditioned and the norm of the residual force vector diverged [41]. An alternative is to refine the mesh ahead of the crack tip or to decrease the maximum interfacial strength while maintaining the same critical fracture energy [27], [42]. Refining the mesh size increases computational time, and lowering the maximum interfacial strength can result in premature initiation of delamination for small cracks. de Borst and Rots [41] used the secant stiffness rather than the tangent stiffness, but the convergence of the residual force vector is slow and in general a converged solution is not guaranteed. Goyal *et al*. [28] modified the tangent stiffness matrix of the interface element such that negative diagonal elements were replaced by zero to improve the convergence rate.

1.9 Intralaminar Progressive Failure Analysis

Material degradation within the damaged ply is evaluated based on the mode of failure. Empirical approaches to material degradation are given by Chang and Lessard [43], Goyal *et al*. [38], and Puck and Schürmann [14]. The thermodynamics of irreversible processes is used to develop constitutive damage models for intralaminar failure mechanisms by Ladevéze and Le Dantec [44], Maimí *et al*. [45], and Hassan and Batra [46].

1.9.1 Empirical material degradation models

Chang and Lessard [43] developed progressive failure analysis of a symmetrically laminated composite plate containing a centrally located open hole subjected to in-plane compression (Fig. **1.9**). Their analysis assumes plane stress, no out of-plane displacement of the

mid-plane of the plate, and geometric linearity. However, their analysis accounts for nonlinear shear stress/strain behavior in the plane of a ply. At the initiation of either tensile or compressive mode of matrix failure in a ply, the transverse modulus E_{22} and Poisson's ratio ν_{12} are abruptly set to zero.

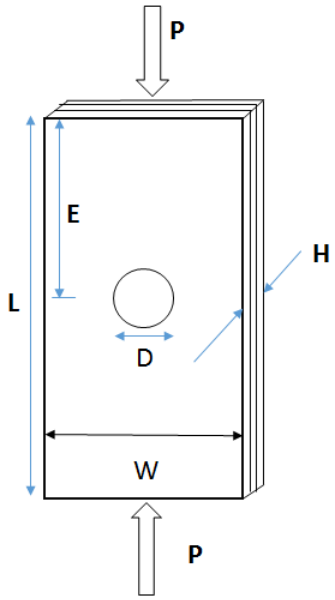

Figure 1.9: The open hole compression specimen studied by Chang and Lessard [43]

The fiber buckling failure mode is assumed to be a catastrophic mode in which the longitudinal modulus E_{11}, the transverse modulus E_{22}, and the shear modulus G_{12} are all abruptly set to zero at the initiation of failure in a ply. A fiber-matrix shearing mode assumes the ply can resist longitudinal and transverse loading, but there is no resistance to in-plane shear loading. The failure index for the fiber-matrix shearing mode is

$$FI_S = \left(\frac{\sigma_{11}}{X_C}\right)^2 + \left(\frac{\sigma_{12}}{S_L}\right)^2; \qquad \sigma_{11} < 0 \tag{1.63}$$

At the initiation of the fiber-matrix shearing mode, the shear modulus G_{12} and Poisson's ratio ν_{12} are abruptly set to zero. Chang and Lessard [43] do not consider the interlaminar failure mode of delamination. Good agreement is cited between the numerical results of the progressive failure analysis and the test data. In Section 1.1.14 of the example problems described in the Abaqus software [47] manual, the progressive failure analysis of Chang and Lessard [43] is implemented with the user defined field (USDFLD) option.

Goyal *et al.* [38] developed a progressive failure analysis of a flat composite panel quasi-statically loaded in shear, and a curved composite panel quasi-statically loaded in compression. Each panel contains a centrally located cutout, and the lamina material properties are for AS4-3502 graphite-epoxy unidirectional tape. The geometrically nonlinear analysis was performed with the Abaqus Software [47] using the shear deformable shell element S4R and the user defined field (USDFLD) option to degrade intralaminar material properties. To model delamination the CZM [28] was implemented as an interface element with the user defined element (UEL) option in Abaqus. Intralaminar failure indices for the matrix, FI_M, and the fiber, FI_F are from Hashin [18], and a fiber-matrix shear failure index, FI_S, given by Eq. (1.13) is extended to include shear stress σ_{13}. Dimensionless damage variables d_F, d_M, and d_S were defined in terms of the failure indices for the fiber, the matrix, and the fiber-matrix shear modes, respectively. Variables d_j, j = F, M, S, are zero for no failure and equal 1.0 at failure. The relationship of the damage variables to the corresponding failure indices is shown in Fig. **1.10**. The damage variables can only increase or remain constant over time; there is no healing. The damage variables at the current time t equal the maximum value throughout the load history, $\tau < t$, for any time τ up to the current time *t*; i.e.,

$$d_j(t) = \max d_j(\tau) \tag{1.64}$$

The lamina material parameters are not abruptly set equal to zero at failure initiation as suggested by the plot in Fig. **1.10**, but are decreased rapidly to a small value. The rules for material property degradation are: the longitudinal modulus E_{11} is decreased by $(1-d_F)$, the transverse modulus E_{22} is decreased by the larger of $(1-d_M)$ or $(1-d_F)$, the Poisson's ratio ν_{12} is decreased by the larger of $(1-d_F)$, $(1-d_M)$, $(1-d_S)$, the longitudinal shear moduli G_{12} and G_{13} are decreased by the larger of $(1-d_S)$ or $(1-d_F)$, and the transverse modulus G_{23} is decreased by $(1-d_F)$. For both the shear and the compression loading, the progressive failure analysis predicted that intralaminar damage induces the initiation of delamination at the free edge of the cut-out in the locations observed in the experimental work.

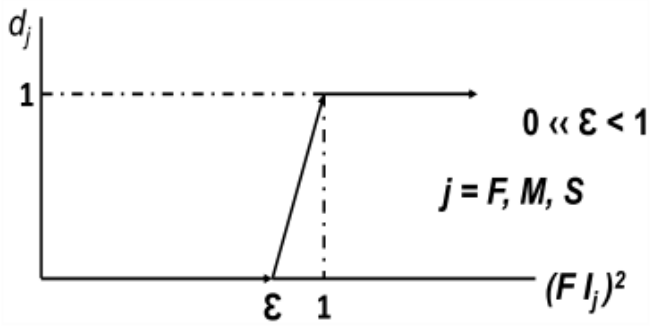

Figure 1.10: Damage variables as a function of the failure indices [39]

1.10 Summary of the Objectives of the Dissertation

The objective of this dissertation is to develop a progressive failure model for laminated composite structures within the finite element framework using the commercial software package, Abaqus [47]. It involves the development of a user defined subroutine to implement Puck and Schürmann's [13, 14] failure criteria which is not a part of the commercial package.

The key aspect of the progressive failure analysis (PFA) is the degradation of the material properties upon the detection of failure. Subsequent to the initiation of matrix failure, elastic moduli are degraded and values of these degradation parameters are found by using a continuum damage mechanics approach. The values of degradation parameters decrease with an increase in the applied load till they reach the limiting value of zero.

1.10.1 Example Problems

The PFA has been performed for several example problems under plane stress conditions. The Abaqus implementation has been verified against either analytical solutions or those obtained using the classical Lamination Plate Theory (CLPT). The computed results have been compared with the available experimental data whenever possible. Two main example problems involving non-homogeneous deformation studied are: (a) composite plate under cylindrical bending, and (b) open hole tension (OHT) specimen.

1.10.2 PFA 3D Framework

The PFA in Abaqus is then modelled for three dimensional problems. A layer-wise technique has been used to model 3D composites in Abaqus. Regarding failure initiation in the matrix a 3D material degradation scheme is developed and implemented.

1.10.3 Organization of the Remaining Portion of the Dissertation

Chapter 2 presents PFA of laminates undergoing homogenous deformation.

Chapter 3 presents PFA of an open hole tension (OHT) laminate.

Chapter 4 presents PFA for three dimensional deformations.

Chapter 5 provides overall conclusions of this dissertation.

Chapter 2

Progressive Failure Analysis in 2D

In this Chapter, we present results for the progressive failure analyses (PFA) of laminates under simple loadings so that deformations can be analyzed either analytically or by using the classical lamination plate theory (CLPT) [48]. A comparison of results from the analytical solution with those from Abaqus will verify the USDFLD that incorporates the Puck and Schürmann failure criteria and the corresponding degradation of material elasticities; the USDFLD has been implemented in Abaqus/Standard. The source code and details of implementation of the USDFLD are given in Appendix A. After failure has initiated at a point, values there of degradation variables, η_a and $\eta^{(-)}$, for a particular applied displacement are numerically calculated in the USDFLD, and supplied to the main program for degrading the material moduli. The boundary-value problem is solved again without incrementing the applied displacement till equilibrium, within a prescribed tolerance, has been established with the degraded values of elastic moduli. Subsequently, the applied displacement is incremented and the iterative process repeated for the new load.

We first analyze deformations of a 30^o off-axis specimen with only one axial strain having non-zero values. Subsequently, we study simple tensile/compressive deformations of $\mathbf{[\pm\theta]_S}$ laminate with only non-zero axial stress to delineate the effect of the angle $\boldsymbol{\theta}$ on the matrix failure mode, and finally study cylindrical bending of a laminate. The first problem studied is an academic exercise and the loading needed may be difficult to realize experimentally. The second problem corresponds to the simple tension/compression test often used to characterize a laminate. For each one of these three problems, the specimen is loaded by applying displacements rather than tractions to simulate deformations after the load has reached its peak value. For the first two problems, the computed solutions are compared with their analytical solutions. For the cylindrical bending problem, the computed solution has been compared with that obtained by using the CLPT. The software based on the CLPT was developed using MATLAB [49].

2.1 PFA of 30º off-axis specimen under uniaxial strain

The 30º off-axis lamina made of E-glass 21xK43 Gevetex fibers and the LY/556/DY063 epoxy matrix is deformed to have only non-zero axial strain in the x-direction, e.g., see Fig. **2.1**. Because of homogeneous deformations, stresses and strains are constant within the lamina and equilibrium equations are identically satisfied with zero body forces. Thus constitutive relations provide surface tractions to be applied to the boundaries of the specimen to produce in it the uniaxial strain.

Values of material parameters in the material principal coordinates, taken from Ref. [5], are: E_1 = 53.48 GPa, E_2 = 17.7 GPa, G_{12} = 5.8 GPa, ν_{12} = 0.278, X_T = 1140 MPa, Y_T =35 MPa, X_C = 570 MPa, Y_C = 114 MPa, S_L = 72 MPa and S_T = 45.6 MPa. For glass epoxy, we set $p_{n1}^{(+)}$ = 0.25 and $p_{n1}^{(-)}$ = 0.25 as suggested by Puck and Schürmann [13, 14].

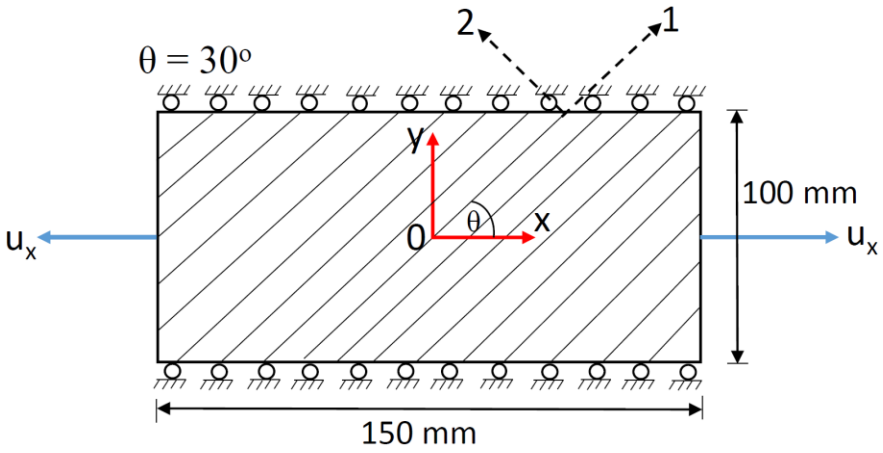

Figure 2.1: 30º off-axis specimen under uniaxial strain state

We assume that the specimen thickness is very small as compared to its in-plane dimensions, and a plane state of stress exists in the specimen. Thus the matrix failure planes are parallel to the fibers. The compliance matrix of the damaged ply with respect to the material principal axes is given by

$$\boldsymbol{S} = \begin{bmatrix} \frac{1}{E_1} & -\frac{\eta_a \nu_{12}}{E_1} & 0 \\ -\frac{\eta_a \nu_{12}}{E_1} & \frac{1}{\eta_a E_2} & 0 \\ 0 & 0 & \frac{1}{\eta_a \eta^{(-)} G_{12}} \end{bmatrix} \tag{2.1}$$

Prior to the initiation of failure, values of η_a and $\eta^{(-)}$equal 1.0. The matrix, $\bar{Q}$, of elastic constants in the global coordinate system is found from [48]:

$$\bar{Q} = T_{\sigma i} S^{-1} T_{\epsilon i} \tag{2.2}$$

where $\mathbf{T_{\sigma i}}$ and $\mathbf{T_{\varepsilon i}}$ are matrices that transform stresses and strains from the material principal axes to the global coordinate axes. For the ply with fibers oriented at 30^o to the global x-axis, equations (2.1) and (2.2) give

$$\bar{Q}_{11} = \frac{3\eta_a \eta^{(-)} G_{12}}{4} + \frac{E_1[9E_1 + E_2\eta_a(1 + 6\eta_a\nu_{12})]}{16[E_1 - E_2\eta_a^3\nu_{12}^2]} \tag{2.3}$$

$$\bar{Q}_{12} = \frac{3\eta_a \eta^{(-)} G_{12}}{4} + \frac{E_1[3E_1 + E_2\eta_a(3 + 10\eta_a\nu_{12})]}{16[E_1 - E_2\eta_a^3\nu_{12}^2]} \tag{2.4}$$

$$\bar{Q}_{16} = \frac{\sqrt{3}\left[3E_1^2 + 4E_2\eta_a^4\eta^{(-)}G_{12}\nu_{12}^2 - E_1\eta_a\left(E_2 + 4\eta^{(-)}G_{12} + 2E_2\eta_a\nu_{12}\right)\right]}{16[E_1 - E_2\eta_a^3\nu_{12}^2]} \tag{2.5}$$

$$\bar{Q}_{21} = \bar{Q}_{12} \tag{2.6}$$

$$\bar{Q}_{22} = \frac{3\eta_a \eta^{(-)} G_{12}}{4} + \frac{E_1[E_1 + 3E_2\eta_a(3 + 2\eta_a\nu_{12})]}{16[E_1 - E_2\eta_a^3\nu_{12}^2]} \tag{2.7}$$

$$\bar{Q}_{26} = \frac{\sqrt{3}\left[E_1^2 - 4E_2\eta_a^4\eta^{(-)}G_{12}\nu_{12}^2 + E_1\eta_a\left(4\eta^{(-)}G_{12} + E_2(-3 + 2\eta_a\nu_{12})\right)\right]}{4} \tag{2.8}$$

$$\bar{Q}_{61} = \bar{Q}_{16} \tag{2.9}$$

$$\bar{Q}_{62} = \bar{Q}_{26} \tag{2.10}$$

$$\bar{Q}_{66} = \frac{3\eta_a \eta^{(-)} G_{12}}{4} + \frac{3E_1[E_1 + E_2\eta_a(1 - 2\eta_a \nu_{12})]}{16[E_1 - E_2\eta_a^3 \nu_{12}^2]} \tag{2.11}$$

where elements of $\bar{Q}$ in the 3rd row and the 3rd column are denoted by subscript 6 rather than 3 to stay consistent with notations used for 3-dimensional problems. Using numerical values of material parameters listed above, stress components in terms of the only non-zero strain component, ε_x, are:

$$\sigma_x = \frac{\left[M_1 + \eta_a\left(M_2 + M_3\eta_a + M_4\eta^{(-)} - M_5\eta_a^3\eta^{(-)}\right)\right]\varepsilon_x}{M_6 - M_7\eta_a^3} \tag{2.12}$$

$$\sigma_y = \frac{\left[M_8 + \eta_a\left(M_9 + M_{10}\eta_a - M_{11}\eta^{(-)} + M_5\eta_a^3\eta^{(-)}\right)\right]\varepsilon_x}{M_6 - M_7\eta_a^3} \tag{2.13}$$

$$\sigma_{xy} = \frac{\left[M_{12} + \eta_a\left(M_{13} - M_{14}\eta_a - M_{15}\eta^{(-)} + M_{16}\eta_a^3\eta^{(-)}\right)\right]\varepsilon_x}{M_6 - M_7\eta_a^3} \tag{2.14}$$

where

$$\begin{gathered} M_1 = 5.47925\ x\ 10^{-21}, M_2 = 2.01493\ x\ 10^{-22}, M_3 = 3.366091\ x\ 10^{-22} \\ M_4 = 7.92313\ x\ 10^{-22}, M_5 = 7.93313x\ 10^{-23}, M_6 = 1.8214\ x\ 10^{-31} \\ M_7 = 4.6588\ x\ 10^{-33}, M_8 = 1.82642x\ 10^{-21}, M_9 = 6.044\ x\ 10^{-22} \\ M_{10} = 5.60151\ x\ 10^{-21}, M_{11} = 1.82642x\ 10^{-21}, M_{12} = 3.16345\ x\ 10^{-22} \\ M_{13} = -3.48997\ x\ 10^{-22}, M_{14} = 1.9402\ x\ 10^{-21}, M_{15} = 4.57442\ x\ 10^{-22} \\ M_{16} = 1.17006\ x\ 10^{-23} \end{gathered} \tag{2.15}$$

Since M_7 is two orders of magnitude smaller than M_6, the denominator in equations (2.12) – (2.14) can be approximated by M_6. For uniaxial tensile strain, $\sigma_x > 0$, a hand calculation gives $\sigma_{22} > 0$; thus the matrix in the ply will fail in mode A and $\eta^{(-)} = 1$. The matrix failure initiates at $\varepsilon_x = 0.004$. For an applied displacement $u_x > 0.004\ L_x$, where L_x is the specimen length in the x-direction, E_2, ν_{12} and G_{12} are reduced by η_a, as indicated in Eq. (2.1). The value of η_a is found by iteratively solving the failure surface equation,

$$g(\eta_a) = \frac{1}{4}\left[\frac{E_1 E_2 \eta_a \varepsilon_x (1 + 3\eta_a \nu_{12}) p_{n1}^{(+)}}{(E_1 - E_2 \eta_a^3 \nu_{12}^2) S_L} + \sqrt{R_1 + R_2 + R_3}\right] = 1 \tag{2.16}$$

where

$$R_1 = \frac{\eta_a^2 \varepsilon_x^2 (-24 E_1 E_2 \eta_a^3 G_{12}^2 \nu_{12}^2)}{(E_1 - E_2 \eta_a^3 \nu_{12}^2)^2 S_L^2} \tag{2.17}$$

$$R_2 = \frac{\eta_a^2 \varepsilon_x^2 (12 E_2^2\, \eta_a^6 G_{12}^2 \nu_{12}^2)}{(E_1 - E_2 \eta_a^3 \nu_{12}^2)^2 S_L^2} \tag{2.18}$$

$$R_3 = \frac{\eta_a^2 \varepsilon_x^2 \left[E_1^2 (12\, G_{12}^2 Y_T^2) + E_2^2 (1 + 3\eta_a \nu_{12})^2 \left(S_L - p_{n1}^{(+)} Y_T\right)^2\right]}{(E_1 - E_2 \eta_a^3 \nu_{12}^2)^2 S_L^2 Y_T^2} \tag{2.19}$$

Using numerical values of material parameters Eq. (2.16) becomes

$$g(\eta_a) = \varepsilon_x \left[\frac{(N_1 + N_2 + N_3) + \sqrt{W}}{N_4}\right] = 1 \tag{2.20}$$

where

$$W = N_5 - N_6 + N_7 + N_8 + N_9 - N_{10} + N_{11} \tag{2.21}$$

and

$$\begin{gathered} N_1 = 1.4013\, x\, 10^{-45}\,, N_2 = 2.79852\, x\, 10^{-30}\eta_a, N_3 = 2.33396\, x\, 10^{-30}\eta_a^2 \\ N_4 = 1.821\, x\, 10^{-31} - 4.6555\, x\, 10^{-33}\eta_a^3\,, \qquad N_5 = 1.53532\, x\, 10^{-89} \\ N_6 = 9.95779\, x\, 10^{-74}\eta_a,\ N_7 = 5.70685\, x\, 10^{-58}\eta_a^2 \\ N_8 = 6.82586\, x\, 10^{-58}\, \eta_a^3, \qquad N_9 = 2.84638\, x\, 10^{-58}\, \eta_a^4, \\ N_{10} = 8.25978\, x\, 10^{-60}\, \eta_a^5,\ \ N_{11} = 1.065635\, x\, 10^{-61}\, \eta_a^8 \end{gathered} \tag{2.22}$$

Recalling that $0 < \eta_a \leq 1$, W ≈ 0. When the matrix just fails at a point, Eqns. (2.20) and (2.12) can be approximated, respectively, by $\varepsilon_x(2.8\,\eta_a + 2.3\,\eta_a^2)/(0.182) = 1$ and $\sigma_x = \frac{[M_1 + \eta_a(M_2 + M_3\eta_a + M_4)]\varepsilon_x}{M_6}$. Values of η_a and σ_x for different values of ε_x found from Eqns. (2.20) and (2.12) are listed in Table 1. These values imply that the slope of the axial stress vs.

Table 2.1: Numerical solution of Eq. (2.20) and corresponding values of σ_x from Eq. (2.12)

ε_x	η_a	σ_x , MPa
0	1	0
0.004	1	153.27
0.0045	0.923515	168.25
0.005	0.85802	183.369
0.006	0.75267	213.629
0.007	0.67142	243.893
0.008	0.607018	274.152
0.009	0.554211	304.401
0.01	0.51018	334.64
0.015	0.366775	485.686
0.02	0.28726	636.542
0.025	0.236413	787.279
0.03	0.201001	937.938

the axial strain curve changes from 38.3 GPa to ~ 30 GPa when damage initiates and subsequently remains constant. In Figs. **2.2** and **2.3 r**esults obtained by using the analytical solution are superimposed upon those computed using Abaqus. It is clear that the two sets of results coincide with each other. Because of homogeneous deformations, the numerical solution of the problem is found by using only one finite element. The matrix failure initiates at axial strain $\varepsilon_x = 0.004$ corresponding to point *P* in Fig. **2.2**. For a prescribed value of $\varepsilon_x > 0.004$ (or $u_x > 0.004\ L_x$) the non-linear Eq. (2.20) is iteratively solved for η_a within a tolerance of 10^{-6}. When using Abaqus, the equilibrium problem is reanalyzed with this newly computed value of η_a till convergence. Subsequently, the applied u_x is incremented and the process continued till the ply has completely failed due to fibers failing in tension at $\varepsilon_x = 0.028$.

We note that Young's modulus of fibers is much higher than that of the matrix. Thus degrading E_2 decreases the slope of the axial stress vs. the axial strain curve only by 29%. Of course, this slope does not equal the modulus of the laminate since uniaxial strain and not uniaxial

stress deformations are being studied. Because of infinitesimal deformations considered fiber rotations, if any, during deformations of the lamina are ignored. The final value 0.2 of η_a implies that the effective Poisson's ratio $\eta_a \nu_{12}$ in Eq. (2.1) has been reduced to zero. Thus the axial stress in the fiber equals E_1 multiplied by the axial strain, 0.75 ε_x in the fiber, or 1123 MPa which is close to the ultimate strength, X_T, of 1140 MPa thereby verifying the value computed using Abaqus.

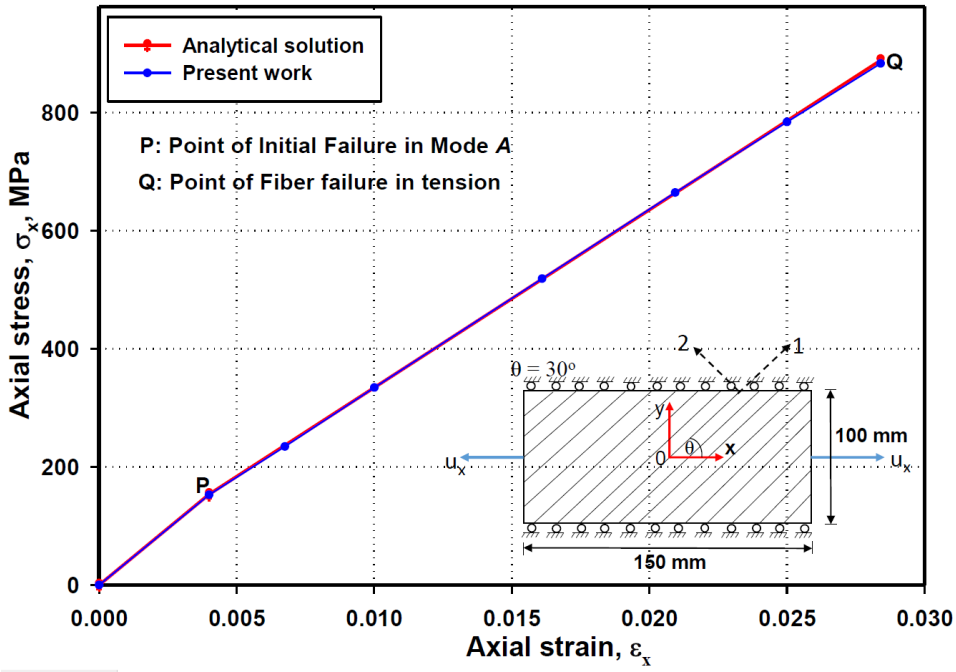

Figure 2.2: Variation of the axial stress with the axial strain for the 30º off-axis lamina with only non-zero axial strain.

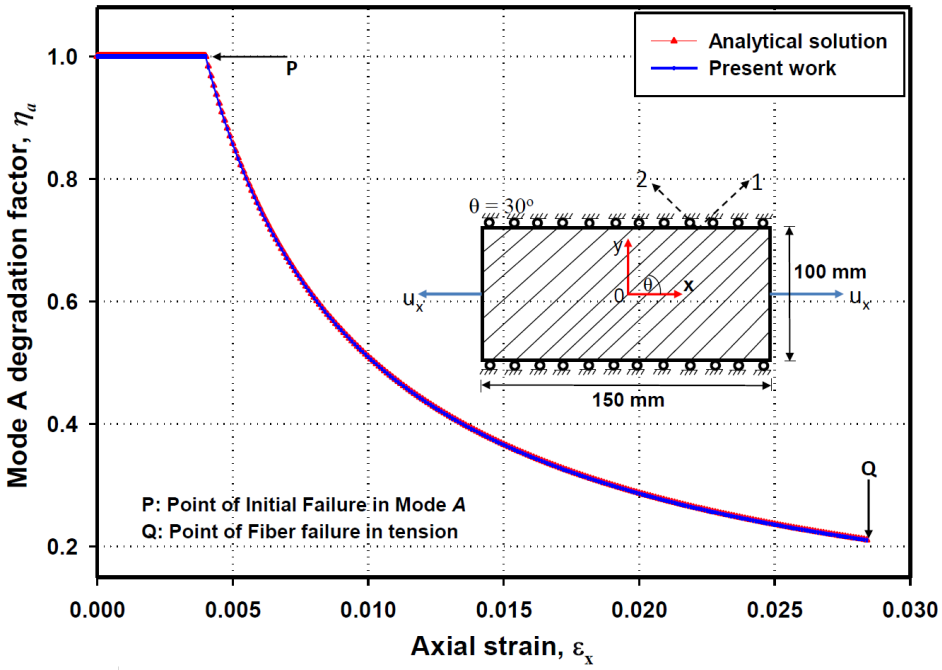

Figure 2.3: Variation of Mode A degradation factor for the 30º off -axis lamina deformed with only non-zero axial strain.

Results plotted in Fig **2.3** imply that the value of the material degradation factor, η_a, drops sharply with increasing values of ε_x but this effect is rather benign in the global stress-strain behavior. We note that in Eq. (2.12) η_a is a function of ε_x. Since matrix elasticities have very little effect on the overall elastic moduli of the laminate and deformations are constrained in the lateral direction, it is not surprising that the slope of the axial stress vs. the axial strain curve does not change much due to the degradation of matrix properties.

2.2 PFA of $[\pm\theta]_S$ laminate under uniaxial tensile/compressive loads

We now analyze matrix failure in uniaxial tensile/compressive deformations of a 4-ply $[\pm\theta]_S$ graphite/epoxy AS4/3501-6 laminate for different values of θ to understand transitions among different matrix failure modes. The material properties with respect to the material principal directions for the laminate are: E_1 = 126 GPa, E_2 = 11 GPa, G_{12} = 6.6 GPa, ν_{12} = 0.28, X_T = 1950 MPa, Y_T = 48 MPa, X_C = 1480 MPa, Y_C = 200 MPa, S_L = 79 MPa, S_T =78.30 MPa, $p_{n1}^{(+)}$ = 0.3, $p_{n1}^{(-)}$ = 0.25, and $p_{nt}^{(-)}$=0.28. The laminate is deformed homogeneously by applying x-

displacements to the smooth opposite edges while keeping the other two edges traction free. Thus with respect to the global coordinate axes, the only non-zero component of stresses is σ_x.

For plane stress deformations, the strain-stress relation for a laminate is [48]:

$$\begin{Bmatrix} \varepsilon_x \\ \varepsilon_y \\ \gamma_{xy} \end{Bmatrix} = \begin{bmatrix} \bar{S}_{11} & \bar{S}_{12} & \bar{S}_{16} \\ \bar{S}_{12} & \bar{S}_{22} & \bar{S}_{26} \\ \bar{S}_{16} & \bar{S}_{26} & \bar{S}_{66} \end{bmatrix} \begin{Bmatrix} \sigma_x \\ \sigma_y \\ \sigma_{xy} \end{Bmatrix} \tag{2.23}$$

where the reduced compliances, $\bar{S}_{ij}$, are given by:

$$\bar{S}_{11} = S_{11}\, m^4 + (2S_{12} + S_{66})n^2m^2 + S_{22}\, n^4 \tag{2.24}$$

$$\bar{S}_{12} = (S_{11} + S_{22} - S_{66})\, n^2m^2 + S_{12}(m^4 + n^4) \tag{2.25}$$

$$\bar{S}_{16} = (2S_{11} - 2S_{12} - S_{66})nm^3 - (2S_{22} - 2S_{12} - S_{66})n^3m \tag{2.26}$$

$$\bar{S}_{22} = S_{11}\, n^4 + (2S_{12} + S_{66})n^2m^2 + S_{22}\, m^4 \tag{2.27}$$

$$\bar{S}_{26} = (2S_{11} - 2S_{12} - S_{66})n^3m - (2S_{22} - 2S_{12} - S_{66})nm^3 \tag{2.28}$$

$$\bar{S}_{66} = 2\,(2S_{11} + 2S_{22} - 4S_{12} - S_{66})n^2m^2 + S_{66}(m^4 + n^4) \tag{2.29}$$

m = Cos (θ), n = Sin (θ), θ being the ply angle, and

$$S_{11} = \frac{1}{E_1}\,, \qquad S_{12} = -\frac{\nu_{12}}{E_1}, \qquad S_{22} = \frac{1}{E_2}\,, \quad S_{66} = \frac{1}{G_{12}} \tag{2.30}$$

Substituting $\sigma_y = 0$ in Eq. (2.23) and solving for ε_y, we get

$$\varepsilon_y = \varepsilon_x\, \frac{\bar{S}_{12}\bar{S}_{66} - \bar{S}_{26}\bar{S}_{16}}{\bar{S}_{11}\bar{S}_{66}\bar{S}_{16}^2} \tag{2.31}$$

Using values of material parameters listed above gives

$$\varepsilon_y = \varepsilon_x \left[\frac{G_1 + G_2\, Cos(4\theta) + G_3\, Cos(8\theta)}{G_4 + G_5\, Cos(2\theta) + G_2\, Cos(4\theta) + G_6\, Cos(6\theta) + G_7\, Cos(8\theta)} \right] \tag{2.32}$$

where

$$\begin{aligned} G_1 &= -\,1.76448\; x\; 10^{-21} & G_2 &= \;1.43019\; x\; 10^{-21} & G_3 &= \;1.17549\; x\; 10^{-38} \\ G_4 &= \;6.05812\; x\; 10^{-21} & G_5 &= -6.2858\; x\; 10^{-21} & G_6 &= -1.88079\; x\; 10^{-37} \\ & & G_7 &= -1.17549\; x\; 10^{-38} & & \end{aligned} \tag{2.33}$$

Considering the magnitudes of G_1 through G_7, terms multiplying G_3, G_6 and G_7 in Eq. (2.32) can be neglected.

The strain components with respect to the material principal directions computed from

$$\begin{Bmatrix}\varepsilon_{11}\\ \varepsilon_{22}\\ \gamma_{12}\end{Bmatrix} = T_{\varepsilon}\begin{Bmatrix}\varepsilon_{x}\\ \varepsilon_{y}\\ \gamma_{xy}\end{Bmatrix} \tag{2.34}$$

are given by

$$\varepsilon_{11} = \varepsilon_x\left[\frac{X_1 + X_2Cos(2\theta) + X_3Cos(4\theta) + X_4Cos(6\theta) + X_4Cos(8\theta) + X_5Cos(10\theta)}{G_4 + G_5\,Cos(2\theta) + G_2\,Cos(4\theta) + G_6\,Cos(6\theta) + G_7\,Cos(8\theta)}\right] \tag{2.35}$$

$$\varepsilon_{22} = \varepsilon_x\left[\frac{X_6 + X_7\,Cos(2\theta) + X_8\,Cos(4\theta) + X_9\,Cos(6\theta) + X_{10}Cos(8\theta) + X_{11}Cos(10\theta)}{G_4 + G_5\,Cos(2\theta) + G_2\,Cos(4\theta) + G_6\,Cos(6\theta) + G_7\,Cos(8\theta)}\right]$$

$$\gamma_{12} = \varepsilon_x\,Cos(\theta)\,Sin(\theta)\left[\frac{X_{12} + X_{13}\,Cos(2\theta) - X_{14}\,Cos(4\theta) + X_{14}\,Cos(6\theta) + X_{15}\,Cos(8\theta)}{G_4 + G_5\,Cos(2\theta) + G_2\,Cos(4\theta) + G_6\,Cos(6\theta) + G_7\,Cos(8\theta)}\right]$$

where

$$\begin{aligned}
&X_1 = 5.75368\,x\,10^{-22} && X_2 = 7.68398\,x\,10^{-22}, && X_3 = -1.41264\,x\,10^{-22}\\
&X_4 = -4.70198\,x\,10^{-38} && X_5 = -5.87747x\,10^{-39} && X_6 = 3.71827\,x\,10^{-21}\\
&X_7 = -7.0542\,x\,10^{-21} && X_8 = 3.00164\,x\,10^{-21} && X_9 = -1.41059\,x\,10^{-37}\\
&X_{10} = 4.70198\,x\,10^{-38} && X_{11} = 5.87747\,x\,10^{-39} && X_{12} = -1.56452\,x\,10^{-20}\\
&X_{13} = 1.25716\,x\,10^{-20} && X_{14} = 3.76158\,x\,10^{-37} && X_{15} = 4.70198\,x\,10^{-38}
\end{aligned} \tag{2.36}$$

We now find stresses with respect to the material principal directions from

$$\begin{Bmatrix}\sigma_{11}\\ \sigma_{22}\\ \sigma_{21}\end{Bmatrix} = \begin{bmatrix}Q_{11} & Q_{12} & 0\\ Q_{12} & Q_{22} & 0\\ 0 & 0 & Q_{66}\end{bmatrix}\begin{Bmatrix}\varepsilon_{11}\\ \varepsilon_{22}\\ \gamma_{12}\end{Bmatrix} \tag{2.37}$$

where

$$Q_{11} = \frac{S_{22}}{S_{11}S_{22} - S_{12}^2}\,,\; Q_{12} = \frac{S_{12}}{S_{11}S_{22} - S_{12}^2}\,,\; Q_{22} = \frac{S_{11}}{S_{11}S_{22} - S_{12}^2}\,,\; Q_{66} = \frac{1}{S_{66}} \tag{2.38}$$

with the following result:

$$\sigma_{11} = \varepsilon_x\left[\frac{X_{16} + X_{17}\,Cos(2\theta) + X_{18}\,Cos(4\theta) + X_{19}\,Cos(6\theta) + X_{20}Cos(8\theta) + X_{21}Cos(10\theta)}{G_4 + G_5\,Cos(2\theta) + G_2\,Cos(4\theta) + G_6\,Cos(6\theta) + G_7\,Cos(8\theta)}\right]$$

$$\sigma_{22} = \varepsilon_x\left[\frac{X_{22} + X_{23}\,Cos(2\theta) + X_{24}\,Cos(4\theta) + X_{25}\,Cos(6\theta) + X_{26}Cos(8\theta) + X_{27}Cos(10\theta)}{G_4 + G_5\,Cos(2\theta) + G_2\,Cos(4\theta) + G_6\,Cos(6\theta) + G_7\,Cos(8\theta)}\right] \tag{2.39}$$

$$\sigma_{21} = \varepsilon_x\,Cos(\theta)\,Sin(\theta)\left[\frac{X_{28} + X_{29}\,Cos(2\theta) - X_{30}\,Cos(4\theta) + X_{30}\,Cos(6\theta) + X_{15}\,Cos(8\theta)}{G_4 + G_5\,Cos(2\theta) + G_2\,Cos(4\theta) + G_6\,Cos(6\theta) + G_7\,Cos(8\theta)}\right]$$

Here

$$X_{16} = 8.44365\ x\ 10^{-11} \quad X_{17} = 7.57576\ x\ 10^{-11} \quad X_{18} = -8.67893\ x\ 10^{-12}$$
$$X_{19} = -6.39903\ x\ 10^{-27} \quad X_{20} = -5.81997\ x\ 10^{-27} \quad X_{21} = -7.27497\ x\ 10^{-28}$$
$$X_{22} = 4.29502\ x\ 10^{-11} \quad X_{23} = -7.57576\ x\ 10^{-11} \quad X_{24} = 3.28074\ x\ 10^{-11} \qquad (2.40)$$
$$X_{25} = -1.70696\ x\ 10^{-27} \quad X_{26} = 3.75968\ x\ 10^{-28} \quad X_{27} = 4.6996\ x\ 10^{-29}$$
$$X_{28} = -1.03258\ x\ 10^{-10} \quad X_{29} = 8.29726\ x\ 10^{-11} \quad X_{30} = 2.48264\ x\ 10^{-27}$$
$$X_{31} = 3.10331\ x\ 10^{-28}$$

We substitute for stress components σ_{22} and σ_{21} into Eqns. (1.50) - (1.52) and set failure mode index equal to 1.0. We thus get a relation between the axial strain ε_x and the fiber orientation angle θ for the matrix to fail in one of the failure modes.

$$FIM_A = f(\varepsilon_x, \theta) = 1 \qquad (2.41)$$

$$FIM_B = f(\varepsilon_x, \theta) = 1 \qquad (2.42)$$

$$FIM_C = f(\varepsilon_x, \theta) = 1 \qquad (2.43)$$

In Figure **2.4** we have plotted solutions of Eqns. (2.41) – (2.43) without considering side conditions required for the relevant mode to prevail and θ varying from 0° to 90°. In Figure **2.5** we have considered the constraint on σ_{22}, described in Eqns. (1.50) – (1.52), and plotted the axial strain vs. the ply angle θ for the three failure modes in the matrix. In Figs. **2.4** and **2.5** the green curve describing mode A corresponds to values of θ for which $\sigma_{2\,2} > 0$, the red curve describing mode B corresponds to the values of θ for which $-S_T \leq \sigma_{22} < 0$, and the purple curve describing mode C corresponds to the values of θ for which $-Y_C < \sigma_{22} < -S_T$. Thus in uniaxial compression of a lamina with fibers oriented at counterclockwise angle θ with the x-axis, the matrix fails in mode A for θ between 5° and 42°, in mode B for θ between 42° and 57° and in mode C for θ between 57° and 90°. We note that fiber failure modes have not been considered for results exhibited in Figs. 2.4 and 2.5. We therefore get unrealistically large values of the failure strain for θ close to 0° and 90°. For θ close to 0° fibers support most of the axial load, and for θ close to 90° the matrix is essentially loaded in axial compression.

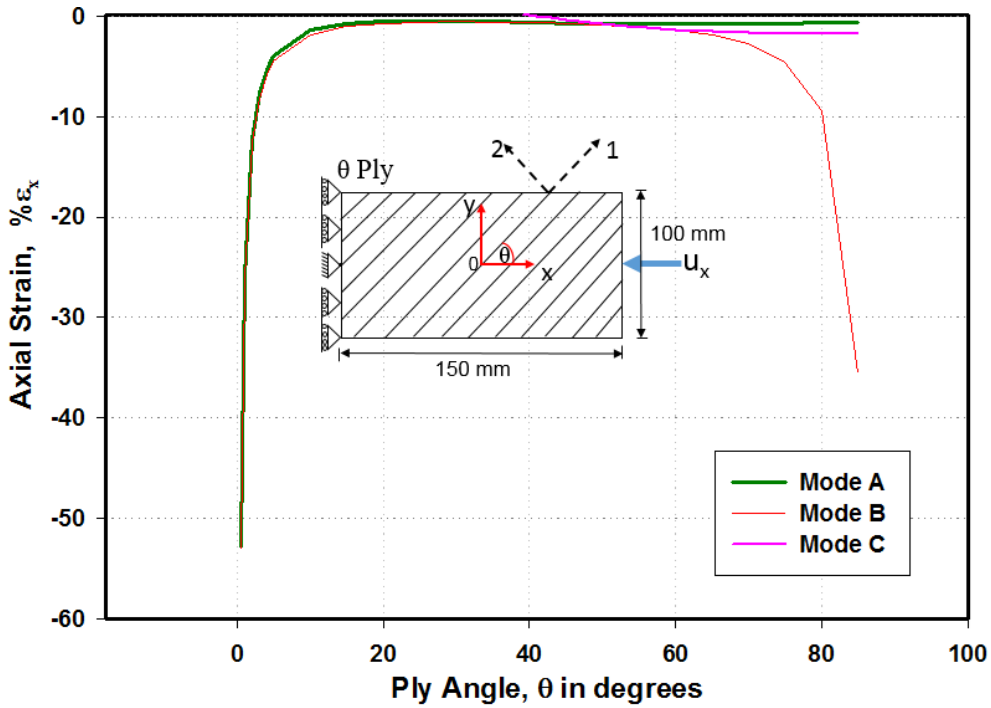

Figure 2.4: Solutions of Equations (2.41) – (2.43) without considering constraints on stresses for the failure mode.

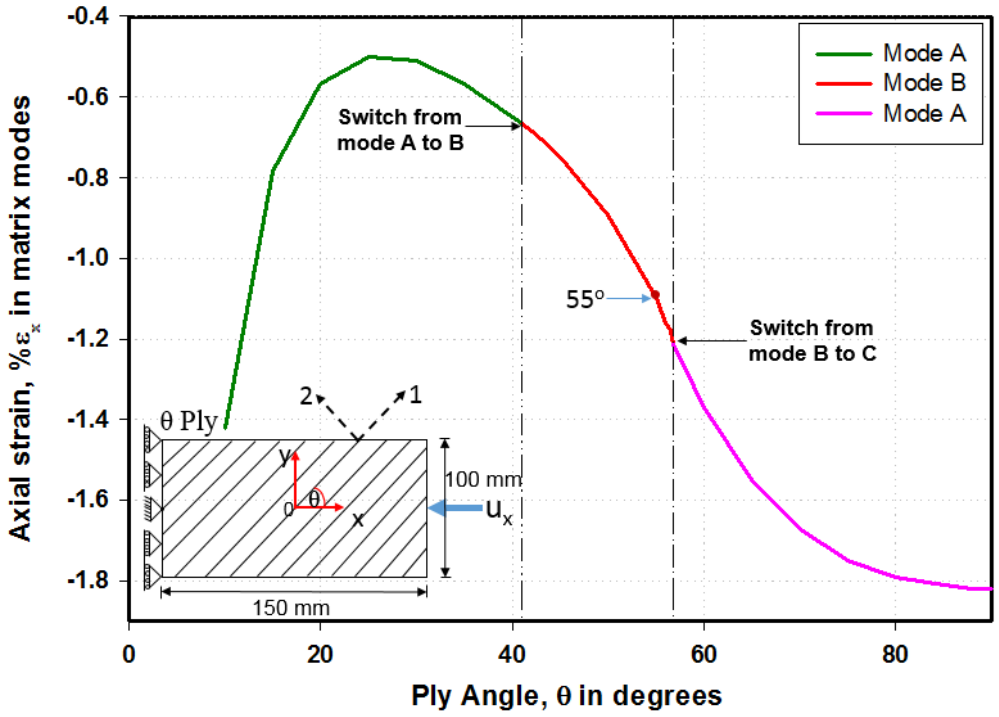

Figure 2.5: Failure strain for matrix modes A, B and C varying with ply angle, θ.

2.2.1 Failure mode switching during monotonic loading

Results presented and discussed above are valid till the initiation of the matrix failure in one of three modes. We now analyze deformations during the post-failure initiation phase, and consider the $[\pm 55^o]_S$ laminate as an example. For $\theta = 55^o$ the relationship between ε_y , ε_x and the degradation parameter $\eta^{(-)}$ is

$$\varepsilon_y = \frac{\varepsilon_x \left[1.88079\, x\, 10^{-37} + \eta^{(-)} \left(-3.49287\, x\, 10^{-21} + 6.32083\, x\, 10^{-22} \eta^{(-)}\right)\right]}{-1.88079\, x\, 10^{-37} + \eta^{(-)} \left(6.4796\, x\, 10^{-21} + 6.32083\, x\, 10^{-22} \eta^{(-)}\right)} \tag{2.44}$$

Expressions for the failure mode indices are:

$$FIM_B = \frac{W_1 \varepsilon_x^2 (\eta^{(-)})^2 [W_2 + (W_3 + W_4\, \eta^{(-)}) \eta^{(-)}]^2}{[\, W_9 + \eta^{(-)} (\, W_{10} + \, W_{11}\, \eta^{(-)})]^2} + \frac{W_5\, \varepsilon_x [\, W_6 + (\, W_7 + \, W_8\, \eta^{(-)})\, \eta^{(-)}]}{-W_9 - \, \eta^{(-)} (W_{10} + \, W_{11}\, \eta^{(-)})}$$

$$FIM_C = -\frac{W_{12}\, \varepsilon_x \left[W_{13} + W_{14}\, \eta^{(-)} + W_{15} (\eta^{(-)})^2 + W_{16} (\eta^{(-)})^3 + W_{17} (\eta^{(-)})^4 + W_{18} (\eta^{(-)})^5 + W_{19} (\eta^{(-)})^6\right]}{W_{20} + \, W_{21}\, \eta^{(-)} + \, W_{22}\, (\eta^{(-)})^2 + \, W_{23}\, (\eta^{(-)})^3 + \, W_{24}\, (\eta^{(-)})^4} \tag{2.45}$$

where

$$W_1 = 1.60231\,x\,10^{-16} \quad W_2 = 2.33292\,x\,10^{-27} \quad W_3 = -6.1849\,x\,10^{-11}$$
$$W_4 = 2.48264\,x\,10^{-27} \quad W_5 = 7.168\,x\,10^{-9} \quad W_6 = -5.14354\,x\,10^{-28}$$
$$W_7 = 3.47726\,x\,10^{-11} \quad W_8 = 8.95637\,x\,10^{-12} \quad W_9 = 1.88079\,x\,10^{-37}$$
$$W_{10} = -6.4796\,x\,10^{-21} \quad W_{11} = -6.32802\,x\,10^{-22} \quad W_{12} = 2.23305\,x\,10^{19} \qquad (2.46)$$
$$W_{13} = 6.614\,x\,10^{-72} \quad W_{14} = -8.9427\,x\,10^{-55} \quad W_{15} = 3.02283\,x\,10^{-38}$$
$$W_{16} = 1.55718\,x\,10^{-38} \quad W_{17} = 9.55311x\,10^{-38} \quad W_{18} = -7.50832\,x\,10^{-54}$$
$$W_{19} = 1.50694\,x\,10^{-70} \quad W_{20} = 1.08012\,x\,10^{-53} \quad W_{21} = -1.10232\,x\,10^{-36}$$
$$W_{22} = 2.51567\,x\,10^{-20}, \quad W_{23} = 8.93642\,x\,10^{-21} \quad W_{24} = 6.32803\,x\,10^{-22}$$

The stresses are related to the axial strain by

$$\sigma_x = \frac{\varepsilon_x\left[2.27434\,x\,10^{-27} + \eta^{(-)}\left(1.77239\,x10^{-11} + \eta^{(-)}\left(9.1179\,x\,10^{-11} - 1.6156\,x\,10^{-27}\eta^{(-)}\right)\right)\right]}{-1.88079\,x\,10^{-37} + \eta^{(-)}(6.4796\,x\,10^{-21} + 6.32803\,x\,10^{-22}\eta^{(-)})} \qquad (2.47)$$

$$\sigma_{xy}^{(55^o)} = \frac{\varepsilon_x\left[3.98267\,x\,10^{-27} + \eta^{(-)}\left(-2.4348\,x10^{-11} + \eta^{(-)}\left(5.557\,x\,10^{-11} - 8.0779\,x\,10^{-28}\,\eta^{(-)}\right)\right)\right]}{-1.88079\,x\,10^{-37} + \eta^{(-)}\left(6.4796\,x\,10^{-21} + 6.32803\,x\,10^{-22}\eta^{(-)}\right)} \qquad (2.48)$$

$$\sigma_{xy}^{(-55^o)} = \frac{\varepsilon_x\left[-3.98267\,x\,10^{-27} + \eta^{(-)}\left(2.4348\,x10^{-11} + \eta^{(-)}\left(-5.557\,x\,10^{-11} + 8.0779\,x\,10^{-28}\,\eta^{(-)}\right)\right)\right]}{-1.88079\,x\,10^{-37} + \eta^{(-)}\left(6.4796\,x\,10^{-21} + 6.32803\,x\,10^{-22}\eta^{(-)}\right)} \qquad (2.49)$$

Once the matrix fails in mode B the value of the material degradation factor $\eta^{(-)}$ will decrease from 1.0 and the new value is found from Eq. (2.45) as described in Section 2.1. Numerical values of the axial stress, the axial strain and the material degradation factor $\eta^{(-)}$ are listed in Table 2.2. At ε_x = - 0.013, the failure mode switched from mode B to mode C because then $\sigma_{22} = -S_T$. The value of $\eta^{(-)}$ is subsequently found by the failure surface for mode C till ultimate failure of the laminate. The global stress-strain response and the variation of the material degradation factor along with the corresponding results computed using Abaqus and the USDFLD are shown in Figs. **2.6** and **2.7.** It is clear that results computed using Abaqus agree well with the analytical solution of the problem.

Table 2.2: During monotonic uniaxial compressive loading of the $[\pm 55^{o}]_{S}$ laminate, values of the axial stress, the axial strain and the material degradations factor

ε_x	$\eta^{(-)}$	σ_x	PFA Feature
-0.005	1	-76.56	No failure
-0.0110836	1	-169.70	Initiation in Mode B
-0.012083	0.9228	-174.271	Degradation in Mode B
-0.0125	0.8946	-176.164	Degradation in Mode B
-0.013	0.86324	-178.432	Mode B to C
-0.0210836	0.51478	-200.327	Degradation in Mode C
-0.0264836	0.358562	-199.095	Degradation in Mode C
-0.029983	0.26714	-189.776	Degradation in Mode C
-0.03720	0.009	-102.5	Degradation in Mode C
-0.03726238	0.001	-102.4	Ultimate failure

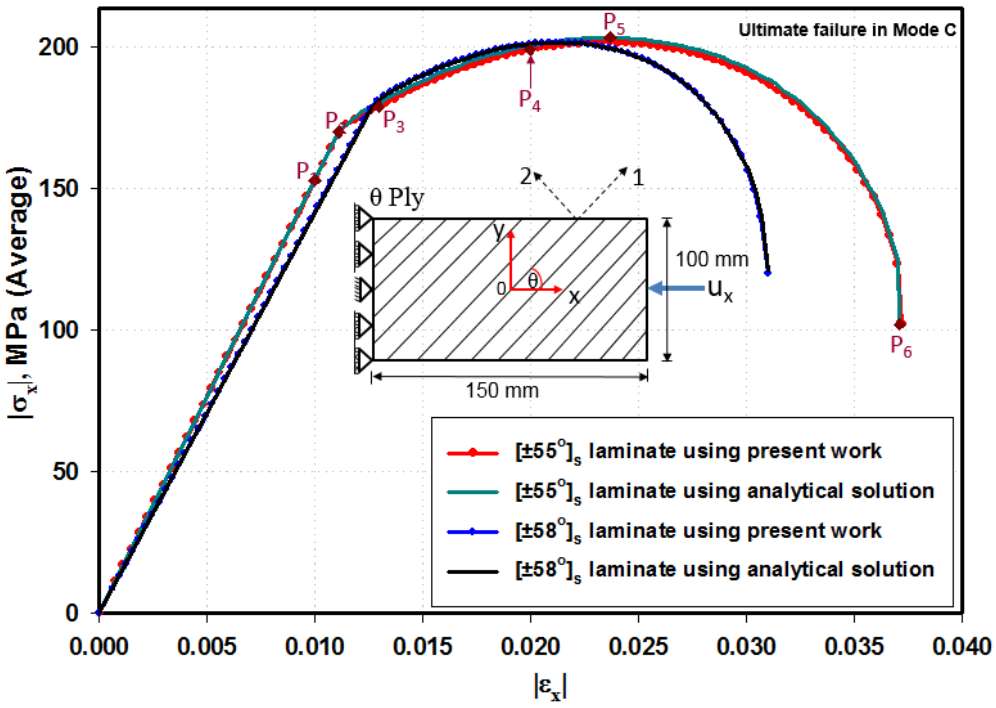

Figure 2.6: Comparison of the global stress-strain response for $[\pm 55^{o}]_{S}$, and $[\pm 58^{o}]_{S}$, laminates using Abaqus and the analytical solution.

The six points P_1, P_2, P_3, P_4, P_5, and P_6 marked on the axial stress – axial strain curve correspond, respectively, to ε_x = - 0.01, - 0.01110, = - 0.01332, - 0.020, - 0.02368, - 0.03710. We note that the matrix failure switches from mode B to mode C at point P_3, the load reaches its maximum value at point P_5, and the ultimate failure occurs at point P_6. Numerical values of the axial stress, the axial strain and the material degradations factor $\boldsymbol{\eta}^{(-)}$ are listed in Tables **2.3** and **2.4.**

Table 2.3: Numerical values of stresses in global coordinates for the +55º plies

	ε_x	ε_y	$\eta^{(-)}$	$\sigma_x^{(55^o)}$, MPa	$\sigma_y^{(55^o)}$, MPa	$\sigma_{xy}^{(55^o)}$, MPa	PFA Feature
P_1	-0.01000	0.0040212382	1	-153.12	0	-43.900	No failure
P_2	-0.01110	0.0044635744	1	-169.96	0	-48.740	Mode B initiation
P_3	-0.01332	0.0056137930	0.84714	-180.302	0	-43.163	Mode B to Mode C
P_4	-0.02000	0.00921173	0.55071	-198.846	0	-18.513	Degradation in Mode C
P_5	-0.02368	0.0112729357	0.43706	-201.797	0	0.20	Degradation in Mode C
P_6	-0.03710	0.0199934131	0.00100	-102.00	0	139.1	Ultimate failure

Table 2.4: Numerical values of stresses in global coordinates for the - 55º plies

	ε_x	ε_y	$\eta^{(-)}$	$\sigma_x^{(-55^o)}$, MPa	$\sigma_y^{(-55^o)}$, MPa	$\sigma_{xy}^{(-55^o)}$, MPa	PFA Feature
P_1	-0.01000	0.0040212382	1	-153.12	0	43.900	No failure
P_2	-0.01110	0.0044635744	1	-169.96	0	48.740	Mode B initiation
P_3	-0.01332	0.0056137930	0.84714	-180.302	0	43.163	Mode B to Mode C
P_4	-0.02000	0.00921173	0.55071	-198.846	0	18.513	Degradation in Mode C
P_5	-0.02368	0.0112729357	0.43706	-201.797	0	-0.20	Degradation in Mode C
P_6	-0.03710	0.0199934131	0.00100	-102.00	0	-139.1	Ultimate failure

Table 2.5: Numerical values of average stresses for the [±55º]s laminate in global coordinates

	ε_x	ε_y	$\eta^{(-)}$	σ_x, MPa	σ_y, MPa	σ_{xy}, MPa	PFA Feature
P_1	-0.01000	0.0040212382	1	-153.12	0	0	No failure
P_2	-0.01110	0.0044635744	1	-169.96	0	0	Mode B initiation
P_3	-0.01332	0.0056137930	0.84714	-180.302	0	0	Mode B to Mode C
P_4	-0.02000	0.00921173	0.55071	-198.846	0	0	Degradation in Mode C
P_5	-0.02368	0.0112729357	0.43706	-201.797	0	0	Degradation in Mode C
P_6	-0.03710	0.0199934131	0.00100	-102.00	0	0	Ultimate failure

Table 2.6: Numerical values of stresses in local coordinates for the +55º plies

	ε_x	ε_y	$\eta^{(-)}$	σ_{11}, MPa (+55º Ply)	σ_{22}, MPa (+55º Ply)	σ_{21}, MPa (+55º Ply)	PFA Feature
P_1	-0.01000	0.0040212382	1	-90.017	-61.32	86.982	No failure
P_2	-0.01110	0.0044635744	1	-101.73	-68.247	96.523	Mode B initiation
P_3	-0.01332	0.0056137930	0.84714	-99.8776	-78.80	99.477	Mode B to Mode C
P_4	-0.02000	0.00921173	0.55071	-82.8985	-116.201	99.8783	Degradation in Mode C
P_5	-0.02368	0.0112729357	0.43706	-66.2035	-135.596	94.7445	Degradation in Mode C
P_6	-0.03710	0.0199934131	0.00100	97.1346	-200.00	0.003	Ultimate failure

Table 2.7: Numerical values of stresses in local coordinates for the -55º plies

	ε_x	ε_y	$\eta^{(-)}$	σ_{11}, MPa (-55º Ply)	σ_{22}, MPa (-55º Ply)	σ_{21}, MPa (-55º Ply)	PFA Feature
P_1	-0.01000	0.0040212382	1	-90.017	-61.32	-86.982	No failure
P_2	-0.01110	0.0044635744	1	-101.73	-68.247	-96.523	Mode B initiation
P_3	-0.01332	0.0056137930	0.84714	-99.8776	-78.80	-99.477	Mode B to Mode C
P_4	-0.02000	0.00921173	0.55071	-82.8985	-116.201	-99.8783	Degradation in Mode C
P_5	-0.02368	0.0112729357	0.43706	-66.2035	-135.596	-94.7445	Degradation in Mode C
P_6	-0.03710	0.0199934131	0.00100	97.1346	-200.00	-0.003	Ultimate failure

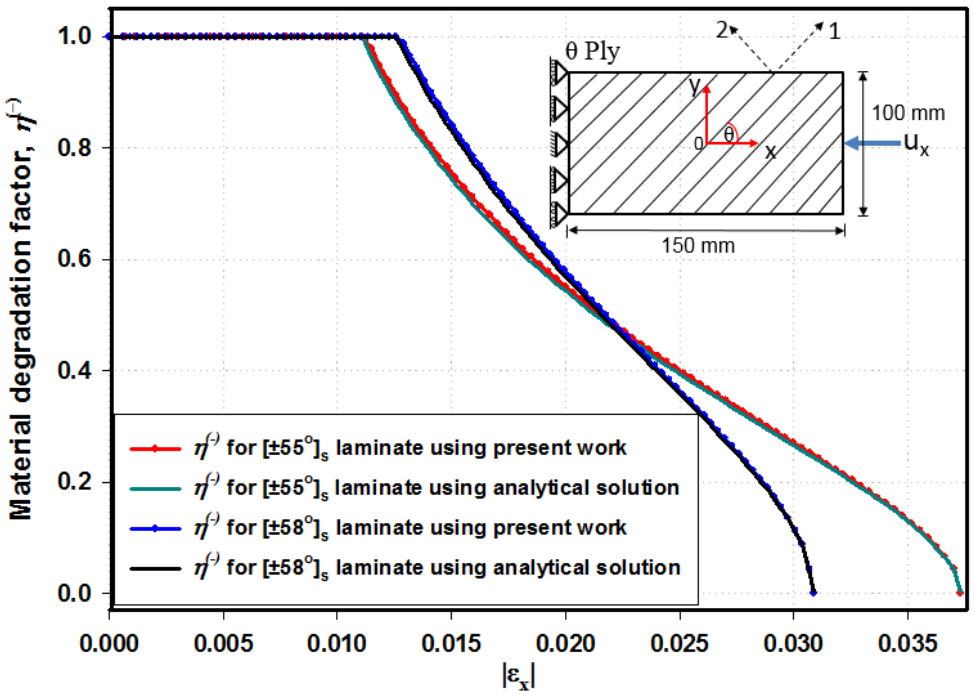

Figure 2.7: Evolution of the material degradation factor, $\eta^{(\cdot)}$, for the $[\pm 55^o]_S$ laminate under uniaxial compression found from the analytical solution and using Abaqus.

The axial stress vs. the axial strain curves and the evolution with the axial strain of the degradation parameters for laminates of different ply angles are exhibited in Figures **2.8** through **2.13**. These results evince that for all these laminates results computed using Abaqus agree well with those from the corresponding analytical solutions. The dependence of the ultimate failure stress upon ply angle θ for $[\pm\theta]_S$ laminates is shown in Fig. **2.14.**

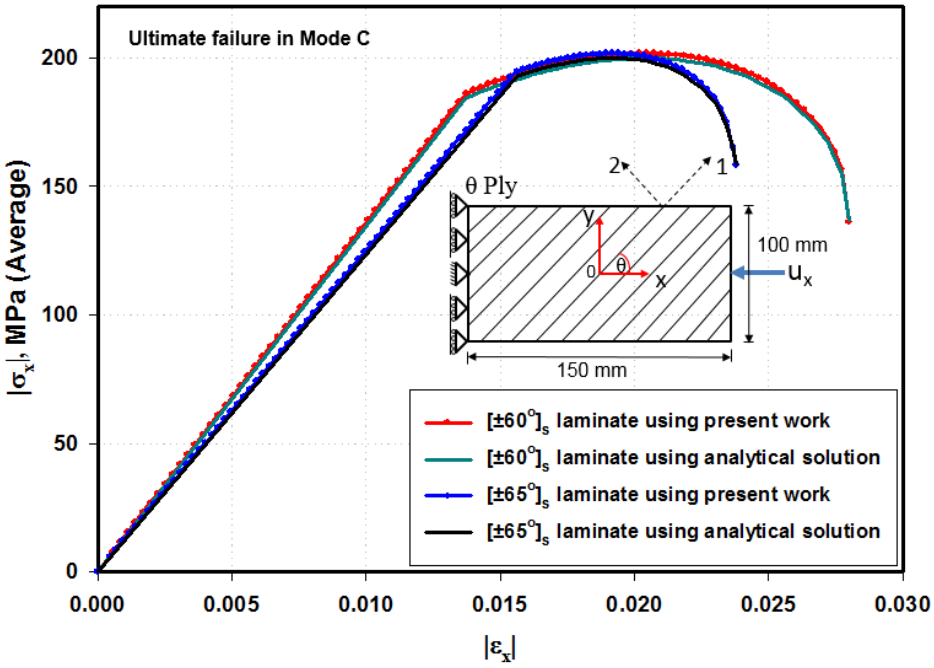

Figure 2.8: Comparison of the global stress-strain response for [±60º]s, and [±65º]s, laminates using Abaqus and analytical solution.

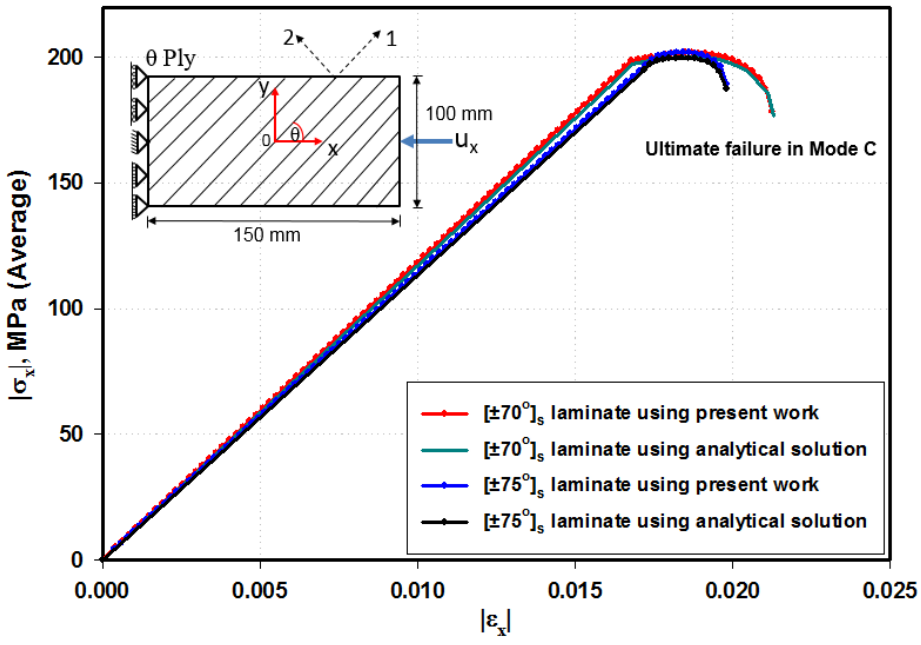

Figure 2.9: Comparison of the global stress-strain response for [±70º]s, and [±75º]s, laminates using Abaqus and analytical solution.

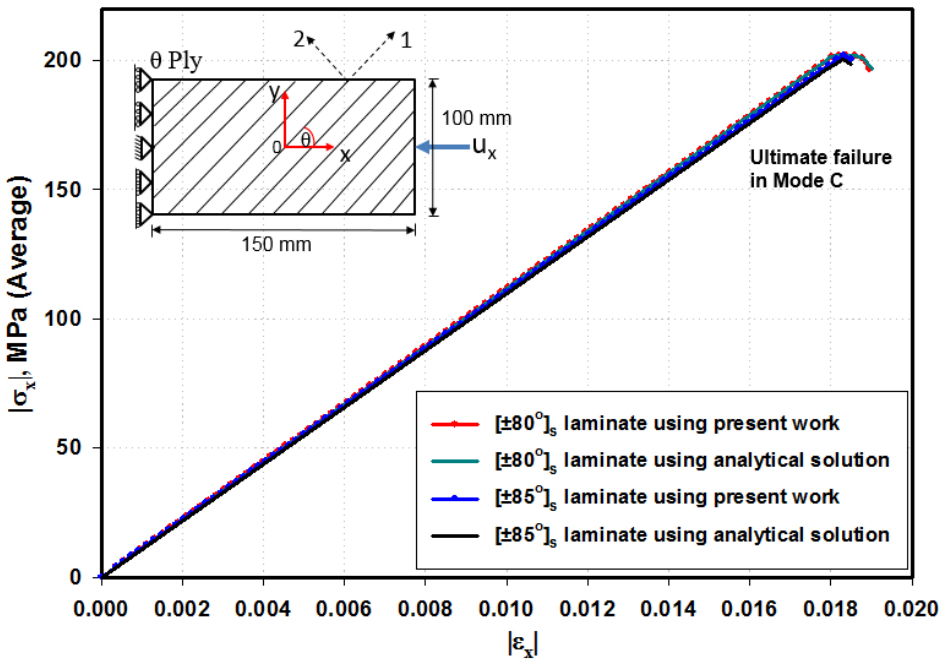

Figure 2.10: Comparison of the global stress-strain response for $[\pm 80^o]_S$, and $[\pm 85^o]_S$, laminates using Abaqus and analytical solution.

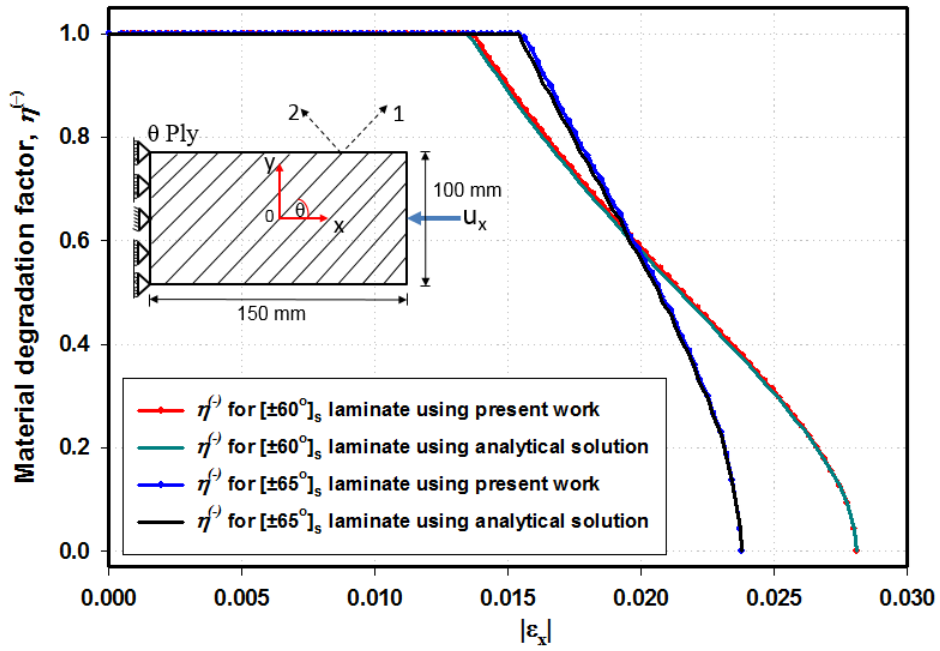

Figure 2.11: Comparison of the evolution of the material degradation factor, $\eta^{(-)}$ for $[\pm 60^o]_S$, and $[\pm 65^o]_S$, laminates using Abaqus and analytical solution.

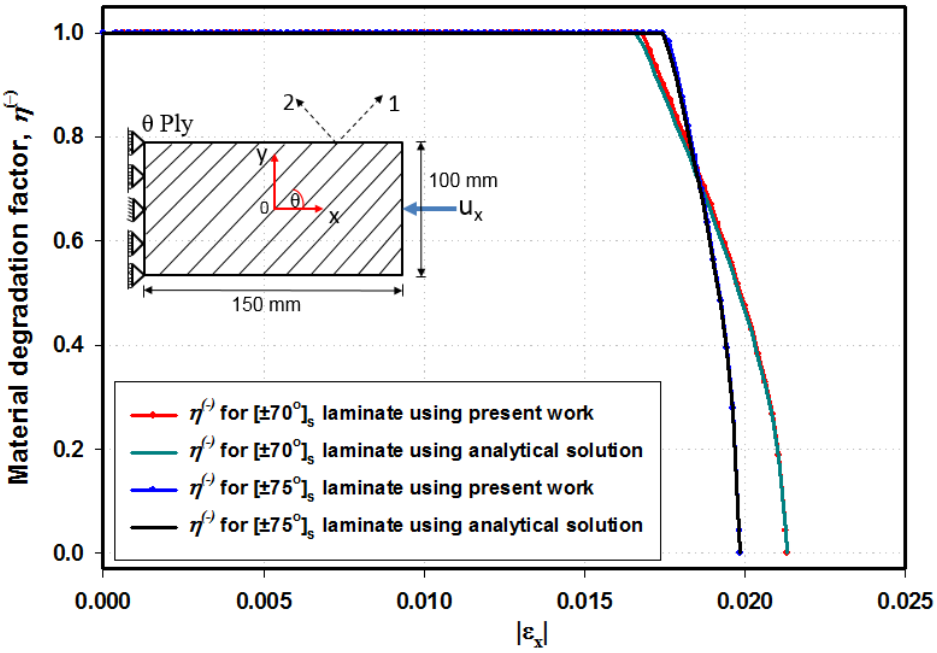

Figure 2.12: Comparison of the evolution of the material degradation factor, $\eta^{(-)}$ for $[\pm 70^o]_S$, and $[\pm 75^o]_S$, laminates using Abaqus and analytical solution.

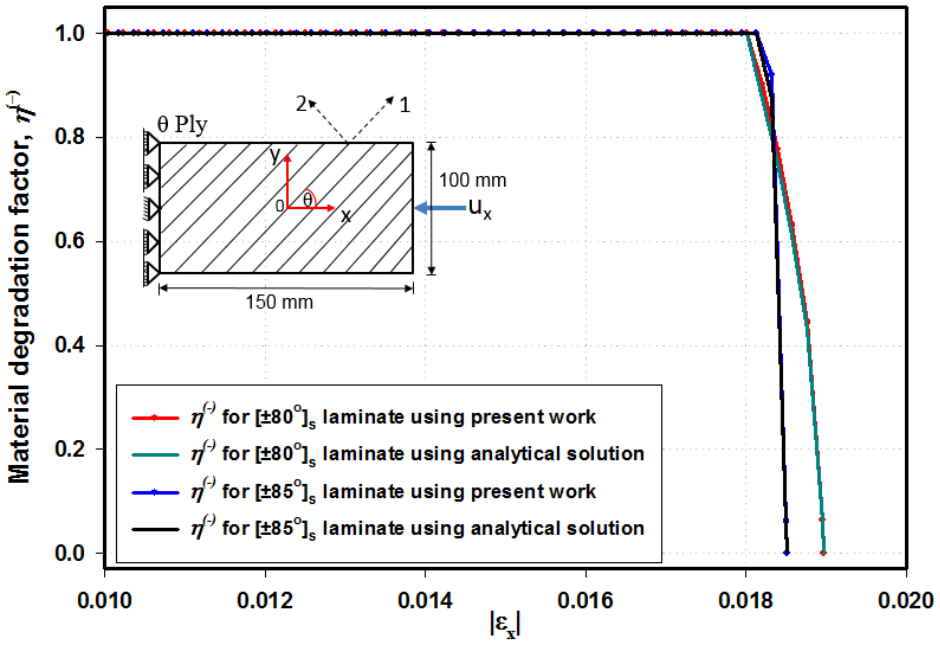

Figure 2.13: Comparison of the evolution of the material degradation factor, $\eta^{(-)}$ for $[\pm 80^o]_S$, and $[\pm 85^o]_S$, laminates using Abaqus and analytical solution.

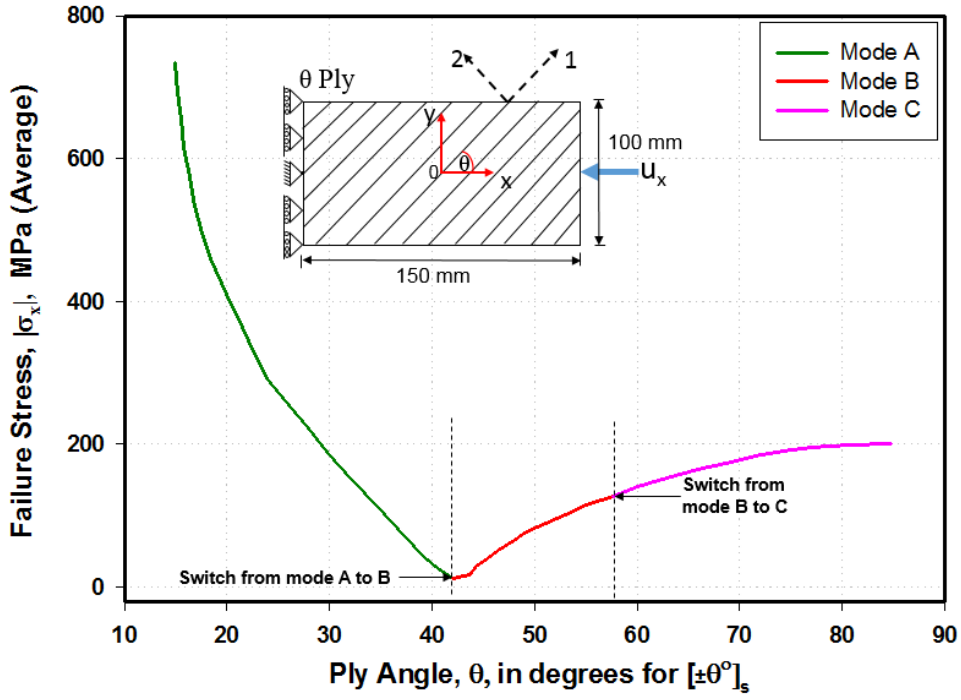

Figure 2.14: Variation of ultimate failure stress with the ply angle θ for $[\pm\theta]_S$ laminates.

2.3 PFA of quasi-isotropic $[0^o/\pm45^o/90^o]_S$ laminate under uniaxial tensile/compressive loads

We analyze uniaxial tensile deformations of a quasi-isotropic $[0^o/\pm45^o/90^o]_S$ laminate made of graphite AS4 fibers and the 3501-6 epoxy matrix with the laminate material properties listed in Section 2.2. A schematic sketch of the problem studied is shown in Fig. **2.15**. The thickness of each equals 0.165 mm.

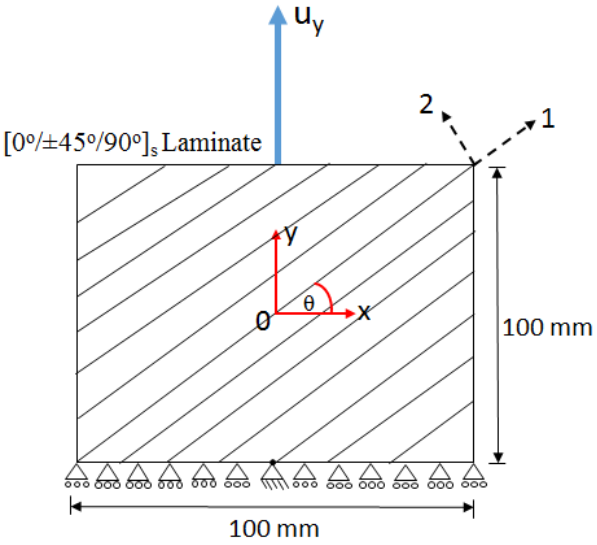

Figure 2.15: Quasi-isotropic $[0^o/\pm45^o/90^o]_s$ laminate under uniaxial tensile loading.

We assume that the specimen deforms homogeneously, and use **S4** shell elements in Abaqus. For uniaxial tensile stresses $\sigma_y > 0$, a hand calculation gives $\sigma_{22} > 0$ for all values of the fiber orientation angle, θ; thus the matrix in a ply can only fail in Mode A. Details of the analytical solution are given later in this section. The axial stress vs. the axial-strain curve with respect to the global coordinate axes is shown in Fig. **2.16**. Results obtained by using the analytical solution are superimposed upon those computed using Abaqus to show a close agreement between them. It is found that the failure first initiates in the 0^o plies in Mode A at $\varepsilon_y = 0.0047$; it corresponds to point **P** in Fig. **2.16**. Failure initiates in the $[\pm45^o]$ plies in mode A at $\varepsilon_y = 0.0064$; it corresponds to point **M** in Fig. **2.16**. The PFA is continued till fibers in the 90^o plies fail in tension at which point the analysis is stopped since the maximum load carrying capacity of the laminate has been reached.

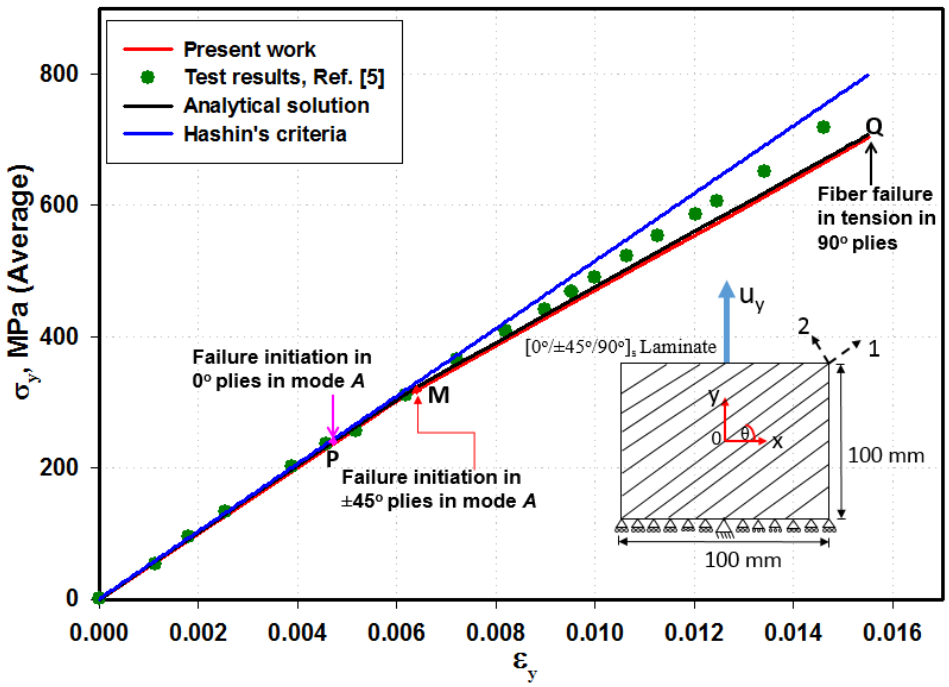

Figure 2.16: Stress-strain response of $[0^o/\pm45^o/90^o]_S$ laminate under uniaxial tensile loading.

In Fig. **2.16** we have also plotted results using Hashin's [18] failure criteria already implemented in Abaqus. Recalling that Hashin's criteria do not consider degradation of material properties, at the instant of laminate failure it predicts a higher value of σ_y than that found using Puck and Schürmann's criteria. The matrix failure initiation at point P in Fig. **2.16** using Hashin's criteria also occurs at $\varepsilon_y = 0.0047$ in matrix tension mode. The fiber failure also occurs at $\varepsilon_y = 0.01555$ but with a higher value of σ_y.

The comparison between stress components, σ_x, σ_y and σ_{xy}, using both Hashin's and Puck and Schürmann's criteria in each ply are shown in Figs. **2.17-2.19**. As a result of using the Hashin's criteria in Abaqus the state of stress depicts linear behavior with increasing strain. The Puck and Schürmann's failure criteria depict non-linear behavior in stress state of the laminate as shown in Fig. **2.17-2.19**.

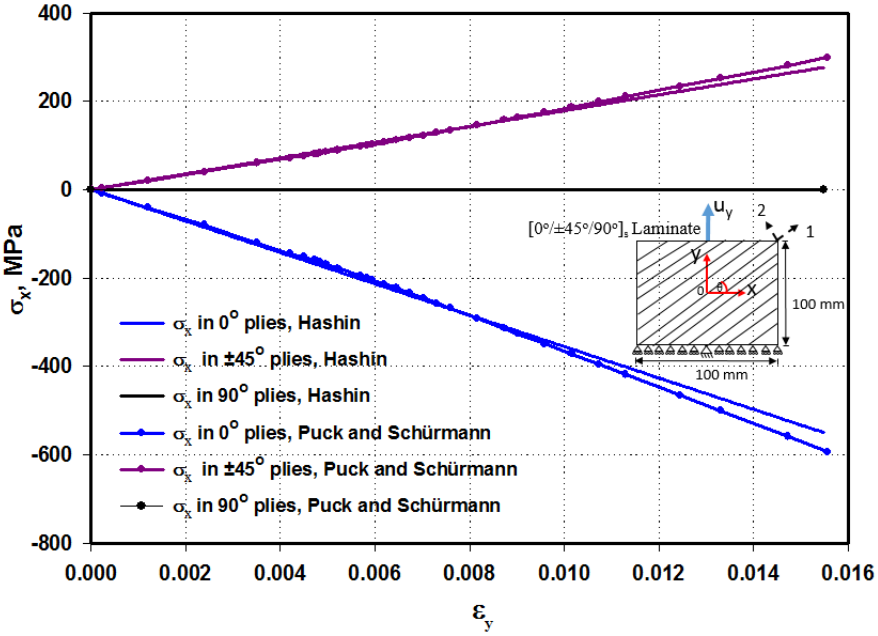

Figure 2.17: The evolution of stress σ_x in the $[0^o/\pm45^o/90^o]_S$ laminate with uniaxial tensile load applied in the y-direction. Comparison between predictions from Hashin's and Puck and Schürmann's failure criteria (Abaqus).

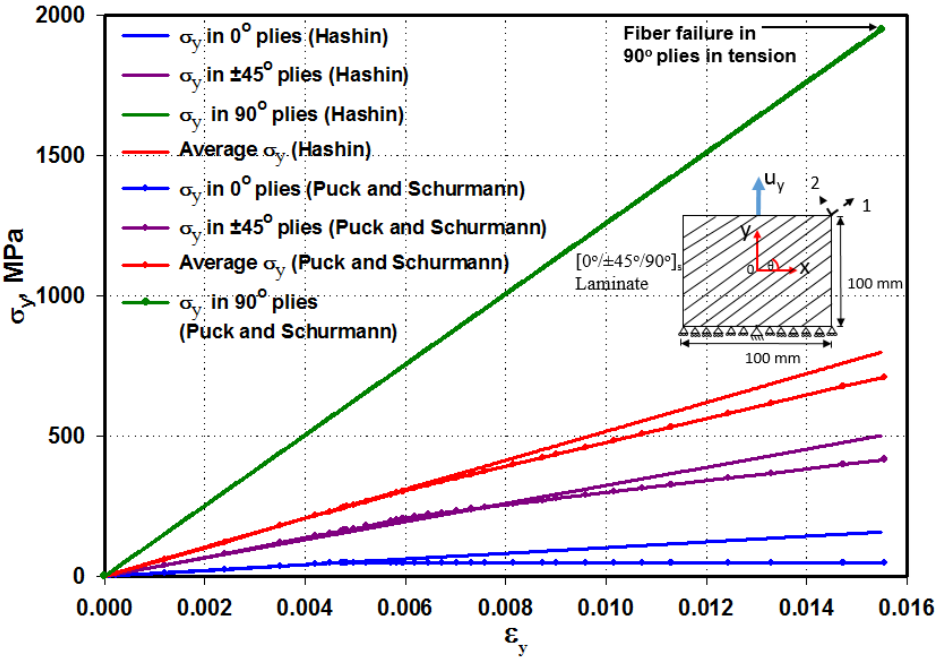

Figure 2.18: The evolution of stress σ_y in the $[0^o/\pm45^o/90^o]_S$ laminate with uniaxial tensile load applied in the y-direction. Comparison between predictions from Hashin's and Puck and Schürmann's failure criteria (Abaqus).

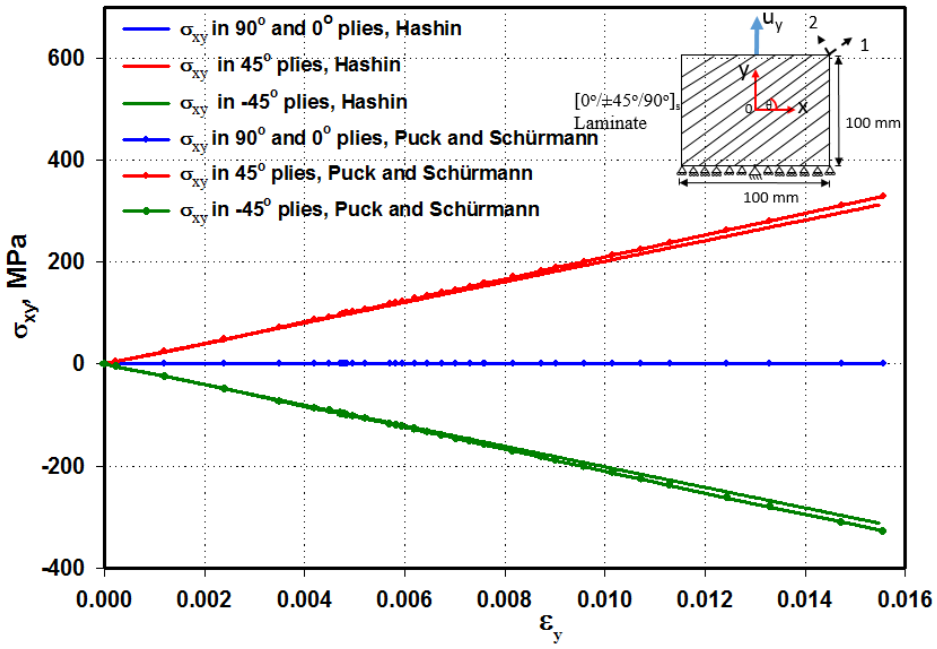

Figure 2.19: The evolution of stress σ_{xy} in the $[0^o/\pm45^o/90^o]_S$ laminate with uniaxial tensile load applied in the y-direction. Comparison between predictions from Hashin's and Puck and Schürmann's failure criteria (Abaqus).

2.3.1 Analytical approach for $[0^o/\pm45^o/90^o]_S$ laminate

For homogeneous deformations of the laminate stress components σ_x and σ_{xy} equal zero, and the strain component ε_x can be written as a function of ε_y from

$$\begin{Bmatrix}\varepsilon_x\\ \varepsilon_y\\ 0\end{Bmatrix} = \begin{bmatrix}a_{11} & a_{12} & a_{16}\\ a_{12} & a_{22} & a_{26}\\ a_{16} & a_{26} & a_{66}\end{bmatrix}\begin{Bmatrix}0\\ N_y\\ 0\end{Bmatrix} \tag{2.50}$$

where $\boldsymbol{A}$ is the laminate compliance matrix [48] and N_y is resultant edge force per unit side length of the laminate. Equation (2.50) gives

$$\varepsilon_x = \frac{a_{12}}{a_{22}}\,\varepsilon_y \tag{2.51}$$

Stresses with respect to the global coordinate axes in each ply are given by [48]:

$$\begin{Bmatrix}\sigma_x\\ \sigma_y\\ \sigma_{xy}\end{Bmatrix} = \begin{bmatrix}\bar{Q}_{11} & \bar{Q}_{12} & \bar{Q}_{16}\\ \bar{Q}_{12} & \bar{Q}_{22} & \bar{Q}_{26}\\ \bar{Q}_{16} & \bar{Q}_{26} & \bar{Q}_{66}\end{bmatrix}\begin{Bmatrix}\varepsilon_x\\ \varepsilon_y\\ 0\end{Bmatrix} \tag{2.52}$$

The reduced stiffnesses $\bar{Q}_{ij}$ of a ply are related to Q_{6ij} by

$$\bar{Q}_{11} = Q_{11}\, m^4 + 2(Q_{12} + 2Q_{66})n^2m^2 + Q_{22}\, n^4 \tag{2.53}$$

$$\bar{Q}_{12} = (Q_{11} + Q_{22} - 4Q_{66})\, n^2m^2 + Q_{12}(m^4 + n^4) \tag{2.54}$$

$$\bar{Q}_{16} = (Q_{11} - Q_{12} - 2Q_{66})nm^3 + (Q_{12} - Q_{22} + 2Q_{66})n^3m \tag{2.55}$$

$$\bar{Q}_{22} = Q_{11}\, n^4 + 2(Q_{12} + 2Q_{66})n^2m^2 + Q_{22}\, m^4 \tag{2.56}$$

$$\bar{Q}_{26} = (Q_{11} - Q_{12} - 2Q_{66})n^3m + (Q_{12} - Q_{22} + 2Q_{66})nm^3 \tag{2.57}$$

$$\bar{Q}_{66} = (Q_{11} + Q_{22} - 2Q_{12} - 2Q_{66})n^2m^2 + Q_{66}(m^4 + n^4) \tag{2.58}$$

The compliance matrix for the matrix failure in mode A is given by Eq. (2.1), which implies that for the laminate, the term $\frac{a_{12}}{a_{22}}$ given in Eq. (2.51) is a function of the material degradation factor in each ply. As the laminate only fails in mode A, we denote the mode A degradation factor in 0^o plies by η_a^0 and that in the 45^o plies by η_a^{45}.

By substituting the values of the material parameters given in section 2.1, and setting $S_f = \frac{a_{12}}{a_{22}}$ we rewrite Eqn. (2.51) as:

$$\varepsilon_x = S_f \varepsilon_y \tag{2.59}$$

where

$$S_f = \frac{ZZ_1 - ZZ_2ZZ_3}{ZZ_4 + ZZ_5ZZ_6} \tag{2.60}$$

$$ZZ_1 = \frac{\mathrm{V}_3}{[V_1 - \mathrm{V}_2\,(\eta_a^{-45})^3]^2} + \frac{V_4(\eta_a^{-45})^2}{[V_1 - V_2(\eta_a^{-45})^3]^2} + \frac{V_3}{[V_1 - V_2(\eta_a^{45})^3]^2}$$

$$+ \frac{V_4(\eta_a^{45})^2}{[V_1 - V_2(\eta_a^{45})^3]^2} - \frac{V_5}{[V_1 - V_2(\eta_a^{-45})^3][V_1 - V_2(\eta_a^{45})^3]}$$

$$+ \frac{\eta_a^{45}[V_6(\eta_a^{-45})^3 - V_6\,(\eta_a^{45})^3]}{[V_1 - V_2(\eta_a^{-45})^3]\,[V_1 - V_2(\eta_a^{45})^3]^2} \tag{2.61}$$

$$+ \frac{\eta_a^{-45}[(\eta_a^{-45})^3[-V_6 + V_7\eta_a^{45}] - V_8\eta_a^{45} + V_6(\eta_a^{45})^3]}{[V_1 - V_2(\eta_a^{-45})^3]^2[V_1 - V_2(\eta_a^{45})^3]}$$

$$ZZ_2 = \frac{V_9\,(\eta_a^{90})^2}{V_1 - V_2(\eta_a^{90})^3} + \frac{V_{10}}{V_1 - V_2(\eta_a^{-45})^3} - \frac{V_{11}\eta_a^{-45}}{V_1 - V_2(\eta_a^{-45})^3} + \frac{V_{12}(\eta_a^{-45})^2}{V_1 - V_2(\eta_a^{-45})^3}$$

$$+ \frac{V_{13}\,(\eta_a^{-45})^4}{V_1 - V_2(\eta_a^{-45})^3} + \frac{V_{10}}{V_1 - V_2(\eta_a^{45})^3} - \frac{V_{11}\eta_a^{45}}{V_1 - V_2(\eta_a^{45})^3} + \frac{V_{12}(\eta_a^{45})^2}{V_1 - V_2(\eta_a^{45})^3}$$

$$+ \frac{V_{13}\,(\eta_a^{45})^4}{V_1 - V_2(\eta_a^{45})^3} + \frac{V_9(\eta_a^{0})^2}{V_1 - V_2(\eta_a^{0})^3} \tag{2.62}$$

$$ZZ_3 = \frac{V_{14}\,\eta_a^{90}}{V_1 - V_2\,(\eta_a^{90})^3} - \frac{V_{13}\,(\eta_a^{90})^4}{V_1 - V_2\,(\eta_a^{90})^3} + \frac{V_{10}}{V_1 - V_2\,(\eta_a^{-45})^3} + \frac{V_{15}\,\eta_a^{-45}}{V_1 - V_2\,(\eta_a^{-45})^3}$$

$$- \frac{V_{12}\,(\eta_a^{-45})^2}{V_1 - V_2\,(\eta_a^{-45})^3} + \frac{V_{10}}{V_1 - V_2(\eta_a^{45})^3} + \frac{V_{15}\,\eta_a^{45}}{V_1 - V_2\,(\eta_a^{45})^3} - \frac{V_{12}(\eta_a^{45})^2}{V_1 - V_2\,(\eta_a^{45})^3}$$

$$+ \frac{V_{14}\,\eta_a^{90}}{V_1 - V_2\,(\eta_a^{90})^3} - \frac{V_{13}\,(\eta_a^{90})^4}{V_1 - V_2\,(\eta_a^{90})^3} \tag{2.63}$$

$$ZZ_4 = -\frac{V_3}{[V_1 - V_2\,(\eta_a^{-45})^3]^2} - \frac{V_4\,(\eta_a^{-45})^2}{[V_1 - V_2\,(\eta_a^{45})^3]^2} - \frac{V_3}{[V_1 - V_2\,(\eta_a^{45})^3]^2}$$

$$- \frac{V_4\,(\eta_a^{45})^2}{[V_1 - V_2\,(\eta_a^{45})^3]^2} + \frac{V_5}{[V_1 - V_2\,(\eta_a^{-45})^3][V_1 - V_2\,(\eta_a^{45})^3]}$$

$$+ \frac{\eta_a^{-45}\,[(\eta_a^{-45})^3(V_6 - V_7\,\eta_a^{45}) + V_6\eta_a^{45} - V_6\,(\eta_a^{45})^3]}{[V_1 - V_2\,(\eta_a^{-45})^3]^2[V_1 - V_2\,(\eta_a^{45})^3]}$$

$$+ \frac{\eta_a^{45}\,[-V_6(\eta_a^{-45})^3 + V_6(\eta_a^{45})^3]}{[V_1 - V_2(\eta_a^{-45})^3][V_1 - V_2\,(\eta_a^{45})^3]^2} \tag{2.64}$$

$$ZZ_5 = \frac{V_{16}\,\eta_a^{-45}}{V_1 - V_2\,(\eta_a^{90})^3} + \frac{V_{10}}{V_1 - V_2(\eta_a^{-45})^3} + \frac{V_{17}\,\eta_a^{-45}}{V_1 - V_2(\eta_a^{-45})^3} + \frac{V_{12}(\eta_a^{-45})^2}{V_1 - V_2(\eta_a^{-45})^3}$$

$$- \frac{V_{13}\,(\eta_a^{-45})^4}{V_1 - V_2(\eta_a^{-45})^3} + \frac{V_{10}}{V_1 - V_2(\eta_a^{45})^3} + \frac{V_{17}\,\eta_a^{45}}{V_1 - V_2(\eta_a^{45})^3} + \frac{V_{12}(\eta_a^{45})^2}{V_1 - V_2(\eta_a^{45})^3}$$

$$- \frac{V_{13}(\eta_a^{45})^4}{V_1 - V_2(\eta_a^{45})^3} + \frac{V_{18}}{V_1 - V_2(\eta_a^{0})^3} \tag{2.65}$$

$$ZZ_6 = \frac{V_{14}\,\eta_a^{0}}{V_1 - V_2\,(\eta_a^{90})^3} - \frac{V_{13}\,(\eta_a^{0})^4}{V_1 - V_2\,(\eta_a^{90})^3} + \frac{V_{10}}{V_1 - V_2\,(\eta_a^{-45})^3} + \frac{V_{15}\,\eta_a^{-45}}{V_1 - V_2\,(\eta_a^{-45})^3}$$

$$- \frac{V_{12}\,(\eta_a^{-45})^2}{V_1 - V_2\,(\eta_a^{-45})^3} + \frac{V_{10}}{V_1 - V_2\,(\eta_a^{45})^3} + \frac{V_{15}\,\eta_a^{45}}{V_1 - V_2\,(\eta_a^{45})^3} - \frac{V_{12}(\eta_a^{45})^2}{V_1 - V_2\,(\eta_a^{45})^3}$$

$$+ \frac{V_{14}\,\eta_a^{0}}{V_1 - V_2\,(\eta_a^{0})^3} - \frac{V_{13}\,(\eta_a^{0})^4}{V_1 - V_2\,(\eta_a^{0})^3} \tag{2.66}$$

Values of different constant are:

$$V_1 = 1.093182911364729\ x\ 10^{-31} \qquad V_{10} = 1.136363636363636\ x\ 10^{-24}$$

$$V_2 = 7.375722455087537\ x\ 10^{-34} \qquad V_{11} = 1.388888888888888\ x10^{-25}$$

$$V_3 = 1.291322314049587\ x\ 10^{-48} \qquad V_{12} = 5.515873015873017\ x\ 10^{-26}$$

$$V_4 = 9.841899722852107\ x\ 10^{-51} \qquad V_{13} = 1.606432350718065\ x\ 10^{-27}$$

$$V_5 = 2.582644628099174\ x\ 10^{-48} \qquad V_{14} = 2.380952380952381\ x\ 10^{-25}$$

$$V_6 = 1.662996585292104\ x\ 10^{-82} \qquad V_{15} = 9.920634920634923\ x\ 10^{-26}$$

$$V_7 = 1.451822415731201\ x\ 10^{-83} \qquad V_{16} = 3.968253968253969\ x\ 10^{-25}$$

$$V_8 = 2.151799318477438\ x\ 10^{-81} \qquad V_{17} = 3.373015873015873\ x\ 10^{-25}$$

$$V_9 = 1.103174603174603\ x\ 10^{-25} \qquad V_{18} = 4.545454545454546\ x\ 10^{-24} \qquad (2.67)$$

Thus stresses in each ply with respect to the material principal axes can be found from those with respect to the global coordinate axes by:

$$\begin{Bmatrix} \sigma_{11} \\ \sigma_{22} \\ \sigma_{21} \end{Bmatrix} = T_\sigma \begin{Bmatrix} \sigma_x \\ \sigma_y \\ \sigma_{xy} \end{Bmatrix} \qquad (2.68)$$

where T_σ is the matrix that transform stresses from the global coordinate axes to the material principal axes. The stresses with respect to the material principal axes in 0^o plies are:

$$\sigma_{11}^0 = \frac{1.37741\ x\ 10^{-20}\ S_f \varepsilon_y}{PP_1 - \ PP_2(\eta_a^0)^3} + \frac{3.34295\ x\ 10^{-22}\ \varepsilon_y(\eta_a^0)^2}{PP_1 - \ PP_2(\eta_a^0)^3} \qquad (2.69)$$

$$\sigma_{22}^0 = \frac{\eta_a^0\ \varepsilon_y\left(1.2025\ x\ 10^{-21} + 3.34295\ x\ 10^{-22} S_f \eta_a^0\right)}{PP_1 - \ PP_2(\eta_a^0)^3} \qquad (2.70)$$

$$\sigma_{21}^0 = 0 \qquad (2.71)$$

where,

$$PP_1 = 1.09318\ x\ 10^{-31},\ \ PP_2 = 7.37572\ x\ 10^{-34} \qquad (2.72)$$

Substituting for σ_{22}^0 and σ_{21}^0 from Eqs. (2.70) - (2.71) into Eq. (1.50) we get the expression for mode A failure index in 0^o plies as:

$$FIM_A^0 = \frac{\eta_a^0\, \varepsilon_y \left(4.56646\, x\, 10^{-30} + 1.26948\, x\, 10^{-30} S_f \eta_a^0\right)}{PP_1 - \ PP_2(\eta_a^0)^3} + LL_1 \frac{(1.86233\, x\, 10^{-39} - 1.25652\, x\, 10^{-41}(\eta_a^0)^3\ )}{PP_1 - \ PP_2(\eta_a^0)^3} \tag{2.73}$$

where

$$LL_1 = \sqrt{\frac{\varepsilon_y^2(\eta_a^0)^2\left(1.44601\, x\, 10^{-42} + \ 8.0398\, x\, 10^{-43} S_f \eta_a^0 + 1.11753\, x\, 10^{-43}\, S_f^2(\eta_a^0)^2\right)}{(PP_1 - \ PP_2(\eta_a^0)^3)^2}} \tag{2.74}$$

Similarly, stresses with respect to the material principal axes in the 45^o plies are:

$$\sigma_{11}^{45} = \frac{\varepsilon_y \left[6.88705\, x\, 10^{-21}\left(1 + S_f\right) + 1.67148\, x\, 10^{-22}(\eta_a^{45})^2\ \left(1 + S_f\right)\right]}{PP_1 - \ PP_2(\eta_a^{45})^3} \tag{2.75}$$

$$\sigma_{22}^{45} = \frac{\varepsilon_y\, \eta_a^{45}\left[6.01251\, x\, 10^{-22} + S_f(6.01251\, x\, 10^{-22} + 1.67148\, x\, 10^{-22}\, \eta_a^{45}) + 1.67148\, x\, 10^{-22}\eta_a^{45}\right]}{PP_1 - \ PP_2\left(\eta_a^{45}\right)^3} \tag{2.76}$$

$$\sigma_{21}^{45} = \left(6.6\, x\, 10^9 - 6.6\, x\, 10^9 * S_f\right)\varepsilon_y \eta_a^{45} \tag{2.77}$$

and the expression for the mode A failure index is

$$FIM_A^{45} = \frac{LL_2\, LL_3}{PP_1 - PP_2\left(\eta_a^{45}\right)^3} \tag{2.78}$$

with

$$LL_2 = \left(\varepsilon_y \eta_a^{45}\left(GG_1 + S_f(GG_1 + \ GG_2\eta_a^{45}) + \eta_a^{45} GG_2\right) + [PP_1 - PP_2(\eta_a^{45})^3]\right) \tag{2.79}$$

$$LL_3 = \left[\frac{\varepsilon_y^2 \left(\eta_a^{45}\right)^2}{\left(PP_1 - PP_2\left(\eta_a^{45}\right)^3\right)^2} \left[GG_3 + GG_4\,\eta_a^{45} + GG_5\left(\eta_a^{45}\right)^2 - GG_6\left(\eta_a^{45}\right)^3 + GG_7\left(\eta_a^{45}\right)^6 + S_f\left(GG_8 + \eta_a^{45}\,GG_9 + GG_{10}\left(\eta_a^{45}\right)^2 + GG_{11}\left(\eta_a^{45}\right)^3 + GG_{12}\left(\eta_a^{45}\right)^6\right) + S_f^2\left(GG_3 + GG_4\,\eta_a^{45} + GG_5\left(\eta_a^{45}\right)^2 - GG_6\left(\eta_a^{45}\right)^3 + GG_{13}\left(\eta_a^{45}\right)^6\right)\right] \right]^{\frac{1}{2}} \tag{2.80}$$

where

$$GG_1 = 2.28323\,x\;10^{-30},\; GG_2 = 6.34738\,x\,10^{-31},\; GG_3 = 1.88326\,x\,10^{-58}$$
$$GG_4 = 5.8333\,x\,10^{-59},\; GG_5 = 8.10829\,x\,10^{-60},\; GG_6 = 1.12554\,x\,10^{-60}$$
$$GG_7 = 3.79702\,x\,10^{-63}\quad GG_8 = 4.30104\,x\,10^{-59}\quad GG_9 = 1.16666\,x\,10^{-58} \tag{2.81}$$
$$GG_{10} = 1.62166x\,10^{-59},\; GG_{11} = 2.25108\,x\,10^{-60},\; GG_{12} = -7.59404x\,10^{-63}$$
$$GG_{13} = 3.79702\,x\,10^{-63}$$

Stresses with respect to the material principal axes in the - 45^o plies are given by

$$\sigma_{11}^{-45} = \frac{\varepsilon_y \left[6.88705\,x\,10^{-21}\left(1+S_f\right) + 1.67148\,x\,10^{-22}(\eta_a^{-45})^2\left(1+S_f\right)\right]}{1.09318\,x\,10^{-31} - 7.37572\,x\,10^{-34}\left(\eta_a^{-45}\right)^3} \tag{2.82}$$

$$\sigma_{22}^{-45} = \frac{\varepsilon_y\,\eta_a^{-45}\left[6.01251\,x\,10^{-22} + S_f(6.01251\,x\,10^{-22} + 1.67148\,x\,10^{-22}\,\eta_a^{-45}) + 1.67148\,x\,10^{-22}\eta_a^{-45}\right]}{1.09318\,x\,10^{-31} - 7.37572\,x\,10^{-34}\left(\eta_a^{-45}\right)^3} \tag{2.83}$$

$$\sigma_{21}^{-45} = \left(-6.6\,x\,10^9 + 6.6\,x\,10^9 S_f\right)\varepsilon_y\eta_a^{-45} \tag{2.84}$$

and the expression for the mode A failure index for the -45^o plies is

$$FIM_A^{-45} = \frac{LL_4\,LL_5}{PP_1 - PP_2\left(\eta_a^{-45}\right)^3} \tag{2.85}$$

where

$$LL_4 = \left(\varepsilon_y\eta_a^{-45}\left(GG_1 + S_f\left(GG_1 + GG_2\eta_a^{-45}\right) + \eta_a^{-45}GG_2\right) + \left[PP_1 - PP_2\left(\eta_a^{-45}\right)^3\right]\right) \tag{2.86}$$

$$LL_5 = \left[\frac{\varepsilon_y^2 \left(\eta_a^{-45}\right)^2}{\left(PP_1 - PP_2\left(\eta_a^{45}\right)^3\right)^2} \left[GG_3 + GG_4\,\eta_a^{45} + GG_5\left(\eta_a^{-45}\right)^2 - GG_6\left(\eta_a^{-45}\right)^3 + GG_7\left(\eta_a^{-45}\right)^6 \right.\right.$$
$$+ S_f\left(GG_8 + \eta_a^{-45}\,GG_9 + GG_{10}\left(\eta_a^{-45}\right)^2 + GG_{11}\left(\eta_a^{-45}\right)^3 + GG_{12}\left(\eta_a^{-45}\right)^6\right) \quad (2.87)$$
$$\left.\left. + S_f^2\left(GG_3 + GG_4\,\eta_a^{-45} + GG_5\left(\eta_a^{-45}\right)^2 - GG_6\left(\eta_a^{-45}\right)^3 + GG_{13}\left(\eta_a^{-45}\right)^6\right)\right]\right]^{\frac{1}{2}}$$

The stresses with respect to the material principal axes in 90° plies are

$$\sigma_{11}^{90} = \frac{\varepsilon_y\left(1.37741\,x\,10^{-20} + S_f\ 3.34295\,x\,10^{-22}(\eta_a^{90})^2\right)}{PP_1 - \ PP_2(\eta_a^{90})^3} \quad (2.88)$$

$$\sigma_{22}^{90} = \frac{1.2025\,x\,10^{-21}\,\eta_a^{90} S_f \varepsilon_y}{PP_1 - \ PP_2(\eta_a^{90})^3} + \frac{3.34295\,x\,10^{-22}\,\varepsilon_y(\eta_a^{90})^2}{PP_1 - \ PP_2(\eta_a^{90})^3} \quad (2.89)$$

$$\sigma_{21}^{90} = 0 \quad (2.90)$$

and the expression for mode A failure index for the 90° plies is

$$FIM_A^{90} = \frac{\eta_a^{90}\,\varepsilon_y\left(4.56646\,x\,10^{-30}S_f + 1.26948\,x\,10^{-30}\eta_a^{90}\right)}{PP_1 - \ PP_2(\eta_a^{0})^3} + LL_6\frac{\left(1.86233\,x\,10^{-39} - 1.25652\,x\,10^{-41}(\eta_a^{90})^3\ \right)}{PP_1 - \ PP_2(\eta_a^{90})^3} \quad (2.91)$$

where

$$LL_6 = \sqrt{\frac{\varepsilon_y^2(\eta_a^{90})^2\left(1.44601\,x\,10^{-42}S_f^2 + \ 8.0398\,x\,10^{-43}S_f\eta_a^{90} + 1.11753\,x\,10^{-43}(\eta_a^{90})^2\right)}{(PP_1 - \ PP_2(\eta_a^{90})^3)^2}} \quad (2.92)$$

Until the failure initiates in mode A in a ply the value of the material degradations factor in that ply equals 1.0. Once the matrix fails in tension E_2, ν_{12} and G_{12} for that ply are degraded by the factor $\eta_a$whose value is found by using the approach outlined above for determining η_a for the 30° off-axis specimen. The global stress σ_y for the laminate is found by taking the average value of σ_y in each ply. The global stress σ_y in different plies is given by

$$\sigma_y^0 = \frac{\eta_a^0\left(\ 1.2025\ x\ 10^{-21}\varepsilon_y + \ 3.34295\ x\ 10^{-22}S_f\varepsilon_y\eta_a^0\right)}{1.09318\ x\ 10^{-31} - 7.37572\ x10^{-34}\ (\eta_a^0)^3} \tag{2.93}$$

$$\sigma_y^{45} = J_1 + J_2 \tag{2.94}$$

where

$$J_1 = \frac{\varepsilon_y[L_1 + \eta_a^{45}(L_2 + L_3\ \eta_a^{45} - L_4\ (\eta_a^{45})^3)]}{1.09318\ x\ 10^{-31} - 7.37572\ x10^{-34}\ (\eta_a^{45})^3} \tag{2.95}$$

$$J_2 = \frac{S_f\varepsilon_y[L_1 + \eta_a^{45}(L_5 + L_3\ \eta_a^{45} + L_4\ (\eta_a^{45})^3)]}{1.09318\ x\ 10^{-31} - 7.37572\ x10^{-34}\ (\eta_a^{45})^3} \tag{2.96}$$

$$L_1 = \ 3.44353\ x\ 10^{-21},\ L_2 = \ \ 1.02213\ x\ 10^{-21},\ L_3 = \ 1.67148\ x\ 10^{-22},$$
$$L_4 = \ 4.86798\ x\ 10^{-24}\ ,\ L_5 = \ -4.20875\ x\ 10^{-22} \tag{2.97}$$

The global stress σ_y in the -45° plies is written as:

$$\sigma_y^{-45} = J_3 + J_4 \tag{2.98}$$

where

$$J_3 = \frac{\varepsilon_y[L_1 + \eta_a^{-45}(L_2 + L_3\ \eta_a^{-45} - L_4\ (\eta_a^{-45})^3)]}{1.09318\ x\ 10^{-31} - 7.37572\ x10^{-34}\ (\eta_a^{-45})^3} \tag{2.99}$$

$$J_4 = \frac{S_f\varepsilon_y[L_1 + \eta_a^{-45}(L_5 + L_3\ \eta_a^{-45} + L_4\ (\eta_a^{-45})^3)]}{1.09318\ x\ 10^{-31} - 7.37572\ x10^{-34}\ (\eta_a^{-45})^3} \tag{2.100}$$

The global stress σ_y in the 90° plies is written as:

$$\sigma_y^{90} = \frac{1.37741\ x\ 10^{-20}\ \varepsilon_y + 3.34295\ x\ 10^{-22}S_f\varepsilon_y(\eta_a^{90})^2}{1.09318\ x\ 10^{-31} - 7.37572\ x10^{-34}\ (\eta_a^{90})^3} \tag{2.101}$$

The average σ_y in the laminate can be written as:

$$\sigma_y^{avg} = \frac{1}{4}\left(\sigma_y^0 + \sigma_y^{45} + \sigma_y^{-45} + \sigma_y^{90}\right) \tag{2.102}$$

Values of the degradation factor in each ply found using the analytical expressions given above and those computed using Abaqus with the USDFLD are compared in Tables 2.8 through 2.9. We see that the two sets of results are very close to each other verifying the implementation in Abaqus of the Puck and Schürmann failure criteria.

Table 2.8: Comparison between computed values using analytical approach and Abaqus for material degradations factors for $[0^o/\pm45^o/90^o]_S$ laminate under uniaxial tensile load

ε_y	η_a^0 *Analytical Solution*	η_a^0 *Abaqus*	η_a^{45} *Analytical Solution*	η_a^{45} *Abaqus*	η_a^{-45} *Analytical Solution*	η_a^{-45} *Abaqus*	η_a^{90} *Analytical Solution*	η_a^{90} *Abaqus*
0	1	1	1	1	1	1	1	1
0.00472	1	1	1	1	1	1	1	1
0.004728	0.99970	0.99975	1	1	1	1	1	1
0.00484	0.9747	0.9746	1	1	1	1	1	1
0.00640	0.7225	0.7226	0.99990	0.99980	0.99990	0.99980	1	1
0.007168	0.641050	0.6416	0.90280	0.90275	0.90280	0.90275	1	1
0.0093760	0.484650	0.48470	0.70550	0.70560	0.70550	0.70560	1	1
0.013400	0.33550	0.3360	0.50495	0.50491	0.50495	0.50491	1	1
0.0150	0.2990	0.29910	0.45380	0.45375	0.45380	0.45375	1	1
0.0155	0.28800	0.28804	0.4393	0.4395	0.4393	0.4395	1	1

Table 2.9: Comparison between computed values using analytical approach and Abaqus for the axial stress σ_y^{avg} for the $[0^o/\pm45^o/90^o]_s$ laminate under uniaxial tensile load

ε_y	σ_y^{avg}, MPa, Analytical	σ_y^{avg}, MPa, Abaqus
0	0	0
0.00472	241.00	240.9913
0.004728	241.40	241.3970
0.00484	246.891	246.8778
0.00640	323.105	323.1007
0.007168	355.668	355.78
0.0093760	449.071	449.21
0.01340000	618.90	619.1
0.0150	686.31	686.61
0.0155	707.27	707.47

The evolution with the applied axial stress of the material degradation factor η_a in each ply is shown in Figure **2.20** wherein significant points when failure initiates in each ply are also marked. Failure initiates in the 0^o plies prior to the failure initiation in the $\pm45^o$ plies. The ultimate failure of the laminate occurs when fibers fail in all of the 90^o plies in which the matrix does not fail.

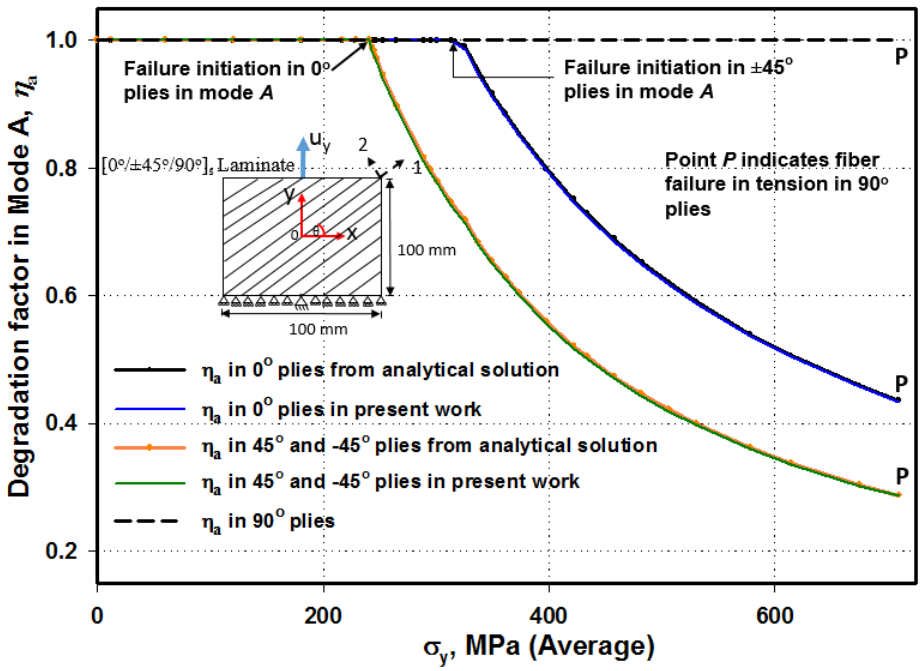

Figure 2.20: Evolution with the axial stress of the Mode A degradation factor, η_a, in each ply of the $[0^o/\pm45^o/90^o]_S$ deformed under uniaxial tension.

2.4 PFA of cylindrical bending of a laminate

We study cylindrical bending of a thin, semi-infinite rectangular laminated plate by using the classical laminated plate theory (CLPT) [48] and the USDFLD implemented in Abaqus. The rectangular Cartesian coordinate system x, y and z with $0 \leq x \leq a$, $-H/2 \leq z \leq H/2$, and $0 \leq y < \infty$, used to describe deformations of the laminate is shown in Fig. **2.21**. Let functions *u(x, y, z)*, *v(x, y, z)* and *w(x, y, z)* denote displacements of a material point in the *x*-, the *y*- and the *z*- directions, respectively. Displacements of a point on the laminate midsurface are described by functions $u_0(x, y) = u(x, y, 0)$, $v_0(x, y) = 0$, and $w_0(x, y) = w(x, y, 0)$.

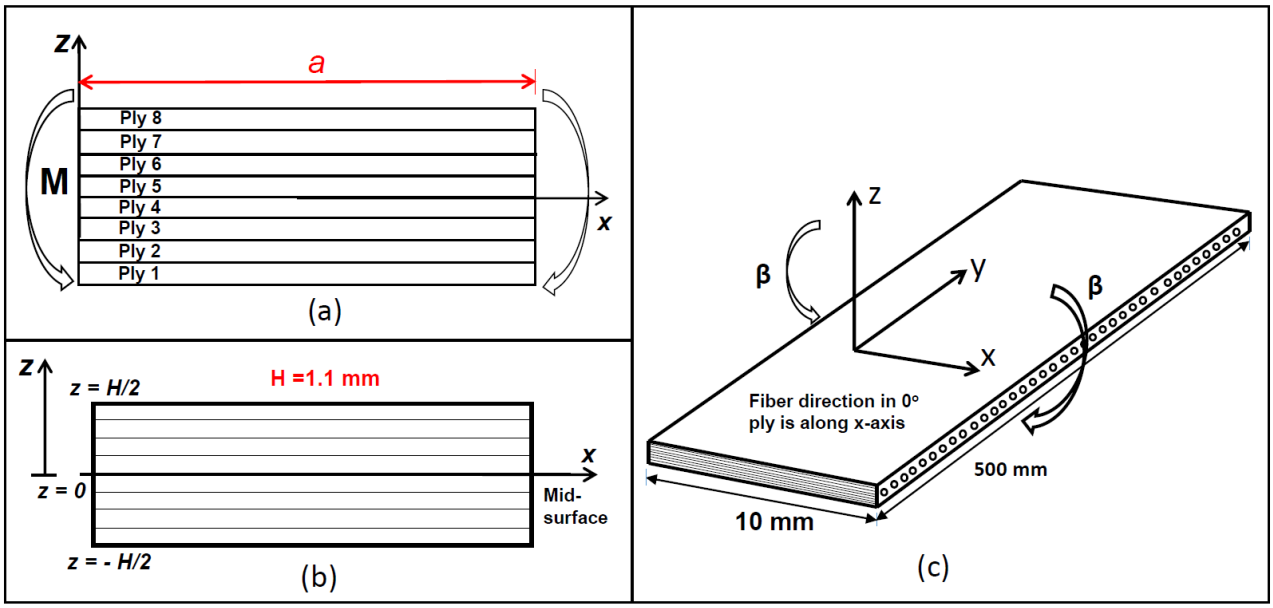

Figure 2.21: (i) Laminate under cylindrical bending; (ii) the coordinate system and mid-surface of the laminate (fibers are along the x-axis); (iii) the laminate showing the fiber direction.

2.4.1 Brief review of the CLPT for cylindrical bending of a laminate

In cylindrical bending all derivatives of displacements with respect to y-coordinate vanish, and the displacement field in the CLPT is assumed to be given by [50]:

$$u(x, y, z) = u_0(x) + z\beta_x(x), \qquad v(x, y, z) = 0, \quad w(x, y, z) = w_0(x) \tag{2.103}$$

where the rotation, β_x, of the normal to the mid-surface about the y-axis is given by

$$\beta_x(x) = -\frac{dw_0}{dx} \tag{2.104}$$

The normal strains, ε_x and ε_y, and the shear strain, γ_{xy}, are given by

$$\varepsilon_x = \frac{du_0}{dx} - z\kappa_x, \qquad \varepsilon_y = 0 \quad \text{and} \quad \gamma_{xy} = \frac{dv_0}{dx} \tag{2.105}$$

where the only non-zero curvature of the mid-surface, denoted by κ_x, is related to the rotation, β_x, by

$$\kappa_x = -\frac{d\beta_x}{dx} \tag{2.106}$$

Stress components in the material principal directions are computed from

$$[\sigma_{11} \;\; \sigma_{22} \;\; \sigma_{12}]^T = S^{-1}T_{\epsilon i}^{-1}\left[\varepsilon_x \;\; 0 \;\; \gamma_{xy}\right]^T \tag{2.107}$$

in which the compliance matrix $\boldsymbol{S}$ is given by Eq. (2.1) for plane stress deformations. Substitution for strains from Eq. (2.105) into Eq. (2.107), transforming stress components from the material principal directions to the global x, y, z axes, and integrating the resulting equations over the laminate thickness, we obtain the following relation between the resultant edge force per unit side length of the laminate, N_x , and strains.

$$N_x = A_{11}\frac{du_0}{dx} + A_{16}\frac{dN_0}{dx} + B_{11}\kappa_x \tag{2.108}$$

$$M_x = B_{11}\frac{du_0}{dx} + B_{16}\frac{dN_0}{dx} + D_{11}\kappa_x \tag{2.109}$$

Here M_x is the bending moment per unit edge length.

Equilibrium equations, in the absence of body forces and distributed loads on the top and the bottom surfaces of the laminate, obtained either from a free body diagram or by integrating over the laminate thickness equations for plane stress deformations are

$$\frac{dN_x}{dx} = 0, \qquad \frac{d^2M_x}{dx^2} = 0 \tag{2.110}$$

Even though we have shown bending moments applied at the two bounding edges of the laminate, in the numerical work, we prescribe rotations at the edges. Thus pertinent boundary conditions are

$$N_x = 0, \quad x = 0, a; \;\; \beta_x(0) = -\beta, \qquad \beta_x(a) = \beta \tag{2.111}$$

Assuming that N_0 = 0, Eqns. (2.110) and (2.111) give $N_x = 0$ for 0 < x < a, and $\frac{dM}{dx}$ = constant. Eqns. (2.108), (2.109) and (2.111) give

$$\frac{du_0}{dx} = \frac{B^{(R)}}{A^{(R)}}(-\kappa_x), \quad \kappa_x = \frac{A^{(R)}}{D^{(R)}}M \tag{2.112}$$

where $M_x = M$ for 0 < x < a, and the reduced plate stiffness are given by

$$A^{(R)} = A_{11}A_{66} - A_{16}^2 \tag{2.113}$$

$$B^{(R)} = A_{66}B_{11} - A_{16}B_{16} \tag{2.114}$$

$$D^{(R)} = D_{11}A^{(R)} - B^{(R)}B_{11} - C^{(R)}B_{16} \tag{2.115}$$

In Eqs. (2.113) - (2.115), A_{11}, A_{66}, A_{16}, B_{11}, B_{16} and D_{11} are elements of the usual *A*, *B* and *D* matrices of the CLPT [48]. The last of Eq. (2.112) shows that the curvature is spatially uniform in the *x*-direction. Consequently, we integrate Eq. (2.106) with respect to *x* subject to the boundary conditions (2.111) to find

$$\kappa_x = \frac{2\beta}{a} \tag{2.116}$$

Prescribing the end rotation β determines the curvature from Eq. (2.116). Then the bending moment *M* and the displacement gradients are found from Eq. (2.112), followed by computation of the strains from Eq. (2.105).

2.4.2 Numerical results for the cylindrical bending of a laminate

For the configuration exhibited in Fig. **2.21**, we assume the laminate material to be carbon/epoxy AS4/3501-6 with ply thickness = 0.1375 mm, a = 10 mm, and values of material parameters listed in Section 2.2. For the cylindrical bending problem the shear stress identically vanishes. Thus matrix will not fail. The fiber failure is governed by Eqs. (1.54) and (1.55).

Cylindrical bending of $[0^o]_8$ laminate

With a gradual increase in the applied rotations at the end faces, *x* = 0 and *a*, the computed bending moment increases linearly with an increase in the applied rotation until ply 1 fails due to fiber failure in compression because $X_C < X_T$. At this instant, M = 355 N-mm/mm and the either the CLPT or the Euler-Bernoulli beam theory gives σ_x = 355 (0.1375 x 3.5)/((1.1)^3/12) = 1540 MPa which is close to X_C = 1480 MPa for the laminate. Thus fibers in ply 1 fail in compression and the ply is deleted from the analysis. With the reduction in the laminate height to 7 x 0.1375 =

0.9625 mm, the neutral axis of the laminate shifts upwards, the magnitude of the maximum axial stress drops from 1480 MPa to 1320 MPa for the same curvature, the bending moment supported by the beam decreases in proportion to the decrease in the moment of inertia, or equivalently to 355 x $(0.9625/1.1)^3$ = 216.2 N-mm/mm. With an increase in the applied rotations at the bounding edges the bending moment increases in proportion to the applied rotations from 228 to 266 N-mm/mm when fibers in ply 2 fail in compression and the bending moment suddenly drops to 167 N-mm/mm. This process continues till all plies have failed, and is illustrated in Fig. **2.22**.

The problem has also been analyzed using **S4** shell elements in ABAQUS/Standard incorporating the USDFLD subroutine, considering *10 mm* x *500 mm* x *1.1 mm* laminate shown in Fig. **2.21(c)**, specifying rotations at the end faces $x = 0$ and a, and keeping other surfaces traction free. The computed moment-rotation curve is superimposed on that found using the CLPT in Fig. **2.22**. Values of the bending moment corresponding to the first peak equal 355 and 341 N-mm/mm from the FE and the CLPT solutions, respectively. Except for these small differences in the bending moments at the peaks and troughs in the two curves, the results from the two approaches are close to each other implying that the implementation of the PFA in USDFLD gives very good results. The redistribution of stress states before and after the fiber failure in ply 1 and in plies 1 through 4 are shown, respectively, in Figs. **2.23** and **2.25**.

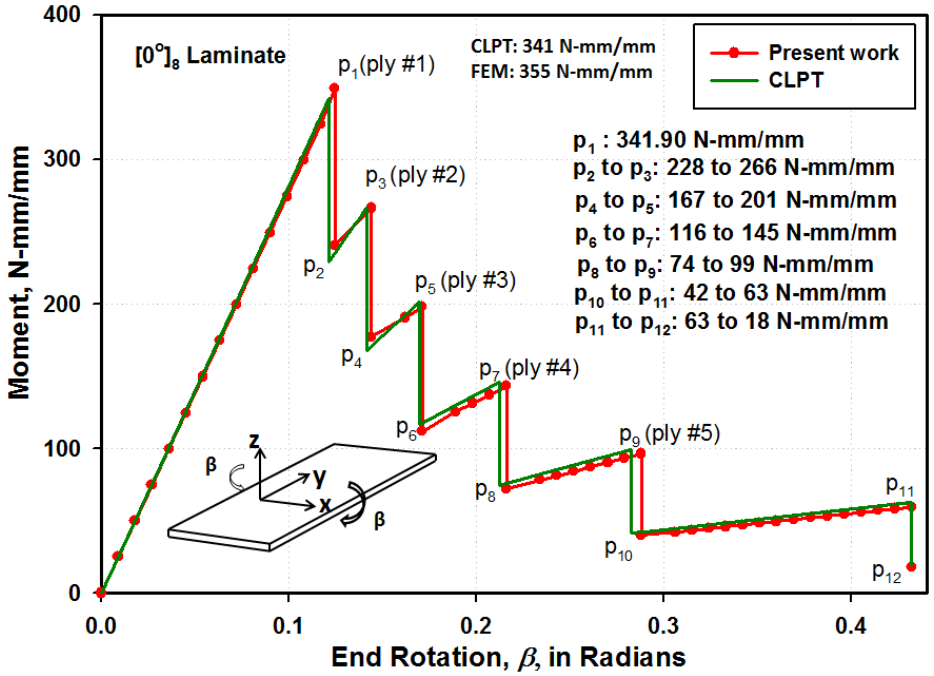

Figure 2.22: Comparison of moment-rotation curves for the $[0^o]_8$ laminate obtained using Abaqus and CLPT (plies are sequentially numbered from bottom to top).

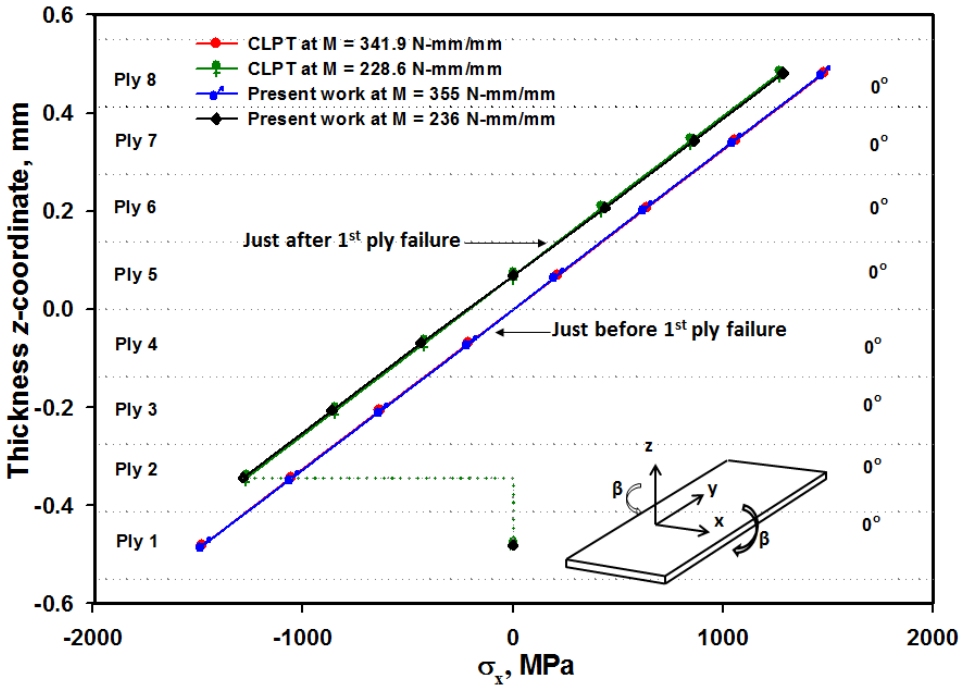

Figure 2.23: Through-the-thickness distribution of the axial stress, σ_x, for the first failure event (moment drop from 341.9 to 228.6 N-mm/mm) for the $[0^o]_8$ laminate

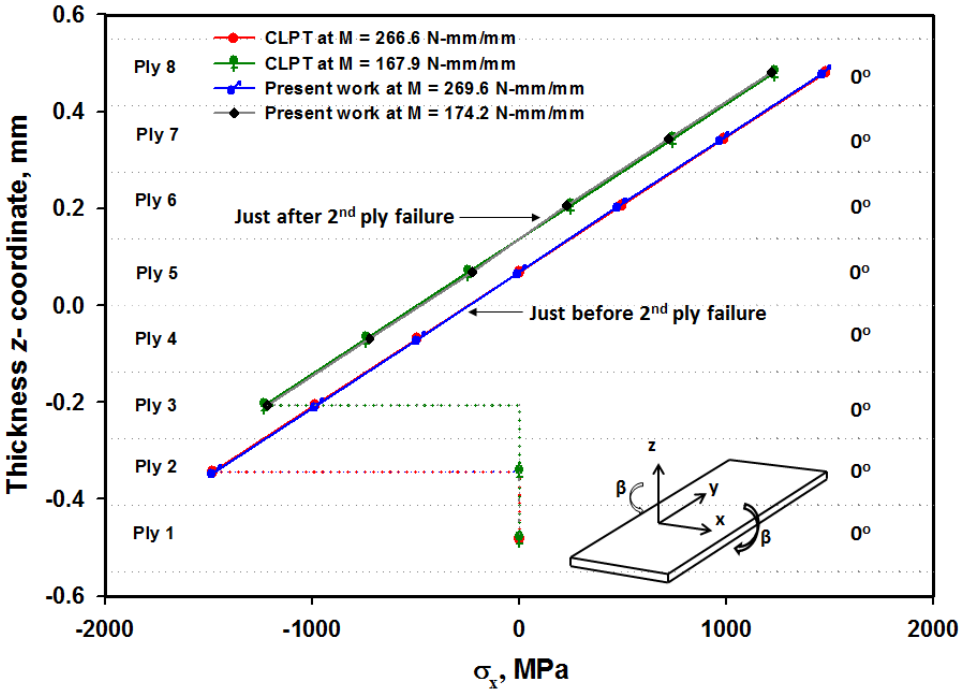

Figure 2.24: Through-the-thickness distribution of the axial stress, σ_x, for the second failure event (moment drop from 266.6 to 167.9 N-mm/mm) for the $[0^o]_8$ laminate

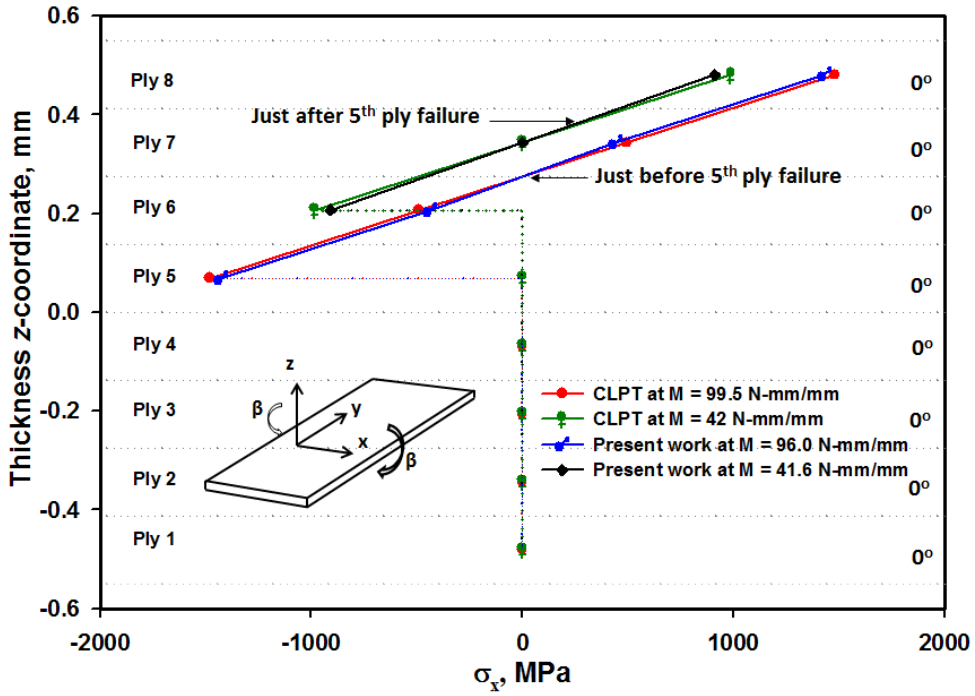

Figure 2.25: Through-the-thickness distribution of the axial stress, σ_x, when fibers in plies 1 through 4 have failed for the $[0^o]_8$ laminate

2.4.3 Cylindrical bending of $[0^o/45^o/90^o/-45^o]_S$ laminate

For the cylindrical bending of the quasi-isotropic laminate, the first failure occurs at M = 163 N-mm/mm in ply 7 due to the matrix failure in Mode A. The sequence of failure and the corresponding bending moments are exhibited in the moment-edge rotation curve plotted in Fig. **2.26**. As stated above, elastic moduli of the ply are degraded due to the matrix failure; however, it still contributes to the load carrying capacity of the laminate. Thus the moment continues to increase with an increase in the rotations applied to the edges $x = 0, a$, until at M = 240 N-mm/mm fibers in ply 1 fail due to the compressive axial stress, and ply 1 is deleted from the analysis. Failure of ply 1 reduces the load carrying capacity of the laminate. In Fig. **2.26** D/L at point q_7 means a possibility of delamination or local buckling of fibers in a ply. For deformations of the laminate corresponding to point q_5 in Fig. **2.26**, three failure modes occur simultaneously, i.e., fibers in ply 2 fail in compression, the matrix in ply 3 completely fails in Mode C, and the Mode C matrix failure initiates in ply 4. We note that at complete failure of the laminate, the edge rotations are very large for the linear theory to be applicable. For all practical purposes, the structure has lost the load carrying capacity when its deformations correspond to point q_7 in Fig. **2.26**. The redistribution of stresses before and after each major drop in the load are shown in Figs. **2.27-2.32** in the global coordinate system. When fibers fail the redistribution of stresses between plies is large**.**

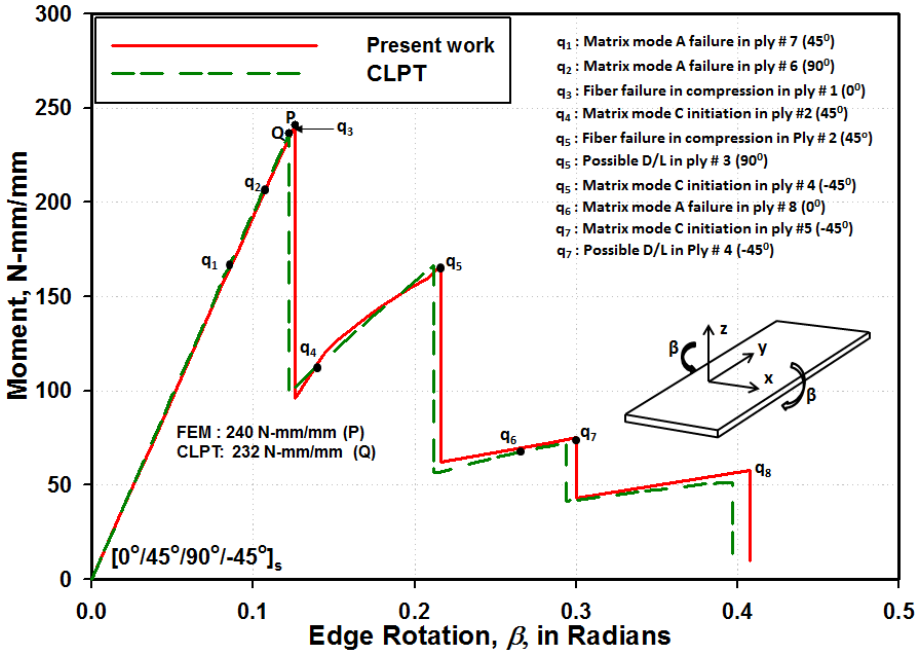

2.26: Comparison of moment-rotation curves for the [0º/45º/90º/-45º]$_S$ laminate obtained using Abaqus and the CLPT

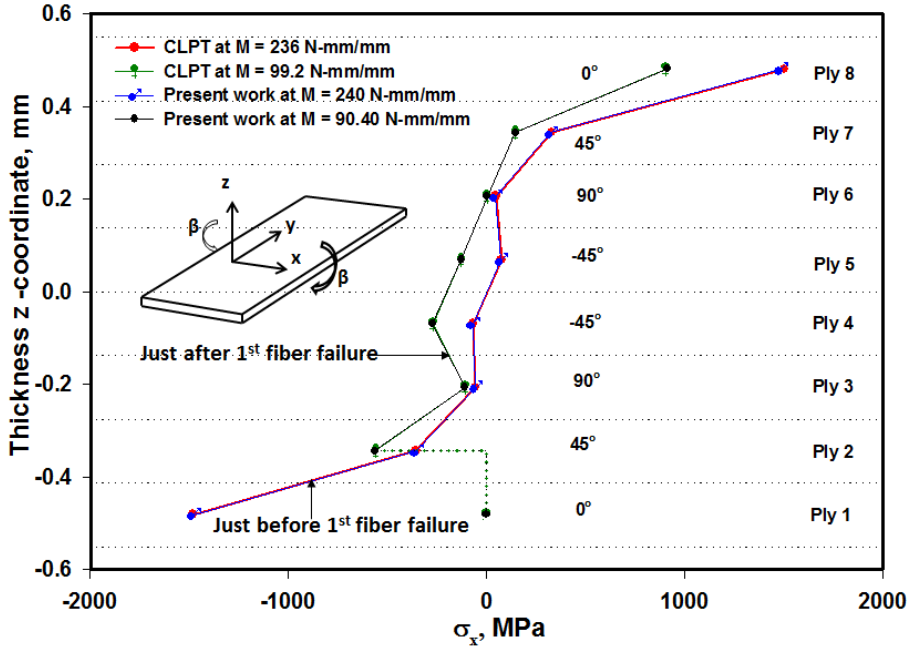

Figure 2.27: Through-the-thickness distribution of the stress, σ_x, for the first fiber failure for the [0º/45º/90º/-45º]$_S$ laminate

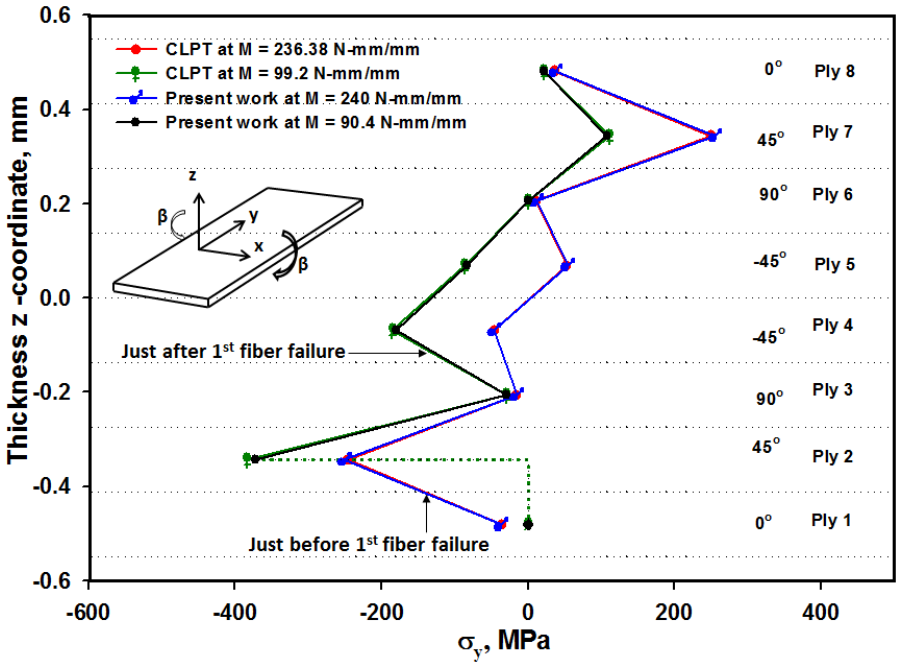

Figure 2.28: Through-the-thickness distribution of the stress, σ_y, for the first fiber failure for the $[0^o/45^o/90^o/-45^o]_S$ laminate.

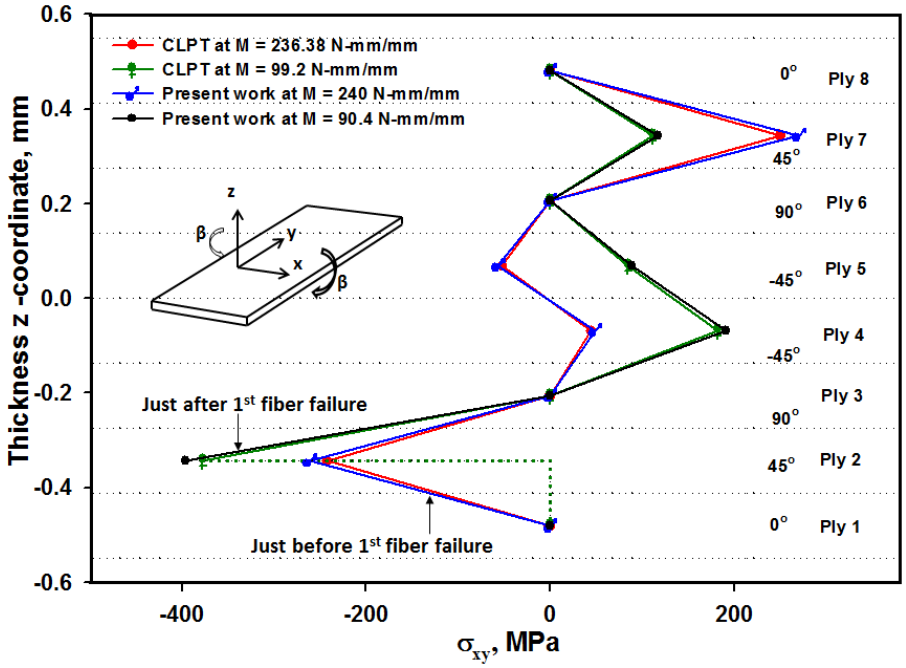

Figure 2.29: Through-the-thickness distribution of the stress, σ_{xy}, for the first fiber failure for the $[0^o/45^o/90^o/-45^o]_S$ laminate.

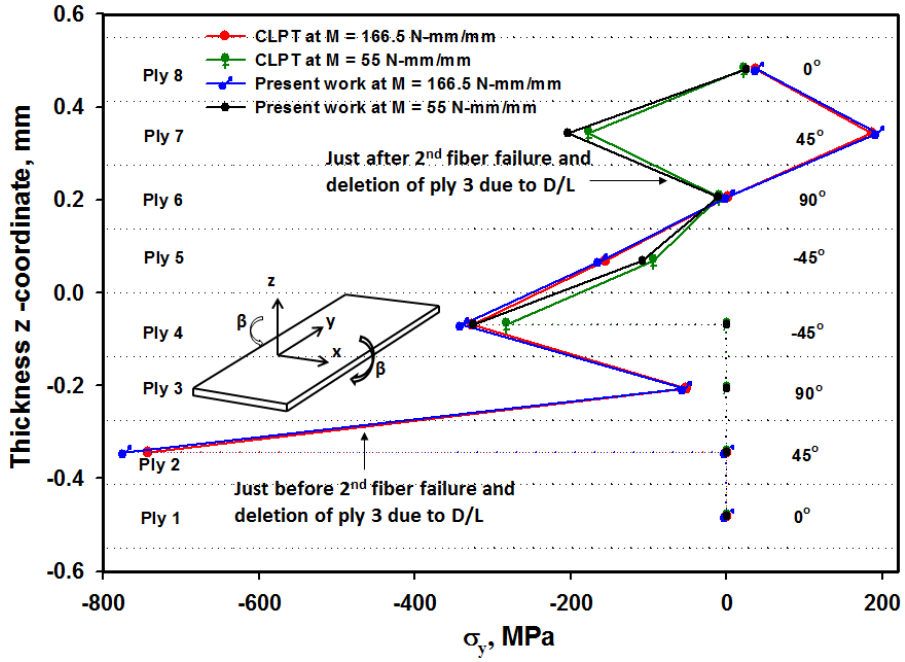

Figure 2.30: Through-the-thickness distribution of the stress, σ_y, for the second major failure event, (moment drop from 166 to 55 N-mm/mm) for the $[0^o/45^o/90^o/-45^o]_S$ laminate.

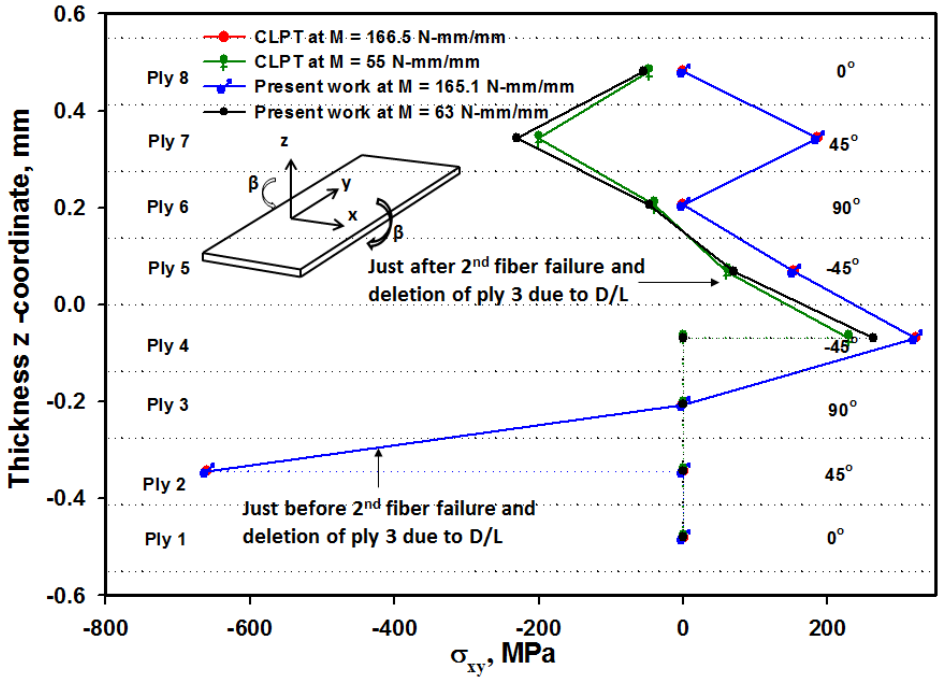

Figure 2.31: Through-the-thickness distribution of the stress, σ_{xy}, for the second major failure event, (moment drop from 166 to 55 N-mm/mm) for the $[0^o/45^o/90^o/-45^o]_S$ laminate.

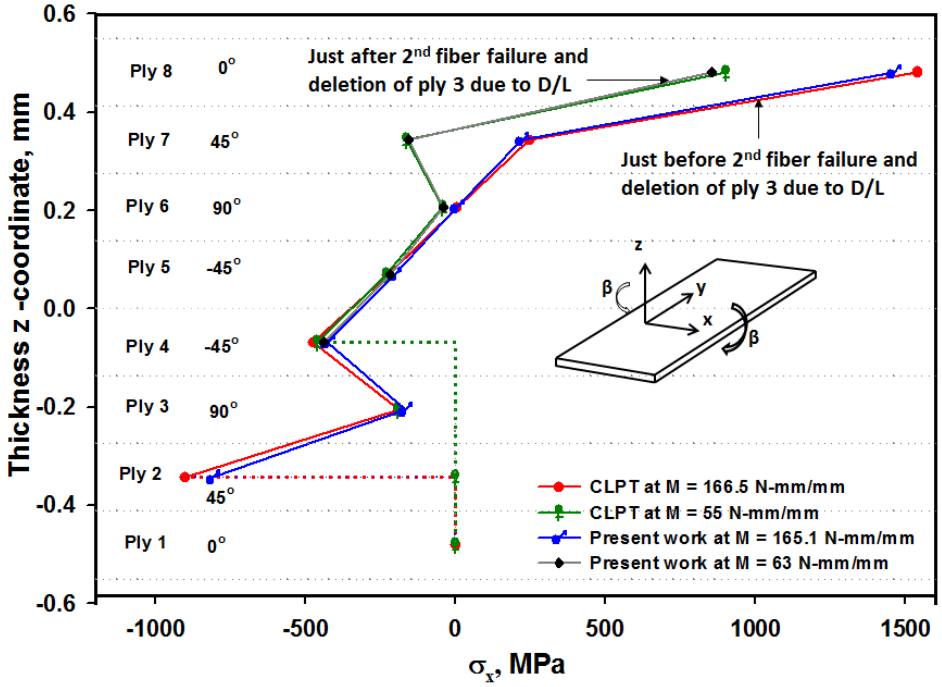

Figure 2.32: Through-the-thickness distribution of the stress, σ_x, for the second major failure event, (moment drop from 166 to 55 N-mm/mm) for the $[0^o/45^o/90^o/-45^o]_S$ laminate.

Chapter 3

PFA of OHT Specimen

3.1 Introduction

The open hole tension (OHT) specimen falls in the category of notched plates. Chang *et al*. [43, 51, 52] developed a two dimensional progressive damage model considering three different failure modes to predict accumulated damage and the strength of composite OHT laminates with loaded and unloaded hole surfaces by using failure criteria of Yamada-Sun and Hashin [53, 18]. The PFA for notched composite laminates subjected to either tensile or compressive axial loads has also been presented by Tan and Nuismer [54], Tan [55] and Tan and Perez [56]. In Ref. [54], the PFA using C-shell elements based on the CLPT and in-plane stresses has been examined. Only in-plane ply failure was evaluated and the out-of-plane failure such as delamination was not considered. Moreover, the ply orientations in the laminate were assumed to be symmetric with respect to the mid-plane of the plate. An interlaminar failure of an OHT coupon has been studied by Satyanarayana and Przekop, [57]. Damage models for describing the matrix cracking and fiber fracture based on the finite element (FE) analysis of notched laminates are presented by Lo *et al*. [58] and Sleight [59]. Experimental studies for OHT specimen are presented by Las and Zemcik [60] and Shahid and Chang [61]. The experimental studies generally show the maximum load at which the structure catastrophically fails.

3.2 Problem description

The two OHT configurations studied in the current work are the same as those analyzed by Knight [62]. The PFA is performed by using Puck and Schürmann's failure theory implemented as a user defined subroutine, USDFLD, in the FE commercial software, Abaqus. Two stacking sequences of $[(0^o/90^o)_4]_S$ and $[(0^o/45^o/90^o/-45^o)_2]_S$ glass epoxy laminate are studied. The response of each ply is assumed to be linear elastic and transversely isotropic with the fiber direction as the axis of transverse isotropy. Values of material parameters with respect to coordinate axes along

the material principal directions, taken from Ref. [62], are: E_1 = 159.96 GPa, E_2 = 8.96 GPa, G_{12} = 6.2 GPa, ν_{12} = 0.278, X_T = 2.840 GPa, Y_T = 60 MPa, X_C = 570 MPa, Y_C = 167 MPa, S_L = 94.80 MPa and S_T = 45.6 MPa. For glass epoxy laminates, we take $p_{n1}^{(+)}$ = 0.25, $p_{n1}^{(-)}$ = 0.25, and $p_{nt}^{(-)}$ = 0.25 as suggested by Puck and Schürmann [13, 14].

The infinitesimal deformations of the laminate have been analyzed by assuming a plane stress state of deformation. The laminate is loaded by applying axial displacements at the two opposite edges while keeping them free of tangential tractions. The other two sides of the laminate and the hole surface are kept traction free. Due to stress concentrations at some points near the hole periphery, the damage induced in the structure is nonuniform. The damage induced in the matrix is used to degrade its elastic moduli. Rather than deleting an element in which the matrix has basically failed, we set its elastic moduli equal to 0.001% of their values for the undamaged laminate. However, upon fiber failure in an element, the modulus, E_1, in the fiber direction is set equal to zero. Thus the fiber failure is instantaneous but the matrix failure is gradual.

The "composite layup" feature in Abaqus has been used to model the stacking sequence of the laminate using **S4** shell elements. Figure **3.1** shows the specimen geometry; it has length = 228.6 mm, width = 25.4 mm, the diameter of the central hole = 6.35 mm, and each ply has a thickness of 0.16383 mm. The region **ABCD** shown in Fig. **3.2** is discretized into very small FEs in order to capture the stress singularity at points on the hole periphery. The axial load on the specimen is found from the normal tractions/reactions on the top surface of the specimen.

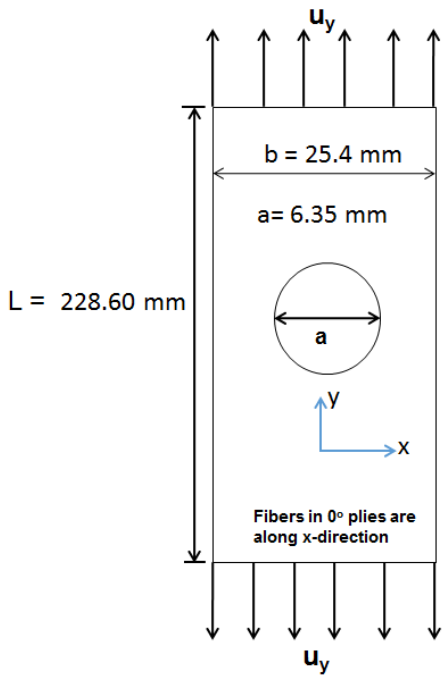

Figure 3.1: The open hole tension (OHT) configuration of Ref. [62].

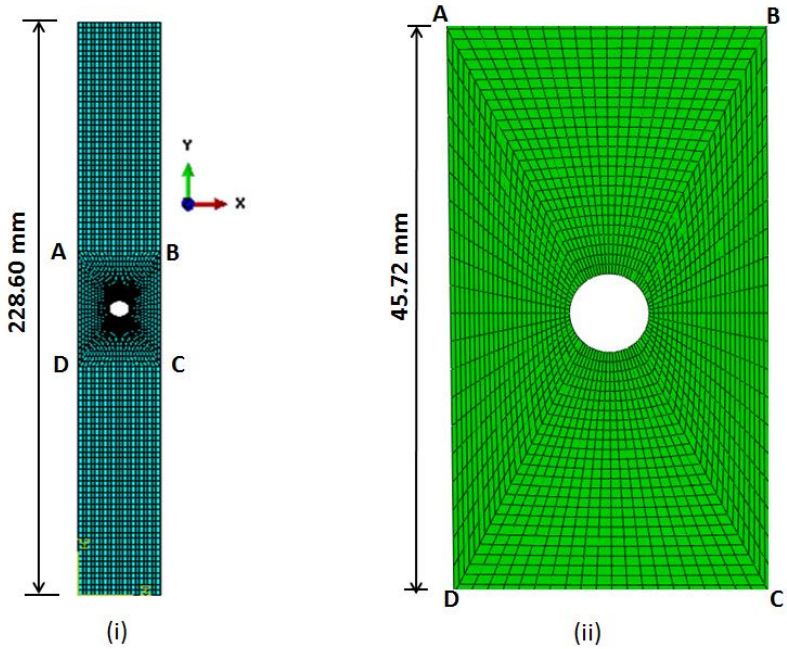

Figure 3.2: (i) FE mesh for the overall structure, (ii) magnified view of the FE mesh around the hole (region ABCD)

The dependence of the maximum load upon the number of elements in region ABCD, exhibited in Fig. **3.3**, reveals that a converged value of the maximum load, 42.8 kN, is found with 1530 elements in this region in each ply.

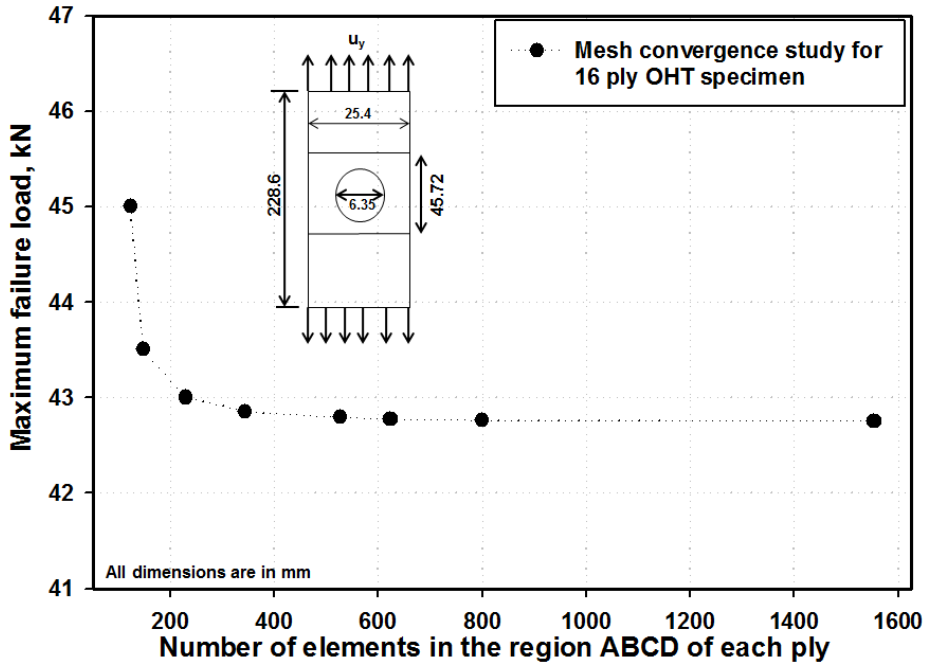

Figure 3.3: Maximum failure load for different FE meshes for the 16 ply OHT specimen. The solution converged for 1530 elements in the region ABCD around the hole in each ply.

3.2.1 Stress Concentration Study

As should be clear from results plotted in Figures **3.4** and **3.5** for the specimen made of isotropic and transversely isotropic materials (i.e., $[0^o]_{24}$ laminate), respectively, the converged values, 3.258 and 6.6, respectively, of the stress concentration factor are obtained by using the FE mesh with 1530 elements in the region ABCD around the hole. These converged values of the stress concentration factor agree well with those reported in the literature. Thus the FE mesh used is adequate for studying the PFA of the laminate.

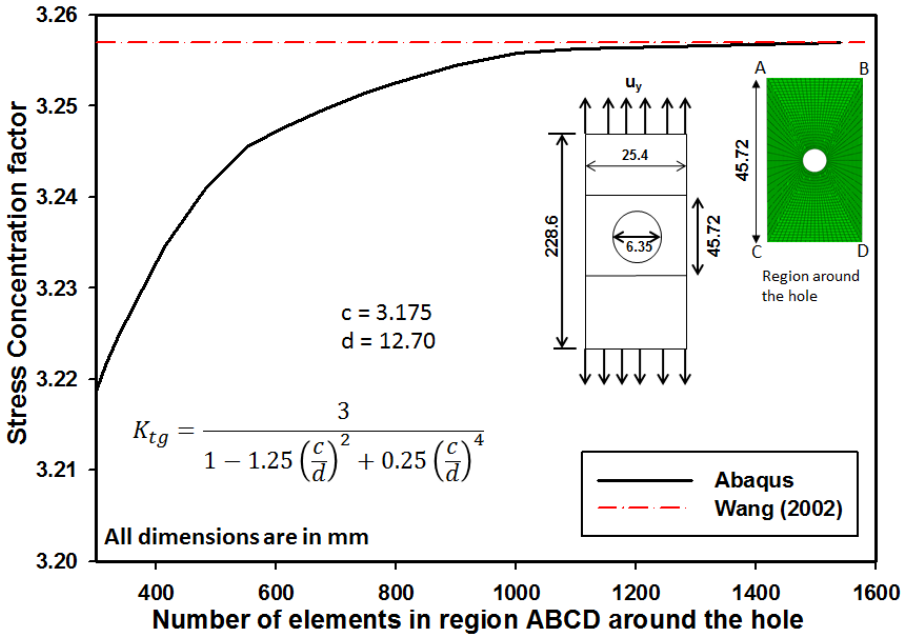

Figure 3.4: Stress concentration factor for an isotropic OHT specimen. The stress concentration factor converged for 1530 elements in the region ABCD around the hole.

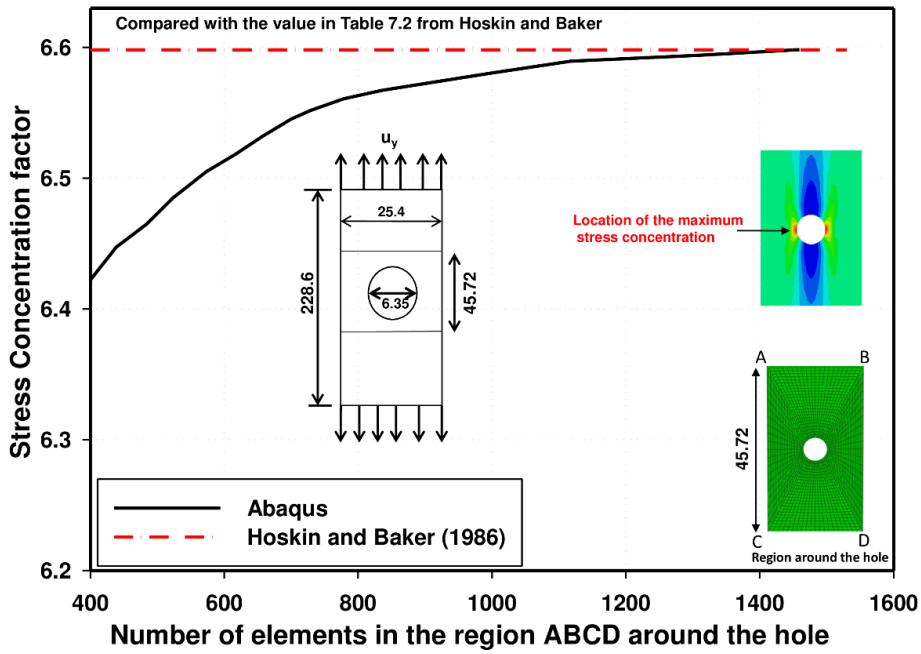

Figure 3.5: Stress concentration factor study for the $[0^o]_{24}$ OHT specimen. The stress concentration factor converged for 1530 elements in the region ABCD around the hole.

3.3 PFA of OHT $[(0^o/90^o)_4]_S$ laminate

The presently computed load-displacement response of the OHT $[(0^o/90^o)_4]_S$ laminate is compared in Fig. **3.6** with that of Knight, Ref. [62], who used three different failure criteria, namely the Tsai-Wu, the maximum stress and the maximum strain. Knight halved the element stiffness every time the failure initiated in either the matrix or the fiber or both. In the present work the material elasticities are degraded at a point after the matrix failure has initiated there. Because of the assumption of plane stress, the failure plane is parallel to the fibers. The value of the degradation parameter is found by ensuring that the failure criterion is satisfied with the degraded material moduli within a prescribed displacement increment. The number of iterations required within a displacement increment is reduced by taking very small increments in the applied displacement. When a fiber fails, the elastic modulus in the fiber direction is reduced to a value close to zero. However, the element can still support some load due to the presence of the matrix. For the problem studied, the maximum applied y-displacement equals 3.556 mm when the symmetric cross ply $[(0^o/90^o)_4]_S$ laminate [62] completely fails. The presently computed ultimate load, 42.8 kN, is slightly higher than the experimental value and that found by Knight using either the maximum stress-based or the maximum strain-based failure criterion. However, Knight's computed value of the peak load with the Tsai-Wu failure criterion is much smaller than that found experimentally.

The presently computed load-displacement curve prior to the onset of failure agrees very well with those computed by Knight using the three failure criteria mentioned above. However, subsequent to failure initiation the post-peak load-displacement curve strongly depends upon the failure criterion and the technique used to degrade material elasticities.

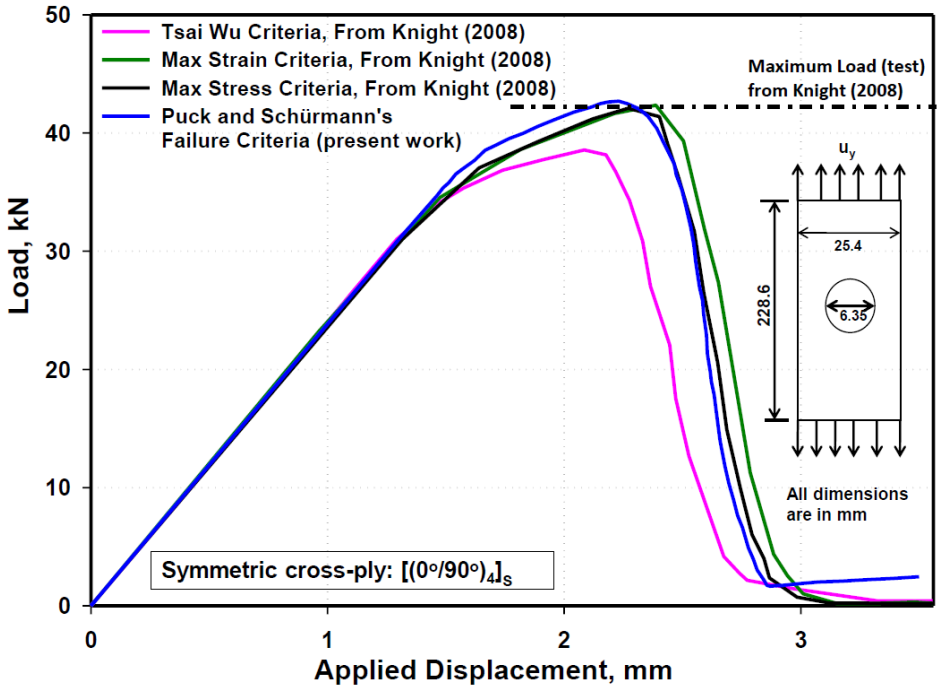

Figure 3.6: Presently computed and those reported in Ref. [62] load-displacement curves for the OHT $[(0^o/90^o)_4]_S$ laminate.

3.3.1 Mesh Dependency of Load-displacement Behavior

The presently computed load-displacement curves for the $[(0^o/90^o)_4]_S$ OHT specimen for two FE meshes with 810 and 1530 elements in the region ABCD (Fig. 3.2) around the hole are plotted in Fig. **3.7**. Whereas the two FE meshes give essentially the same value of the peak load, the post-peak load-displacement responses of the laminate are slightly different. Also, the maximum displacement at which the laminate completely fails is slightly higher for the finer mesh.

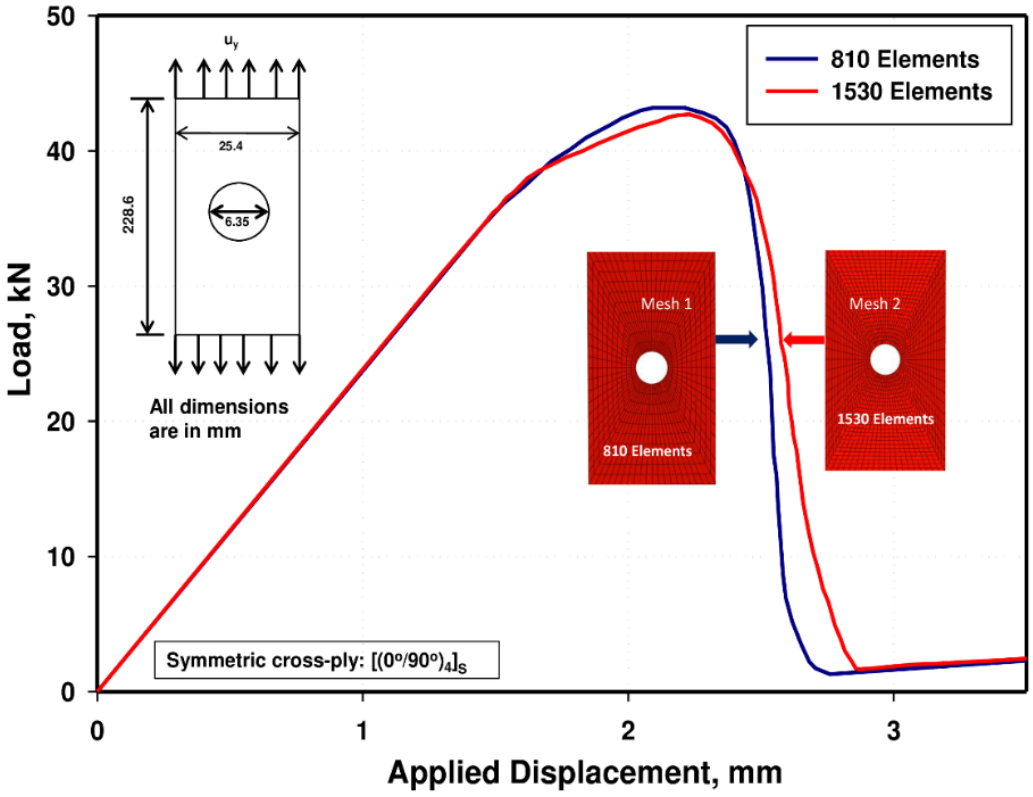

Figure 3.7: Load displacement curves for the OHT $[(0^o/90^o)_4]_S$ laminate for two different finite element meshes.

3.3.2 Failure Propagation in the OHT $[(0^o/90^o)_4]_S$ Laminate

Failure events for the OHT specimen are marked in Fig. **3.8** on the global load-displacement curve. The matrix failure initiates at points near the hole periphery in the 0^o plies in Mode A, followed by Mode A matrix failure in the 90^o plies. The first fiber failure occurs in the 90^o plies in tension. The failure sequence is described in some detail in sections 3.3.3 and 3.3.4. The stress concentration factor in the 90^o plies of the $[(0^o/90^o)_4]_S$ laminate was found to be 4.46.

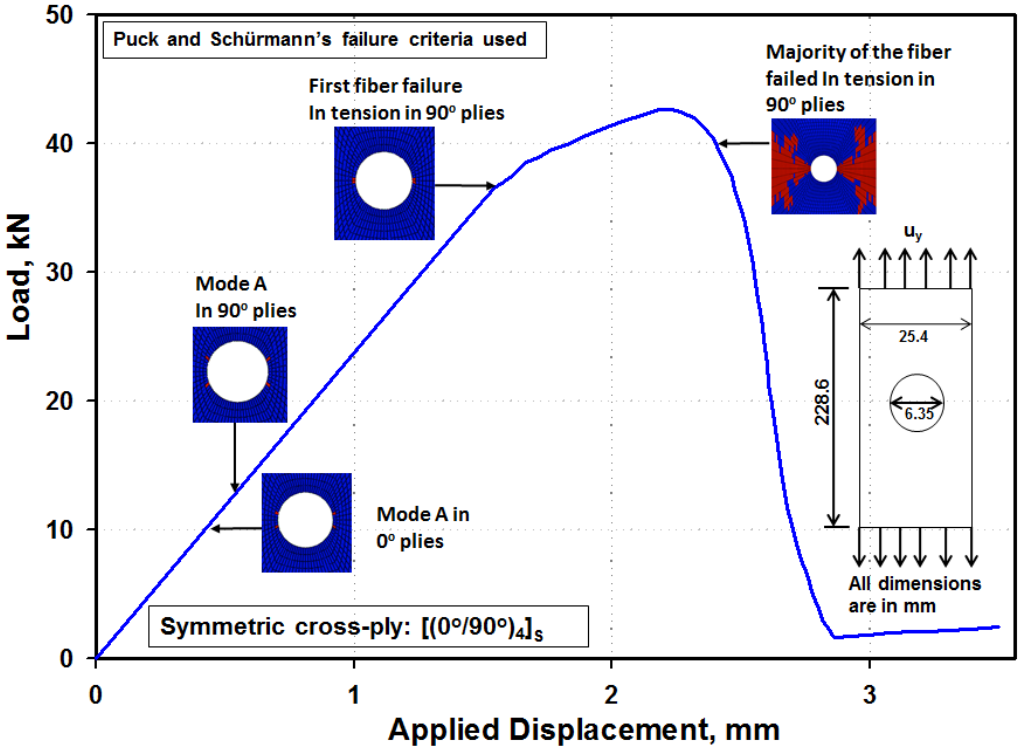

Figure 3.8: Load displacement curve for the OHT $[(0^o/90^o)_4]_S$ laminate showing instances of failure initiations.

3.3.3 Matrix Failure

Failure initiates at some points around the hole periphery in all 0^o plies (with fibers perpendicular to the applied displacement/load) in Mode A for the $[(0^o/90^o)_4]_S$ laminate at u_y = 0.4338 mm. Failure initiation in the matrix for the 90^o plies occurs in Mode A at u_y = 0.5440 mm. The Mode A degradation factors, η_a, in 0^o and 90^o plies with increasing applied displacement are shown in Figs. **3.9-3.15**. Whereas the matrix failure in the 0^o ply initiates in the 4 elements around the hole periphery that are very close to the horizontal axis passing through the hole center, that in the 90^o plies occurs in elements that are about one-third of the circumference away from the horizontal axis and at a higher value of the applied displacement. With an increase in the applied displacement the matrix failure spreads in elements first around the hole circumference and then in other elements along the loading direction. The matrix in the central region of the 0^o and the 90^o plies above and below the hole does not fail. Even though the matrix around the horizontal axis passing through the hole center has failed in the 0^o plies at

u_y = 2.2296 mm, that in the 90° plies has not. This could be due to fibers carrying most of the applied load in the 90° plies.

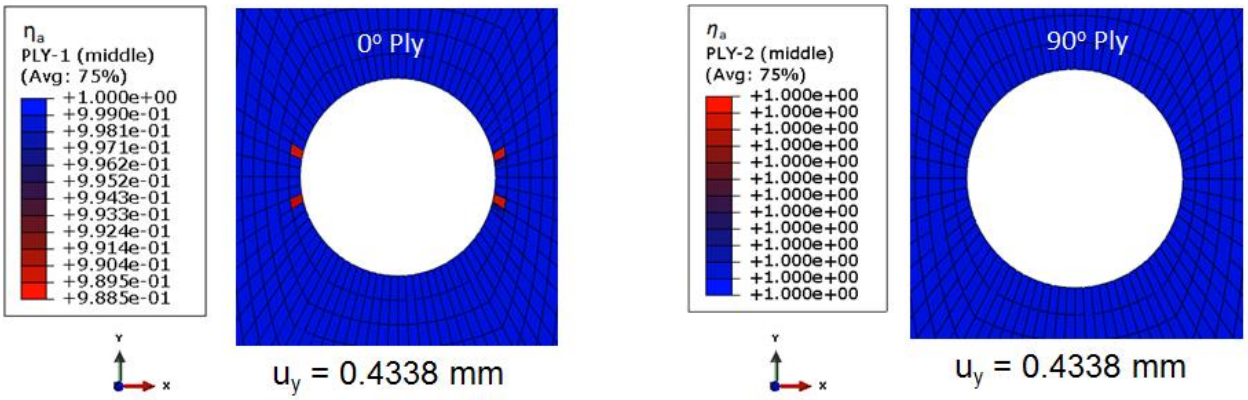

Figure 3.9: Fringe plot of the Mode A degradation factor, η_a, in 0° and 90° plies for the $[(0°/90°)_4]_S$ laminate at u_y = 0.4338 mm.

.

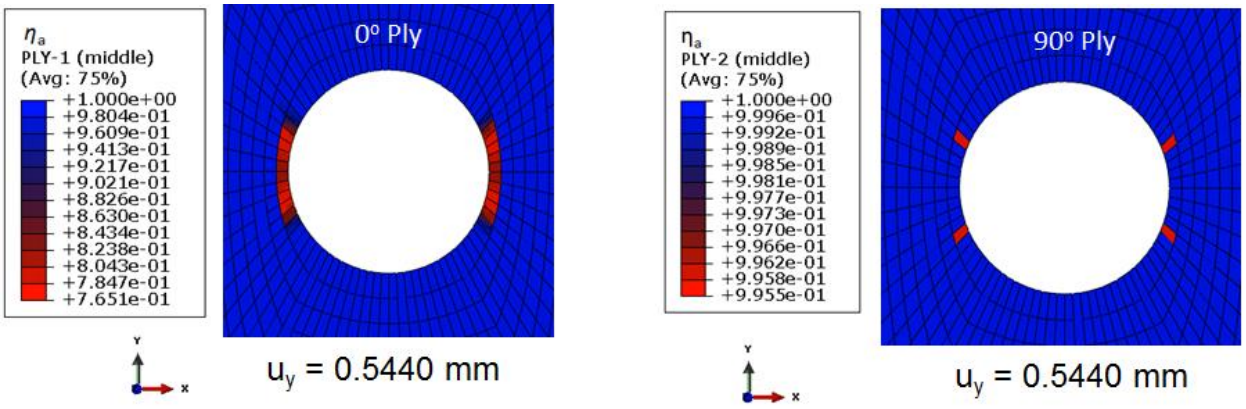

Figure 3.10: Fringe plot of the Mode A degradation factor, η_a, in 0° and 90° plies for the $[(0°/90°)_4]_S$ laminate at u_y = 0.5440 mm.

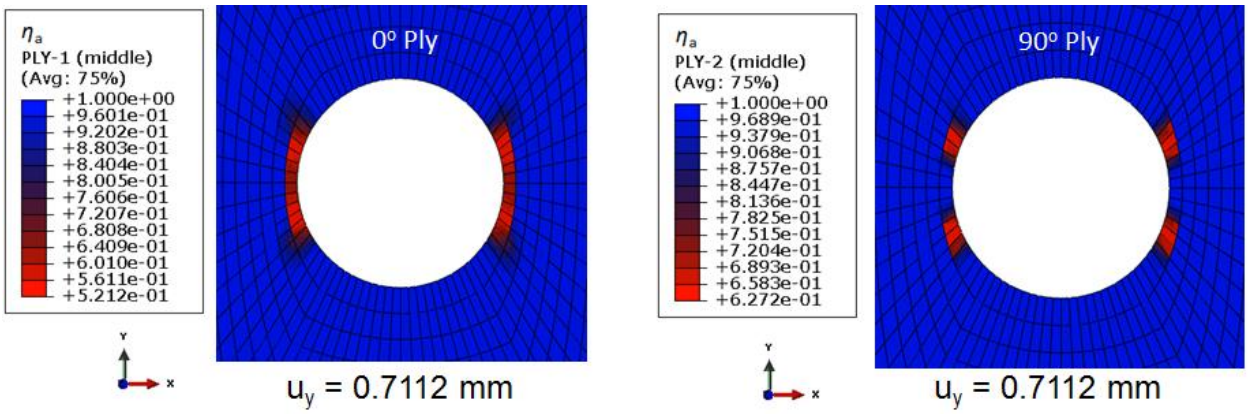

Figure 3.11: Fringe plot of the Mode A degradation factor, η_a, in 0° and 90° plies for the $[(0°/90°)_4]_S$ laminate at u_y = 0.7112 mm.

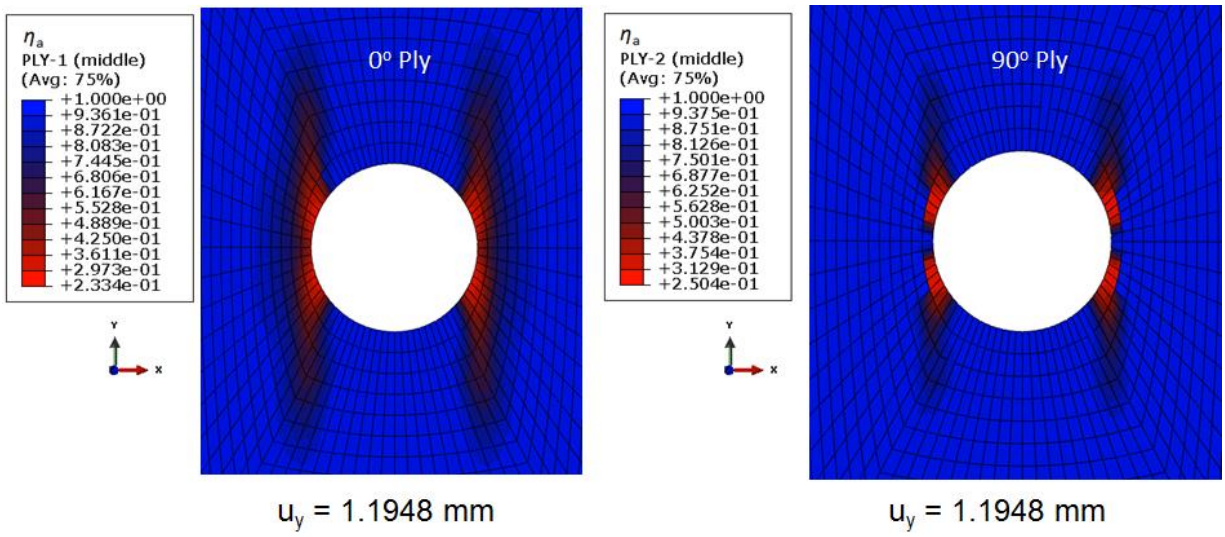

Figure 3.12: Fringe plot of the Mode A degradation factor, η_a, in 0° and 90° plies for the $[(0°/90°)_4]_S$ laminate at u_y = 1.1948 mm.

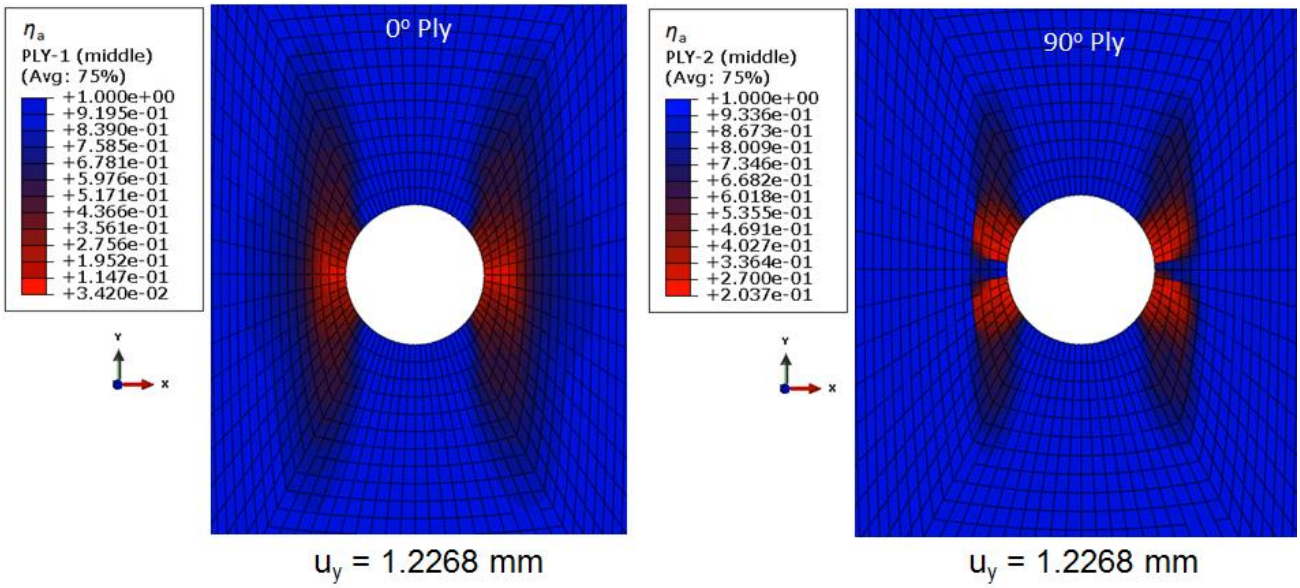

Figure 3.13: Fringe plot of the Mode A degradation factor, η_a, in 0° and 90° plies for the $[(0^o/90^o)_4]_S$ laminate at u_y = 1.2268 mm.

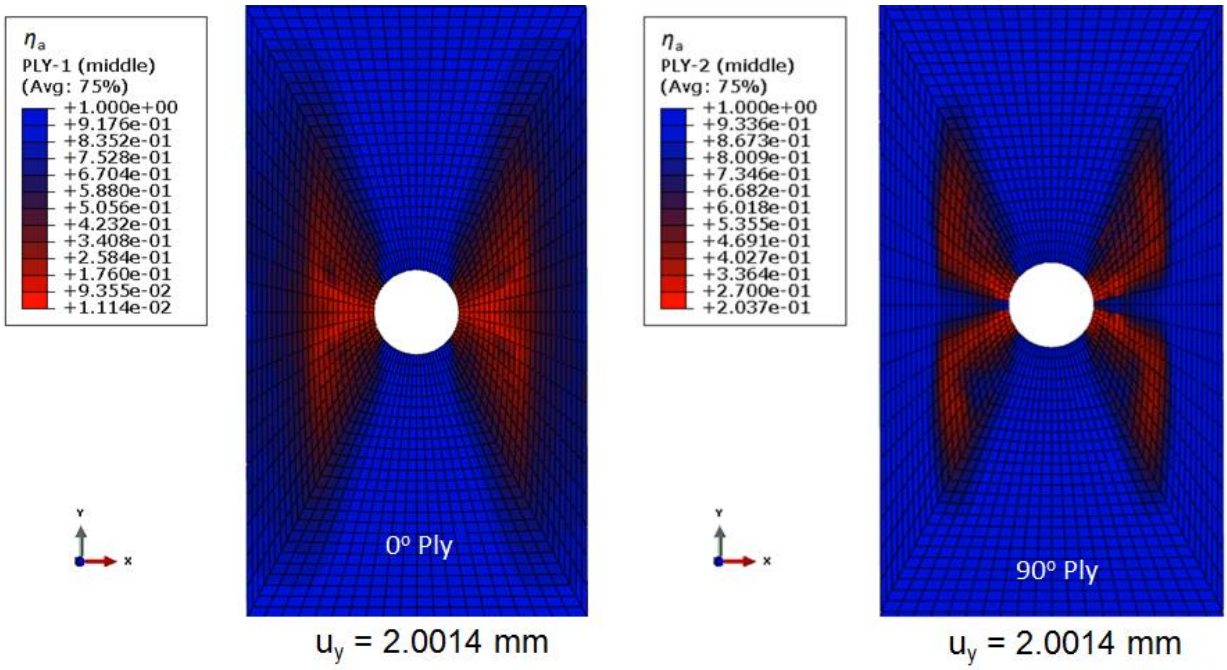

Figure 3.14: Fringe plot of the Mode A degradation factor, η_a, in 0° and 90° plies for the $[(0^o/90^o)_4]_S$ laminate at u_y = 2.0014 mm.

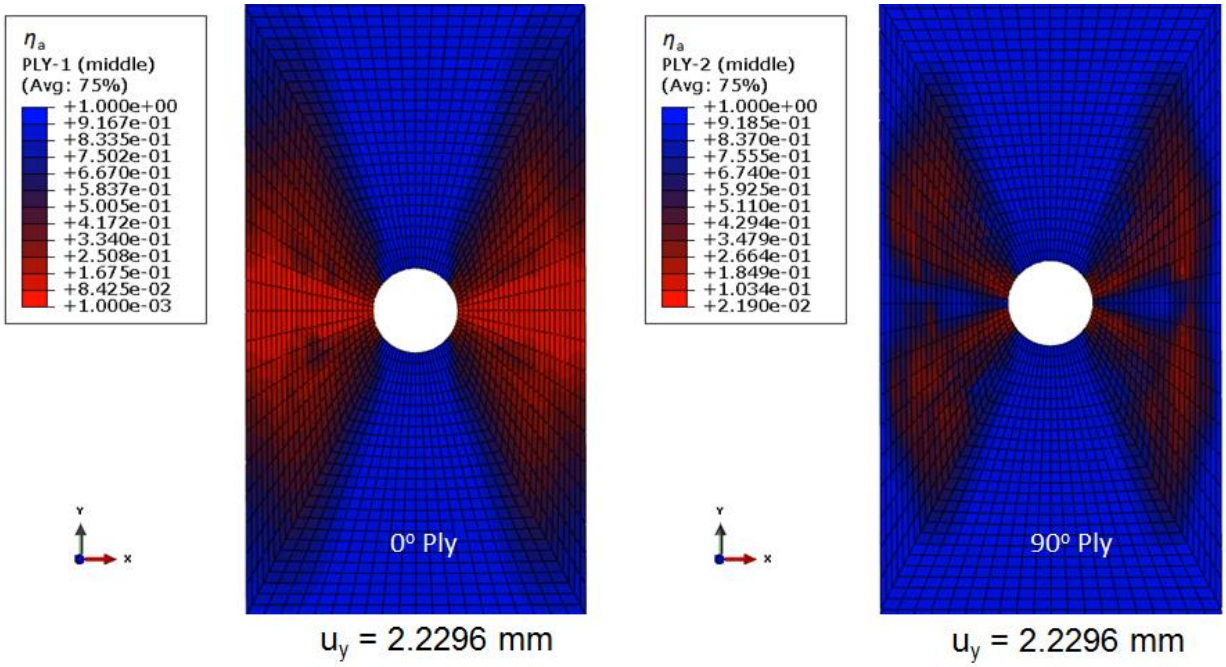

Figure 3.15: Fringe plot of the Mode A degradation factor, η_a, in 0º and 90º plies for the $[(0^o/90^o)_4]_S$ laminate at u_y = 2.2296 mm.

3.3.4 Fiber Failure

Fiber failure occurs in tension only in the 90º plies and no fiber failure is detected in the 0º plies of the laminate. As mentioned above, fibers in the 90º plies carry most of the applied load. The fiber failure regions are shown in Fig. **3.16** for the $[(0^o/90^o)_4]_S$ laminate at u_y = 2.34 mm beyond which the overall load carrying capacity of the laminate drops significantly. The fringe plots of the fiber failure indicate that all fibers on the horizontal centroidal axis in the 90º plies have failed thereby reducing their load carrying capacity to zero. The matrix in this region of the 0º plies has also either failed or has been severely weakened and contributes very little to the load carrying capacity of the laminate.

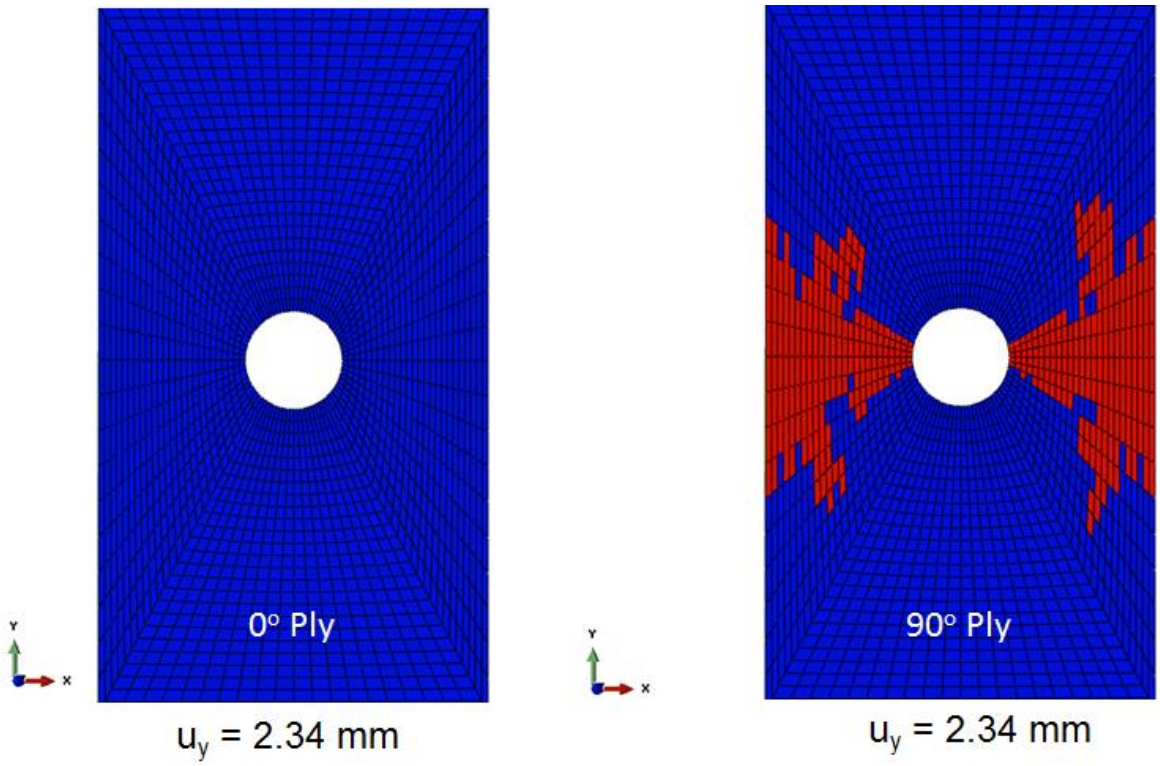

Figure 3.16: Fiber failure regions for the 0° and the 90° plies in the $[(0^o/90^o)_4]_S$ laminate at u_y = 2.34 mm.

3.3.5 Stress State Distribution in the OHT $[(0^o/90^o)_4]_S$ Laminate

The fiber failure in an element significantly affects the state of stress in that and adjoining elements. Subsequent to the fiber failure in an element, the load carrying capacity of the element decreases significantly. As a result the neighboring elements carry increased load and hence have higher values of stresses as shown in Figs. **3.17-3.20**. The fringe plots of the normal stresses σ_x and σ_y (normalized by E_1) for the 90° ply are shown in Fig. **3.17** for u_y = 1.491 mm. It is clear that σ_y has high values in two elements on the hole periphery that are also on either side of the horizontal centroidal axis. Fibers in these elements have failed when u_y = 1.51 mm and high values of σ_y now occur in the next two elements. For u_y = 1.544 large values of σ_y occur in six elements with fibers about to fail. We note that stresses σ_x and σ_{xy} have very small values as compared to that of σ_y and hence do not contribute much to the material failure in the 90° plies.

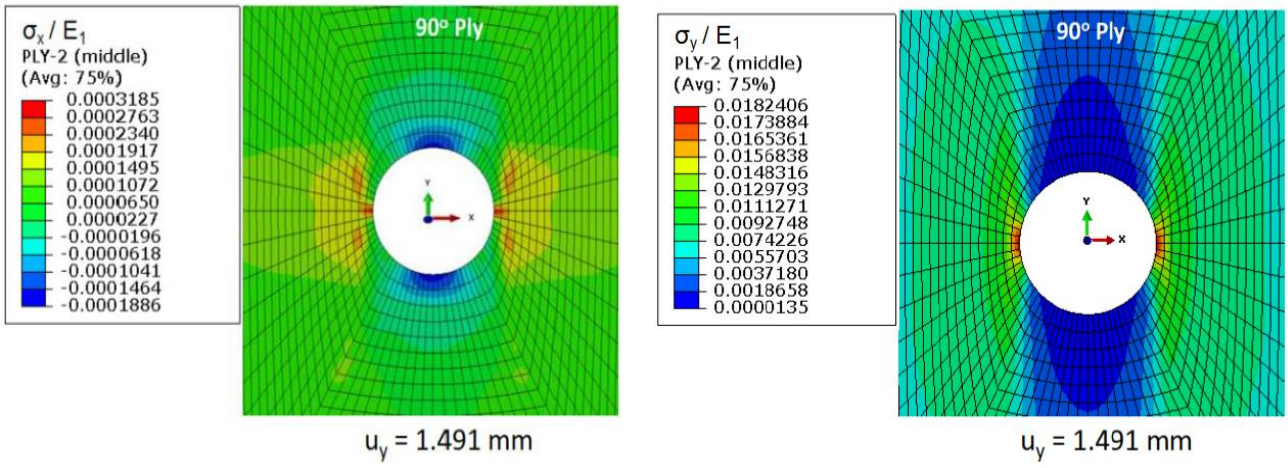

Figure 3.17: Fringe plots of σ_x and σ_y in 90º plies in the $[(0^o/90^o)_4]_S$ laminate at u_y = 1.491 mm.

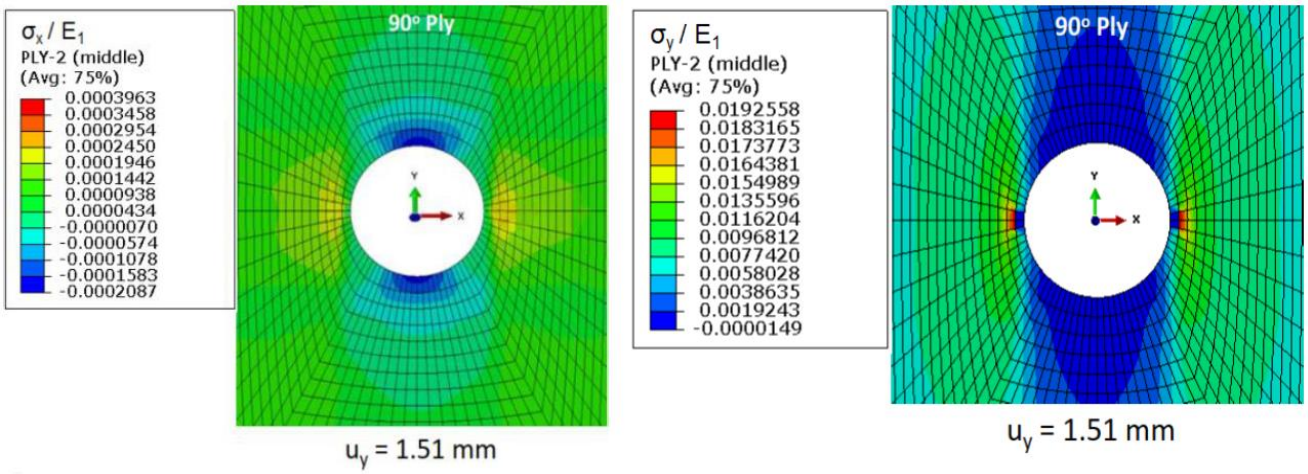

Figure 3.18: Fringe plots of σ_x and σ_y in 90º plies in the $[(0^o/90^o)_4]_S$ laminate at u_y = 1.51 mm.

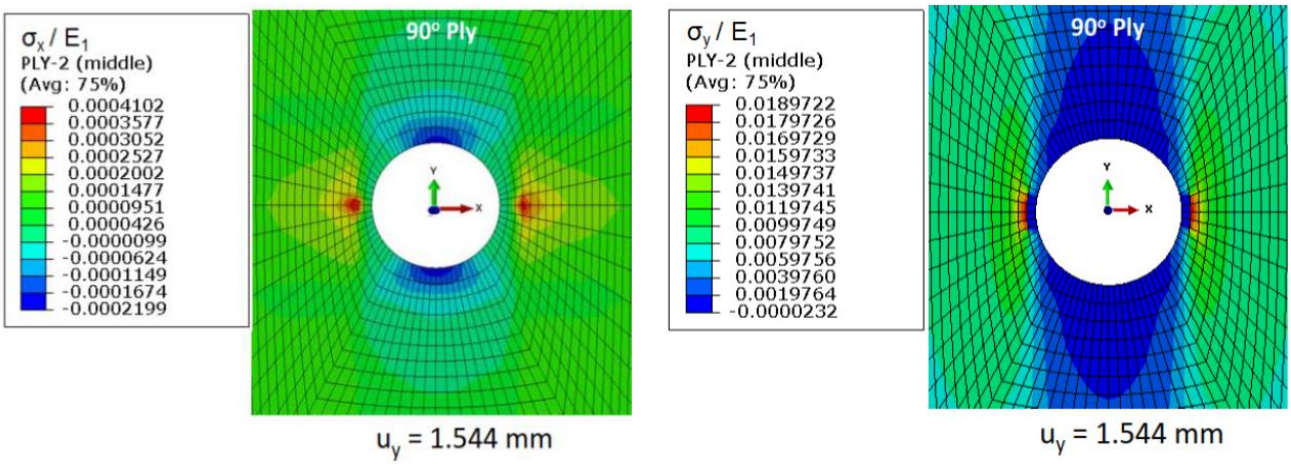

Figure 3.19: Fringe plots of σ_x and σ_y in 90° plies in the $[(0^o/90^o)_4]_S$ laminate at u_y = 1.544 mm.

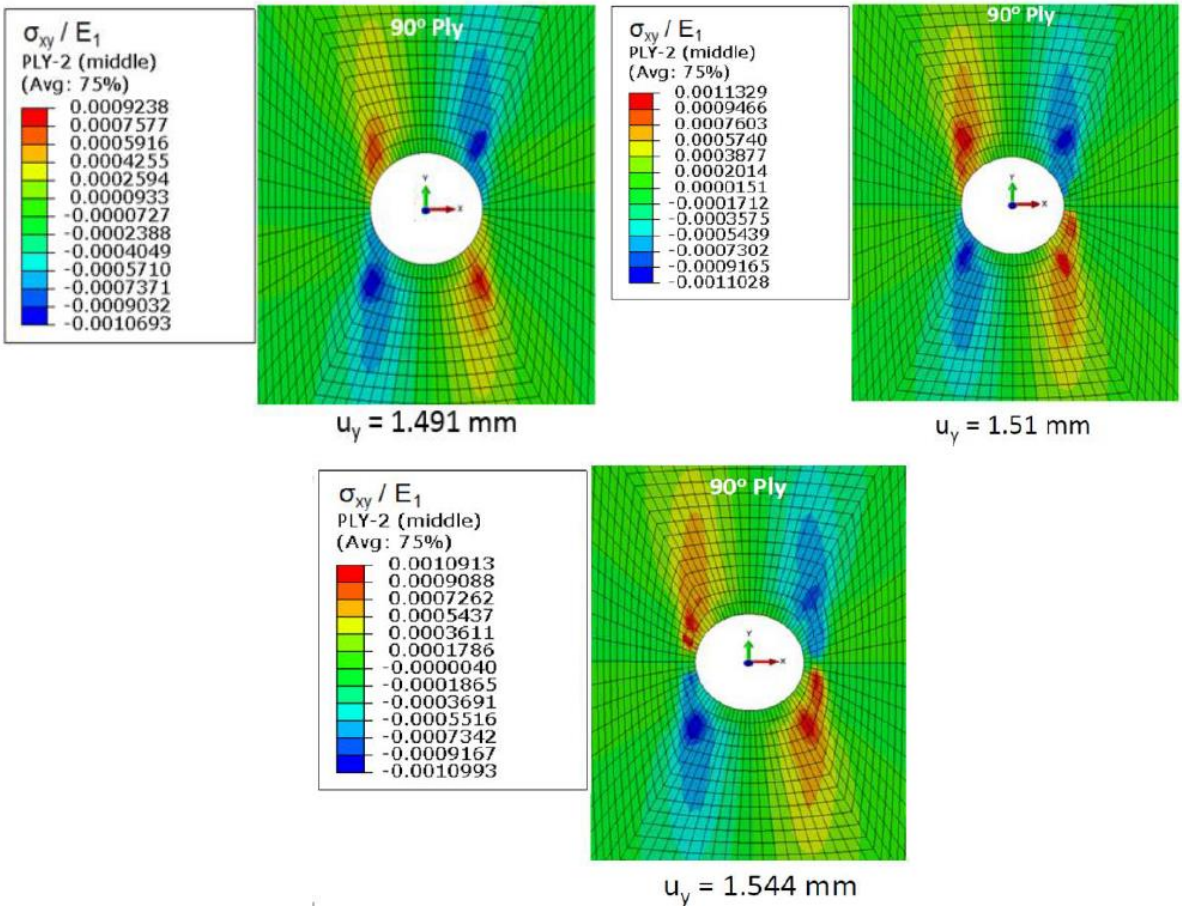

Figure 3.20: Fringe plots of σ_{xy} in 90° plies in the $[(0^o/90^o)_4]_S$ laminate at u_y = 1.491, 1.510, and 1.544 mm.

3.4 PFA of OHT Quasi-isotropic $[(0^o/45^o/90^o/-45^o)_2]_S$ Laminate

We now analyze the progressive failure of the OHT quasi-isotropic $[(0^o/45^o/90^o/-45^o)_2]_S$ laminate that has also been studied by Knight [62] with the goal of understanding the effect of stacking sequence on the laminate failure. The specimen geometry and the material properties are the same as those in the previous example problem. The load-displacement curve, depicted in Fig. **3.21**, reveals that the laminate completely fails at the maximum applied *y*-displacement of 5.08 mm as compared to 3.556 mm for the symmetric cross ply $[(0^o/90^o)_4]_S$ laminate. The computed maximum load of 31 kN supported by the laminate is slightly less than the experimental value of 33 kN but is little higher than that found by Knight [62] with the maximum stress and the maximum strain criteria. Knight also showed that the Hashin failure criteria gave the maximum load of 26.62 kN which is much less than the experimental value of 33 kN. It is because there is no material degradation considered in Hashin's failure criteria and the laminate is assumed to have failed when either the matrix or the fiber has failed in only one element. Thus it severely underestimates the load carrying capacity of the laminate. We recall that the maximum load supported by the symmetric cross ply $[(0^o/90^o)_4]_S$ laminate equaled about 42.8 kN.

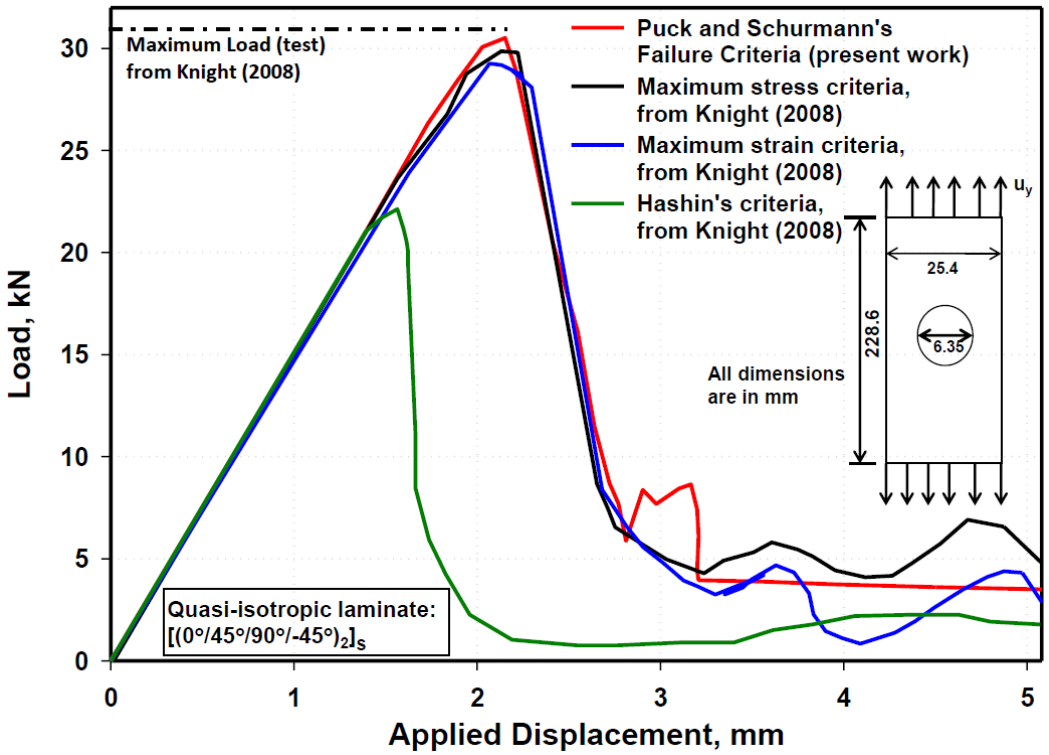

Figure 3.21: Presently computed and those reported in Ref. [62] load-displacement curves for the OHT $[(0^o/45^o/90^o/-45^o)_2]_S$ laminate.

3.4.1 Failure propagation in the $[(0^o/45^o/90^o/-45^o)_2]_S$ laminate

First failure occurrences for the OHT specimen are depicted on the global load - displacement curve in Fig. **3.22**. The matrix failure initiates in the 0^o plies in Mode A for u_y = 0.8636 mm and is followed by the matrix Mode A failure in the $\pm 45^o$ plies at u_y = 1.016 mm. The matrix does not fail in the 90^o plies mainly because fibers carry most of the load. The first fiber failure in tension occurs in the 90^o plies at a much larger value of u_y. After the computed reaction force at the top and the bottom edges has peaked, fibers in nearly all elements on the horizontal centroidal axis in the 0^o and the 90^o plies fail in tension, and the load carrying capacity of the laminate rapidly diminishes to zero. However, fibers in many but not all elements of the $\pm 45^o$ plies that are near the horizontal centroidal axis have failed. The asymmetry in the failed elements in the $+45^o$ and the -45^o plies is most likely due to truncation errors in the numerical solution.

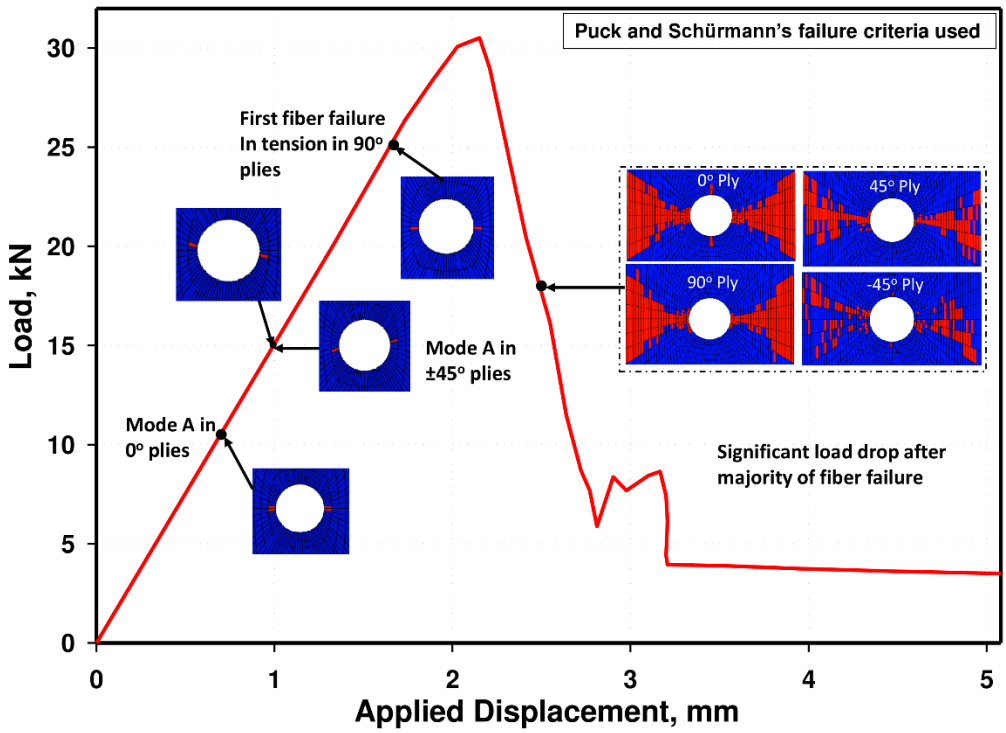

Figure 3.22: **Load-displacement curve for the OHT $[(0^o/45^o/90^o/-45^o)_2]_S$ laminate showing instances of failure initiations.**

Fringe plots of the Mode A degradation factor, η_a, in the 0^o, 90^o, 45^o and -45^o plies are shown in Figs. **3.23-3.32**. Fringe plots of the Mode A degradation parameter in the 45^o and -45^o plies are shown side by side in Figs. **3.23-3.32** at a fixed applied displacement to depict symmetry/antisymmetry in the progression of the damage in the two plies. As expected, due to stress concentration, the matrix Mode A failure initiates first at $u_y = 0.8386$ mm in the four elements on the hole periphery of the 0^o ply that are also on the centroidal horizontal axis. With the increase in the applied y-displacement to 1.016 mm the matrix failure spreads to two additional elements on the hole periphery in the 0^o ply, and initiates in two elements on the hole periphery of the $+45^o$ and the -45^o plies. With further increase in the y-displacement, the damaged regions in these plies first propagate essentially circumferentially, and then also radially. At $u_y = 2.286$ mm, the matrix in all elements on the horizontal centroidal axis in these plies has completely failed. We recall that the matrix in the 90^o plies does not fail mainly because fibers in these plies carry most of the load.

Fiber failure initiates in tension in the 90^o plies at u_y = 1.6713 mm, and at u_y = 2.540 mm fibers in all elements either on or close to the horizontal centroidal axes have failed thereby severely reducing the load carrying capacity of the laminate. The fiber failure regions are shown in Figs. **3.23** through **3.24** for the $[(0^o/45^o/90^o/-45^o)_2]_S$ laminate for different values of u_y.

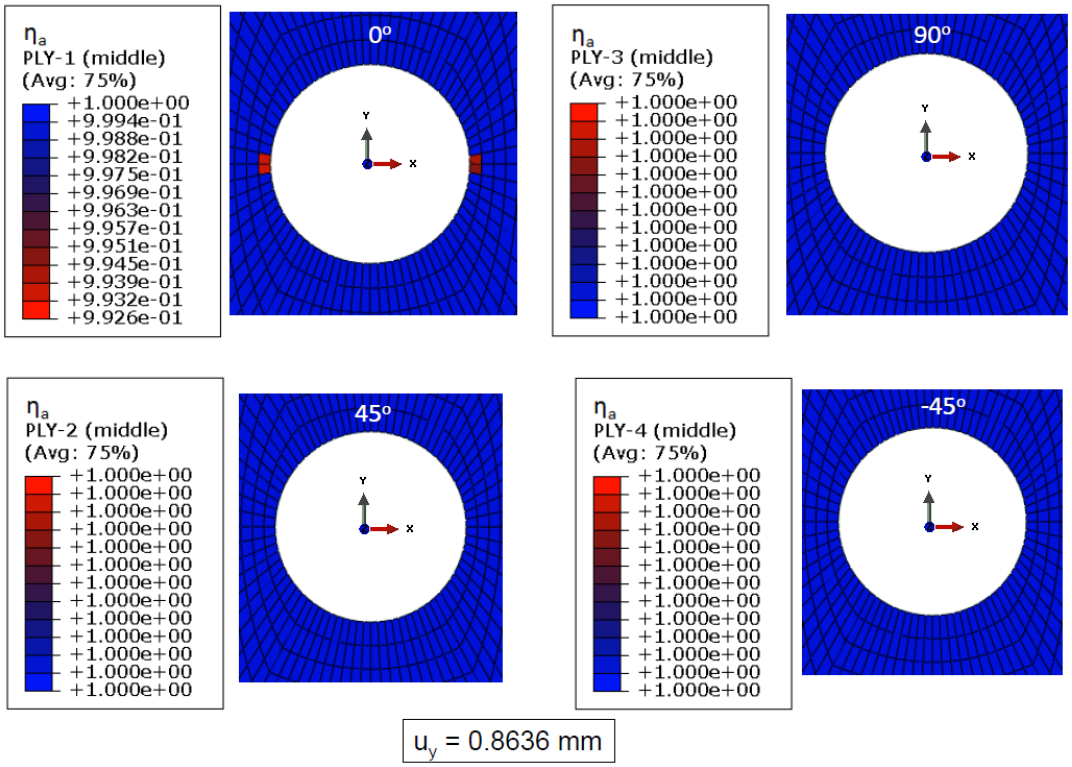

Figure 3.23: Fringe plots of the Mode A degradation factor, η_a, in 4 plies of the $[(0^o/45^o/90^o/-45^o)_2]_S$ laminate at u_y = 0.8636 mm.

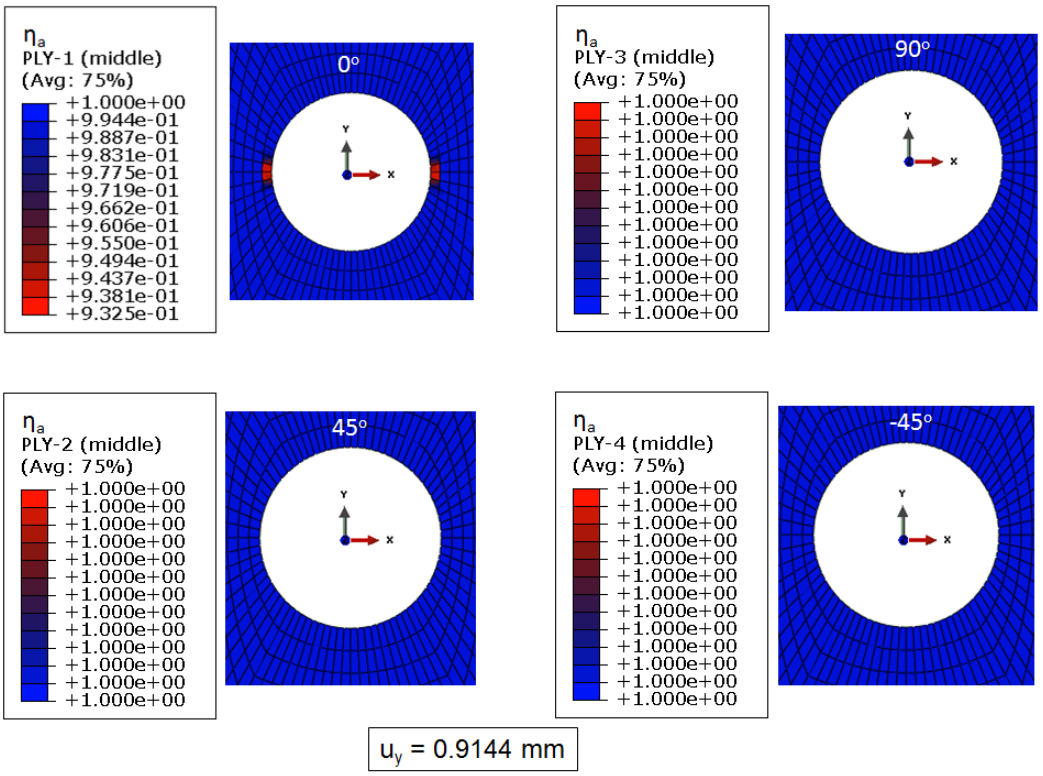

Figure 3.24: Fringe plots of the Mode A degradation factor, η_a, in 4 plies of the $[(0^o/45^o/90^o/-45^o)_2]_S$ laminate at u_y = 0.9144 mm.

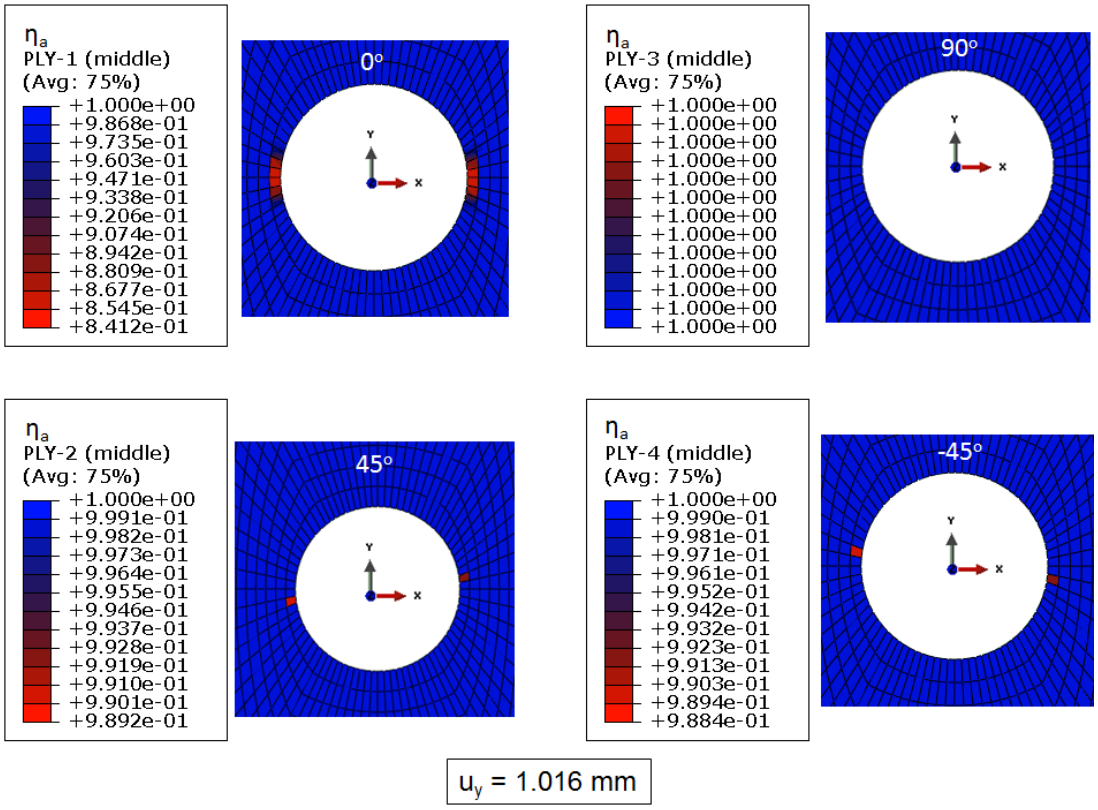

Figure 3.25: Fringe plots of the Mode A degradation factor, η_a, in 4 plies of the $[(0^o/45^o/90^o/-45^o)_2]_S$ laminate at u_y = 1.016 mm.

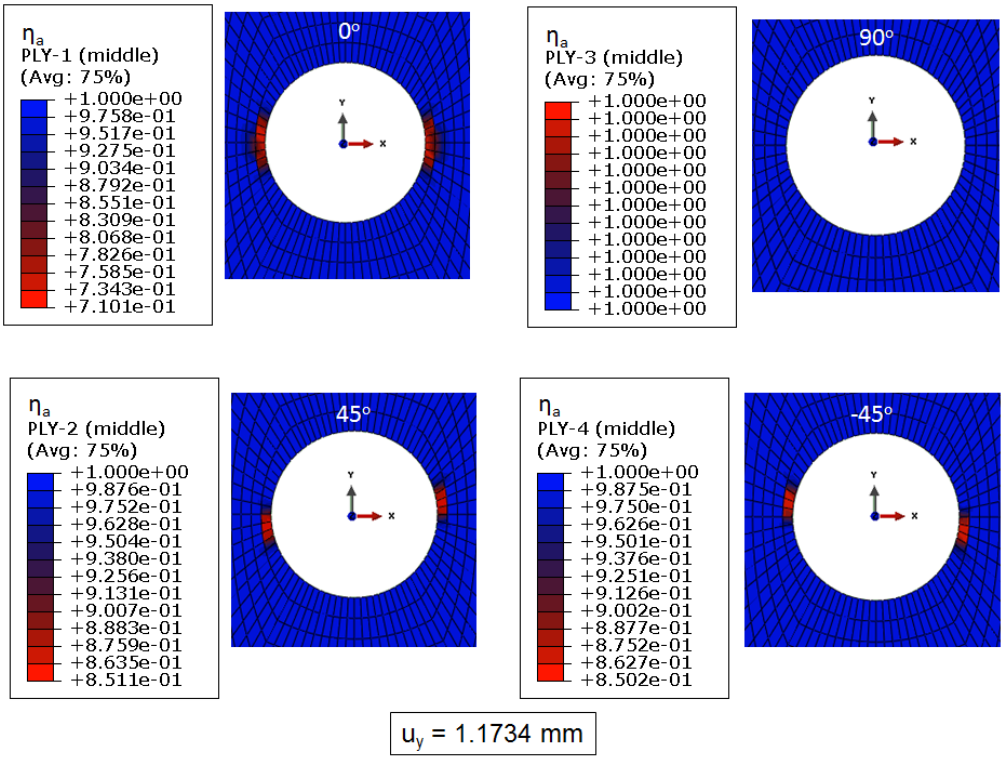

Figure 3.26: Fringe plots of the Mode A degradation factor, η_a, in 4 plies of the $[(0^o/45^o/90^o/-45^o)_2]_S$ laminate at u_y = 1.1734 mm.

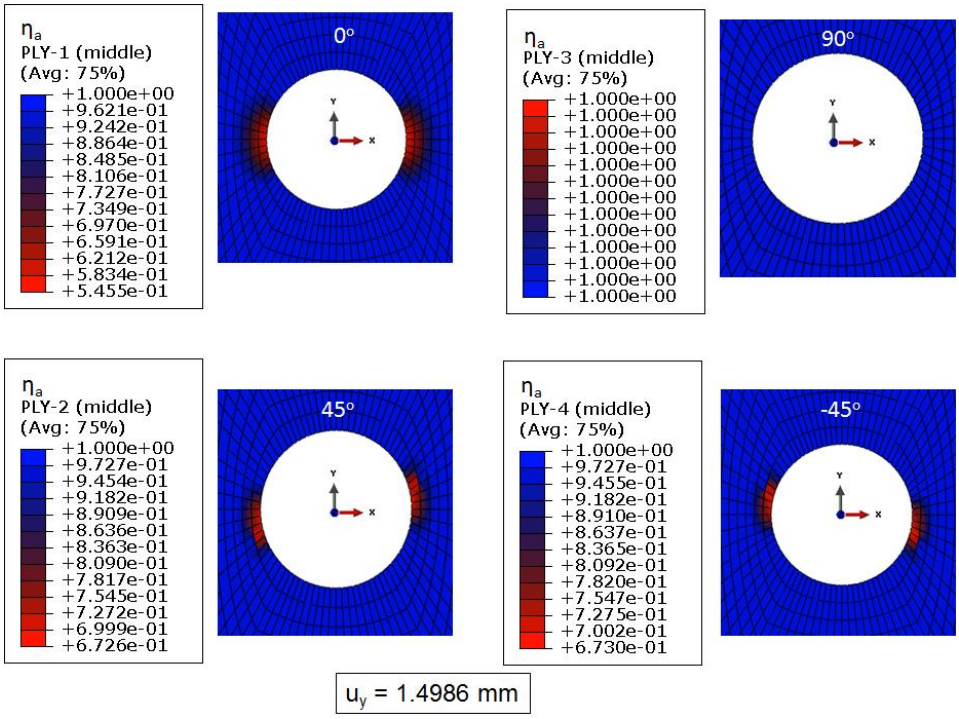

Figure 3.27: Fringe plots of the Mode A degradation factor, η_a, in 4 plies of the $[(0^o/45^o/90^o/-45^o)_2]_S$ laminate at u_y = 1.4986 mm.

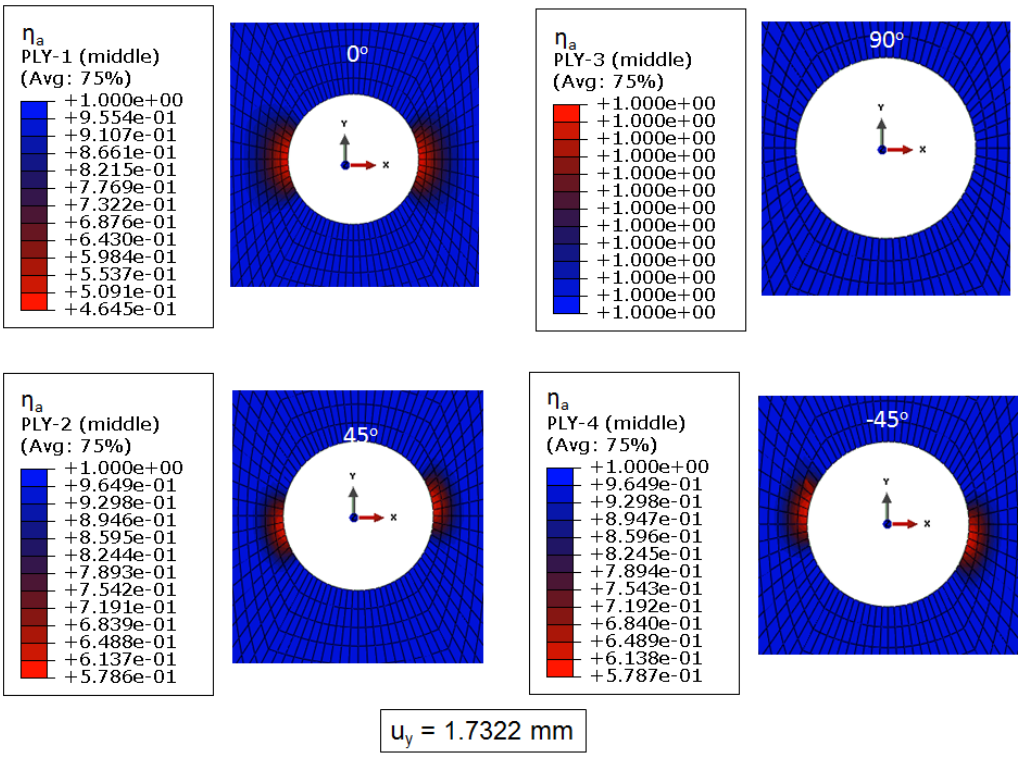

Figure 3.28: Fringe plots of the Mode A degradation factor, η_a, in 4 plies of the $[(0^o/45^o/90^o/-45^o)_2]_S$ laminate at u_y = 1.7322 mm.

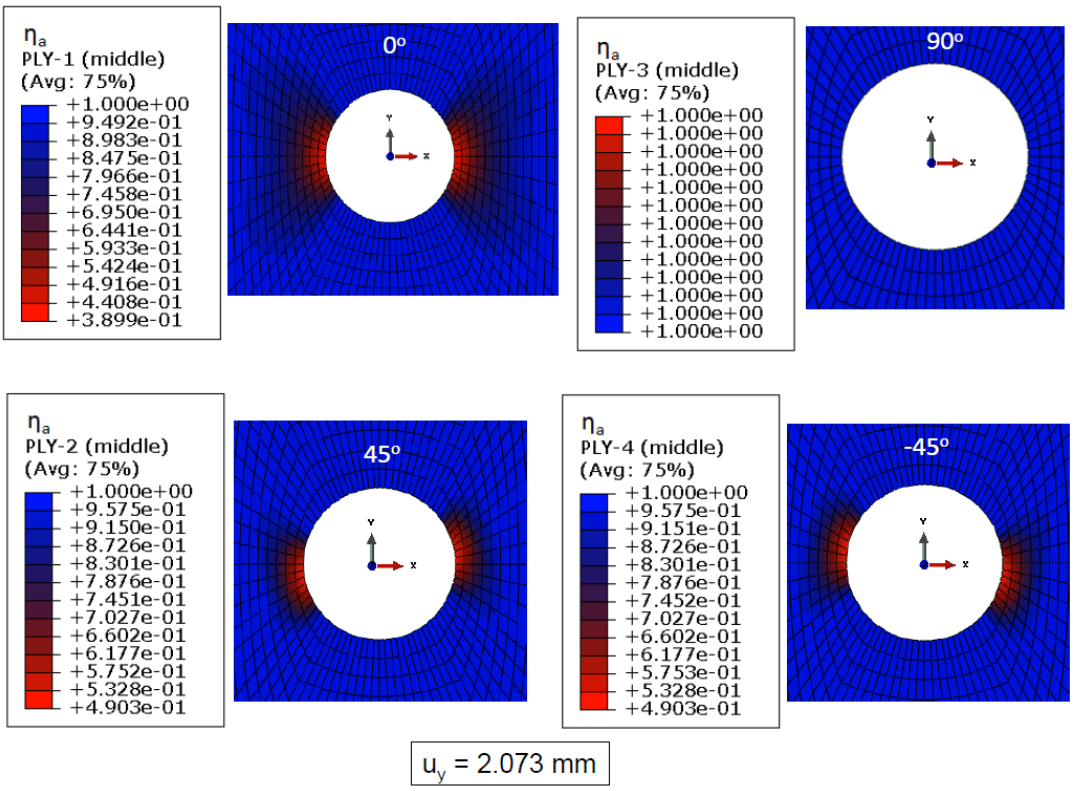

Figure 3.29: Fringe plots of the Mode A degradation factor, η_a, in 4 plies of the $[(0^o/45^o/90^o/-45^o)_2]_S$ laminate at u_y = 2.073 mm.

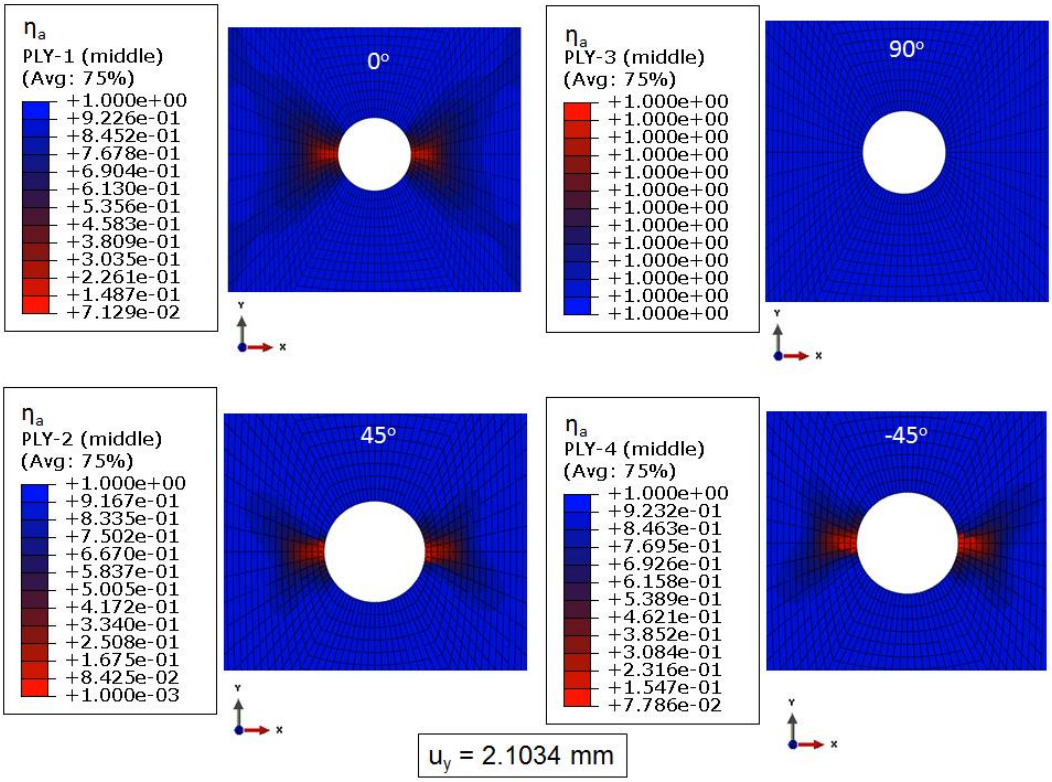

Figure 3.30: Fringe plot of the Mode A degradation factor, η_a, in 4 plies of the $[(0^o/45^o/90^o/-45^o)_2]_S$ laminate at u_y = 2.1034 mm.

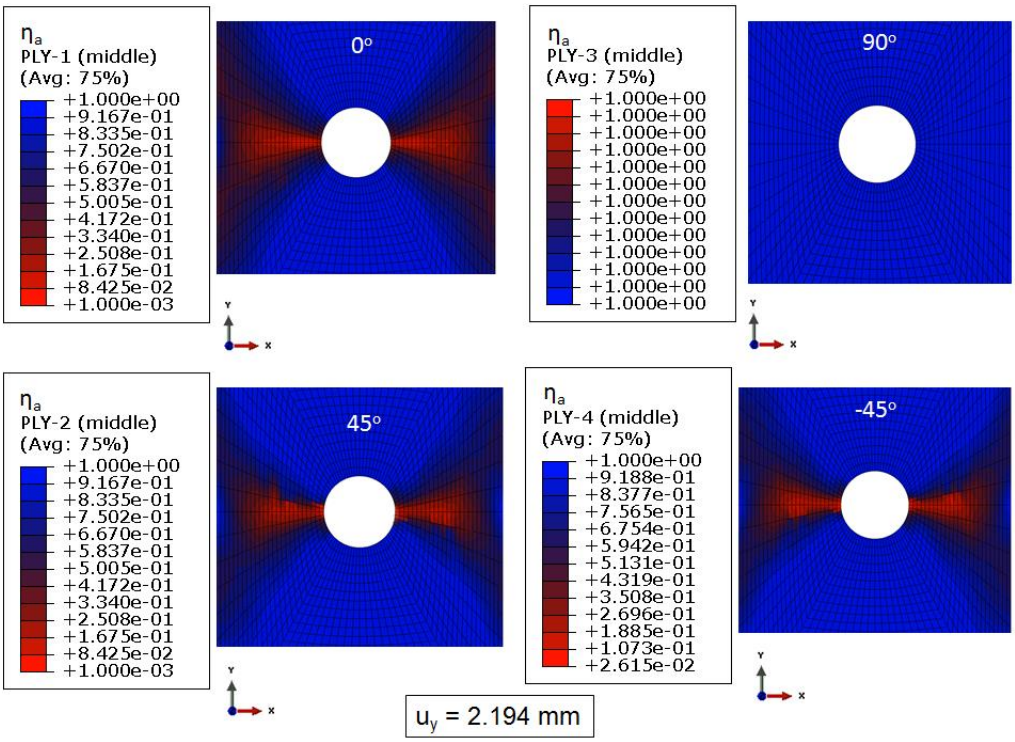

Figure 3.31: Fringe plots of the Mode A degradation factor, η_a, in 4 plies of the $[(0^o/45^o/90^o/-45^o)_2]_S$ laminate at u_y = 2.194 mm.

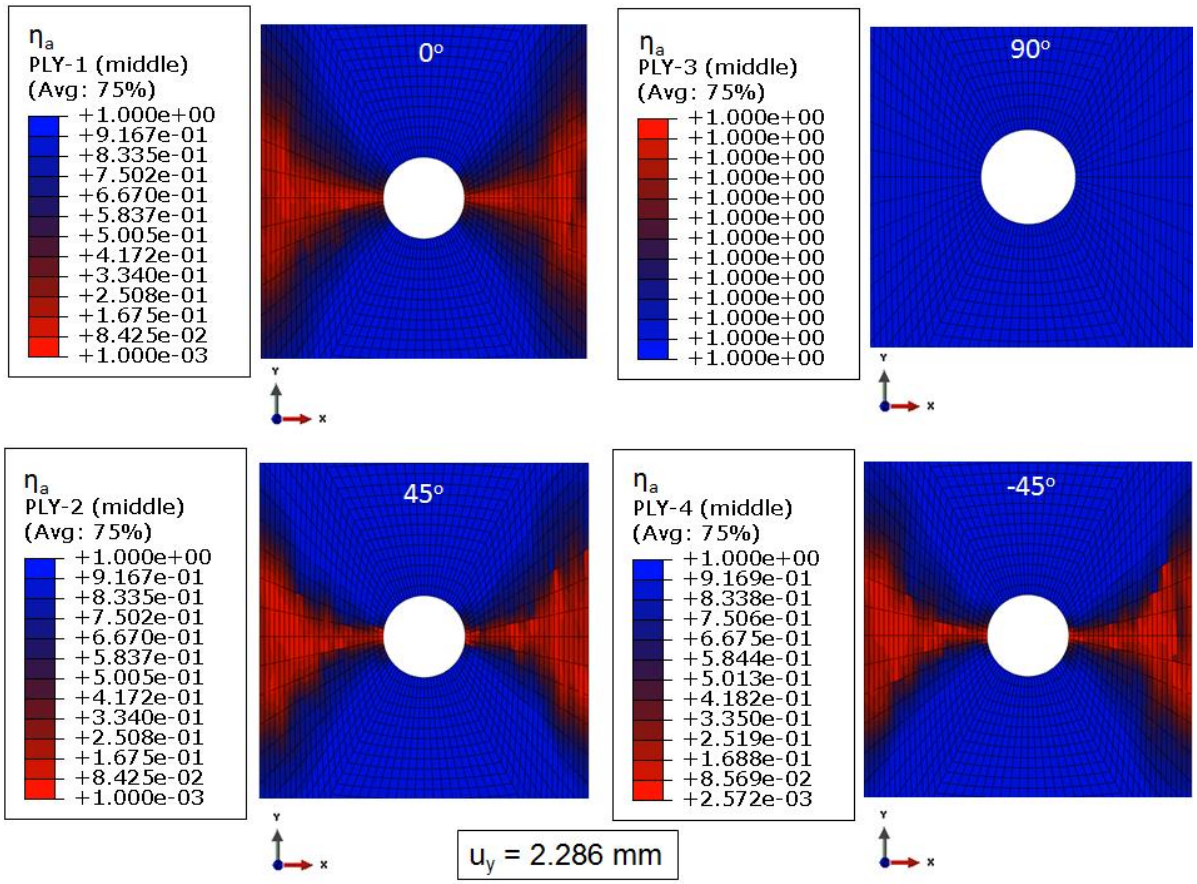

Figure 3.32: Fringe plots of the Mode A degradation factor, η_a, in 4 plies of the $[(0^o/45^o/90^o/-45^o)_2]_S$ laminate at u_y = 2.286 mm.

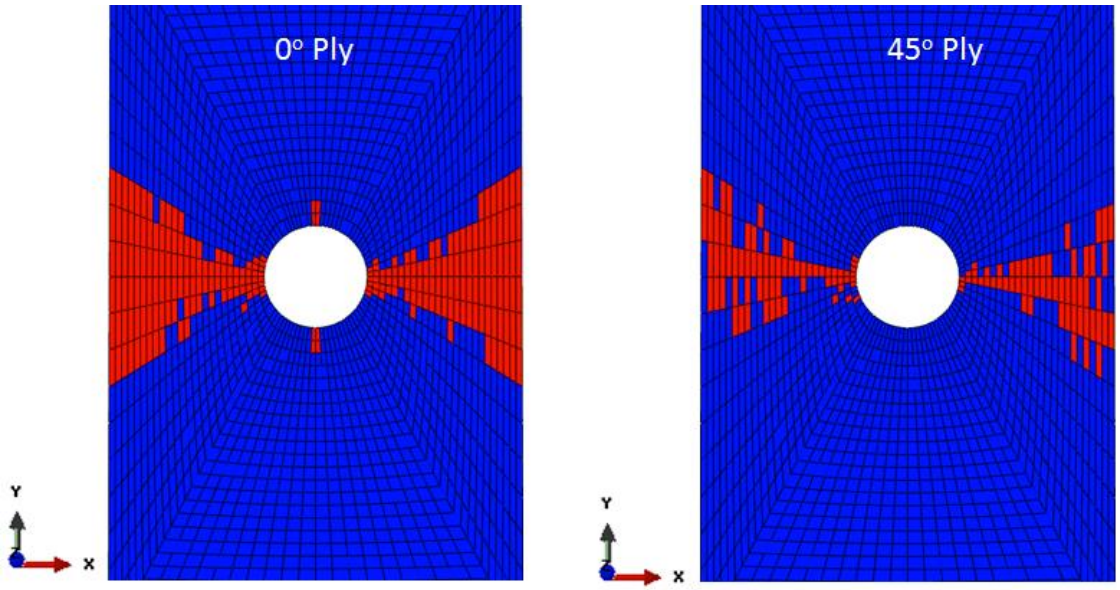

Figure 3.33: Fiber failure regions for the 0º and the 45º plies of the $[(0^º/45^º/90^º/-45^º)_2]_S$ laminate at u_y = 2.540 mm.

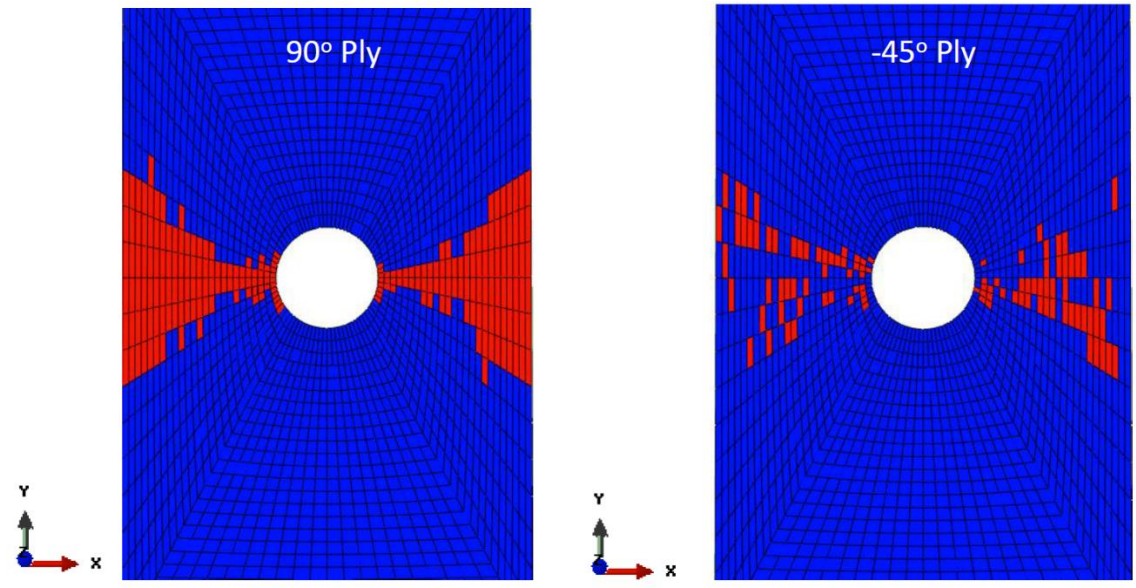

Figure 3.34: Fiber failure regions for the 90º and the - 45º plies in the $[(0^º/45^º/90^º/-45^º)_2]_S$ laminate at u_y = 2.540 mm.

3.5 Energy Balance for OHT specimens

In order to assess the accuracy of the numerical solution we have checked the energy balance for the two OHT mechanical problems studied. That is, the work, *ALLWK*, done by external forces must equal the strain energy, *ALLIE*, stored in the body and that lost due to deleting the failed elements; the latter was not output from the software. As should be clear from the plots of Figs. **3.35** and **3.36,** at each value of the applied displacement, the strain energy is very close to the work done by the external force, and the difference, ETOTAL, between the two quantities is at most 2%. Thus very little energy is dissipated in failed elements.

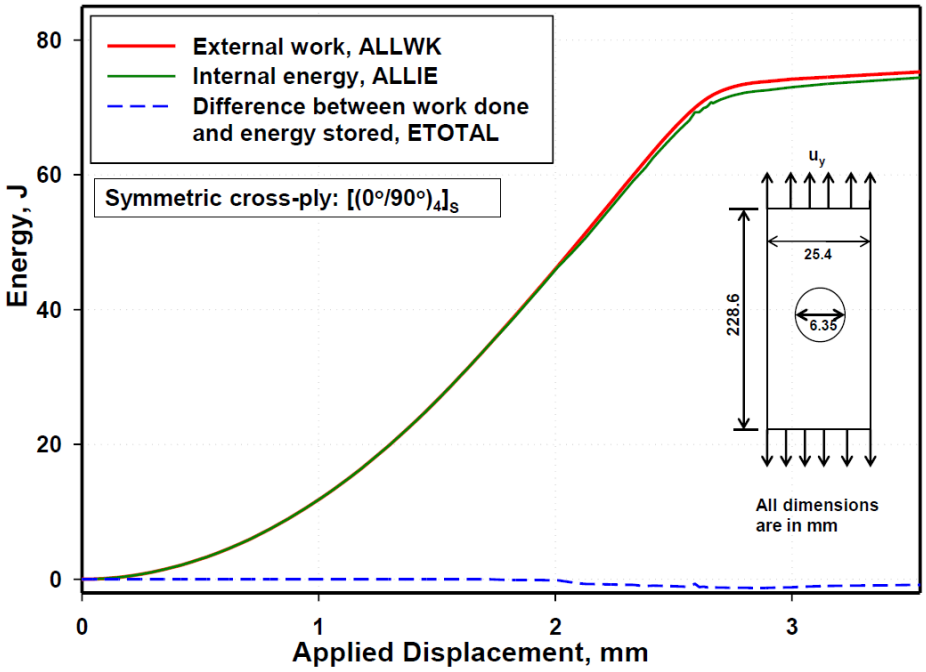

Figure 3.35: Energy balance for the OHT [(0º/90º)$_4$]$_S$ laminate.

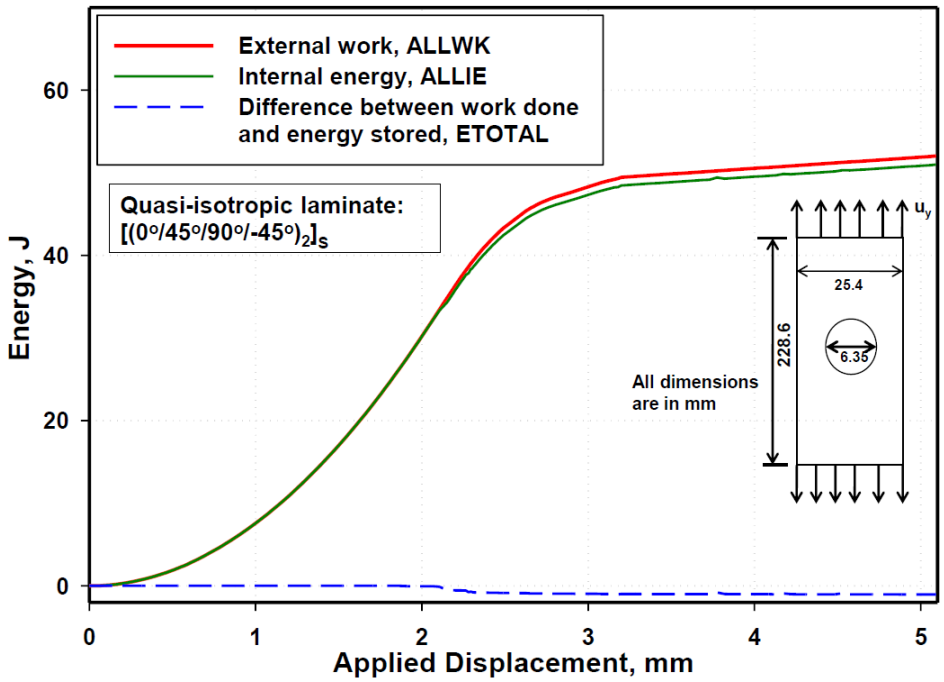

Figure 3.36: Energy balance for the OHT $[(0^o/45^o/90^o/-45^o)_2]_S$ laminate.

3.6 Summary of PFA of OHT Coupons

The peak loads found using the progressive failure analyses of two OHT laminates and different failure criteria are summarized in Table 3.1. Except for the Tsai-Wu and the Hashin failure criteria that ignore damage initiation and progression, the other three criteria, namely the maximum stress, the maximum strain and the Puck and Schürmann, give nearly the same value of the maximum load for the $[(0^o/90^o)_4]_S$ laminate. However, for the $[(0^o/45^o/90^o/-45^o)_2]_S$ laminate, the peak load predicted by the Puck and Schürmann failure criteria is about 14% less than that found by using the maximum stress and the maximum strain criteria. For both laminates and for each failure criterion that considers damage initiation and progression, the computed peak load agrees well with that found experimentally. Whereas Knight [62] degraded the element stiffness by ½ every time either the fiber or the matrix or both failed in the element we found the degradation factor for the matrix by ensuring that the stress state in the failed element lies on the failure surface for the relevant failure mode. The fiber failure criteria used in this and Knight's work are essentially the same but the degradation factors equal 0 and ½, respectively, in the two works.

Table 3.1: Summary of the peak loads for the cross-ply and the quasi-isotropic 16-layer graphite-epoxy open-hole-tension laminates using different failure criteria.

Failure Criteria	Peak Load, kN	Peak Load, kN
	$[(0^o/90^o)_4]_S$	$[(0^o/45^o/90^o/-45^o)_2]_S$
Max. Stress [62]	42.40	35.47
Max. Strain [62]	42.8	35.32
Tsai-Wu [62]	38.50	35
Hashin [62]	31.70	26.62
Puck and Schürmann	42.83	30.60
Experiment [62]	42.72	32.90

Chapter 4

Progressive Failure in 3D Deformations

Introduction

Composite materials have been used, albeit sporadically, in several industrial applications since the 1950's because of their high specific stiffness and anisotropic material properties that enable one to tailor material stiffness in desired directions. It is only recently that composites have truly started to replace conventional materials in commercial structural assemblies. The automotive industry has begun to incorporate fiber reinforced composites (FRCs) in peripheral structural parts, crash boxes and car bodies. As mentioned in Chapter 1, the weight-sensitive aerospace sector has started to use FRCs for building load-carrying assemblies like fuselages. The Airbus A380's wing box, made entirely of FRCs, is an important structural component as it transfers the aerodynamic load from the wings to the fuselage. This large scale use of FRCs has been made possible by the immense increase in the computing power and our improved understanding of the failure of FRCs. A safe design of lightweight FRC structures requires an efficient and reliable failure prediction model for a general three-dimensional (3-D) state of stress.

Laminated structures commonly have geometries with thicknesses small relative to their lateral dimensions. The deformations of such structures are usually analyzed by using a 2-D structural model that is based on the plane stress state assumption. The governing equations and the associated boundary conditions of the reduced-order model are derived by making suitable kinematic assumptions on the displacement field in the thickness direction, and integrating through the thickness various moments with respect to the thickness coordinate of the partial differential equations governing 3-D deformations of a continuous body [64, 65]. Usually adjoining layers are assumed to be perfectly bonded to each other. The interlaminar boundaries that are surfaces of abrupt discontinuities in material properties [66-68] are usually sites of failure initiation in the form of interlaminar cracks and/or delaminations.

The analysis of an ultra-thick laminate requires studying 3-D deformations and employing

the pertinent failure theories. Even though computational analysis of 3-D deformations and experimental validation [69] of the failure criteria have been attempted, there is no consensus on the failure theories. The 3-D progressive damage and failure analyses have been conducted on FRC laminates containing holes and subjected to tensile loading [70, 71] with the continuum damage mechanics (CDM) approach used to simulate the matrix failure and the maximum strain criteria to model fiber failure [70]. A stiffness reduction approach is used to simulate progressive failure while analyzing deformations by using the finite element method (FEM) [70, 72]. Hahin's [73] failure criteria have been supplemented with the progressive damage models [74, 75] to simulate damage accumulation in bolted single-lap composite joints under in-plane tensile loading. These models could predict well the residual strength and the residual stiffness of laminates with arbitrary lay-ups, geometries and bolt position [76, 77]. Using the CDM approach, 3-D failures of laminated structures under low velocity impact have also been studied [46, 78-83]. A second World Wide Failure Exercise was organized to determine how accurately can different failure theories predict the experimentally observed failure for 3-D deformations of laminated FRCs [84, 85]. Predictions from the failure theories of Pinho [86], Carrere [87], and Puck [88] were found to be within 10% of the corresponding experimental values.

In this chapter, we describe the implementation in the commercial FE software, Abaqus, of the stress based progressive failure criteria proposed by Puck and Schürmann [13,14] for 3-D deformations of unidirectional (UD) FRC laminates. We note that Deuschle and Koreplin [89, 90] also implemented these failure criteria in Abaqus as a user defined material subroutine, UMAT. We were not aware of their works when we started the project in 2011. Also, the chapter was written as a paper for presentation at a conference. Thus some statements of previous chapters are repeated here. Whereas the fiber is assumed to instantaneously fail once stresses in it satisfy the failure criterion, the matrix properties are assumed to degrade upon failure initiation and, depending upon the structure geometry and the applied loads the ultimate failure may be significantly delayed. Deuschle [91] has also considered the nonlinear constitutive behavior of the matrix material. Besides implementing the failure criteria, we have also proposed which material elasticities should be degraded when matrix fails on a plane with normal stress either tensile or compressive. Subsequent to the initiation of the matrix failure at a point, values of degradation

parameters are found by numerically solving nonlinear algebraic equations so that one is always on a failure surface within a load increment. Values of the degradation parameters vary from point to point, and at one material point they vary with the applied load. However, they are not allowed to decrease at a material point meaning that a failed material point cannot heal. The implementation of the PFA criteria is illustrated by analyzing two example problems: (i) homogeneous deformations of a laminate deformed in shear, and (ii) homogeneous deformations of a laminate deformed due to combined triaxial and in-plane shear strains.

4.1 Puck and Schürmann failure criteria for 3-D Deformations

For UD FRCs, Puck and Schürmann [13,14] postulated different stress-based failure initiation criteria for the fiber and the matrix. Both the matrix and the fiber are assumed to deform linear elastically and undergo brittle failure implying that inelastic effects are neglected and deformations envisaged are infinitesimal. Furthermore, for the matrix the failure plane is assumed to be parallel to the fibers, and the failure initiation criterion depends upon whether the normal stress on the plane is tensile or compressive. The compressive normal stress on the plane is assumed to impede the sliding of one surface over the other. For the matrix failure, material elasticities are degraded subsequent to failure initiation but the fiber failure is assumed to be catastrophic in the sense that the fiber is assumed to fail instantaneously when the failure criterion is satisfied.

Let x_1, x_2, x_3 denote the material principal directions (Fig. **4.1**) in a lamina, with the x_1-axis along the fiber direction and the x_3-axis parallel to the thickness direction. The UD FRC lamina is modeled as a linear elastic transversely isotropic material with the x_1-axis (i.e., the fiber direction) as the axis of transverse isotropy. The stress-strain relation can be written as

$$\begin{Bmatrix} \varepsilon_{11} \\ \varepsilon_{22} \\ \varepsilon_{33} \\ \gamma_{23} \\ \gamma_{13} \\ \gamma_{12} \end{Bmatrix} = \begin{bmatrix} \frac{1}{E_1} & -\frac{\nu_{12}}{E_1} & -\frac{\nu_{12}}{E_1} & 0 & 0 & 0 \\ -\frac{\nu_{12}}{E_1} & \frac{1}{E_2} & -\frac{\nu_{23}}{E_2} & 0 & 0 & 0 \\ -\frac{\nu_{12}}{E_1} & -\frac{\nu_{23}}{E_2} & \frac{1}{E_2} & 0 & 0 & 0 \\ 0 & 0 & 0 & \frac{2(1+\nu_{23})}{E_2} & 0 & 0 \\ 0 & 0 & 0 & 0 & \frac{1}{G_{12}} & 0 \\ 0 & 0 & 0 & 0 & 0 & \frac{1}{G_{12}} \end{bmatrix} \begin{Bmatrix} \sigma_{11} \\ \sigma_{22} \\ \sigma_{33} \\ \sigma_{23} \\ \sigma_{13} \\ \sigma_{12} \end{Bmatrix} \tag{4.1}$$

The elasticity matrix is given by

$$C = \begin{bmatrix} C_{11} & C_{12} & C_{13} & 0 & 0 & 0 \\ C_{12} & C_{22} & C_{23} & 0 & 0 & 0 \\ C_{13} & C_{23} & C_{33} & 0 & 0 & 0 \\ 0 & 0 & 0 & C_{44} & 0 & 0 \\ 0 & 0 & 0 & 0 & C_{55} & 0 \\ 0 & 0 & 0 & 0 & 0 & C_{66} \end{bmatrix} \tag{4.2}$$

where

$$C_{11} = \frac{E_1}{1-\nu_{23}^2} D\,, \quad C_{22} = \frac{E_1 E_2}{E_1 - E_2 \nu_{12}^2} D, \qquad C_{33} = \frac{E_1 E_2}{E_1 - E_2 \nu_{12}^2} D$$

$$C_{12} = \frac{E_1^2}{E_2 \nu_{12} + E_2 \nu_{12} \nu_{23}} D\,, \qquad C_{13} = \frac{E_1^2}{E_2 \nu_{12} + E_2 \nu_{12} \nu_{23}} D$$

$$C_{23} = \frac{E_2}{\nu_{12}^2 + \nu_{13}} D,\ C_{44} = G_{23},\ C_{55} = G_{13},\ C_{66} = G_{12}$$

$$\textbf{with} \quad D = \frac{E_1}{E_1 - 2E_2 \nu_{12}^2 (1-\nu_{23}) - E_1 \nu_{23}^2}$$

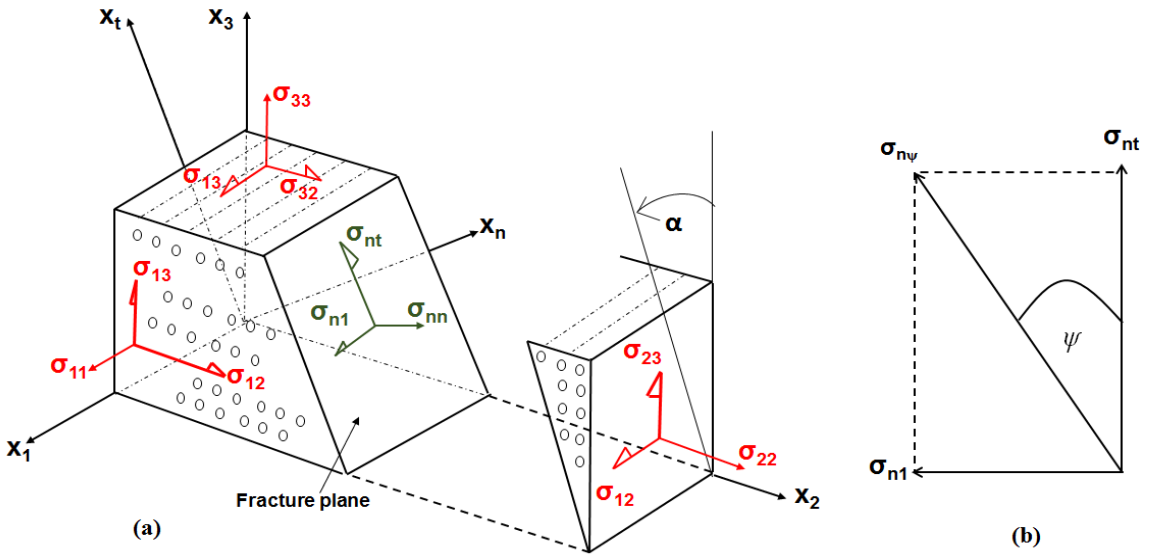

Figure 4.1: The coordinate system along the material principal directions, stress components on coordinate planes, and stresses on a potential fracture plane passing through a point

In Eqs. (4.1) and (4.2), E_1 is the elastic modulus in the x_1-direction, E_2 the modulus along any direction in the x_2x_3-plane, G_{12} the shear modulus in the x_1x_2-plane, ν's are Poisson's ratios, σ_{ij}'s are stress components, ε_{ij}'s are normal strain components, and γ_{ij}'s are shear strain components. Thus there are five independent elastic constants. In order that the work done by external forces on the body be non-negative during its deformations, the compliance matrix in Eq. (4.1) or the elasticity matrix in Eq. (4.2) must have non-negative eigenvalues which is the case if the following conditions are satisfied.

$$E_1, E_2, G_{12}, G_{23} > 0, \quad |\nu_{12}| < \sqrt{\frac{E_1}{E_2}} \quad \text{and } |\nu_{23}| < 1\,. \tag{4.3}$$

4.1.1 Fiber Failure

For 3-D deformations [90], the influence of transverse normal stresses, σ_{22} and σ_{33}, on the fiber failure is considered because fibers are confined in the matrix. Puck and Schürmann hypothesized that (i) the effect of transverse normal stresses σ_{22} and σ_{33} on the axial strain induced in the fiber is enhanced due to the presence of the matrix, (ii) at failure the axial strain in the fiber embedded in a ply deformed in uniaxial tension equals that in an isolated fiber deformed in uniaxial tension.

For an isolated fiber subjected to three normal stresses, Hooke's law gives

$$\varepsilon_1 = \frac{\sigma_{11}}{E_1} - \frac{\nu_{12}}{E_1}(\sigma_{22} + \sigma_{33}) \tag{4.4}$$

for the axial strain in the fiber. The axial strain in a fiber embedded in an UD fiber-reinforced ply is assumed to be given by the following modified Hooke's law

$$\varepsilon_{1f} = \frac{\sigma_{11f}}{E_{1f}} - \frac{\nu_{12f}}{E_{2f}} m_{\sigma f}(\sigma_{22} + \sigma_{33}) \tag{4.5}$$

with

$$\frac{\nu_{12f}}{E_{2f}} = \frac{\nu_{21f}}{E_{1f}} \tag{4.6}$$

In Eq. (4.5) the magnification factor, $m_{\sigma f}$, enhances the effect of the transverse normal stresses on the axial deformations of the fiber. Puck has proposed taking $m_{\sigma f}$ equal to 1.1 for the carbon fiber-reinforced polymeric (FRP) composites and 1.3 for the glass FRP composites. In Eqs. (4.5) and (4.6) the subscript *f* on a quantity implies its value when it is embedded in a ply.

The assumption (ii) stated above implies that a fiber in a ply fails when $\varepsilon_{1f} = \varepsilon_1^{fail}$. For deformations of the lamina and the isolated fiber under uniaxial loading, we have at failure

$$X_{f1T} = E_{1f}\varepsilon_{1f}^{fail},\ X_T = E_1\varepsilon_1^{fail} \text{ and } X_{f1T} = \frac{E_{1f}}{E_1} X_T \tag{4.7}$$

Furthermore, at failure, $\sigma_{11f} = X_{f1T}$. Equating the axial strains in the fiber given by Eqs. (4.4) and (4.5) (i.e., setting $\varepsilon_1 = \varepsilon_{1f}$), solving the resulting equation for σ_{11f} and using $\sigma_{11f} = X_{f1T}$, we get the following relation among the axial stresses at the instant of fiber failure.

$$\frac{E_{1f}}{E_1} X_T = E_{1f}\left[\frac{\sigma_{11}}{E_1} - \frac{\nu_{12}}{E_1}(\sigma_{22} + \sigma_{33})\right] + \nu_{12f} m_{\sigma_f}(\sigma_{22} + \sigma_{33}) \tag{4.8}$$

We define the fiber failure index, FF_T, by

$$FF_T = \frac{1}{X_T}\left[\sigma_{11} - \left(\nu_{12} - \nu_{12f} m_{\sigma_f}\frac{E_1}{E_{1f}}\right)(\sigma_{22} + \sigma_{33})\right] \tag{4.9}$$

Thus for 3-D deformations, a fiber in a UD lamina fails in tension and compression when

$$FF_T = 1, and\ \ FF_C = 1 \tag{4.10}$$

respectively. The expression for FF_C is obtained from that for FF_T by substituting X_C for X_T where X_C is the strength of the isolated fiber in compression.

4.1.2 Matrix Failure

Assume that the failure ensues at a matrix point on a plane obtained by counterclockwise rotation through angle α about the x_1-axis, as shown in Fig. **4.1**. Using the stress transformation equations, the normal stress, σ_{nn}, and the shear stresses, σ_{nt}, σ_{n1}, acting on the plane are given by

$$\sigma_{n1} = \sigma_{21}\, Cos\, \alpha \; + \; \sigma_{31}\, Sin\, \alpha \tag{4.11}$$

$$\sigma_{nn} = \left(\frac{\sigma_{22} + \sigma_{33}}{2}\right) + \left(\frac{\sigma_{22} - \sigma_{33}}{2}\right)\; Cos\; 2\alpha + \; \sigma_{23}\, Sin\; 2\alpha \tag{4.12}$$

$$\sigma_{nt} = \left(\frac{\sigma_{22} - \sigma_{33}}{2}\right) Sin\; 2\alpha + \;\; \sigma_{23}\, Cos\; 2\alpha \tag{4.13}$$

The matrix failure indices, $FI_{MT}(\alpha)$ and $FI_{MC}(\alpha)$, are defined as

$$FI_{MT}(\alpha) = \sqrt{\left[1 - p_{n\psi}^{(+)}\frac{Y_T}{S_\psi}\right]^2\left[\frac{\sigma_{nn}(\alpha)}{Y_T}\right]^2 + \left[\frac{\sigma_{nt}\,(\alpha)}{S_T}\right]^2 + \left[\frac{\sigma_{n1}(\alpha)}{S_L}\right]^2} + \frac{p_{n\psi}^{(+)}\sigma_{nn}(\alpha)}{S_\psi}\;;\;\; \sigma_{nn} \geq 0 \tag{4.14}$$

$$FI_{MC}(\alpha) = \sqrt{\left[\frac{\sigma_{nt}(\alpha)}{S_T}\right]^2 + \left[\frac{\sigma_{n1}(\alpha)}{S_L}\right]^2 + \left[\frac{p_{n\psi}^{(-)}}{S_\psi}\sigma_{nn}(\alpha)\right]^2} + \left(\frac{p_{n\psi}^{(-)}}{S_\psi}\right)\sigma_{nn}(\alpha);\; \sigma_{nn} < 0, \tag{4.15}$$

where the shear strength resultant, S_ψ, on the failure plane is given by

$$S_\psi = \left[\frac{S_L^2\sigma_{nt}^2 + \sigma_{n1}^2 S_T^2}{S_L^2(\sigma_{n1}^2 + \sigma_{nt}^2)S_T^2}\right]^{-\frac{1}{2}} \tag{4.16}$$

Here the subscript 'MT' ('MC') denotes the tension (compression) mode of failure, the inclination slope parameters, $p_{n\psi}^{(+)}$, $p_{n\psi}^{(-)}$, and $p_{nt}^{(+)}$, are determined from experimental data [13, 14] and depend upon the material of the UD FRC. Furthermore, Y_T is the transverse (x_2- direction) ultimate strength of the UD FRC in uniaxial tension test along the x_2-axis, and S_T and S_L are, respectively, transverse shear strengths along the thickness and the transverse directions, and the angle ψ is depicted in Fig. **4.1 (b)**.

The expression for S_ψ given in Eq. (4.16) is derived from definitions of the inclination parameters of the failure surface [13, 14]. These definitions imply that

$$\frac{p_{n\psi}^{(+)}}{S_\psi} = \frac{p_{nt}^{(+)}}{S_T}\, Cos^2\psi + \frac{p_{n1}^{(+)}}{S_L}\, Sin^2\psi \tag{4.17}$$

where $Cos^2\psi = \frac{\sigma_{nt}^2}{\sigma_{nt}^2+\sigma_{n1}^2}$ and $Sin^2\psi = \frac{\sigma_{n1}^2}{\sigma_{nt}^2+\sigma_{n1}^2}$. If $[\sigma_{nt}(\alpha)]^2 + [\sigma_{n1}(\alpha)]^2 = 0$ and $\sigma_{nn}(\alpha) < 0$ on the failure plane, then no failure occurs on that plane. That is, a matrix point is assumed not to fail on a plane that has only normal compressive stress.

The failure is assumed to initiate at a point on that plane for which the failure index equals 1. Thus for a given state of stress at a point, the failure will initiate on the plane for which either $FI_{MT}(\alpha)$ or $FI_{MC}(\alpha)$ equals 1 first. It is possible that both $FI_{MT}(\alpha)$ and $FI_{MC}(\alpha)$ simultaneously equal 1 on different planes passing through the point. The angle α that gives an extreme value of $FI_{MT}(\alpha)$ is given by

$$\frac{\partial FI_{MT}(\alpha)}{\partial \alpha} = 0 \tag{4.18}$$

This equation is numerically solved for α in the range $-90^o < \alpha < 90^o$ within 10^{-8} tolerance.

4.1.3 Degradation of material elasticities

The fiber failure is assumed to be catastrophic, and E_1 is assigned a very small value after a fiber has failed either in tension or compression.

Matrix failure in tension

Different elasticities of the composite lamina are degraded upon the initiation of the matrix failure in tension and compression. In order to determine which elastic parameters to degrade, we note that for a transversely isotropic material with the x_1-axis as the axis of transverse isotropy,

$$E_n = E_3 = E_2,\ G_{nt} = G_{23},\ G_{n1} = G_{31} \tag{4.19}$$

In physical experiments when the matrix at a point fails in tension, a crack forms with null surface tractions on the crack surfaces. That is, σ_{nn}, σ_{n1}, σ_{nt} vanish there. However, according to Puck and Schürmann's [14] analysis of progressive failure, we don't simulate cracks, assume that they are smeared out, and the corresponding material has lower values of elastic constants than the virgin matrix material. We thus degrade values of E_n, G_{nt}, and G_{n1} by the same factor, η_T, ($0 < \eta_T$

≤ 1), to keep the analysis simple. Note that values of Poisson's ratios ν_{23} and ν_{12} are not degraded. The value of η_T is found by requiring that the failure condition, $FI_{MT}(\alpha, \eta_T) = 1$, is always satisfied. Thus subsequent to the initiation of failure at a point in the matrix, we solve

$$FI_{MT}(\alpha, \eta_T) - 1 = 0 \quad \text{and} \quad \frac{\partial [FI_{MT}(\alpha, \eta_T)]}{\partial \alpha} = 0 \tag{4.20}$$

for α and η_T. In order to keep computations stable, the lowest value we assign to η_T is 0.05. The degradation of values of elastic constants at a point affects the stress distribution at its neighboring points and may enhance failure initiation there. For easy reference, we list below the stress-strain relation at a point where the failure has initiated. Of course, setting $\eta_T = 1$ in these equations gives the stress-strain relations (inverse of Eq. (4.1)) for a virgin transversely isotropic material.

$$\sigma_{11} = \frac{E_1[-E_2(\varepsilon_{22} + \varepsilon_{33}) + E_1\varepsilon_{11}(-1 + \eta_T\nu_{23})]}{2E_2\eta_T\nu_{12}^2 + E_1(-1 + \eta_T\nu_{23})} \tag{4.21}$$

$$\sigma_{22} = \frac{E_2\eta_T[E_2(\varepsilon_{22} - \varepsilon_{33})\eta_T\nu_{12}^2 + E_1(\varepsilon_{22} + \varepsilon_{11}\nu_{12} + \varepsilon_{33}\eta_T\nu_{23} + \varepsilon_{11}\eta_T\nu_{12}\nu_{23})]}{(1 + \eta_T\nu_{23})[2E_2\eta_T\nu_{12}^2 + E_1(-1 + \eta_T\nu_{23})]} \tag{4.22}$$

$$\sigma_{33} = \frac{E_2\eta_T[E_2(\varepsilon_{33} - \varepsilon_{22})\eta_T\nu_{12}^2 - E_1(\varepsilon_{33} + \varepsilon_{11}\nu_{12} + \varepsilon_{22}\eta_T\nu_{23} + \varepsilon_{11}\eta_T\nu_{12}\nu_{23})]}{(1 + \eta_T\nu_{23})[2E_2\eta_T\nu_{12}^2 + E_1(-1 + \eta_T\nu_{23})]} \tag{4.23}$$

$$\sigma_{23} = \frac{E_2\eta_T\gamma_{23}}{2(1+\nu_{23})} = \eta_T G_{23}\gamma_{23} \tag{4.24}$$

$$\sigma_{13} = \eta_T G_{12}\gamma_{13} \tag{4.25}$$

$$\sigma_{12} = \eta_T G_{12}\gamma_{12} \tag{4.26}$$

Matrix failure in compression

When the failure occurs at a matrix point with the normal stress on the failure plane being compressive, we assume that the material on either side of the failure plane stays in contact and only relative sliding occurs between the contacting material points. We thus assume that E_n is unaffected by the failure, and to account for the damage induced due to sliding we reduce G_{nt} and

$G_{n1,}$ or equivalently G_{12} and G_{32} by the same factor, η_C, to keep the analysis simple. For the transversely isotropic material,

$$G_{23} = \frac{E_2}{2(1+\nu_{23})} \tag{4.27}$$

Since E_2 is not being degraded but G_{23} is, in order to preserve the relation (4.27), we degrade ν_{32} by the factor η_v given by

$$\eta_C G_{23} = \frac{E_2}{2(1+\eta_v \nu_{23})} \tag{4.28}$$

Substitution for G_{23} from Eq. (4.27) into Eq. (4.28) gives

$$\eta_v = \frac{1+\nu_{23}-\eta_C}{\eta_C \nu_{23}} \tag{4.29}$$

we note that as $\eta_C \to 0, \eta_v \to \infty$. However, for the degraded Poisson's ratio ($\eta_v \nu_{23}$) to satisfy the constraint expressed by Eq. (4.3), the minimum value η_C can take is the larger of $(1+\nu_{23})/2$ and zero. When η_C either equals $(1+\nu_{23})/2$ or 0, the material point is assumed to have completely failed. The stress-strain relations for the degraded material are

$$\sigma_{11} = \frac{E_1[-E_2(\varepsilon_{22}+\varepsilon_{33})\nu_{12} + E_1\varepsilon_{11}(-1+\eta_v\nu_{23})]}{2E_2\nu_{12}^2 + E_1(-1+\eta_v\nu_{23})} \tag{4.30}$$

$$\sigma_{22} = \frac{E_2[E_2(\varepsilon_{22}-\varepsilon_{33})\nu_{12}^2 - E_1(\varepsilon_{22}+\varepsilon_{11}\nu_{12}+\varepsilon_{33}\eta_v\nu_{23}+\varepsilon_{11}\eta_v\nu_{12}\nu_{23})]}{(1+\eta_v\nu_{23})[2E_2\eta_T\nu_{12}^2 + E_1(-1+\eta_v\nu_{23})]} \tag{4.31}$$

$$\sigma_{33} = -\frac{E_2[E_2(\varepsilon_{22}-\varepsilon_{33})\nu_{12}^2 + E_1(\varepsilon_{33}+\varepsilon_{11}\nu_{12}+\varepsilon_{22}\eta_v\nu_{23}+\varepsilon_{11}\eta_v\nu_{12}\nu_{23})]}{(1+\eta_T\nu_{23})[2E_2\nu_{12}^2 + E_1(-1+\eta_v\nu_{23})]} \tag{4.32}$$

$$\sigma_{23} = \frac{\eta_C G_{23} \gamma_{23}}{2(1+\nu_{23})} \tag{4.33}$$

$$\sigma_{13} = \eta_C G_{12} \gamma_{13} \tag{4.34}$$

$$\sigma_{12} = \eta_C G_{12} \gamma_{12} \tag{4.35}$$

4.2 Numerical Implementation and Two Example Problems

The above described failure initiation criteria and the degradation of material properties have been implemented as an USDFLD subroutine written in FORTRAN in the commercial FE software, Abaqus. The main program provides stresses at an integration (quadrature) point to the USDFLD. The subroutine uses the Golden Search Algorithm [92] first to find planes on which the failure indices $FI_{MT}(\alpha)$ and $FI_{MC}(\alpha)$ have maximum values, and then their maximum values. Only when the matrix failure has ensued either in tension or in compression, the subroutine computes degradation factors for the material elasticities by numerically solving nonlinear algebraic equations (4.20) within the prescribed tolerance of 10^{-8}. The analysis is repeated without further incrementing the load to ensure that equilibrium equations are satisfied with the just computed degraded values of the material elasticities. If the material at the integration point had failed earlier but now the stress state there does not satisfy the matrix failure criteria due to either unloading or the redistribution of stresses there, previous values of the degradation parameters are returned to the main program. That is, there is no healing of the damaged material.

4.2.1 Homogeneous shear deformations

The first example problem studied involves homogeneous deformations of a rectangular UD FRC lamina loaded by uniformly distributed tangential tractions that produce homogeneous deformations and result in only non-zero stresses $\sigma_{23} = \sigma_{32} > 0$. We note that there is no axial stress induced in the fibers, and they don't fail for this state of stress. Eqns. (4.11) - (4.13) simplify to

$$\sigma_{n1} = 0 \tag{4.36}$$

$$\sigma_{nn} = \sigma_{23}\, Sin\, 2\alpha \tag{4.37}$$

$$\sigma_{nt} = \sigma_{23}\, Cos\, 2\alpha \tag{4.38}$$

Thus for the matrix to fail in tension, α must have values between 0^o and 90^o; otherwise the matrix may fail in compression. Regardless of the value of σ_{23}, no failure occurs on the plane $\alpha = -45^o$ since $\sigma_{nn} < 0$ and there is no shear stress on this plane. For $\alpha = 0$, the only non-zero component

of stress on the failure plane is $\sigma_{nt} = \sigma_{23}$, and according to Eq. (4.14) the matrix will fail in tension when $\sigma_{23} = S_T$. In order to investigate if the matrix fails for $\sigma_{23} < S_T$, we substitute from Eqns. (4.36) - (4.38) into Eqns. (4.14) and (4.15), and get following expressions for the matrix failure indices.

$$\frac{FI_{MT}(\alpha)}{\sigma_{23}} = \frac{p_{n\psi}^{(+)} Sin(2\alpha)}{S_T} + \frac{1}{Y_T}\sqrt{\left(\frac{Y_T^2}{S_T^2}\cos^2(2\alpha) + \left(\frac{p_{n\psi}^{(+)} Y_T}{S_T} - 1\right)^2 \sin^2(2\alpha)\right)} \tag{4.39}$$

$$\frac{S_T\, FI_{MC}(\alpha)}{\sigma_{23}} = p_{n\psi}^{(-)} Sin(2\alpha) + \sqrt{\left(cos^2(2\alpha) + \left(p_{n\psi}^{(-)}\right)^2 sin^2(2\alpha)\right)} \tag{4.40}$$

Noting that these expressions involve values of material parameters, we assign them the following values taken from Kaddour and Hinton [93]: E_1= 129 GPa, E_2 = 5.6 GPa, E_3 = 5.6 GPa, G_{12} = 1.33 GPa, G_{13} = 1.33 GPa, G_{23} = 1.86 GPa, ν_{12} = 0.318, ν_{13} = 0.318, ν_{23} = 0.5, X_T = 1378 MPa, Y_T = 40 MPa, X_C = 950 MPa, Y_C = 125 MPa, S_L= 97 MPa, S_T = 48 MPa, E_{1f} = 231 GPa, ν_{12f} = 0.2 and $m_{\sigma f}$ = 2. For the graphite epoxy composite, we set $p_{n\psi}^{(+)}$ = 0.30, $p_{n1}^{(-)}$ = 0.30 and, $p_{n\psi}^{(-)}$=0.30 as suggested by Puck and Schürmann [13,14]. Equation (4.16) gives S_ψ = 97 MPa. The failure indices, $FI_{MT}(\alpha)$ and $FI_{MC}(\alpha)$ normalized by S_T/σ_{23}, versus the angle, α, are plotted in Fig. **4.2**. Since $S_T < Y_C$ the maximum value of the $FI_{MT}(\alpha)$ is higher than that of $FI_{MC}(\alpha)$, the matrix will first fail in tension on the plane for which α = 45°, and the failure will occur when $\sigma_{23} = S_T$. This value of α could have been found by setting equal to zero the first derivative with respect to α of expressions in Eqns. (4.39) and (4.40). The plot of Fig. 4.2 shows that there are no other values of α for which these expressions take extreme values.

In a displacement controlled test (or simulation) the shear stress will linearly increase with γ_{23} till $\sigma_{23} = S_T$. Subsequently with an increase in γ_{23}, the degradation factor η_T will be inversely proportional to γ_{23} for $\eta_T G_{23}\gamma_{23} = S_T$. Thus the graph of η_T vs. γ_{23} will be a hyperbola passing the point (S_T/G_{23}, 1).

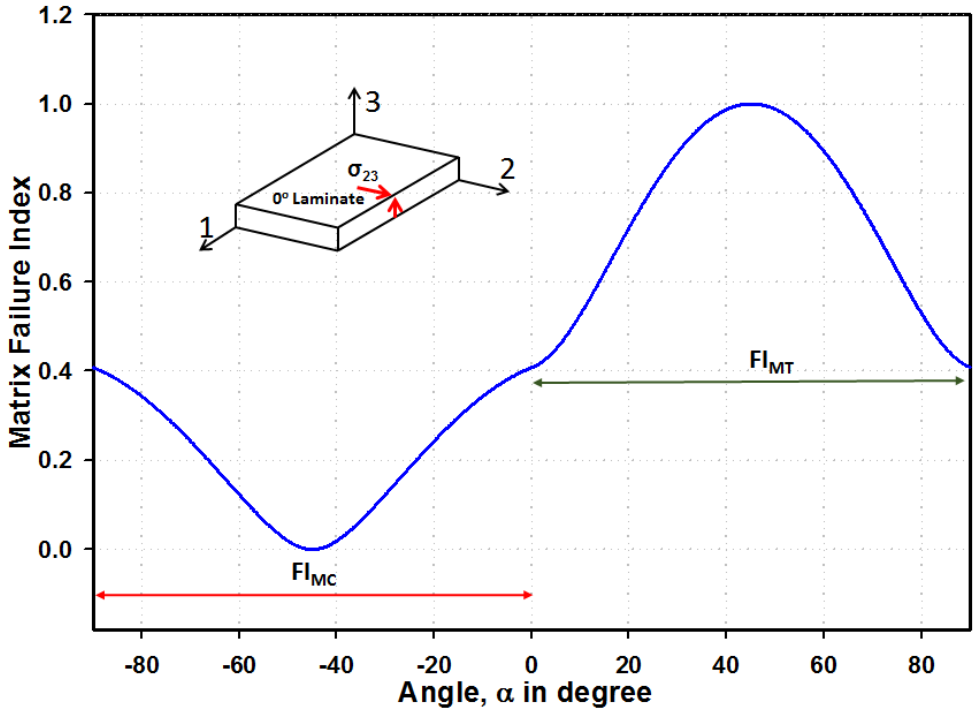

Figure 4.2: Variation of the normalized matrix failure index with the fracture plane angle, α

4.2.2 Homogeneous combined axial and shear deformations

We now study the failure of a rectangular UD FRC lamina loaded under combined shear and axial deformations. The problem is numerically solved by first applying axial displacements along the three material principal directions that correspond to a state of hydrostatic pressure. Subsequently, the axial strains are kept fixed and displacements corresponding to a shear strain in the x_1x_2-plane are applied to analyze the progressive failure of the lamina. For $\sigma_{11} = \sigma_{22} = \sigma_{33} = \lambda$, the axial strains found using Hooke's law are given by

$$\varepsilon_{11} = \lambda\left[\frac{-2\nu_{12} + 1}{E_1}\right] \tag{4.41}$$

$$\varepsilon_{22} = \varepsilon_{33} = \lambda\left[\frac{-\nu_{12}E_2 + E_1 - E_1\nu_{23}}{E_2E_1}\right] \tag{4.42}$$

For homogeneous deformations of a body the displacement field in it must be an affine function of coordinates of a point. Assuming that the rigid body motion has been eliminated by suitably

fixing points in the body, the displacement field for coupled triaxial and simple shear deformations is given by

$$u_1 = Ax_1 + \frac{\gamma}{2}\, x_2, u_2 = Bx_2 + \frac{\gamma}{2} x_1, u_3 = Bx_3\ , \tag{4.43}$$

where A = ε_{11}, B = ε_{22}, and $\gamma = \gamma_{12}$. Substitution of $\sigma_{11} = \sigma_{22} = \sigma_{33} = \lambda$, $\sigma_{13} = \sigma_{23} = 0$ in Eqs. (4.11) - (4.13) gives

$$\sigma_{n1} = \sigma_{21}\, Cos\, \alpha \tag{4.44}$$

$$\sigma_{nn} = \lambda \tag{4.45}$$

$$\sigma_{nt} = 0 \tag{4.46}$$

Thus

$$FI_{MT}(\alpha) = \frac{\lambda p_{n\psi}^{(+)}}{S_L} + \sqrt{\frac{\lambda^2}{Y_T^2}\left(\frac{p_{n\psi}^{(+)} Y_T}{S_L} - 1\right)^2 + \frac{\sigma_{21}^2 cos^2\alpha}{S_L^2}} \tag{4.47}$$

$$FI_{MC}(\alpha) = \frac{1}{S_L}\left(p_{n\psi}^{(-)}\lambda + \sqrt{\left(p_{n\psi}^{(-)}\right)^2 \lambda^2 + \sigma_{21}^2 cos^2\alpha}\right),\ \sigma_{21} > 0, \tag{4.48}$$

$$FF_T = \frac{\lambda}{X_T}\left[1 - 2\left(\nu_{12} - \nu_{12f} m_{\sigma_f} \frac{E_1}{E_{1f}}\right)\right] \tag{4.49}$$

$$FF_C = \frac{\lambda}{X_C}\left[1 - 2\left(\nu_{12} - \nu_{12f} m_{\sigma_f} \frac{E_1}{E_{1f}}\right)\right] \tag{4.50}$$

We assume that the lamina material is the same as that studied in the first example problem. For $\sigma_{21} = 0$, $\sigma_{nn} = \lambda$ on every plane through a point. Thus the matrix will initially fail in tension when $\lambda = Y_T$. The fiber will fail in tension (compression) for λ = 1700 (-1171) and 2105 (-1451) MPa, respectively, for $m_{\sigma f}$ = 2 and 1.3.

When $\sigma_{21} \neq 0$, expressions for the matrix failure indices given in Eqns. (4.47) and (4.48) have maximum values for $\alpha = 0$. Thus the matrix failure plane will be perpendicular to the x_2-axis. By setting $\alpha = 0$ and the failure index = 1, we get equations of the initial failure surface in the $\lambda - \sigma_{21}$ plane. For values of material parameters listed above, it is exhibited in Fig. **4.3**. For $\lambda = 0$,

Eqns. (4.47) and (4.48) give the same value of σ_{21} at failure initiation. Thus the plot in Fig. 4.3 is continuous.

In order to numerically study the PFA we assume that displacements computed from Eq. (4.43) are applied on the bounding surfaces of the rectangular laminate. For $\lambda \geq 0$, A and B are determined using Eqs. (4.41) and (4.42), and the failure indices are evaluated for increasing values of γ. For example, when λ= 20 MPa, failure initiates in the matrix in tension at γ = 0.0605 or σ_{21} = 80.47 MPa. For failure initiation in compression with λ= -200 MPa, the matrix failure initiates at γ = 0.109, or equivalently at σ_{21} = 145 MPa. The initial failure envelope presented in Fig. **4.3** differs from the one found in the World Wide failure exercise [85] because of the nonlinear shear stress-shear strain response of the laminate observed experimentally but linear response assumed here. Of course, there is the possibility of incorrect values of various material parameters and inclination parameters.

Recalling Eq. (4.14), the fiber failure depends on the stress magnification factor $m_{\sigma f}$. Puck and Schürmann recommended $m_{\sigma f}$ = 1.3 for CFRP materials [14]. For $m_{\sigma f}$ = 1.3, the fiber failure occurs at $\sigma_{11} = \sigma_{22} = \sigma_{33}$ = -1460 MPa when σ_{21} = 0; this corresponds to point **P** in Fig. **4.3**. The non-interactive fiber failure criterion of Eq. (1.55) results in fiber failure occurring at $\sigma_{11} = \sigma_{22} = \sigma_{33}$ = -950 MPa (point R in Fig. **4.3**). Experimental data imply that the fibers fail at $\sigma_{11} = \sigma_{22} = \sigma_{33}$ = -1176 MPa [90], represented by point **Q** in Fig. **4.3**. This value corresponds to $m_{\sigma f}$ = 2. For studying the failure progression beyond the failure initiation we have used $m_{\sigma f}$ = 2.

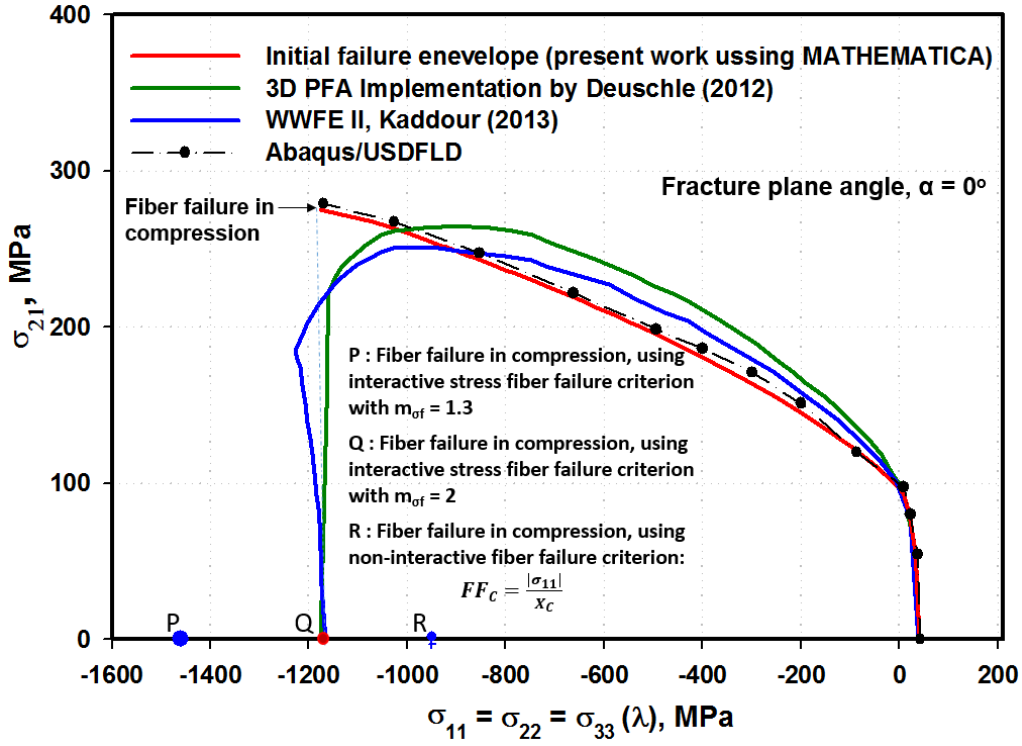

Figure 4.3: Failure envelope for the laminate in the hydrostatic pressure and shear stress plane.

Degradation of Material Elasticities

Because different elasticities are degraded when the matrix fails in tension and compression, we separately study these two cases.

Matrix failure in tension

Strains computed from displacements (4.43) are substituted into the stress-strain relations given by Eqns. (4.21) – (4.26), the resulting stresses into Eqns. (4.11) – (4.13) that give normal and shear stresses on a prospective failure plane, and these stresses into the matrix failure index given by Eqn. (4.14). For values of material parameters listed above, we get the following expression for the matrix failure index using the expression given by Eq. (4.16) for $S\psi$:

$$FI_{MT}(\alpha) = -\frac{E_1E_2(B+A\eta_T\nu_{12})p_{n\psi}^{(+)}}{\left(2E_2\eta_T^2\nu_{12}^2+E_1(-1+\eta_T\nu_{23})\right)S_L} + \sqrt{\frac{E_1^2E_2^2(B+A\eta_T\nu_{12})^2\left(\left(p_{n\psi}^{(+)}\right)^2Y_T^2+S_L^2\left(1-2p_{n\psi}^{(+)}\frac{Y_T}{S_L}\right)\right)}{\left[2E_2\eta_T^2\nu_{12}^2+E_1(-1+\eta_T\nu_{23})\right]^2Y_T^2S_L^2} + \frac{\eta_T^2G_{12}^2\gamma^2cos^2\alpha}{S_L^2}} \quad (4.51)$$

Using the numerical values of elasticities, Eqn. (4.51) becomes:

$$FI_{MT}(\alpha) = \frac{1972.7B + 627.78A\eta_T}{113.89 - \eta_T(56.94 + \eta_T)} + \frac{\sqrt{Q_1 + \gamma^2\eta_T^2 cos^2\alpha\ (Q_2 + Q_3 + Q_4 + Q_5)}}{113.90 - \ \eta_T(56.94 + \eta_T)} \qquad (4.52)$$

where

$$Q_1 = 1.95 \times 10^8 B^2 + A\eta_T(1.241 \times 10^8 B + 1.97 \times 10^7 A\eta_T)$$

$$Q_2 = 2.439\ \times 10^6\ (1 - \eta_T)$$

$$Q_3 = 5.6692 \times 10^5\ \eta_T^2$$

$$Q_4 = 2.1414 \times 10^4\ \eta_T^3$$

$$Q_5 = 188\ \eta_T^4$$

We note that the maximum value of $FI_{MT}(\alpha)$ occurs for $\alpha = 0$. Thus the orientation of the failure plane remains unaffected when material elasticities are degraded for this loading.

Matrix failure in compression

Proceeding in the same way as that for the matrix failure in tension, the matrix failure index for failure in compression is given by

$$FI_{MC}(\alpha) = -\frac{E_1E_2\eta_C(B+A\nu_{12})p_{n\psi}^{(-)}}{\left(2E_2\eta_C\nu_{12}^2+E_1(1-2\eta_C+\nu_{23})\right)S_L} + \sqrt{\eta_C^2\left[\frac{E_1^2E_2^2(B+A\nu_{12})^2\left(p_{n\psi}^{(-)}\right)^2}{\left\{2E_2\eta_C\nu_{12}^2+E_1(1-2\eta_C+\nu_{23})\right\}^2S_L^2} + \frac{G_{12}^2\gamma^2cos^2\alpha}{S_L^2}\right]} \qquad (4.53)$$

Using the numerical values Eq. (4.53) becomes:

$$FI_{MC}(\alpha) = \frac{\eta_C\ (2.765\ A\ + 8.679\ B\ )}{\eta_C - 0.753307} + \eta_C\sqrt{\left[\frac{7.65\ A^2+48.1\ AB+75.6\ B^2}{(0.753307-\eta_C)^2} + 187.90\gamma^2cos^2\alpha\right]} \qquad (4.54)$$

As for the matrix failure in tension, the failure plane for the matrix failure in compression remains unchanged when material elasticities are degraded for this loading.

The effect of material degradation upon the failure propagation has been studied by keeping the hydrostatic pressure constant and monotonically increasing the shear loading. As noted above, for λ = -200 MPa, the matrix fails in compression at σ_{12} = 145 MPa. With values of A and B in Eqn. (4.43) kept constant corresponding to λ = -200 MPa, the shear loading (γ_{12}) is monotonically

increased until the fibers fail. For each increment in γ_{12} the value of the material degradation factor η_C is found by setting $\alpha = 0$ and the failure index = 1 in Eq. (4.54). The computed global shear stress-shear strain curve is plotted in Fig. **4.4,** and the evolution of η_C is shown in Fig. **4.5**. Although the axial strains $\varepsilon_{11} = A$ and $\varepsilon_{22} = \varepsilon_{33} = B$ are kept constant after failure initiation in the matrix, the normal stresses change because of the degradation of elastic constants, e.g., see Eqns. (4.30) – (4.33). Thus σ_{11} differs from σ_{22} and σ_{33}. For values of elasticities used here, the normal stresses (in Pascals) are given by

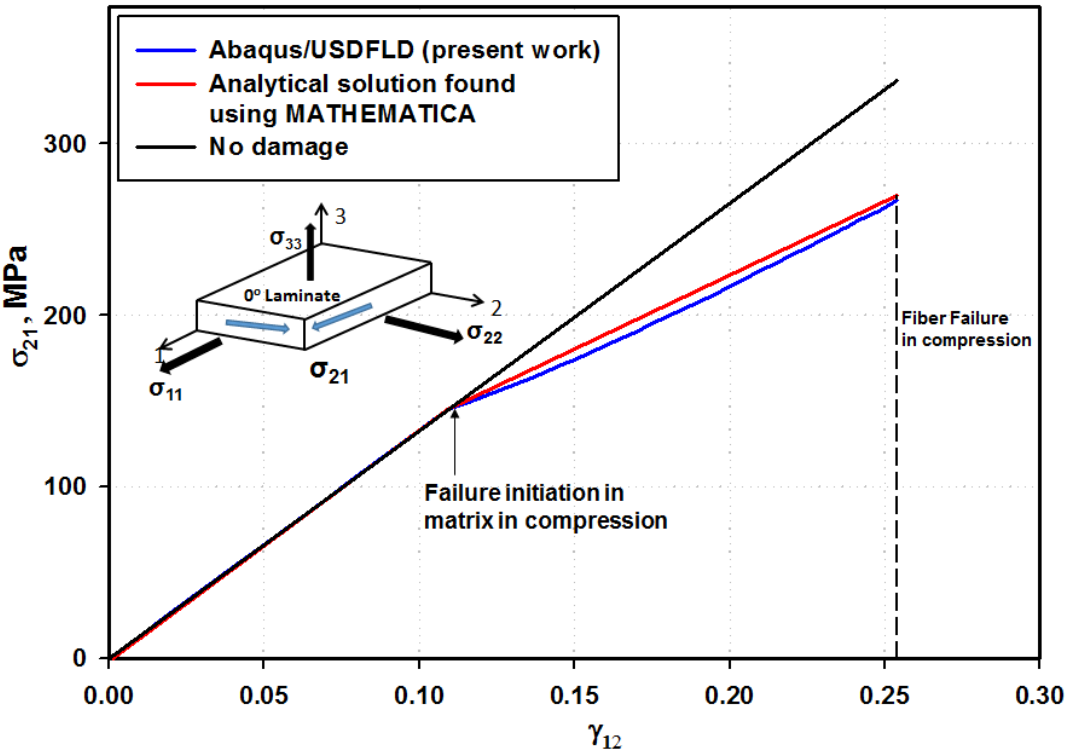

Figure 4.4: Global shear stress-shear strain response for PFA analysis of a laminate

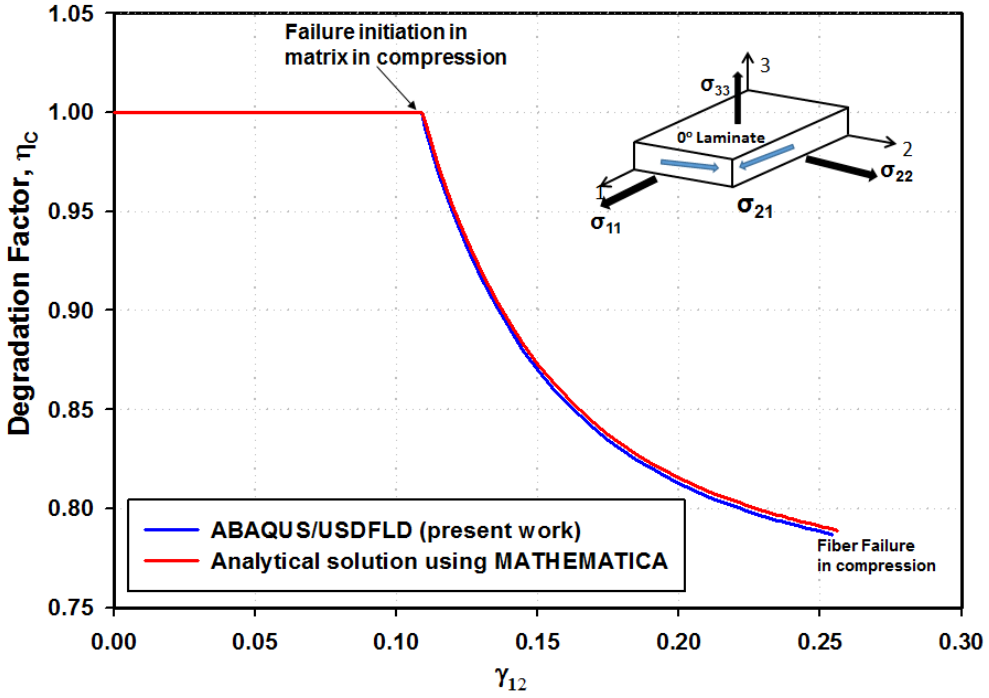

Figure 4.5: Evolution with the shear strain of the material degradation factor η_C for matrix failure under compression

$$\sigma_{11} = 10^9 \left[\frac{A(290.756\,\eta_C - 218.06)}{2.24402\,\eta_C - 1.6904429} + \frac{4.01378\,B\,\eta_C}{1.6904429 - 2.24402\,\eta_C}\right] \tag{4.55}$$

$$\sigma_{22} = \left[\frac{-2.0068939\,A\,\eta_C - 6.3109871\,B\,\eta_C}{1.6904429 - 2.24402\,\eta_C}\right] 10^9 \tag{4.56}$$

$$\sigma_{33} = \left[\frac{-2.0068939\,A\,\eta_C - 6.3109871\,B\,\eta_C}{1.6904429 - 2.24402\,\eta_C}\right] 10^9 \tag{4.57}$$

The evolution of the normal stresses σ_{11}, σ_{22}, and σ_{33} is exhibited in Fig. **4.6**.

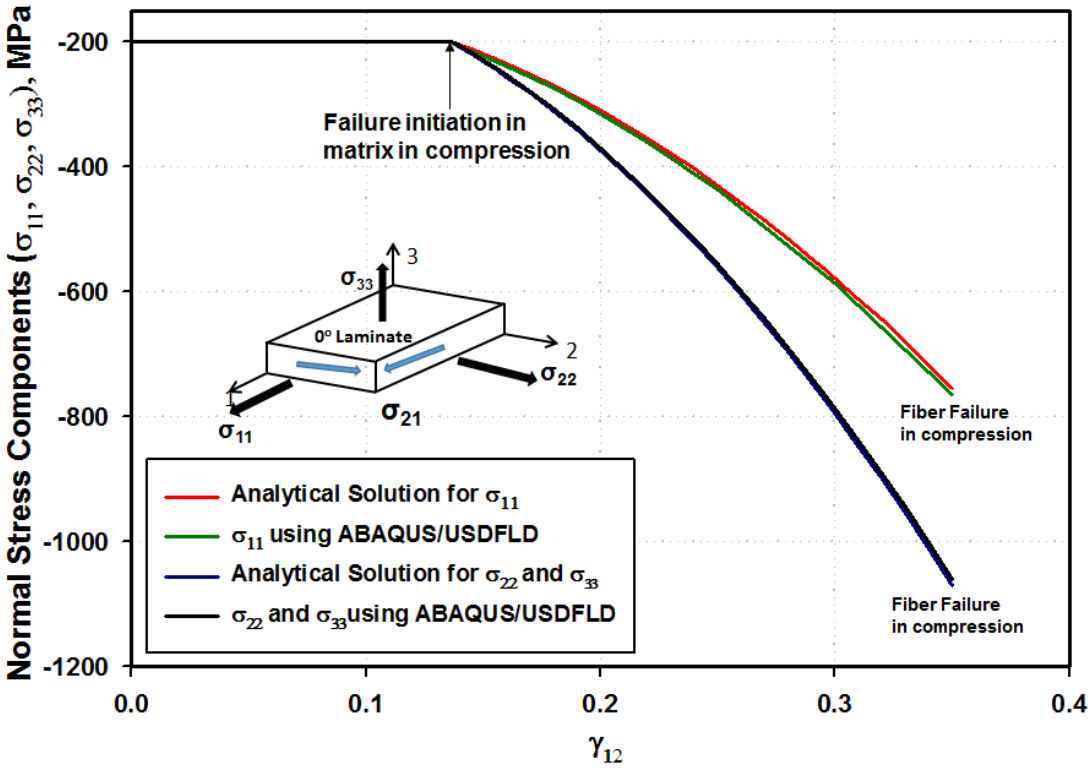

Figure 4.6: Variation with the shear strain of the normal stress components during the PFA analysis

In Table 4.1 we have listed numerical values of various variables to illustrate the variation in the normal stresses as the material is degraded with an increase in the applied shear strain. We note

Table 4.1: Values of variables for PFA under fixed triaxial strains and increasing shear strain

γ	A	B	η_C	σ_{11}, MPa	σ_{22}, MPa	σ_{33}, MPa	σ_{21}, MPa	Failure
0	-0.0005643	-0.01736	1	-200	-200	-200	0	
0.04	-0.0005643	-0.01736	1	-200	-200	-200	53.20	
0.08	-0.0005643	-0.01736	1	-200	-200	-200	106.4	
0.109085	-0.0005643	-0.01736	1	-200	-200	-200	145.08	Initiation
0.110	-0.0005643	-0.01736	0.995505	-201.78	-202.80	-202.8	145.64	Degradation
0.115	-0.0005643	-0.01736	0.972769	-211.89	-218.69	-218.69	148.79	Degradation
0.16	-0.0005643	-0.01736	0.85658	-333.07	-409.23	-409.23	182.78	Degradation
0.2540	-0.0005643	-0.01736	0.7899	-748.59	-1062.6	-1062.6	266.93	Fiber failure

that the fibers fail when η_C = 0.7899 and the matrix has not been fully degraded. This could be due to the assumption that the laminate can be modeled as a transversely isotropic material even after the failure has initiated in the matrix.

For the problem studied, the variation of the three normal stresses with the shear strain and the degradation parameter is exhibited in Fig. **4.7**.

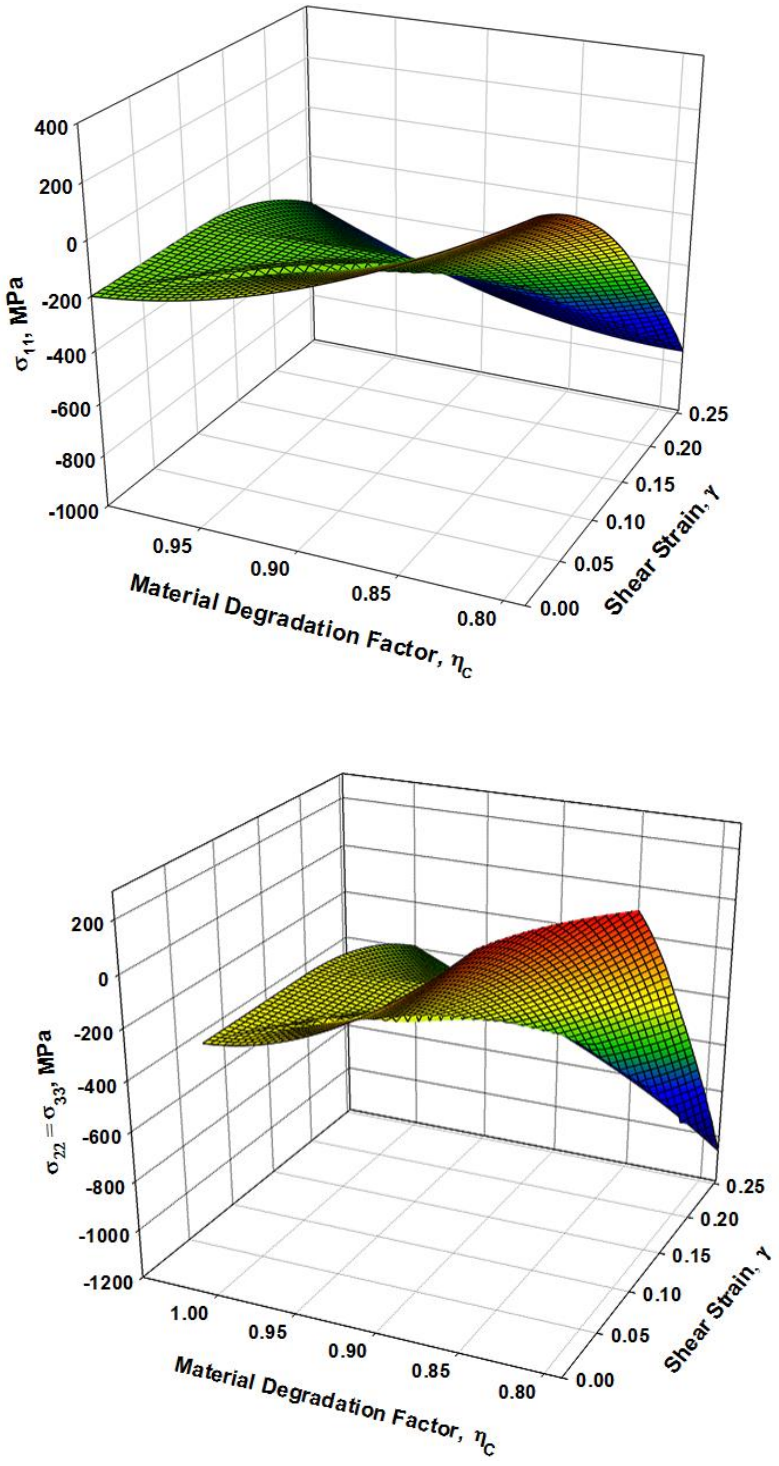

Figure 4.7: Variation of the normal stresses with the shear strain and the degradation parameter for the specific loading scenario considered

4.3 Summary

The progressive failure analysis (PFA) of laminated structures for simple three-dimensional deformations has been studied. A user defined subroutine capable of performing the PFA based on the Puck and Schürmann's failure criteria is developed for the commercial finite element software package, Abaqus. Two example problems are presented comparing analytical and FE solutions. Good agreements are found between the analytical and the FE solutions.

Chapter 5

Summary

The main objective of this dissertation was to review some of the literature on the Progressive Failure Analysis (PFA) of fiber-reinforced laminated composites, and implement through an USDFLD Puck and Schürmann's [13, 14] failure initiation and propagation criteria in the commercial finite element software, ABAQUS. Theoretical foundations of the Puck and Schürmann's [13, 14] failure criteria have been reviewed in Chapter 1. The implementation of the criteria in ABAQUS is described in Appendices. Some simple example problems illustrating predictions and implications of the Puck and Schürmann criteria have been discussed in Chapters 2, 3 and 4. The concluding remarks are in Section 1 below and suggestions to extend the work are given in Section 2.

5.1 Concluding Remarks

The concluding remarks are divided into the following subsections:

- Review of the failure criteria and material degradation available in the literature, and of reported development and identifications of key features of Puck and Schürmann's failure criteria presented in Chapter 1.
- Applications of Puck and Schürmann's failure criteria for plane stress problems presented in Chapters 2 and 3.
- The three dimensional progressive failure model discussed in Chapter 4.

5.1.1 Failure Criteria and Discussions

It is hard to come up with a universal definition for what constitutes "failure" of a composite structure since many failure theories and analytical models are available in the literature. The World Wide Failure exercise (WWFE) [3] summarized twenty three different failure criteria. All test cases presented in the WWFE are laminates assembled from continuous fiber reinforced unidirectional laminae subjected to 2D in-plane loading [3]. Objectives of the WWFE included:

(i) identify leading failure theories for fiber reinforced laminates, (ii) test the general applicability of the theories across a range of problems, (iii) compare predictions from these theories, (iv) compare predictions from the theories against experimental observations, and (v) summarize conclusions of the exercise. Among the twenty three failure criteria studied in the WWFE, predictions from Puck and Schürmann's failure criteria showed good agreement with most of the experimental data.

The current state of some failure criteria was described in Chapter 1. The revolutionary Hashin's [18] failure criteria for FRP composites based on the concept of failure plane were discussed in some detail, and correlations between Puck and Schürmann's and Hashin's failure criteria are reviewed. Puck and Schürmann's failure criteria can be used to determine the shear strength transverse to the failure plane.

5.1.2 Finite Element Analysis and USDFLD Subroutine

The PFA based on Puck and Schürmann's failure criteria has been implemented in the finite element commercial software package, Abaqus/CAE as a user defined subroutine, USDFLD in **FORTRAN**. Separate failure modes are considered for the matrix and the fiber of the laminates. Regarding the failure initiation and propagation in the matrix, the material degradation factors or the damage parameters are found using an iterative root finding process within the subroutine. Furthermore, the failure flags are generated for the corresponding modes of the fiber failure (tension or compression). The material degradation factors or the fiber failure flags are supplied to the main Abaqus program to reduce the material properties of the lamina. The development of the subroutine widens the capability of the software for PFA using the finite element method.

5.1.3 Structural Level Applications

The predictive capabilities of the analytical and the computational tools to perform the PFA are demonstrated with numerical simulations of laminated composite structures in Abaqus.

5.1.4 Specimens with Homogeneous Deformation

Several plane stress example problems with homogenous state of stress were considered. The results obtained using Abaqus were superimposed on the ones found using either an

analytical approach or the Classical Lamination Plate Theory (CLPT). As a first step for validation, deformations of a 30° off-axis specimen under uniaxial tension were studied. Then deformations of a quasi-isotropic $[0^o/45^o/90^o/-45^o]_S$ laminate under uniaxial tension were simulated and the results were compared against those from the CLPT, available experimental data and a simulation using built-in Hashin's failure criteria in Abaqus. Deformations of several laminates of $[\pm\theta]_S$ con-figuration under uniaxial compression are then studied. For these laminates the effect of the fiber orientation angle on the failure initiation stresses was observed. It was found that changing the fiber orientation for the laminates under compression can significantly change the ultimate failure load. Several example problems from the WWFE were also simulated and results were compared to the experimental results available in Ref. [5]. The results obtained using Abaqus were superimposed on the ones found using the CLPT. Good agreements have been found between these two sets of solutions.

5.1.5 Specimen Deforming under Cylindrical Bending

A laminated plate under cylindrical bending is considered to simulate the PFA for a non-uniform stress distribution through the thickness. The cylindrical bending of two laminate configurations of $[0^o]_8$ and $[0^o/45^o/90^o/-45^o]_S$ are studied, and the computed results are compared with those derived analytically from the CLPT.

With a gradual increase in the applied rotations at the end faces of the $[0^o]_8$ laminate the computed bending moment increased linearly with an increase in the applied rotation. For the problem studied, the maximum bending moment reached 355 N-mm/mm before it dropped to 228 N-mm/mm after the bottom-most ply failed due to fiber failure and was deleted from the analysis. The maximum bending moment was predicted to be 341 N-mm/mm using the CLPT. The overall computed structural responses of the laminate using the CLPT and the FE software Abaqus agreed with each other. Further gradual increase in the applied rotations shifted the neutral axis of the laminate upwards from the mid-surface.

The maximum bending moment reached 232 N-mm/mm using Abaqus for the quasi-isotropic laminate under cylindrical bending. Failure first initiated in the matrix. After the first fiber failure the bending moment dropped from 232 N-mm/mm to 99 N-mm/mm. The Abaqus

solutions are superimposed on those from the CLPT solutions. At a higher bending moment the laminate experienced the possibility of delamination or local buckling. A close agreement between the two set of results verified the Abaqus implementation of the PFA based on the Puck and Schürmann failure theory.

5.1.6 Open-Hole Tension (OHT) Specimen

The structural level verification is then extended to the PFA for a rectangular laminated plate with a circular hole at the centroid and loaded in uniaxial tension (OHT specimen). Thin symmetric cross-ply and a quasi-isotropic lay-up are modelled. Computed results included the axial load with increasing applied axial displacement for several different finite element meshes for convergence study and the sequence in which elements fail. The computed maximum load agreed well with that found experimentally, and is much higher than that at which the first element failed. Thus, designs based on the first ply failure load may be too conservative. The ultimate strength found using the Puck and Schürmann's failure theory is noticeably higher than that computed using the Hashin's failure theory which does not consider damage evolution. A detailed progression of failure has been presented on a ply-by-ply basis. The evolution of failure in the matrix **is** found to be gradually propagating throughout the structure.

5.2 Extension to 3D PFA

A three dimensional PFA of laminated composite structures, with the goal of studying failure in thick laminates, is presented in chapter 4. A layer by layer analysis technique was used to model composites. Each layer was required to be modelled individually based upon its fiber orientation angle.

Two fundamental stages of the PFA, failure initiation, and propagation are considered in the current work for the structures when 3D effects become significant. A numerical search method, the Golden Section Search was adapted to determine the failure plane in the matrix. The damage parameters known as material degradation factors and the angle α of the failure plane are found by solving a system of non-linear equations which satisfy the matrix failure criteria. The anisotropic material properties along and normal to the plane of failure are derived to determine which material properties need to be modified. For matrix failure under

compression where $\sigma_{nn} \leq 0$, it was found that Poission's ratio ν_{23} has to be increased to maintain the transverse isotropy of the material. Parameter η_ν is used to increase ν_{23} from its original value as a function of the compression degradation parameter η_C; i.e,

$$\eta_\nu = \frac{1 + \nu_{23} - \eta_C}{\eta_C \nu_{23}} \tag{5.1}$$

The material degradation process was then implemented in Abaqus and an USDFLD program was written to simulate the failure initiation and propagation by numerically solving for the material degradation factors (η_T and η_C) and the failure plane angle.

5.3 Conclusions

The major conclusions of this dissertation are summarized below.

- Progressive failure analyses of laminated composite structures significantly depend upon the failure criteria used. For the tensile loading of a laminate with an open hole, the Puck and Schürmann's failure criteria accurately predicted the failure load.
- In order to model PFA using the FEM, commercial software like Abaqus requires modifications to simulate progressive damage and eventual failure.
- The development and implementation of USDFLD subroutine in Abaqus enabled us to analyze progressive failure for different loadings. These illustrative examples can be used to study more realistic problem geometries and loading scenarios.
- Extending the PFA to three-dimensional problems is very challenging. A noteworthy point is that for matrix failure in compression it is necessary to degrade Poisson's ratio ν_{23} if the material symmetry is assumed to stay unaffected by failure initiation.

APPENDIX A

Implementation of PFA in Abaqus Software Package

A1. Finite Element Implementation in Abaqus

One of the key objectives of the present research is to develop capabilities for simulating failure scenarios for laminated composites based on failure models which are not currently implemented in the Abaqus package. A method to simulate progressive material damage of laminated composite structures in Abaqus [47] is through a User Defined Field implemented as a FORTRAN subroutine, identified as USDFLD. This USDFLD is based on Puck and Schürmann [14] failure criteria for unidirectional fiber-reinforced composite materials on a ply-by-ply basis. Abaqus requires the user written USDFLD subroutine in conjunction with a unique input file to numerically implement the PFA model. The Abaqus/CAE module at present is limited to Hashin's [18] failure criteria.

A2. Modelling Composite in Abaqus

The Abaqus/CAE package provides built-in composite modeling capability. Abaqus allows the user to define composite layups for three types of elements. These element types are referred to as continuum shell elements, conventional shell elements, and solid elements. Abaqus also has an extensive list of solid 3-D elements that are described in Chapter 23.1.4 of the Abaqus documentation [47]. When analyzing composites with Abaqus, the user should only use solid elements when (i) the transverse shear effects are predominant, (ii) the normal stress cannot be ignored, and (iii) accurate interlaminar stresses are desired [47].

The feature is referred to the as "Composite Layup" feature, and offers the user an opportunity to specify ply angles, material properties, ply thicknesses, and number of section points in each ply where the output is desired through its main Graphical User Interface (GUI). A schematic of the layup as defined by the "Composite Layup" feature in Abaqus is shown in Fig. **A.1**.

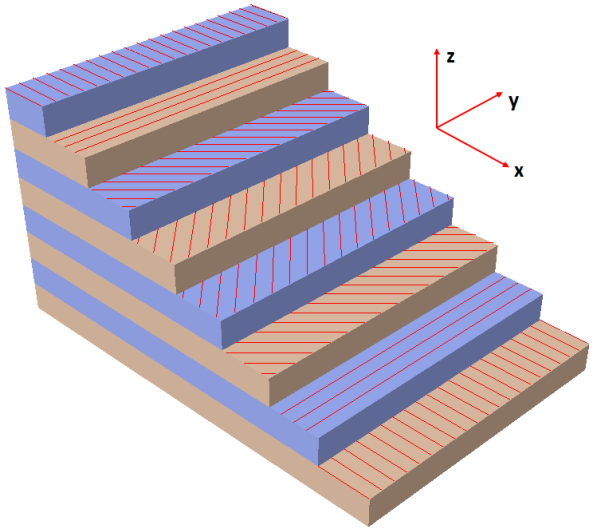

Figure A.1: Composite layer orientation used in Abaqus [47]

Meshing using the "Composite Layup" is very specific to shell elements (S4, S4R, S3/S3R, S8R). It is recommended to use shell elements suitable for modelling layered structures and to account for the influence of shear flexibility. In the current work all analyses are performed using the 4-noded S4 shell element available in the Abaqus library.

A3. USDFLD Subroutine

The user defined subroutine, USDFLD, generates field variables which are eventually supplied to the main Abaqus solver. The subroutine redefines field variables at each material point of the structure. USDFLD allows the user to define field variables at an integration point as functions of time or any of the available material point quantities listed in the Output Variable Identifiers table with the exception of the user-defined output variables. The solution-dependent material properties may readily be defined as functions of field variables, as the field variables are supplied back and forth between Abaqus and USDFLD. The USDFLD is used at all of the material points of the elements for which the material definition includes user-defined field variables. USDFLD also enables one to update state variables in Abaqus

A3.1 USDFLD Subroutine Interface

The subroutine was developed using the basic FORTRAN interface provided within

Abaqus documentation. Figure **A.2** shows the interface in which the USDFLD subroutine may be developed. Several variables are imported by the USDFLD subroutine from the Abaqus main program. Table A.1 gives descriptions of these variables.

```
      SUBROUTINE USDFLD(FIELD,STATEV,PNEWDT,DIRECT,T,CELENT,
     1 TIME,DTIME,CMNAME,ORNAME,NFIELD,NSTATV,NOEL,NPT,LAYER,
     2 KSPT,KSTEP,KINC,NDI,NSHR,COORD,JMAC,JMATYP,MATLAYO,LACCFLA)
     C
       INCLUDE 'ABA_PARAM.INC'
      C
       CHARACTER*80 CMNAME,ORNAME
       CHARACTER*3  FLGRAY(15)
       DIMENSION FIELD(NFIELD),STATEV(NSTATV),DIRECT(3,3),
     1 T(3,3),TIME(2)
       DIMENSION ARRAY(15),JARRAY(15),JMAC(*),JMATYP(*),COORD(*)
       User coding to define FIELD and, if necessary, STATEV and PNEWDT

       RETURN
       END
```

Figure A.2: The USDFLD interface used for development of the subroutine

Table A.1: Description of the variables supplied from main Abaqus program to the USDFLD subroutine [47]

Variables Supplied from Abaqus	Description
DTIME	Time increment
CMNAME	User-specified material name, left justified
ORNAME	User-specified local orientation name
NFIELD	Number of field variables defined at a material point
NSTATV	User-defined number of solution-dependent state variables
NOEL	Element number
NPT	Integration point number
LAYER	Layer number used in the case of composite shells and layered solids
KSPT	Section point number within the current layer
KSTEP	Step number
KINC	Increment number
NDI	Number of stress components at an integration point
NSHR	Number of shear stress components at an integration point

COORD	Coordinates of an integration point
JMAC, JMATYP, MATLAYO, LACCFLA	Variable that must be passed in to the GETVRM utility routine to access an output variable

Detailed discussions of several of these variables are given below:

Field

An array containing the field variables at the current material point is assigned as Field in the USDFLD subroutine. These are passed with values interpolated each nodes at the end of the current increment, as specified with initial condition definitions, predefined field variable definitions, or user subroutine UFIELD. The UFIELD subroutine allows the user to prescribe predefined field variables at the nodes of a model, where the predefined field variables at a node can be updated individually, or a number of field variables at the node can be updated simultaneously. The interpolation is performed using the same scheme as that used to interpolate temperatures where an average value is used for linear elements and an approximate linear variation is used for quadratic elements (also see "Solid (con- tinuum) elements," Section 22.1.1 of the Abaqus Analysis User's Manual). The updated values are used to calculate values of material properties that are dependent on field variables and are passed into other user subroutines that are called at this material point.

STATEV (NSTATV) or SDVs

SDVs are arrays containing the solution-dependent state variables. These are passed in as the values at the beginning of each had increment. In all cases, STATEV may be updated in this subroutine and the updated values are passed into other user subroutines that are called at this material point. These state variables are eventually transferred back into the main Abaqus program.

PNEWDT

PNEWDT is a variable controlling the time increment in Abaqus. If PNEWDT is assigned a value less than 1.0, Abaqus/Standard must abandon the time increment and attempt it again with a smaller time increment. The suggested new time increment provided to the

automatic time integration algorithms is PNEWDT x DTIME, where the PNEWDT used is the minimum value for all calls to user sub- routines that allow redefinition of PNEWDT for a given iteration. If automatic time increment is not selected in the analysis procedure, values of PNEWDT that are greater than 1.0 will be ignored and values of PNEWDT that are less than 1.0 will cause the main Abaqus job to terminate.

DIRECT (3,3)

The variable DIRECT (3,3) is an array containing the direction cosines of the material principal directions in terms of the global basis directions. DIRECT(1,1), DIRECT(2,1), DIRECT(3,1) give the (1, 2, 3) components of the first material principal direction; DIRECT(1,2), DIRECT(2,2) and DIRECT(3,2) give the second material principal direction. For a shell element, the first two directions are in the plane of the element and the third direction is normal to the plane.

T(3,3)

An array containing the direction cosines of the material principal orientation components relative to the element basis directions. This is the orientation that defines the material principal directions (DIRECT) in terms of the element basis directions. For continuum elements T and DIRECT are identical. For shell element $T(1, 1) = \cos\theta$, $T(1, 2) = \sin\theta$, $T(2, 1) = \sin\theta$, $T(2, 2) = \cos\theta$, $T(3, 3) = 1$, and all other components are zero, where θ is the counterclockwise rotation around the normal vector that defines the orientation of the ply. If no orientation is used, T is defined as an identity matrix.

A4. Field Variables in USDFLD for PFA

Initially the field variables are set equal to one. A major function of the USDFLD is the capability to import values of stresses and strains from Abaqus/CAE. Another utility subroutine called GETVRM is used to call the stresses and strains at each integration point for each load step in Abaqus. In USDFLD, these stresses are used to evaluate the failure process and the consequent material degradation to determine the damage variables for a particular load step. Once the values of the stresses are obtained from Abaqus, the subroutine checks for failure conditions at all integration points in a particular time increment. In the case of matrix failure, the damage parameters are solved using the numerical procedure and stored as solution dependent

variables. For Mode A failure, the value of the damage parameter is obtained within the subroutine and then is sent to Abaqus as a field variable where the material properties are reduced based upon the value of the damage parameters. The values of the solution data provided are from the beginning of the current increment. The subroutine USDFLD requires defining the field variables (FV's) as the dam- age variables or the material degradation factors for PFA. The field variables are generally processed as nodal data by Abaqus. When Abaqus begins to calculate the element stresses and stiffnesses (i.e., in the element loop), it interpolates the field variables using their nodal values to the integration (material) points of each element. When the USDFLD is used, the interpolated field variables are replaced by the values computed in the USDFLD subroutine before the material properties of an element are calculated. However, the values defined by the USDFLD are not stored in Abaqus. In order to access the previous values of a field variable, one must save them as solution-dependent variables (SDV's) inside the USDFLD. Abaqus/Standard allows the field variables to be defined as functions of solution data such as stress or strain at the material point. For an implementation of Puck and Schürmann [13, 14] failure criteria, all four damage parameters are modeled as field variables. Table A.2 shows the definitions of the field variables used in the subroutine. For the fiber failure, FV3 and FV4 are the fiber tensile and compressive damage parameters, respectively, and are defined through Heaviside step functions, or unit step functions, H [x].

$$FV3 = H\left[1 - \frac{\sigma_{11}}{X_T}\right]_{\sigma_{11}>0} \tag{A.1}$$

$$FV3 = H\left[1 - \frac{|-\sigma_{11}|}{|X_C|}\right]_{\sigma_{11}<0} \tag{A.2}$$

Table A.2: Description of field variables for USDFLD subroutine

Field Variable	Description	Values	Properties degraded
FV1	Mode A degradation factor, η_a when $\sigma_{22} > 0$	$0 \leq \eta_a \leq 1$ 0 complete failure 1 No failure	Degradation of E_2, ν_{12} and G_{12}
FV2	Mode B and C degradation factor, $\eta^{(-)}$ when $\sigma_{22} < 0$	$0 \leq \eta^{(-)} \leq 1$ 0 complete failure 1 No failure	Degradation of G_{12}
FV3	Flag for fiber failure In tension	0 complete failure 1 No failure	Set $E_1=0$ at fiber failure in tension
FV4	Flag for fiber failure In compression	0 complete failure 1 No failure	Set $E_1=0$ at fiber failure in compression

A4.1 Solution Dependent Variables

Table A.3 shows descriptions of all of the solution-dependent variables used in the subroutine. All field variables are stored as solution dependent variables in order to access their values from the previous time increments. The SDVs can be considered as variables containing the PFA history.

Table A.3: Descriptions of solution dependent variables in the USDFLD subroutine

Solution Dependent variable	Descriptions	Values
SDV1	Mode A degradation factor, η_a, when $\sigma_{22} > 0$	$0 < \eta_a \leq 1$, 1 means no failure, 0 means complete failure
SDV2	Mode A failure index	Between 0 and 1
SDV3	Strain measure, ε_{11}, in a particular load step	Attained in a load step
SDV4	Strain measure, ε_{22} in a particular load step	Attained in a load step
SDV5	Strain measure, γ_{12} in a particular load step	Attained in a load step
SDV6	Mode B/C degradation factor, $\eta^{(-)}$ when $\sigma_{22} < 0$	$0 < \eta^{(-)} \leq 1$, 1 means no failure, 0 means complete failure
SDV7	Mode B/C failure index	Between 0 and 1
SDV8	Flag for fiber failure in tension stored as field variable	0 complete failure 1 no failure
SDV9	Flag for fiber failure in compression stored as field variable	0 complete failure 1 no failure

A5. Flow chart for PFA implementation in USDFLD

Flow charts of the PFA in Abaqus are presented in this section of the dissertation. Fig. **A.3** shows a flow chart of the Abaqus main program which includes calling the USDFLD subroutine. A flow chart describing the algorithm of the USDFLD subroutine is shown in Fig. **A.4**. A sample Abaqus input file and the USDFLD subroutine developed for plane stress conditions are given in sections A7, A8, and A9. The flow chart in Fig. **A.4** corresponds to the subroutine given in the Appendix.

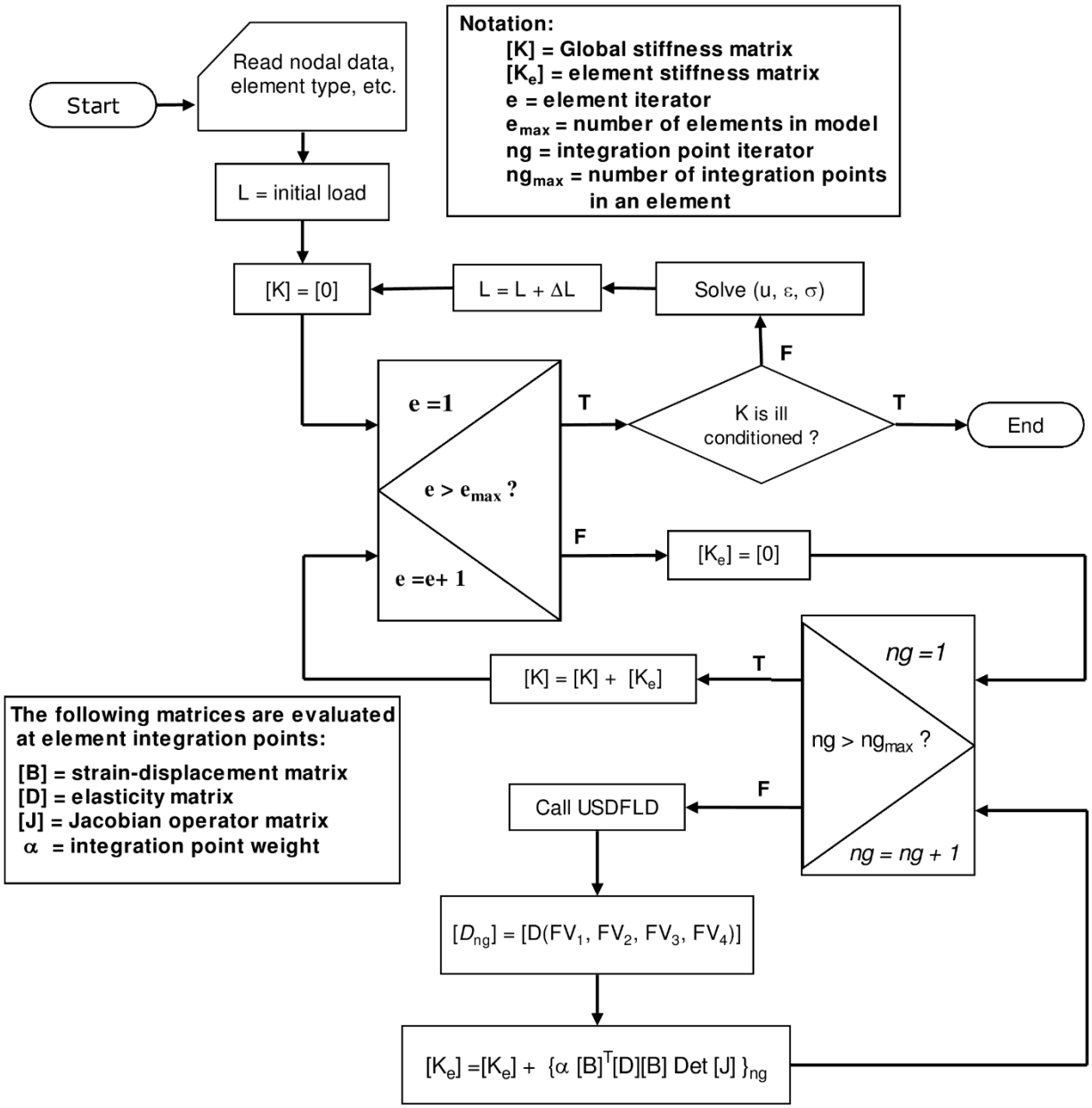

Figure A.3: Flow chart of overall analysis flow chart in Abaqus.

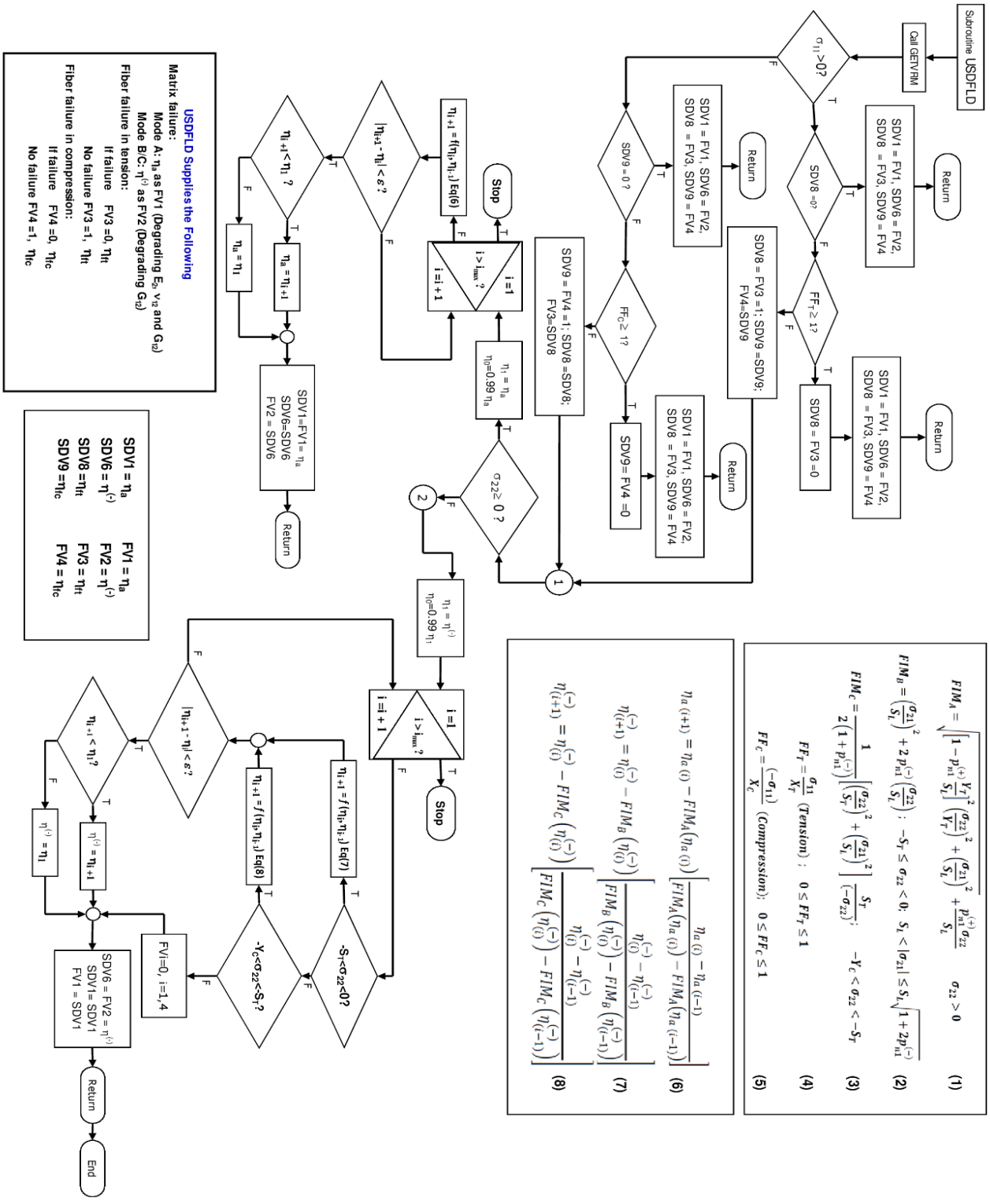

Figure A.4: USDFLD flow chart for PFA using Puck and Schürmann's failure criteria under plane stress assumption.

A5.1 Premise of the USFLD flowchart

The basic premise of the flowchart presented in Fig. **A.4** is described below:

- Abaqus calls the USDFLD subroutine at each integration point during the analysis. Once the subroutine is entered, a utility subroutine referred to as "GETVRM" imports values of stresses and strains at each integration point of every finite element used to model the structure.
- According to Table A.3, SDV8 is assigned to the fiber failure flag in tension, SDV9 is assigned to the fiber failure flag in compression, SDV1 is assigned to η_a, and SDV6 is assigned to $\eta^{(-)}$. The strain components ε_{11}, ε_{22} and γ_{12} are assigned as SDV2, SDV3, and SDV4, respectively.
- According to Table A.2 FV1 is assigned to η_a, FV2 is assigned to $\eta^{(-)}$. FV3 is assigned to the fiber failure flag in tension, and FV4 is assigned to the fiber failure flag in compression.
- If σ_{11} is greater than zero then it is checked whether SDV8 is zero or not from the previous load increment. If SDV8=0, then values of all four field variables (FV1, FV2, FV3, and FV4) are returned. If SDV8=0 then fiber failure in tension mode is checked. If fiber failure in tension is detected by satisfying $FF_T \geq 1$, then SDV8 and FV1 are set to zero and returned to the main Abaqus solver along with other field variables. If $FF_T < 1$, then the values SDV8, SDV9, FV3, and FV4 are returned as their previous values to the Abaqus main solver.
- If σ_{11} is less than zero then we check whether SDV9 is zero or not from the previous load increment. If SDV9=0, then values of all four field variables (FV1, FV2, FV3, and FV4) are returned. If SDV9 $\neq$ 0 then fiber failure in compression mode is checked. If fiber failure in compression is detected by satisfying $FF_C \geq 1$, then SDV9 and FV2 are set to zero and returned to the main Abaqus solver along with other field variables. If $FF_C < 1$, then the values SDV8, SDV9, FV3, and FV4 are returned as their previous values to the Abaqus main solver.
- If fiber failure is not detected then the sign of σ_{22} is checked for the modes of the

matrix failure. If $\sigma_{22} \geq 0$, then failure in matrix Mode A is checked. If failure criterion in Mode A is satisfied then the value of the material degradation factor η_a is found by solving the non-linear equation using the secant method. The value of η_a is saved in SDV1 and FV1 and supplied to the Abaqus main solver.

- If $\sigma_{22} < 0$, then matrix failure in Mode B is checked by evaluating the range of σ_{22} between $-S_T < \sigma_{22} < 0$, otherwise failure in Mode C is checked between $-Y_C < \sigma_{22} < -S_T$. If the failure criterion in either Mode B or Mode C is satisfied then the value of the material degradation factor $\eta^{(-)}$ is found by solving the non-linear equation using the secant method. The value of $\eta^{(-)}$ is saved in SDV6 and FV2 and supplied to the Abaqus main solver.

A6. USDFLD Subroutine Linkage to Abaqus/CAE

In order to perform the finite element analysis in Abaqus in association with the USDFLD subroutine, it is necessary to introduce the field variables as part of the material manager. Three features in Abaqus/CAE material manager are required to be activated while running the analysis in conjunction with the USDFLD sub- routine. The feature regarding the solution dependent variables (SDV's) may be introduced by activating a feature called Depvar in the material manager of the Abaqus/CAE. An image of the Abaqus/CAE material manager method for specifying the feature for solution dependent variable is shown in Fig. **A.5**. It should be specified that there are a total of nine solution dependent variables for studying PFA using Puck and Schürmann's [14] criteria.

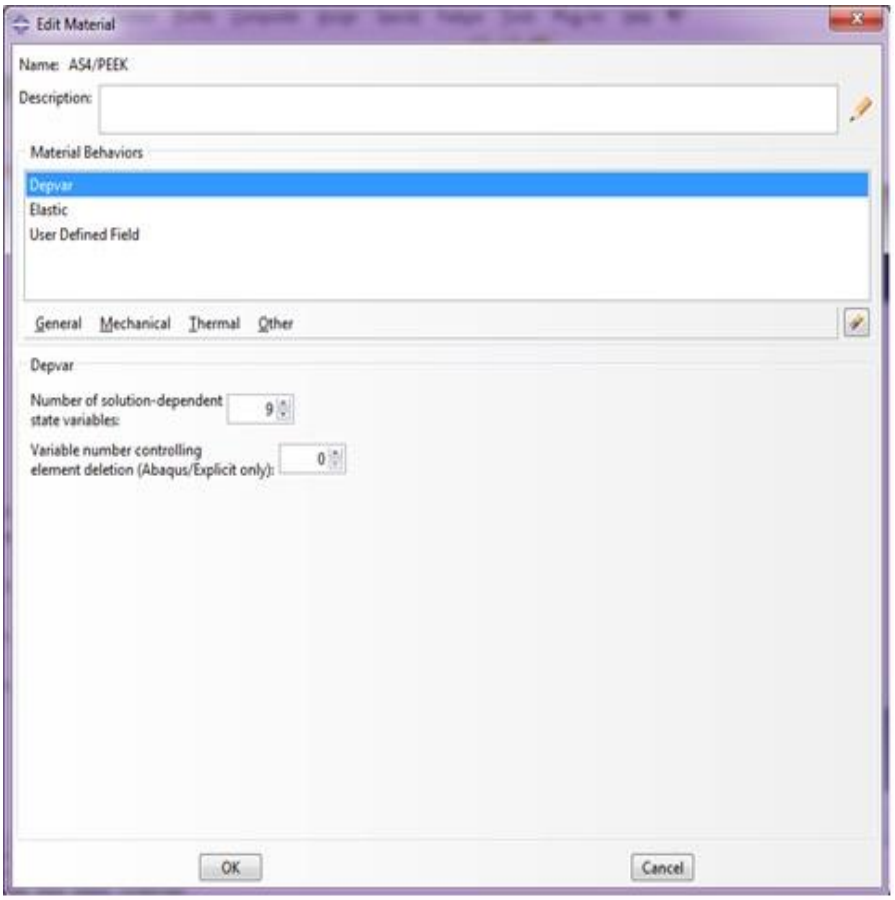

Figure A.5: Abaqus/CAE tab depicting features of solution dependent variables

The elastic material properties are specified through the use of Elastic feature in the Abaqus/CAE material manager. The Lamina properties are specified for a plane stress problem. An image of Abaqus/CAE material manager is shown in Fig. **A.6** for specifying the elastic material properties for a lamina. The tables specified under the Elastic section of the material manager also include the field variables. The total number of field variables is specified as four. The image in Fig. A.6 also indicates which material property should be reduced for the corresponding mode of failure. For example, in the case of Mode A failure in the matrix, field variable one (FV1) is set to zero by holding other field variables as one.

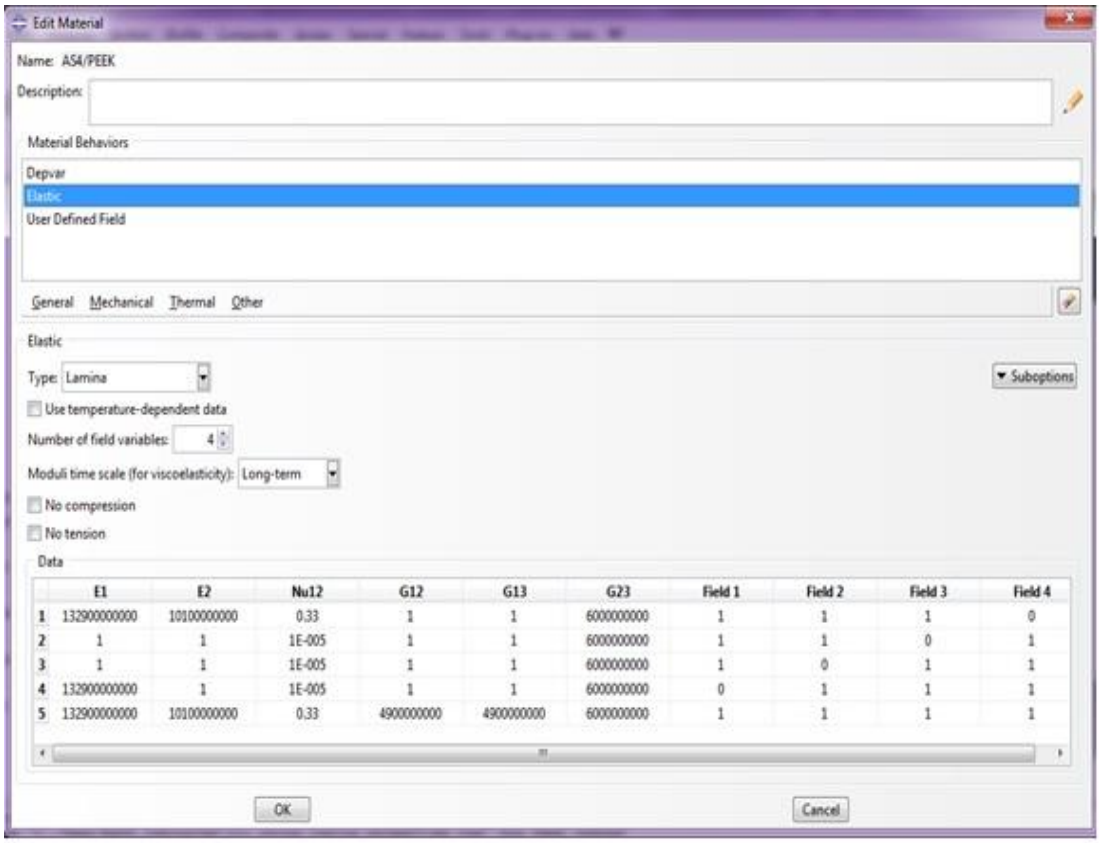

Figure A.6: Abaqus/CAE tab to specify elastic properties and field variables

In order to specify that the current analysis requires using the USDFLD subroutine, a feature called "User Defined Field" must be activated in the Abaqus material manager. The method for specifying the user defined field feature in Abaqus/CAE material manager is shown in Fig. **A.7**.

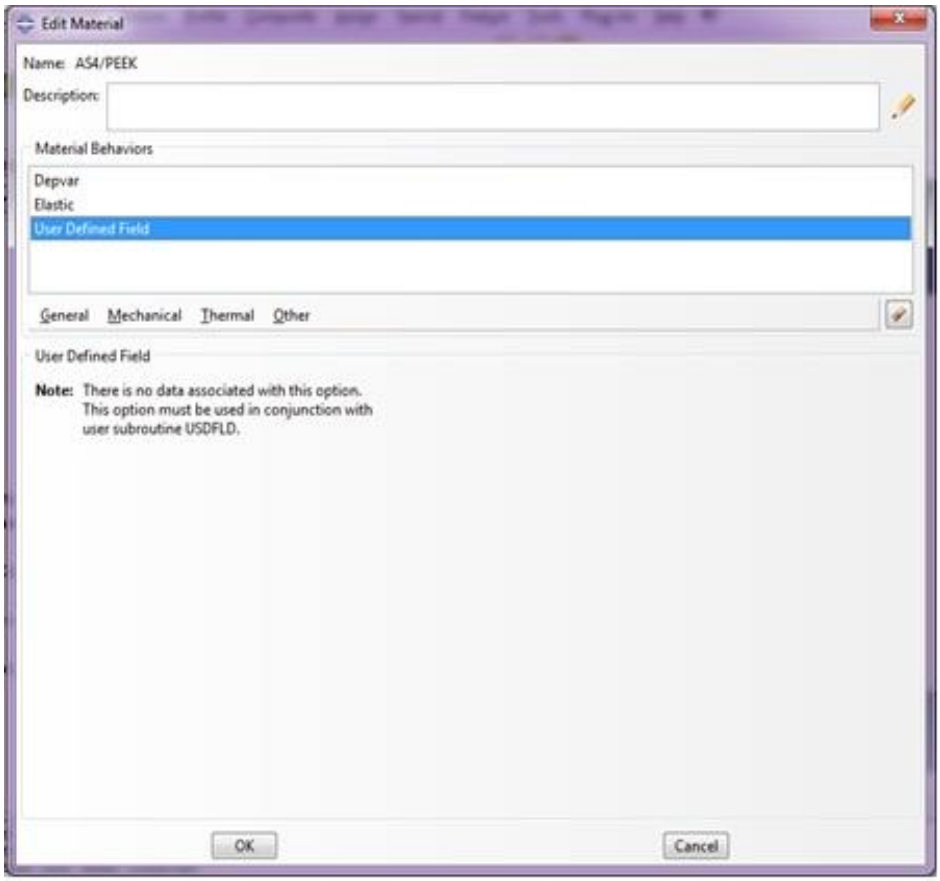

Figure A7: Abaqus/CAE tab to activate the feature for user defined

A7. ABAQUS Input file

The following ABAQUS input file is an example for the 30^{o}-off axis specimen described in section 2.1.

```
*Heading
** Job name: 30lamina Model name: Model-1
** Generated by: Abaqus/CAE 6.14-1
*Preprint, echo=NO, model=NO, history=NO, contact=NO
**
** PARTS
**
*Part, name=Part-1
*Node
      1,           0.,           0.,           0.
      2,  0.075000003,           0.,           0.
      3,  0.150000006,           0.,           0.
      4,           0., 0.0500000007,           0.
      5,  0.075000003, 0.0500000007,           0.
      6,  0.150000006, 0.0500000007,           0.
      7,           0.,  0.100000001,           0.
      8,  0.075000003,  0.100000001,           0.
      9,  0.150000006,  0.100000001,           0.
*Element, type=S4
1, 1, 2, 5, 4
2, 2, 3, 6, 5
3, 4, 5, 8, 7
4, 5, 6, 9, 8
** Region: (CompositeLayup-1-1: Generated From Layup)
*Elset, elset=CompositeLayup-1-1, generate
 1,  4,  1
** Section: CompositeLayup-1-1
*Shell Section, elset=CompositeLayup-1-1, composite,
layup=CompositeLayup-1
0.001, 3, Material-1, 30., Ply-1
*End Part
**
**
** ASSEMBLY
**
*Assembly, name=Assembly
**
*Instance, name=Part-1-1, part=Part-1
```

```
*End Instance
**
*Nset, nset=Set-1, instance=Part-1-1, generate
 1,  7,  3
*Elset, elset=Set-1, instance=Part-1-1
 1, 3
*Nset, nset=Set-2, instance=Part-1-1
 1,
*Nset, nset=Set-3, instance=Part-1-1, generate
 3,  9,  3
*Elset, elset=Set-3, instance=Part-1-1
 2, 4
*Nset, nset=Set-4, instance=Part-1-1, generate
 1,  7,  3
*Elset, elset=Set-4, instance=Part-1-1
 1, 3
*Nset, nset=Set-5, instance=Part-1-1, generate
 3,  9,  3
*Elset, elset=Set-5, instance=Part-1-1
 2, 4
*Nset, nset=Set-6, instance=Part-1-1
 1,
*Nset, nset=Set-7, instance=Part-1-1
 1, 2, 3, 7, 8, 9
*Elset, elset=Set-7, instance=Part-1-1, generate
 1,  4,  1
*Nset, nset=Set-8, instance=Part-1-1, generate
 1,  3,  1
*Elset, elset=Set-8, instance=Part-1-1
 1, 2
*Nset, nset=Set-9, instance=Part-1-1, generate
 7,  9,  1
*Elset, elset=Set-9, instance=Part-1-1
 3, 4
*Elset, elset=_Surf-1_E3, internal, instance=Part-1-1
 3, 4
*Surface, type=ELEMENT, name=Surf-1
_Surf-1_E3, E3
*Elset, elset=_Surf-2_E3, internal, instance=Part-1-1
 3, 4
*Surface, type=ELEMENT, name=Surf-2
_Surf-2_E3, E3
*Elset, elset=_Surf-3_E2, internal, instance=Part-1-1
 2, 4
*Surface, type=ELEMENT, name=Surf-3
```

```
_Surf-3_E2, E2
*End Assembly
**
** MATERIALS
**
*Material, name=Material-1
*Depvar
      9,
*Elastic, dependencies=4, type=ENGINEERING CONSTANTS
       0.1,      0.1,      0.1,   0.0001,   0.0001,      0.4,
0.0001,   0.0001
    6e+09, ,       1.,       1.,       1.,       0.
       0.1,      0.1,      0.1,   0.0001,   0.0001,      0.4,
0.0001,   0.0001
    6e+09, ,       1.,       1.,       0.,       1.
 5.348e+10, 1.77e+10, 1.77e+10,    0.278,    0.278,      0.4,
0.001,   0.0001
    6e+09, ,       1.,       0.,       1.,       1.
 5.348e+10,    0.001,    0.001,    1e-05,    1e-05,      0.4,
0.0001,   0.0001
    6e+09, ,       0.,       1.,       1.,       1.
 5.348e+10, 1.77e+10, 1.77e+10,    0.278,    0.278,      0.4,
5.83e+09, 5.83e+09
    6e+09, ,       1.,       1.,       1.,       1.
*User Defined Field
**
** BOUNDARY CONDITIONS
**
** Name: BC-2 Type: Displacement/Rotation
*Boundary
Set-4, 1, 1
Set-4, 3, 3
Set-4, 4, 4
Set-4, 5, 5
Set-4, 6, 6
** Name: BC-4 Type: Displacement/Rotation
*Boundary
Set-6, 2, 2
Set-6, 3, 3
Set-6, 4, 4
** ----------------------------------------------------------------
---
**
** STEP: Step-1
**
```

```
*Step, name=Step-1, nlgeom=NO
*Static
1., 1., 1e-05, 1.
**
** BOUNDARY CONDITIONS
**
** Name: BC-2 Type: Displacement/Rotation
*Boundary, op=NEW
Set-4, 1, 1
Set-4, 3, 3
Set-4, 4, 4
Set-4, 5, 5
** Name: BC-3 Type: Displacement/Rotation
*Boundary, op=NEW
Set-3, 1, 1, 0.00015
** Name: BC-4 Type: Displacement/Rotation
*Boundary, op=NEW
Set-6, 1, 1
Set-6, 2, 2
Set-6, 3, 3
** Name: BC-5 Type: Displacement/Rotation
*Boundary, op=NEW
Set-8, 2, 2
** Name: BC-6 Type: Displacement/Rotation
*Boundary, op=NEW
Set-9, 2, 2
**
** OUTPUT REQUESTS
**
*Restart, write, frequency=0
**
** FIELD OUTPUT: F-Output-1
**
*Output, field, variable=PRESELECT
**
** HISTORY OUTPUT: H-Output-1
**
*Output, history, variable=PRESELECT
*End Step
```

A8. USDFLD Subroutine Written Using FORTRAN in 2D

```
C     ABAQUS USER DEFINED FIELD VARIABLE (USDFLD) DEVELOPED FOR PROGRESSIVE
C     FAILURE ANALYSIS OF LAMINATED COMPOSITE STERUCUTRES IN 2D FRMAEWORK.

C     THE PUCK AND SCHURMANN FAILURE CRITRIA ARE USED

C     THE SUBROUINE IMPORTS STRESS VALUES ALONG THE MATERIAL PRINCIPAL
      DIRECTION, THE 1-2-3 COORDINATE SYSTEM OF EACH PLY. THE LAMINATE IS
      MODELLED USING THE THE COMPOSITE LAYUP MANAGER, WHICH IS A BUILT-IN
      FEATURE OF ABAQUS/CAE. THE S4 (4-NODDED CONVENTIONAL SHELL) ELEMENTS ARE
      USED.

C     THE SUBROUINE IS EVALUATED AT EACH INTEGRATION POINT OF EACH PLY
      OF THE LAMINATE
C SUBROUINE STARTS HERE
      SUBROUTINE USDFLD(FIELD,STATEV,PNEWDT,DIRECT,T,CELENT,TIME,DTIME,
     1 CMNAME,ORNAME,NFIELD,NSTATV,NOEL,NPT,LAYER,KSPT,KSTEP,KINC,
     2 NDI,nshr,coord,jmac,jmtyp,matlayo,laccflg)
C
      INCLUDE 'ABA_PARAM.INC'

C MATERIAL AND STRENGTH PARAMETERS
      CHARACTER*80 CMNAME,ORNAME
      CHARACTER*3 FLGRAY(15)
      DIMENSION FIELD(NFIELD),STATEV(NSTATV),DIRECT(3,3),T(3,3),TIME(2),
     *  coord(*),jmac(*),jmtyp(*)
      DIMENSION ARRAY(20),JARRAY(20)
C  VARIABLES IN MODE A
      DOUBLE PRECISION:: SL,YT, p1, p2, p3, YC, XT, XC
      DOUBLE PRECISION:: E_1, E_2, NU_12, NU_21, G_12
      DOUBLE PRECISION :: ETA_OLD,ETA_NEW,ETA
      DOUBLE PRECISION :: G_FN_NEW,G_FN_OLD
      DOUBLE PRECISION, DIMENSION (2):: VECT_ETA, VECT_G_FN
      DOUBLE PRECISION :: CALC_ETA,TMP_1,TMP_2,TMP_3, TMP_4
      DOUBLE PRECISION, DIMENSION (3,1):: STRAIN_NEW
      DOUBLE PRECISION :: S11,S22,S12, FF,GG
      DOUBLE PRECISION :: A, B, C, D, E, FMA
C  VARIABLES IN MODE B AND C
      DOUBLE PRECISION :: ETA_OLDBC,ETA_NEWBC,G_FN_NEWBC,G_FN_OLDBC,ETABC
      DOUBLE PRECISION, DIMENSION (2):: VECT_ETABC, VECT_G_FNBC
      DOUBLE PRECISION :: CALC_ETABC,TMPBC_1,TMPBC_2,TMPBC_3, TMPBC_4
      DOUBLE PRECISION :: S11BC,S22BC,S12BC, H, P, R
      DOUBLE PRECISION :: MODEBC,SR1,SR2,SR3,SR4
      DOUBLE PRECISION :: ST, p3, TAU21C, KK, LL
      INTEGER :: IFLAG, LOGIC_CRIT
C VARIABLES FOR FIBER FAILURE IN TENSION
      DOUBLE PRECISION :: FFT
C VARIABLES FOR FIBER FAILURE IN COMPRESSION
      DOUBLE PRECISION :: FFC


C**********************************************************************
```

```
C MATERIAL PROPERTISES AND PARAMETERS
C**********************************************************************
C     GET E_1: VALUES IN Pascal
      open (unit=24, file="Z:\\sandbox\\abaqus-test\\E1.txt")
      read(24,*)E1
      close(24)
C     GET E_2: VALUES IN Pascal
      open (unit=48, file="Z:\\sandbox\\abaqus-test\\E2.txt")
      read(48,*)E2
      close(48)
C     GET NU_12
      open (unit=96, file="Z:\\sandbox\\abaqus-test\\NU12.txt")
      read(96,*)NU_12
      close(96)
C     GET G_12: VALUES IN Pascal
      open (unit=120, file="Z:\\sandbox\\abaqus-test\\G12.txt")
      read(120,*)G_12
      close(120)
C     GET SL, IN PLANE SHEAR STRENGHT: VALUES IN Pascal
      open (unit=144, file="Z:\\sandbox\\abaqus-test\\SL.txt")
      read(144,*)SL
      close(144)
C     GET YT, TENSILE STRENGTH IN TRANSVERSE DIRECTION: VALUES IN Pascal
      open (unit=168, file="Z:\\sandbox\\abaqus-test\\YT.txt")
      read(168,*)YT
      close(168)
C     GET YC, COMPRESSIVE STRENGTH IN TRANSVERSE DIRECTION: VALUES IN Pascal
      open (unit=192, file="Z:\\sandbox\\abaqus-test\\YC.txt")
      read(192,*)YC
      close(192)
C     GET XT, VALUE OF THE TENSILE STRENGTH ALONG FIBER : VALUES IN Pascal
      open (unit=216, file="Z:\\sandbox\\abaqus-test\\XT.txt")
      read(216,*)XT
      close(216)
C     GET XC, VALUE OF THE COMPRESSIVE STRENGTH ALONG FIBER:VALUES IN Pascal
      open (unit=240, file="Z:\\sandbox\\abaqus-test\\XC.txt")
      read(240,*)XC
      close(240)
C     GET p1, INCLINATION SLOPE p_(n1)^(+)
      open (unit=264, file="Z:\\sandbox\\abaqus-test\\p1.txt")
      read(264,*)p1
      close(264)
C     GET p2, INCLINATION SLOPE p_(n1)^(+)
      open (unit=288, file="Z:\\sandbox\\abaqus-test\\p2.txt")
      read(288,*)p2
      close(288)

C CALCULATING TRANSVERSE SHEAR STRENGHT, ST IN Pa
      ST =(SL/(2*p2))*((SQRT(1+(2*p2*YC/SL)))-1)
      p3 = p2*ST/SL; ! INCLINATION SLOPE pnt
      TAU21C = SL*SQRT(1+2*p3) !LIMIT OF ST

C**********************************************************************
C PRINT OUT LOAD INCREMENT
```

```
C**********************************************************************
      WRITE (*,*) "TIME", TIME(1)

C**********************************************************************
C       SUMMARY OF THE FILED VARIABLES
C**********************************************************************
C       FV1: MODE A DEGRADATION FACTOR, ETA_A
C       FV2: MODE B OR C DEGRADATION FACTOR, ETA^(-)
C       FV3: FLAG FOR FIBER FAILURE IN TENSION, ETA_FT
C       FV4: FLAG FOR FIBER FAILURE IN COMPRESSION, ETA_FC

C       SUMMARY OF THE SOLUTION DEPENDENT VARIABLES (SDV'S)

C       SDV1 (STATEV(1)): MODE A DEGRADATION FACTOR, ETA_A
C       SDV2 (STATEV(2)): STORES MODE A FAILURE INDEX
C       SDV3 (STATEV(3)): STORES VALUES OF EPSILON_11
C       SDV4 (STATEV(4)): STORES VALUES OF EPSILON_22
C       SDV5 (STATEV(5)): STORES VALUES OF EPSILON_12
C       SDV6 (STATEV(6)): MODE B OR C DEGRADATION FACTORS, ETA^(-)
C       SDV7 (STATEV(7)): STORES MODE BH OR C FAILURE INDEX
C       SDV8 (STATEV(8)): STORES FLAG FOR FIBER FAILURE IN TENSION, ETA_FT
C       SDV9 (STATEV(9)): STORES FLAG FOR FIBER FAILURE IN COMPRESSION,
C                         ETA_FC

C**********************************************************************
C GET STRINS FROM ABAQUS MAIN SOLVER
C**********************************************************************
      CALL GETVRM('E',ARRAY,JARRAY,FLGRAY,jrcd,
     $     jmac, jmtyp, matlayo, laccflg)
      STRAIN_NEW(1,1) = ARRAY(1)           !SAVE IMPORTED VALUES OF EPSILON11
      STRAIN_NEW(2,1) = ARRAY(2)           !SAVE IMPORTED VALUES OF EPSILON22
      STRAIN_NEW(3,1)=  ARRAY(4)             !SAVE IMPORTED VALUES OF GAMMA12

C**********************************************************************
C STRESS FROM ABAQUS MAIN SOLVER
C**********************************************************************
      CALL GETVRM('S',ARRAY,JARRAY,FLGRAY,jrcd,
     $     jmac, jmtyp, matlayo, laccflg)
      T11 =  ARRAY(1)                        !SAVE IMPORTED VALUES OF SIGMA11
      T22 =  ARRAY(2)                        !SAVE IMPORTED VALUES OF SIGMA22
      T12 =  ARRAY(4)                        !SAVE IMPORTED VALUES OF SIGMA21

C**********************************************************************
C CHECKS FOR THE FIBER FAILURE IN TENSION
C**********************************************************************
C INITIALIZE FAILURE FLAGS FROM STATEV
  STATEV(8)= FIELD(3)
  IF(T11.GT.0.0D0)THEN                  !CHECK FOR TENSION MODE SIGMA_11 > 0
      FFT = T11/XT
  END IF
C CHECK IF THERE ARE FIBER FAILURE PREVIOUSLY IN TENSION
  IF(STATEV(8).LE.0.0D0)THEN
      FIELD(3) = STATEV(8)
  END IF
```

```
  IF(FFT.GE.1.0D0)THEN                        !CHECK FOR FBER FAILURE IN TENSION
      Write (*,*), FFT, "FFT"
      FIELD(3) =0.0D0                          !FOR FAILURE FV3 = 0; ETA_FT IS 0
      FIELD(3) =STATEV(8)                              !SDV8 SAVES VALUE OF FV3
    ELSE
      STATEV(8) = FIELD(3)
  END IF

C*************************************************************************
C CHECKS FOR THE FIBER FAILURE IN COMPRESSION
C*************************************************************************
C INITIALIZE FAILURE FLAGS FROM STATEV
  STATEV(9)= FIELD(4)
  IF(T11.LT.0.0D0)THEN                !CHECK FOR COMPRESSION MODE SIGMA_11 < 0
      FFC = ABS(T11)/XC
  END IF
C CHECK IF THERE ARE FIBER FAILURE PREVIOUSLY IN COMPRESSION
  IF(STATEV(9).LE.0.0D0)THEN
      FIELD(4) = STATEV(9)
  END IF

IF(FFC.GE.1.0D0)THEN                   !CHECK FOR FIBER FAILURE IN COMPRESSION
      Write (*,*), FFC, "FFC"
      FIELD(4) =0.0D0                          !FOR FAILURE FV4 = 0; ETA_FC IS 0
      FIELD(4) =STATEV(9)                              !SDV9 SAVES VALUE OF FV4
    ELSE
      STATEV(9) = FIELD(4)                !FOR NO FAILURE FV4 =1 AND ETA_FC =1
  END IF



C*************************************************************************
C       MODE A FAILURE INITIATION AND DEGRADATION
C*************************************************************************
C INITIATE SOLUTION DEPEVENDENT VARIABLE (SDV)
      IF (TIME(1).EQ.0.0D0)THEN                                !INITIAL ETA_A = 1
      ETA_OLD=1.0D0                                 !ETA_A IS STORED UNDER SDV1
      STATEV(1) = ETA_OLD
      ELSE
      ETA_OLD=STATEV(1)
      END IF
      G_FN_OLD=STATEV(2)           !MODE FAILURE A INDEX IS STORED UNDER SDV2
 IF(T22.GE.0.0D0)THEN                       !Mode A FAILURE CHECK WHEN SIGMA22≥0
         A= (T12/SL)*(T12/SL)                 !Mode A FAILURE EQUATION IN PIECES
         B= (1-(p1*YT/SL))                    !Mode A FAILURE EQUATION IN PIECES
         B=B*B                                !Mode A FAILURE EQUATION IN PIECES
         C=(T22/YT)                           !Mode A FAILURE EQUATION IN PIECES
         C=C*C                                !Mode A FAILURE EQUATION IN PIECES
         D=B*C                                !Mode A FAILURE EQUATION IN PIECES
         E= (p1*T22/SL)                       !Mode A FAILURE EQUATION IN PIECES
         FMA = SQRT(A+D)+E                        !Mode A FAILURE INDEX COMBINED
         G_FN_NEW = FMA-1                     !FAILURE INDEX TO CHECK INITIATION
         WRITE(*,*)'FMA',FMA
C LOOP FOR SECANT METHOD
```

```
      IF (FMA .LT. 1.0D0)THEN
          ETA_NEW  = ETA_OLD            !BEFORE FAILURE INITIATION  ETA_A =1
          STATEV(2)= G_FN_NEW                        !SDV FOR FAILURE INDEX
          FIELD(1) = ETA_NEW                !FV FOR INITIAL VALUE OF ETA=1
         DO J=1,3
           STATEV(J+2)=STRAIN_NEW(J,1)                        !UPDATE STRAIN
         END DO
        ELSE
       DO I=1,20
        IF (I.EQ.1)THEN
         VECT_ETA(1)  = ETA_OLD
         VECT_G_FN(1) = G_FN_OLD
         VECT_ETA(2)=0.99*ETA_OLD
         ETA = VECT_ETA(2)
         A= (T12/SL)                                !MODE A FAILURE EQUATION
         A = A*A
         B= (1-(p1*YT/SL))
         B=B*B
         C=(T22/YT)
         C=C*C
         D=B*C
         E= (p1*T22/SL)
         FMA = SQRT(A+D)+E                            !Mode A FAILURE INDEX
         VECT_G_FN(2)= FMA-1           !FAILURE INDEX TO CHECK INITIATION
        ELSE
        DO J=1,2
           ETA=VECT_ETA(J)
           !STRESSES IN EACH PLY AS FUNCTION OF ETA_A
           GG = E_1*(E_1*STRAIN_NEW(1,1)+E_2*STRAIN_NEW(2,1)*
     &          ETA*ETA*NU_12)
           !SIGMA_11 AS A FUNCTION OF ETA_A
           S11= GG/(E_1-E_2*ETA*ETA*ETA*NU_12*NU_12)
           FF = E_1*E_2*ETA*(STRAIN_NEW(2,1)+STRAIN_NEW(1,1)*ETA*NU_12)
           !SIGMA_22 AS A FUNCTION OF ETA_A
           S22= FF/(E_1-E_2*ETA*ETA*ETA*NU_12*NU_12)
           !SIGMA_21 AS A FUNCTION OF ETA_A
           S12= STRAIN_NEW(3,1)*ETA*G_12

           A= (S12/SL)          !MODE A FAILURE EQUATION AS FUNCTION OF ETA_A
           A = A*A
           B= (1-(p1*YT/SL))
           B=B*B
           C=(S22/YT)
           C=C*C
           D=B*C
           E= (p1*S22/SL)!
           MODEA = SQRT(A+D)+E
       VECT_G_FN(J) =MODEA-1      !MODE A FAILURE INDEX AS FUNCTION OF ETA_A
        END DO
      END IF
         WRITE(*,*)"VECT_ETA", VECT_ETA(1), VECT_ETA(2)
         WRITE(*,*)"VECT_G_FN", VECT_G_FN(1), VECT_G_FN(2)
C    START CHECKING FOR CONVERGENCE OF ETA_A USING SECANT METHOD
         TMP_1 = VECT_G_FN(2)-VECT_G_FN(1)
```

```
          TMP_2 = VECT_ETA(2)-VECT_ETA(1)
          TMP_3 = TMP_2/TMP_1
          TMP_4 = VECT_G_FN(2)*TMP_3
          CALC_ETA= VECT_ETA(2)-TMP_4
          VECT_ETA(1)=VECT_ETA(2)
          VECT_ETA(2)=CALC_ETA                                    !UPDATE ETA_A

          IF (ABS(VECT_G_FN(2)).LE.1E-8)EXIT   !CHECK FOR COVERGENCE OF ETA_A
              IF(I .EQ. 20000)THEN
                  STOP
              END IF
          END DO
          STATEV(1)= VECT_ETA(2)        !SOLVED VALUES OF ETA_A SAVED IN SDV1
          STATEV(2)=VECT_G_FN(2)              !VALUES OF MODE A INDEX IN SDV2
          FIELD(1)=VECT_ETA(2)        !COVERGED VALUES OF ETA_A PASSED TO FV1
      DO J=1,3
          STATEV(J+2)=STRAIN_NEW(J,1)
        END DO
      END IF
END IF
C CHECK IF ETA_A IS GREATER THAN THE PREVIOUS VALUE SAVED IN SDV1
      IF (VECT_ETA(2).GT.ETA_OLD) THEN
      WRITE (*,*)'caution'
      STATEV(1)= ETA_OLD
      ELSE
      VECT_ETA(2)=STATEV(1)
      END IF

C*************************************************************************
C MODE B/C FAILURE INITIATION AND DEGRDATION
C*************************************************************************
C INITIATE SOLUTION DEPEVENDENT VARIABLES FOR MODE B/C FAILURE
      IF (TIME(1).EQ.0.0D0)THEN                                 !INITIAL ETA_A = 1
      ETA_OLDBC=1.0D0                             !ETA_A IS STORED UNDER SDV1
      STATEV(6) = ETA_OLDBC
      ELSE
      ETA_OLD=STATEV(6)
      END IF
      G_FN_OLDBC=STATEV(7)         !MODE FAILURE A INDEX IS STORED UNDER SDV2

      SR1 = ABS(T22/T12)                          !RATIO TO FIND RANGE OF MODE B
      SR2 = ST/ABS(TAU21C)                        !RATIO TO FIND RANGE OF MODE B
      SR3 = ABS(T12/T22)                          !RATIO TO FIND RANGE OF MODE C
      SR4 = ABS(TAU21C)/ST                        !RATIO TO FIND RANGE OF MODE C
      WRITE(*,*)'SR1',SR1,'SR2',SR2
      WRITE(*,*)'SR3',SR3,'SR4',SR4
IF(T22.LT.0.D0.AND.T22.GT.-YC)THEN                !CHECK FOR MODE B/C FAILURE
     IF(SR1.LT.SR2)THEN                           !CHECK FOR LIMITS OF MODE B
         MODEBC =(T12/SL)*(T12/SL)+(2*p2*T22/SL)                !MODE B CHECK
         WRITE(*,*)'B', MODEBC
        ELSE
         H =1/(2*(1+p2))                        !IF NOT MODE B CHECK FOR MODE C
         P = (T22/ST)*(T22/ST)              !MODE C FAILURE EQUATION IN PIECES
         R = (T12/SL)*(T12/SL)              !MODE C FAILURE EQUATION IN PIECES
```

```
         MODEBC = (P+R)*H*(-ST/T22)                    !MODE C FAILURE INDEX
         WRITE(*,*)'C', MODEBC
      END IF
         G_FN_NEWBC = MODEBC-1     !FAILURE INDEX TO CHECK EITHER MODE B OR C
C LOOP FOR SECANT METHOD
      IF (MODEBC .LT. 1.0D0)THEN
          ETA_NEWBC  = ETA_OLDBC !ETA^(-)
          STATEV(7)= G_FN_NEWBC            !SDV FOR FAILURE INDEX MODE B OR C
          FIELD(2) = ETA_NEWBC                !FV FOR ETA^(-)FOR MODE B OR C
            DO J=1,3                        !UPDATE STATE OF STRAIN
                STATEV(J+2)=STRAIN_NEW(J,1)
            END DO
         ELSE
         DO I=1,20
            IF (I.EQ.1)THEN
             VECT_ETABC(1)  = ETA_OLDBC        !INITIAL VALUES OF ETA^(-) = 1
             VECT_G_FNBC(1) = G_FN_OLDBC
             VECT_ETABC(2)=0.98*ETA_OLDBC
             ETABC = VECT_ETABC(2)

          IF(SR1.LT.SR2)THEN
             MODEBC =(T12/SL)*(T12/SL)+(2*p2*T22/SL)
            ELSE
             H =1/(2*(1+p2))                   !IF NOT MODE B CHECK FOR MODE C
             P = (T22/ST)*(T22/ST)          !MODE C FAILURE EQUATION IN PIECES
             R = (T12/SL)*(T12/SL)          !MODE C FAILURE EQUATION IN PIECES
             MODEBC=(P+R)*H*(-ST/T22)                  !MODE C FAILURE INDEX
          END IF
            VECT_G_FNBC(2)= MODEBC-1
          ELSE
           DO J=1,2
            ETABC=VECT_ETABC(J)
            !STRESSES IN EACH PLY AS FUNCTION OF ETA^(-)
            KK = E_1*(E_1*STRAIN_NEW(1,1)+E_2*STRAIN_NEW(2,1)*
     &           NU_12)
            !SIGMA_11 AS A FUNCTION OF ETA^(-)
            S11BC= KK/(E_1-E_2*NU_12*NU_12)
            LL = E_1*E_2(STRAIN_NEW(1,2)+E_2*STRAIN_NEW(1,1)*
     &           NU_12)
            !SIGMA_22 AS A FUNCTION OF ETA^(-)
            S22BC=LL/(E_1-E_2*NU_12*NU_12).
            !SIGMA_21 AS A FUNCTION OF ETA^(-)
            S12BC= STRAIN_NEW(3,1)*ETABC*G_12

         IF(SR1.LT.SR2)THEN
            MODEBC =(S12BC/SL)*(S12BC/SL)+(2*p2*S22BC/SL)
            ELSE
             H =1/(2*(1+p2))                   !IF NOT MODE B CHECK FOR MODE C
             P = (S22BC/ST)*(S22BC/ST)      !MODE C FAILURE EQUATION IN PIECES
             R = (S12BC/SL)*(S12BC/SL)      !MODE C FAILURE EQUATION IN PIECES
             MODEBC = (P+R)*H*(-ST/S22BC)      !MODE C FAILURE INDEX COMBINED
          END IF
            !MODE A FAILURE INDEX AS FUNCTION OF ETA^(-)
            VECT_G_FNBC(J) =MODEBC-1
```

```
          END DO
          END IF
          WRITE(*,*)"VECT_ETABC", VECT_ETABC(1), VECT_ETABC(2)
          WRITE(*,*)"VECT_G_FNBC", VECT_G_FNBC(1), VECT_G_FNBC(2)
C    START CHECKING FOR CONVERGENCE OF ETA^(-) USING SECANT METHOD
           TMPBC_1 = VECT_G_FNBC(2)-VECT_G_FNBC(1)
           TMPBC_2 = VECT_ETABC(2)-VECT_ETABC(1)
           TMPBC_3 = TMPBC_2/TMPBC_1
           TMPBC_4 = VECT_G_FNBC(2)*TMPBC_3
           CALC_ETABC= VECT_ETABC(2)-TMPBC_4
           VECT_ETABC(1)=VECT_ETABC(2)
           VECT_ETABC(2)=CALC_ETABC                              !UPDATE ETA^(-)
         IF (ABS(VECT_G_FNBC(2)).LE.1E-8)EXIT !CHECK FOR COVERGENCE OF ETA^(-)
         IF(I .EQ. 20000)THEN
           STOP
         END IF
         END DO
           STATEV(6)= VECT_ETABC(2)     !SOLVED VALUES OF ETA^(-) SAVED IN SDV6
           STATEV(7)=VECT_G_FNBC(2)          !VALUES OF MODE B/C INDEX IN SDV7
           FIELD(2)=VECT_ETABC(2)     !COVERGED VALUES OF ETA^(-) PASSED TO FV2
         DO J=1,3
           STATEV(J+2)=STRAIN_NEW(J,1)
         END DO
       END IF
  END IF
C CHECK IF ETA^(-)IS GRETER THAN THE PREVIOUS VALUE SAVED IN SDV6
       IF (VECT_ETABC(2).GT.ETA_OLDBC) THEN
       WRITE (*,*)'caution'
       ETA_OLDBC = STATEV(6)
       ELSE
       STATEV(6)=ETA_OLDBC
       END IF
C    CHECK IF SIGMA22 THAN -YC
       IF (T22.LT.-YC)THEN
             FIELD(1)=0.0D0
             STATEV(1) = FIELD(1)
       END IF
       IF (T22.LT.-YC)THEN
             FIELD(2)=0.0D0
             STATEV(6) = FIELD(2)
       END IF
       IF (T22.LT.-YC)THEN
             FIELD(3)=0.0D0
             STATEV(8) = FIELD(3)
       END IF
       IF (T22.LT.-YC)THEN
             FIELD(4)=0.0D0
             STATEV(9) = FIELD(4)
       END IF
RETURN
END
C END OF SUBROUINE HERE
```

A9. USDFLD Subroutine Written Using FORTRAN in 3D

```
C**********************************************************************
C   USDFLD Subroutine for modelling progressive failure analysis in 3D
C   Failure inititaation using golden section search techniqe and failure
C   progression using Continuum damage mechanic approach
C**********************************************************************
3C    SUBROUINTE STARTS HERE
      SUBROUTINE USDFLD(FIELD,STATEV,PNEWDT,DIRECT,T,CELENT,TIME,DTIME,
     1 CMNAME,ORNAME,NFIELD,NSTATV,NOEL,NPT,LAYER,KSPT,KSTEP,KINC,
     2 NDI,nshr,coord,jmac,jmtyp,matlayo,laccflg)
      INCLUDE 'ABA_PARAM.INC'
      CHARACTER*80 CMNAME,ORNAME
      CHARACTER*3 FLGRAY(15)
      DIMENSION FIELD(NFIELD),STATEV(NSTATV),DIRECT(3,3),T(3,3),TIME(2),
     *  coord(*),jmac(*),jmtyp(*)
      DIMENSION ARRAY(20),JARRAY(20)

      DOUBLE PRECISION:: ETA_OLDT, ETA_OLDC, AL_OLDT, AL_OLDC
      DOUBLE PRECISION:: STRAIN_NEW(6,1)
      integer :: nn, nter, iter, k
      integer, parameter  :: m = 2
      DOUBLE PRECISION, parameter :: tol = 1.0E-10
      DOUBLE PRECISION, dimension(m)  :: u,uu,un,ur,fvalue
      DOUBLE PRECISION :: pi
      DOUBLE PRECISION :: theta1, theta2, theta3, theta4, tau, epsilon
      DOUBLE PRECISION :: FIM_3, FIM_4
      DOUBLE PRECISION :: S11, S22, S33, S23, S13, S12
      DOUBLE PRECISION :: E1, E2, E3
      DOUBLE PRECISION :: NU12, NU13, NU23, NU21, NU31, NU32
      DOUBLE PRECISION :: G12, G13, G23
      DOUBLE PRECISION :: SNN_3, SNN_4
      DOUBLE PRECISION :: E11, E22, E33, E23, E13, E12
      DOUBLE PRECISION :: SHI1, SHI2, SHI3, SHI4
      DOUBLE PRECISION :: SHI5, SHI6, SHI7, SHI8
      DOUBLE PRECISION :: SHI9, SHI10, SHI11, SHI12
      DOUBLE PRECISION :: SHI13, SHI14, SHI15, SHI16
      DOUBLE PRECISION :: SHI17, SHI18, SHI19, SHI20
      DOUBLE PRECISION :: SHI21, SHI22,SHI23
      DOUBLE PRECISION :: SHI24, SHI25, SHI26, SHI27, SHI28
      DOUBLE PRECISION :: SHI29, SHI30, SHI31
      DOUBLE PRECISION :: FIMCOMD, FFT, FFC
      DOUBLE PRECISION :: psp, psn, XT, XC, YT, SL, pntn, YC, Spsi, ST
      DOUBLE PRECISION :: JJ1, JJ2, JJ3, JJ4, JJ5, JJ6, JJ7, JJ8, HH1,
     &                    HH2, HH3, HH4

      interface
      function funcv(E11, E22, E33, E23, E13, E12, x)
      implicit none
      DOUBLE PRECISION, intent(in) :: E11, E22, E33, E23, E13, E12
      DOUBLE PRECISION, dimension(:), intent(in) :: x
      DOUBLE PRECISION, dimension(size(x)+1) :: funcv
```

```
      end function funcv


C**********************************************************************
C MATERIAL PROPERTISES AND PARAMETERS
C**********************************************************************
C     GET E_1: VALUES IN Pascal
      open (unit=20, file="Z:\\sandbox\\abaqus-test\\E1.txt")
      read(20,*)E1
      close(20)

C     GET E_2: VALUES IN Pascal
      open (unit=21, file="Z:\\sandbox\\abaqus-test\\E2.txt")
      read(21,*)E2
      close(21)

C     GET E_3: VALUES IN Pascal
      open (unit=22, file="Z:\\sandbox\\abaqus-test\\E3.txt")
      read(22,*)E3
      close(22)

C     GET NU_12
      open (unit=23, file="Z:\\sandbox\\abaqus-test\\NU12.txt")
      read(23,*)NU12
      close(23)

C     GET NU_13
      open (unit=24, file="Z:\\sandbox\\abaqus-test\\NU13.txt")
      read(24,*)NU13
      close(24)

C     GET NU_23
      open (unit=25, file="Z:\\sandbox\\abaqus-test\\NU23.txt")
      read(25,*)NU23
      close(25)

C     GET G_12: VALUES IN Pascal
      open (unit=26, file="Z:\\sandbox\\abaqus-test\\G12.txt")
      read(26,*)G12
      close(26)

C     GET G_13: VALUES IN Pascal
      open (unit=27, file="Z:\\sandbox\\abaqus-test\\G13.txt")
      read(27,*)G13
      close(27)
C     GET SL, IN PLANE SHEAR STRENGHT: VALUES IN Pascal
      open (unit=144, file="Z:\\sandbox\\abaqus-test\\SL.txt")
      read(144,*)SL
      close(144)
C     GET YT, TENSILE STRENGTH IN TRANSVERSE DIRECTION: VALUES IN Pascal
      open (unit=168, file="Z:\\sandbox\\abaqus-test\\YT.txt")
      read(168,*)YT
      close(168)
C     GET YC, COMPRESSIVE STRENGTH IN TRANSVERSE DIRECTION: VALUES IN Pascal
```

```
      open (unit=192, file="Z:\\sandbox\\abaqus-test\\YC.txt")
      read(192,*)YC
      close(192)
C     GET XT, VALUE OF THE TENSILE STRENGTH ALONG FIBER : VALUES IN Pascal
      open (unit=216, file="Z:\\sandbox\\abaqus-test\\XT.txt")
      read(216,*)XT
      close(216)
C     GET XC, VALUE OF THE COMPRESSIVE STRENGTH ALONG FIBER:VALUES IN Pascal
      open (unit=240, file="Z:\\sandbox\\abaqus-test\\XC.txt")
      read(240,*)XC
      close(240)
C     GET p1, INCLINATION SLOPE p_(n1)^(+)
      open (unit=264, file="Z:\\sandbox\\abaqus-test\\p1.txt")
      read(264,*)p1
      close(264)
C     GET p2, INCLINATION SLOPE p_(n1)^(+)
      open (unit=288, file="Z:\\sandbox\\abaqus-test\\p2.txt")
      read(288,*)p2
      close(288)

      subroutine fdjac(E11, E22, E33, E23, E13, E12, x,fvec,df,dfiv)
      implicit none
      double precision, intent(in) :: E11, E22, E33, E23, E13, E12
      double precision, dimension(:), intent(in) :: fvec
      double precision, dimension(:), intent(inout) :: x
      double precision, dimension(:,:), intent(out) :: df,dfiv
      double precision :: EPS
      integer :: j,n
      double precision, dimension(size(x)) :: xsav, xph, h
      end subroutine fdjac
      end interface

      double precision, dimension(m+1) :: fvec
      double precision, dimension(m,m) :: df, dfiv

      WRITE (*,*) "_____________________________________"
      WRITE (*,*) "TIME", TIME(1)
      WRITE (*,*) "_____________________________________"


C**********************************************************************
C     INITIALIZATION OF STATE VARIABLES
C**********************************************************************
      IF (TIME(1).EQ.0.0D0)THEN
      ETA_OLDT = 1.0D0                !VALUE OF ETA_T FORM UNDAMAGED LAMINATE
      ETA_OLDC = 1.0D0                !VALUE OF ETA_C FORM UNDAMAGED LAMINATE
      AL_OLDT = 0.1D0
      AL_OLDC = 0.1D0
      STATEV(1) = ETA_OLDT
      STATEV(2) = AL_OLDT
      STATEV(3) = ETA_OLDC
      STATEV(4) = AL_OLDC
      ELSE
      ETA_OLDT = STATEV(1)
```

```
      AL_OLDT = STATEV(2)
      ETA_OLDC = STATEV(3)
      AL_OLDC = STATEV(4)
      END IF
      FIM_3 =STATEV(5)
      FIM_4 =STATEV(6)
      SNN_4 = STATEV(7)


C**********************************************************************
C     STRESS FROM ABAQUS
C**********************************************************************
      CALL GETVRM('E',ARRAY,JARRAY,FLGRAY,jrcd,
     $     jmac, jmtyp, matlayo, laccflg)
      STRAIN_NEW(1,1) = ARRAY(1)
      STRAIN_NEW(2,1) = ARRAY(2)
      STRAIN_NEW(3,1) = ARRAY(3)
      STRAIN_NEW(4,1) = ARRAY(4)
      STRAIN_NEW(5,1) = ARRAY(5)
      STRAIN_NEW(6,1)=  ARRAY(6)

C**********************************************************************
C     STRESS FROM ABAQUS
C**********************************************************************
      CALL GETVRM('S',ARRAY,JARRAY,FLGRAY,jrcd,
     $     jmac, jmtyp, matlayo, laccflg)
      S11 =  ARRAY(1)
      S22 =  ARRAY(2)
      S33 =  ARRAY(3)
      S12 =  ARRAY(4)
      S13 =  ARRAY(5)
      S23 =  ARRAY(6)
C**********************************************************************
C     STRAIN FROM ABAQUS
C**********************************************************************
      E11 = STRAIN_NEW(1,1)
      E22 = STRAIN_NEW(2,1)
      E33 = STRAIN_NEW(3,1)
      E12 = STRAIN_NEW(4,1)
      E13 = STRAIN_NEW(5,1)
      E23 = STRAIN_NEW(6,1)

C**********************************************************************
C CHECKS FOR THE FIBER FAILURE IN TENSION
C**********************************************************************
C INITIALIZE FAILURE FLAGS FROM STATEV
  STATEV(8)= FIELD(3)
  IF(T11.GT.0.0D0)THEN                  !CHECK FOR TENSION MODE SIGMA_11 > 0
      FFT = T11/XT
  END IF
C CHECK IF THERE ARE FIBER FAILURE PREVIOUSLY IN TENSION
  IF(STATEV(8).LE.0.0D0)THEN
      FIELD(3) = STATEV(8)
  END IF
```

```
  IF(FFT.GE.1.0D0)THEN                        !CHECK FOR FBER FAILURE IN TENSION
      Write (*,*), FFT, "FFT"
      FIELD(3) =0.0D0                          !FOR FAILURE FV3 = 0; ETA_FT IS 0
      FIELD(3) =STATEV(8)                              !SDV8 SAVES VALUE OF FV3
    ELSE
      STATEV(8) = FIELD(3)
  END IF

C*************************************************************************
C CHECKS FOR THE FIBER FAILURE IN COMPRESSION
C*************************************************************************
C INITIALIZE FAILURE FLAGS FROM STATEV
  STATEV(9)= FIELD(4)
  IF(T11.LT.0.0D0)THEN                !CHECK FOR COMPRESSION MODE SIGMA_11 < 0
      FFC = ABS(T11)/XC
  END IF
C CHECK IF THERE ARE FIBER FAILURE PREVIOUSLY IN COMPRESSION
  IF(STATEV(9).LE.0.0D0)THEN
      FIELD(4) = STATEV(9)
  END IF

IF(FFC.GE.1.0D0)THEN                   !CHECK FOR FIBER FAILURE IN COMPRESSION
      Write (*,*), FFC, "FFC"
      FIELD(4) =0.0D0                          !FOR FAILURE FV4 = 0; ETA_FC IS 0
      FIELD(4) =STATEV(9)                              !SDV9 SAVES VALUE OF FV4
    ELSE
      STATEV(9) = FIELD(4)                !FOR NO FAILURE FV4 =1 AND ETA_FC =1
  END IF

C*************************************************************************
C*************************************************************************
C     GOLDEN SECTION SEARCH
C*************************************************************************
C*************************************************************************
      pi=datan(1.d0)* 4.d0     !RANGE OF SEARCH SECTION BETWEEN -pi/2 to pi/2
      theta1 = -Pi/2.0
      theta2 =  Pi/2.0
      tau = (((5.0)**0.5-1.0)/2.0)                  !GOLDEN SECTION PARAMETER

      theta3=theta1+(1-tau)*(theta2-theta1)
      theta4=theta1+tau*(theta2-theta1)

      epsilon=0.000001
      nter= 500
      k=0

      u(1) = 1.0; u(2) = theta3
      fvalue = funcv(E11, E22, E33, E23, E13, E12, u)
      FIM_3 = fvalue(1)+1
      SNN_3 = fvalue(3)
      u(1) = 1.0; u(2) = theta4
      fvalue = funcv(E11, E22, E33, E23, E13, E12, u)
      FIM_4 = fvalue(1)+1
      SNN_4 = fvalue(3)
```

```
      DO WHILE ((abs(theta2-theta1) .GT. epsilon) .AND. (k .LT. nter))

            k=k+1;
       IF (FIM_3 .GT. FIM_4) THEN
            theta2=theta4;
            theta4=theta3;
            theta3=theta1+(1-tau)*(theta2-theta1);

            u(2) = theta3
            fvalue = funcv(E11, E22, E33, E23, E13, E12, u)
            FIM_3 = fvalue(1)+1
            SNN_3 = fvalue(3)

            u(2) = theta4
            fvalue = funcv(E11, E22, E33, E23, E13, E12, u)
            FIM_4 = fvalue(1)+1
            SNN_4 = fvalue(3)

       IF ( (FIM_3 .GE. 1.D0) .OR. (FIM_4 .GE. 1.D0) )  GOTO 10
        ELSE
            theta1=theta3
            theta3=theta4
            theta4=theta1+tau*(theta2-theta1)
            u(2) = theta3
            fvalue = funcv(E11, E22, E33, E23, E13, E12, u)
            FIM_3 = fvalue(1)+1
            SNN_3 = fvalue(3)

            u(2) = theta4
            fvalue = funcv(E11, E22, E33, E23, E13, E12, u)
            FIM_4 = fvalue(1)+1
            SNN_4 = fvalue(3)

     IF ( (FIM_3 .GE. 1.D0) .OR. (FIM_4 .GE. 1.D0) ) GOTO 10
             k=k+1
10   END IF

      END DO

C CHOOSE MAXIMUM POINT OF THE FUNTION
       IF(FIM_3 .GT. FIM_4) THEN
            write (*,*) "theta3", theta3
            write (*,*) "FIM_3", FIM_3
            write (*,*) "SNN_3", SNN_3
            IF (FIM_3 .GT. 1.0) THEN
               u(2) = theta3
               STATEV(5) = FIM_3
               STATEV(6) = FIM_4
               GOTO 40
            ELSE
                IF (SNN_3 .GT. 0.0 ) THEN
                STATEV(1) = 1.0
                STATEV(2) = theta3
```

```
                FIELD(1)= 1.0
                u(2) = theta3
                ELSE
                STATEV(3) = 1.0
                STATEV(4) = theta3
                FIELD(2)= 1.0
                u(2) = theta3
                END IF
                GOTO 50
            END IF
        ELSE
            write (*,*) "theta4", theta4
            write (*,*) "FIM_4", FIM_4
            write (*,*) "SNN_4", SNN_4
            IF (FIM_4 .GE. 1.0) THEN
               u(2) = theta4
               GOTO 40
            ELSE
                IF ( SNN_4 .GT. 0.0 ) THEN
                STATEV(1) = 1.0
                STATEV(2) = theta4
                FIELD(1)= 1.0
                u(2) = theta4
                ELSE
                STATEV(3) = 1.0
                STATEV(4) = theta4
                FIELD(2)= 1.0
                u(2) = theta4
                END IF
                GOTO 50
            END IF
        END IF
C**********************************************************************
c  CHECK THE VALUE OF FIM, DECIDE TO USE NEWTON RAPHSON OR NOT
C**********************************************************************
C
C  Give initial values of x
C
40    nn = 10000
      u(1) = 0.99          ! ETA = u(1)
C      u(2) = 0.0           ! Al = u(2)
C      write(*,*)
C      write(*,*) "Initial Values of Point x are"
C      write(*,*) "--------------------------------"
C      write(*,*) " ", u, "          "
C      write(*,*) "--------------------------------"

      uu(1) = u(1)
      uu(2) = u(2)

      do while ( nn > 0 )
          call fdjac(E11, E22, E33, E23, E13, E12, uu,fvec,df,dfiv)
          if ( abs(df(1,1)*df(2,2) - df(1,2)*df(2,1)) < tol ) then
              write(*,*) "Error: Sigular Jacobian"
```

```
              stop
           end if
         fvec = funcv(E11, E22, E33, E23, E13, E12, uu)
         un(1) = uu(1) - ( dfiv(1,1)*fvec(1) + dfiv(1,2)*fvec(2) )
         un(2) = uu(2) - ( dfiv(2,1)*fvec(1) + dfiv(2,2)*fvec(2) )
         fvec = funcv(E11, E22, E33, E23, E13, E12, un)
            IF ( (abs(fvec(1))<tol) .and. (abs(fvec(2))<tol) ) then
                ur(1)=un(1); ur(2)=un(2)
                iter = 1000 - nn
                IF ( fvec(3) .gt. 0.0 ) then
                  STATEV(1) = ur(1)
                  STATEV(2) = ur(2)
                  FIELD(1)= ur(1)
                  write(*,*) "Tension"
                  write(*,*) "ETA is:", ur(1)
                  write(*,*) "Alpha is:", ur(2)
c                  STAVE = fvec(3)
                ELSE
C  Changes Made
                  STATEV(1) = ur(1)
C                 STATEV(3) = ur(1)
                  STATEV(4) = ur(2)
                  FIELD(2)= ur(1)
                  write(*,*) "Compression"
                  write(*,*) "ETA is:", ur(1)
                  write(*,*) "Alpha is:", ur(2)
                end if
                go to 20
           end if
         nn = nn - 1
         uu(1)=un(1); uu(2)=un(2)
       end do
20     write(*,*)
       write(*,*) "iteration steps of nn is:"
       write(*,*)                              nn


C       write(*,*) "convergence results of the roots are:"
C       write(*,*) "--------------------------------"
C       write(*,*) " ", ur, "          "
C       write(*,*) "--------------------------------"
50       end

C CHECK IF ETA_T IS GRETER THAN THE PREVIOUS VALUE SAVED IN SDV1
       IF (ur(1).GT. ETA_OLDT) THEN
       WRITE (*,*)'caution'
       ETA_OLDT = STATEV(1)
       ELSE
       STATEV(1)= ETA_OLDT
       END IF

C CHECK IF ETA_C IS GRETER THAN THE PREVIOUS VALUE SAVED IN SDV3
       IF (ur(1).GT. ETA_OLDC) THEN
       WRITE (*,*)'caution'
```

```
      ETA_OLDC = STATEV(3)
      ELSE
      STATEV(3)= ETA_OLDC
      END IF

C**********************************************************************
C**********************************************************************
      subroutine fdjac(E11, E22, E33, E23, E13, E12, x,fvec,df,dfiv)
      implicit none
      DOUBLE PRECISION, intent(in) :: E11, E22, E33, E23, E13, E12
      DOUBLE PRECISION, dimension(:), intent(in) :: fvec
      DOUBLE PRECISION, dimension(:), intent(inout) :: x
      DOUBLE PRECISION, dimension(:,:), intent(out) :: df, dfiv
      interface
      function funcv(E11, E22, E33, E23, E13, E12, x)
      implicit none
      DOUBLE PRECISION, intent(in) :: E11, E22, E33, E23, E13, E12
      DOUBLE PRECISION, dimension(:), intent(in) :: x
      DOUBLE PRECISION, dimension(size(x)+1) :: funcv
      end function funcv
      end interface
      DOUBLE PRECISION, parameter :: EPS = 1.0e-04
      integer :: j,n

     DOUBLE PRECISION, dimension(size(x)) :: xsav, xph1, xph2,
     &                                  h, h_double, x2, x1

      n = size(x)
      xsav = x
      h = EPS*abs(xsav)

      where (h <= EPS) h = EPS

      xph2 = xsav + h               ! Trick to reduce finite precision error
      xph1 = xsav - h
      h_double = xph2 - xph1

      x2 = x
      x1 = x
      do j = 1 , n
         x2(j) = xph2(j)
         x1(j) = xph1(j)
C       Central difference formula
         df(:,j) = (funcv(E11, E22, E33, E23, E13, E12, x2)
     &      - funcv(E11, E22, E33, E23, E13, E12, x1)) / h_double(j)
         x2(j) = xsav(j)
         x1(j) = xsav(j)
      end do
C
C Check and Inverse the Jacobian
      if ( (df(1,1)*df(2,2) - df(1,2)*df(2,1)) == 0.0) then
         write (*,*) " Singular Jacobian "
      end if
       dfiv(1,1) =  df(2,2)  /  (df(1,1)*df(2,2) - df(1,2)*df(2,1))
```

```
        dfiv(1,2) = -df(1,2)   /   (df(1,1)*df(2,2) - df(1,2)*df(2,1))
        dfiv(2,1) = -df(2,1)   /   (df(1,1)*df(2,2) - df(1,2)*df(2,1))
        dfiv(2,2) =  df(1,1)   /   (df(1,1)*df(2,2) - df(1,2)*df(2,1))

      end subroutine fdjac
C***********************************************************************
C***********************************************************************
      function funcv(E11, E22, E33, E23, E13, E12, x)
      implicit none

      double precision, intent(in) :: E11, E22, E33, E23, E13, E12
      double precision, dimension(:), intent(in) :: x
      double precision, dimension(size(x)+1) :: funcv
      DOUBLE PRECISION :: E1, E2, E3
      DOUBLE PRECISION :: NU12, NU13, NU23, NU21, NU31, NU32
      DOUBLE PRECISION :: G12, G13, G23
      DOUBLE PRECISION :: SHI1, SHI2, SHI3, SHI4
      DOUBLE PRECISION :: SHI5, SHI6, SHI7, SHI8
      DOUBLE PRECISION :: SHI9, SHI10, SHI11, SHI12
      DOUBLE PRECISION :: SHI13, SHI14, SHI15, SHI16
      DOUBLE PRECISION :: SHI17, SHI18, SHI19, SHI20
      DOUBLE PRECISION :: SHI21, SHI22,SHI23
      DOUBLE PRECISION :: SHI24, SHI25, SHI26, SHI27, SHI28
      DOUBLE PRECISION :: SHI29, SHI30, SHI31, SN1, SNT

      DOUBLE PRECISION ::  TM1, TM2, TM3
      DOUBLE PRECISION ::  TM4, TM5, TM6
      DOUBLE PRECISION ::  TM7, TM8, TM9
      DOUBLE PRECISION ::  TM10, TM11, TM12
      DOUBLE PRECISION ::  TM13, TM14, TM15
      DOUBLE PRECISION ::  TM16, TM17, TM18
      DOUBLE PRECISION ::  TM19, TM20, TM21
      DOUBLE PRECISION ::  AK1, AK2, AK3, AK4, FIMT, FIMTD
      DOUBLE PRECISION ::  BK1, BK2, BK3, BK4, BK5, BK6

      DOUBLE PRECISION :: SFP1, SFP2, SFP3, SFP4, SFP5, SFP11
      DOUBLE PRECISION :: SFP6, SFP7, SFP8, SFP9, SFP10, SNN

      DOUBLE PRECISION :: psp, psn, XT, XC, YT, SL, pntn, YC, Spsi, ST

      DOUBLE PRECISION :: JJ1, JJ2, JJ3, JJ4, JJ5, JJ6, JJ7, JJ8,
     &                    HH1, HH2, HH3, HH4

        E1 = 129D9;
        E2 = 5.5D9;
        E3 = 5.5D9;
        NU12 = 0.318;
        NU13 = 0.318;
        NU23 = 0.5;
        G12 = 5.66D9;
        G13 = 1.33D9;
        G23 = 1.86D9;

        NU21 = NU12*E2/E1;
```

```
      NU31 = NU13*E3/E1;
      NU32 = NU23*E2/E3;

      psp = 0.3;
      psn = 0.3;
      XT = 1378D6;
      XC = 950D6;
      YT = 40D6;
      SL = 97D6;
      pntn = 0.3;
      YC = 125D6;
      ST = YC/(2*(1+pntn));
      Spsi =1/SQRT(SL**2*SNT**2+SN1**2*ST**2/(SL**2*ST**2*(SN1**2+SNT**2)));

C*************************************************************************
C     MATRIX FAILURE IN COMPRESSION
C*************************************************************************
C
      SHI1=1/(E1*E2*x(1)**3*G12*G13*G23)
     &   -NU12**2/(E1**2*x(1)**3*G12*G13*G23)
      SHI2=1/(E1*E3*x(1)**3*G12*G13*G23)-
     &  (NU13**2)/(E1**2*x(1)**3*G12*G13*G23)
      SHI3=(-(NU12*NU13)/(E1**2)-(1-x(1)+NU23)/(E1*E2*x(1)))
      SHI4 = NU13/(E1*E2)+(NU12*(1-x(1)+NU23))/(E1*E2*x(1))
      SHI5=(-(NU12*NU13)/(E1**2)-(E2*(1-x(1)+NU23))/(E1*E3**2*x(1)))
      SHI6 =NU13/(E1*E2)+(E2*NU12*(1-x(1)+NU23))/(E1*E3**2*x(1))
      SHI7=(-NU12/(E1*E3)-(NU13*(1-x(1)+NU23))/(E1*E2*x(1)))
      SHI8=(1/(E1*E2)-(NU12**2)/(E1**2))/E3
      SHI9=(E2*(1-x(1)+NU23)*SHI3)/(E3**2*x(1))
      SHI10=(NU13*SHI4)/E1
      SHI11=SHI8+SHI9-SHI10

      SHI12=((x(1)*E12*G12*COS(x(2))+
     &    x(1)*E13*G13*SIN(x(2))))**2/(SL*SL)

      SHI13=(E33*x(1)**3*G12*G13*G23*SHI1)/SHI11

      SHI14=(E22*x(1)**3*G12*G13*G23*SHI2)/SHI11
      SHI15=(SHI13+SHI14-(E33*SHI3)/SHI11-(E22*SHI5)/SHI11+
     &   (E11*SHI6)/SHI11-(E11*SHI7)/SHI11)

      SHI16=(-SHI13+SHI14-(E33*SHI3)/SHI11+
     &   (E22*SHI5)/SHI11-(E11*SHI6)/SHI11-(E11*SHI7)/SHI11)

      SHI17=0.5*x(1)*E13*G13*SHI16*COS(x(2))
      SHI18=x(1)*E23*G23*SIN(2*x(2))
      SHI19=x(1)*E23*G23*COS(2*x(2))
      SHI20=0.5*SHI15+SHI17+SHI18
      SHI21=x(1)*E13*G13*COS(x(2))
      SHI22=x(1)*E12*G12*SIN(x(2))
      SHI23=x(1)*E12*G12*COS(x(2))
      SHI24=x(1)*E13*G13*SIN(x(2))
      SHI25=0.5*x(1)*E13*G13*SHI16*SIN(x(2))
      SHI26=(SHI19+0.5*SHI16*SIN(2*x(2)))
```

```
      SHI27=(2*(SHI21-SHI22)*(SHI23+SHI24))/(SL*SL)
      SHI28=(2*SHI19-SHI25)
      SHI29=(SHI16*Cos(2*x(2))-2*SHI18)
      SHI30=1/((ST*ST))
      SHI31=1/((Spsi*Spsi))


      JJ1 = (1/Spsi)*psn*(SHI13-(E13*(SHI3)*(SHI11)*Sin(x(2)))
     &      /(2*(SHI2)))

      JJ2 = (1/SL**2)*2*(SHI21)*(SHI22)

      JJ3 = (1/(Spsi**2))*2*(psn**2)
     &      *(SHI13-(E13*(SHI3)*(SHI11)*SIN(x(2)))/(2*(SHI2)))
      JJ4 = ((1/2)*(SHI12)+(e13*(SHI3)*(SHI11)*COS(x(2)))
     &      /(2*(SHI2))+SHI18)
      JJ5 = 1/(ST**2)*2*((SHI11)*COS(2*x(2))-SHI19)
     &      *(SHI20+(1/2)*(SHI11)*SIN(2*x(2)))

      JJ6 = (1/SL**2)*(SHI21)**2
      JJ7 = (1/Spsi**2)*psn**2*((1/2)*(SHI12)
     &      +(E13*(SHI3)*(SHI11)*COS(x(2)))/(2*(SHI2))+SHI18)**2
      JJ8 = 1/(ST**2)*(SHI20+(1/2)*(SHI11)*SIN(2*x(2)))**2

      HH1 = (psn/Spsi)*
     &      ( 0.5*SHI12 + E13*SHI3*SHI11*COS(x(2))/2/SHI2+ SHI18 )
      HH2 = (1/SL**2)* ((1/SHI2)*E12*(SHI10)*COS(x(2))+SHI15)**2
      HH3 = (1/Spsi**2)*(psn**2)*
     &      (0.5 *SHI12+E13*SHI3*SHI11*COS(x(2))/2/SHI2+SHI18)**2
      HH4 = (1/ST**2)* (SHI20 + 0.5 *SHI11* SIN(2*x(2)))**2



C*************************************************************************
C*************************************************************************
C     STRESS ON THE FRACTURE PLANE, SIGMA_NN
C*************************************************************************
C*************************************************************************
      SFP1 = 1/(E1*E2*E3*G12*G13*G23)
     &      -(NU12*NU21)/(E1*E2*E3*G12*G13*G23)
     &      -(NU13*NU31)/(E1*E2*E3*G12*G13*G23)
     &      -(NU12*NU23*NU31)/(E1*E2*E3*G12*G13*G23)
     &      -(NU13*NU21*NU32)/(E1*E2*E3*G12*G13*G23)
     &      -(NU23*NU32)/(E1*E2*E3*G12*G13*G23)


      SFP2 = 1/(E1*E2*E3*G12*G23) - (NU12*NU21)/(E1*E2*E3*G12*G23)
     &      - (NU13*NU31)/(E1*E2*E3*G12*G23)
     &      - (NU12*NU23*NU31)/(E1*E2*E3*G12*G23)
     &      - (NU13*NU21*NU32)/(E1*E2*E3*G12*G23)
     &      - (NU23*NU32)/(E1*E2*E3*G12*G23)

      SFP3 = (1/(E1*E2*E3*G12*G13) - (NU12*NU21)/(E1*E2*E3*G12*G13)
     &      - (NU13*NU31)/(E1*E2*E3*G12*G13)
```

```
     &         - (NU12*NU23*NU31)/(E1*E2*E3*G12*G13)
     &         - (NU13*NU21*NU32)/(E1*E2*E3*G12*G13)
     &         - (NU23*NU32)/(E1*E2*E3*G12*G13))

       SFP4 = (1/(E1*E2*G12*G13*G23) - (NU12*NU21)/(E1*E2*G12*G13*G23))

       SFP5 = ((NU13*NU21)/(E1*E2*G12*G13*G23)
     &         + NU23/(E1*E2*G12*G13*G23))

       SFP6 = (NU13/(E1*E2*G12*G13*G23)
     &         + (NU12*NU23)/(E1*E2*G12*G13*G23))

       SFP7 = (1/(E1*E3*G12*G13*G23) - (NU13*NU31)/(E1*E3*G12*G13*G23))

       SFP8 = ((NU12*NU31)/(E1*E3*G12*G13*G23)
     &         + NU32/(E1*E3*G12*G13*G23))

       SFP9 = (NU12/(E1*E3*G12*G13*G23)
     &         + (NU13*NU32)/(E1*E3*G12*G13*G23))

       SFP10 = (E33*SFP4/SFP1 + (E22*SFP5)/SFP1 + (E11*SFP6)/SFP1
     &         + (E22*SFP7)/SFP1 + (E33*SFP8)/SFP1 + (E11*SFP9)/SFP1)


       SFP11 = (-(E33*SFP4/SFP1) - (e22*SFP5)/SFP1 - (e11*SFP6)/SFP1
     &        + (E22*SFP7)/SFP1 + (E33*SFP8)/SFP1 + (E11*SFP9)/SFP1)

       SNN = 0.5* (SFP10) + (E13*(SFP2)*SFP11*COS(x(2)))/(2*(SFP1))
     &        + (E23*SFP3*SIN(2*x(2)))/SFP1


C*************************************************************************
C*************************************************************************
C    MATRIX FAILURE IN TENSION
C*************************************************************************
C*************************************************************************

          TM1 = (1/(E1*E2*E3*x(1)**4*G12*G13)
     &         - NU12**2/(E1**2*E3*x(1)**3*G12*G13)
     &         - NU13*2/(E1**2*E2*x(1)**3*G12*G13)
     &         -(NU12*NU13*NU23)/(E1**2*E2*x(1)**2*G12*G13)
     &         -(E2*NU12*NU13*NU23)/(E1**2*E3**2*x(1)**2*G12*G13)
     &         - NU23**2/(E1*E3**2*x(1)**2*G12*G13))

          TM2 = 1/(E1*E2*E3*x(1)**5*G12*G13*G23)
     &         - NU12**2/(E1**2*E3*x(1)**4*G12*G13*G23)
     &         - NU13*2/(E1**2*E2*x(1)**4*G12*G13*G23)
     &         - (NU12*NU13*NU23)/(E1**2*E2*x(1)**3*G12*G13*G23)
     &         -(E2*NU12*NU13*NU23)/(E1**2*E3**2*x(1)**3*G12*G13*G23)
     &         - NU23**2/(E1*E3**2*x(1)**3*G12*G13*G23)

          TM3 =  (1/(E1*E2*E3*x(1)**4*G12*G23)
     &          - NU12**2/(E1**2*E3*x(1)**3*G12*G23)
```

```
&          - NU13**2/(E1**2*E2*x(1)**3*G12*G23)
&          -  (NU12*NU13*NU23)/(E1**2*E2*x(1)**2*G12*G23)
&          -(E2*NU12*NU13*NU23)/(E1**2*E3**2*x(1)**2*G12*G23)
&          - NU23**2/(E1*E3**2*x(1)**2*G12*G23))

      TM4 = (1/(E1*E2*x(1)**4*G12*G13*G23)
&          - NU12**2/(E1**2*x(1)**3*G12*G13*G23))

      TM5 = (1/(E1*E3*x(1)**4*G12*G13*G23)
&          - NU13**2/(E1**2*x(1)**3*G12*G13*G23))

      TM6 = ((NU12*NU13)/(E1**2*x(1)**3*G12*G13*G23)
&          + NU23/(E1*E2*x(1)**3*G12*G13*G23))

      TM7 = ((NU12*NU13)/(E1**2*x(1)**3*G12*G13*G23)
&          + (E2*NU23)/(E1*E3**2*x(1)**3*G12*G13*G23))

      TM8 = (NU13/(E1*E2*x(1)**4*G12*G13*G23)
&          +(NU12*NU23)/(E1*E2*x(1)**3*G12*G13*G23))

      TM9 = (NU12/(E1*E3*x(1)**4*G12*G13*G23)
&          +(E2*NU13*NU23)/(E1*E3**2*x(1)**3*G12*G13*G23))

      TM10 = (1/(E1*E2*E3*x(1)**4*G13*G23)
&          - NU12**2/(E1**2*E3*x(1)**3*G13*G23)
&          - NU13**2/(E1**2*E2*x(1)**3*G13*G23)
&          -(NU12*NU13*NU23)/(E1**2*E2*x(1)**2*G13*G23)
&          -(E2*NU12*NU13*NU23)/(E1**2*E3**2*x(1)**2*G13*G23)
&          -NU23**2/(E1*E3**2*x(1)**2*G13*G23))

      TM11 = (1/(E1*E2*E3*x(1)**4*G12*G23)
&           - NU12**2/(E1**2*E3*x(1)**3*G12*G23)
&           - NU13**2/(E1**2*E2*x(1)**3*G12*G23)
&           -(NU12*NU13*NU23)/(E1**2*E2*x(1)**2*G12*G23)
&           - (E2*NU12*NU13*NU23)/(E1**2*E3**2*x(1)**2*G12*G23)
&           - NU23**2/(E1*E3**2*x(1)**2*G12*G23))

      TM12 = (-((E33*TM4)/TM2) + (E22*TM5)/TM2 - (E22*TM6)/TM2
&           + (E33*TM7)/TM2 - (E11*TM8)/TM2 + (E11*TM9)/TM2)

      TM13 = ((E33*TM4)/TM2 + (E22*TM5)/TM2 + (E22*TM6)/TM2
&           + (E33*TM7)/TM2 + (E11*TM8)/TM2 + (E11*TM9)/TM2)

      TM14 = 2*E23*TM1*COS(2*x(2))/TM2

      TM15 = ((E12*TM10*COS(x(2)))/TM2 + (E13*TM11*SIN(x(2)))/TM2)

       TM16 = ((E13*TM11* COS(x(2)))/TM2 - (E12*TM10*SIN(x(2)))/TM2)

       TM17 = (E23*TM1*SIN(2*x(2)))/TM2

       TM18 = (E23*TM1*COS(2*x(2)))/TM2

       TM19 = (2* E23* TM1* SIN(2*x(2)))/TM2
```

```
      TM20 = (0.5)*TM13 + (E13*TM3*TM12*COS(x(2)))/(2*(TM2)) + TM17

      TM21 = (TM18 + 0.5*TM12*SIN(2*x(2)))

      AK1 = ((1/Spsi)*psp*((0.5)*TM13
     &     + (E13*TM3*TM12*COS(x(2)))/(2*(TM2))+TM17))

      AK2 = (((E12*TM10*COS(x(2)))/TM2
     &     + (E13*TM11*SIN(x(2)))/TM2)**2)/SL**2

      AK3 = (1/YT**2)*(1-(psp*YT)/Spsi)**2*(TM20)**2

      AK4 = (1/ST**2)* (TM21)**2


      BK1 = (1/Spsi)*psp*(TM14- (E13*TM3*TM12*SIN(x(2)))/(2*(TM2)))

      BK2 = (1/SL**2)*2*TM15*TM16
      BK3 = (1/YT**2)*2*((1 - (psp* YT)/Spsi)**2)
     &      *(TM14-(E13*TM3*TM12*SIN(x(2)))/(2*(TM2)))*TM20
      BK4 = (1/ST**2)*2*(TM12*COS(2*x(2))-TM19)*TM21

      BK5 = 2*SQRT((TM15**2/SL**2)+ (1/YT**2)
     &      *((1 - (psp*YT)/Spsi)**2)*TM20**2 + (1/ST**2)*TM21**2)
      BK6 = BK2+BK3+BK4


C*************************************************************************
C*************************************************************************
C     LOGIC FOR CHOOSING THE MODE OF FAILURE
C*************************************************************************
C*************************************************************************
      IF (SNN .GT. 0.0) THEN
          funcv(2) = (1/Spsi)*psn*SHI28 +(SHI27 +
     $     SHI31**2*psn**2*SHI28*
     $    (SHI20)+ SHI30*2*SHI29*SHI26)/(2*SQRT((SHI12+
     $    SHI31*psn**2*(SHI20)**2 + SHI30*SHI26**2)))


        funcv(1) =( (1/Spsi)*psn*(SHI20) +sqrt((SHI12 +
     $    (1/Spsi**2)*psn**2*(SHI20)**2 +
     $    (1/ST**2)*(SHI19 + SHI21)**2))) -1

C          funcv(1) = AK1+ SQRT(AK2+AK3+AK4)-1.0
C          funcv(2) = BK1+ (BK6/BK5)

      ELSE
        funcv(2) = (1/Spsi)*psn*SHI28 +(SHI27 +
     $     SHI31**2*psn**2*SHI28*
     $    (SHI20)+ SHI30*2*SHI29*SHI26)/(2*SQRT((SHI12+
     $    SHI31*psn**2*(SHI20)**2 + SHI30*SHI26**2)))
```

```
            funcv(1) =( (1/Spsi)*psn*(SHI20) +sqrt((SHI12 +
     $       (1/Spsi**2)*psn**2*(SHI20)**2 +
     $       (1/ST**2)*(SHI19 + SHI21)**2))) -1

          END IF

            funcv(3) = SNN

        end function funcv

C-------------------------------------------------------------------------------

C*******************************************************************************
C*******************************************************************************
```

REFERENCES

[1]"Airbus, and EADS Company", ", http://www.airbus.com/aircraftfamilies/. Accessed 4/27/2013.

[2] "Federal Aviation Administration", http://www.airporttech.tc.faa.gov/safety/bagot2.asp. Accessed 4/27/2013.

[3] Hinton, M. J., Kaddour, A.S. and Soden, P.D., "Failure Criteria in Fibre Rein- forced Polymer Composites: The World-Wide Failure Exercise", *A Composite Science and Technology Compendium*, Elsevier, 2004.

[4] Soden, P.D, Hinton, M. J. and Kaddour, A.S., "Lamina Properties, Lay-up Con- figurations and loading Conditions for A Range of Fiber-Reinforced Composite Laminates," *Composites Science and Technology*. Vol -58, 1998, pp. 1011-1022.

[5] Soden, P. D., Hinton, M., J., and Kaddour, A. S., "A Comparison of the Predictive Capabilities of Current Failure Theories for Composite Laminates," *Composite Science and Technology*, Vol. 58, 1998, pp. 1225 -1254.

[6] Special issue of *Composites Science and Technology*, Vol. 58, No. 7, 1998.

[7] Special issue of *Composites Science and Technology*, Vol. 62, Nos. 12-13, 2002.

[8] Special issue of *Composites Science and Technology*, Vol. 64, 2004.

[9] Hinton, M. J., Kaddour, A. S., and Soden P .D., "A Comparison of the Predictive Capabilities of Current Failure Theories for Composite Laminates, Judged Against Experimental Evidence," *Composite Science and Technology*, Vol. 62, 2002, pp. 1725-1797.

[10] Hinton, M. J., Kaddour, A. S., and Soden P. D., "Evaluation of Failure Prediction in Composite Laminate: Background to Part C of the Exercise," *Composite Science and Technology*,

Vol. 64, 2004, pp. 321-327.

[11] Kaddour, A. S., Hinton, M. J., and Soden P. D., "Recommendations for Designers and Researchers Resulting From the World-wide Failure Exercise," *Composite Science and Technology*, Vol. 64, 2004, pp. 589-604.

[12] Cuntze, R., "The Predictive Capability of Failure Mode Concept-based Strength Criteria for Multidirectional Laminates. WWFE-I, Part B", *Composite Science and Technology*, Vol. 64, 2004, pp. 487-516.

[13] Puck, A., and Schürmann, H.,"Failure Analysis of FRP Laminates by Means of Physically Based Phenomenological Models," *Composite Science and Technologies*, Vol. 58, 1998, pp. 1045-1067.

[14] Puck, A., and Schürmann, H.,"Failure Analysis of FRP Laminates by Means of Physically Based Phenomenological Models," *Composite Science and Technologies*, Vol.62, 2002, pp. 1633-1662.

[15] Chaboche, J.L., "Continuum Damage Mechanics part I - General Concepts," *Journal of Applied Mechanics*, Vol.55, 1988, pp. 59-64.

[16] Chaboche, J.L., "Continuum Damage Mechanics part II - Damage Growth, Crack Initiation and Crack Growth," *Journal of Applied Mechanics*, Vol.55, 1988, pp. 65-72.

[17] Hashin, Z., and Rotem, A., "A Fatigue Failure Criterion for Fiber Reinforced Materials," *Journal of Composite Materials*, Vol. 7, 1973, pp. 448-464.

[18] Hashin, Z., "Failure criteria for unidirectional fiber composites," *Journal of Applied Mechanics*, Vol. 47, 1980, pp. 329-334.

[19] Dávila, C. G., Camanho, P. P., and Rose, C. A., "Failure Criteria for FRP Laminates," *Journal*

of Composite Materials, Vol. 39, No. 4, 2005, pp. 323-345.

[20] Pinho, S. T., Dávila, C. G., Camanho, P. P., Iannucci, L., and Robinson, P., "Failure Models and Criteria for FRP Under In-plane or Three-dimensional Stress States Including Shear Non-linearity," National Aeronautics and Space Administration, U.S.A., NASA/TM 213530, Langley Research Center, Hampton, VA 23681, February 2005.

[21] Paris, F., "A Study of Failure Criteria of Fibrous Composite Materials," National Aeronautics and Space Administration, U.S.A., Tech. Rep. NASA/TM-2001-210661, 2001.

[22] Puck, A., Kopp, J., and Knops, M., "Guidelines for the determination of the parameters in Puck's action plane strength criterion," *Composites Science and Technology,* Vol. 62, 2002, pp. 371-378.

[23] Rybicki, E. F., and Kanninen, M. F., "A Finite Element Calculation of Stress Intensity Factors by a Modified Crack Closure Integral," *Engineering Fracture Mechanics*, Vol. 9, 1977, pp. 931-838.

[24] Krueger, R., "The Virtual Crack Closure Technique: History, Approach and Applications," National Aeronautics and Space Administration, U.S.A., NASA/CR-2002-211628 and ICASE Report No. 2002-10, Langley Research Center, Hampton, VA 23681, April 2002.

[25] Glaessgen, E. H., Riddell, W. T., and Raju, I., "Nodal Constraint, Shear Deformation and Continuity Effects Related to The Modeling of Debonding Laminates, Using Plate Elements," CMES, Vol. 3, No. 1, NASA Langely Research Center, Hampton, VA, U.S.A., 2002, pp. 103-116.

[26] Camacho, G. T., and Ortiz, M., "Computational Modeling of Impact Damage in Brittle Materials," International Journal of Solids and Structures, Vol. 33, 1996, pp. 2899-2939.

[27] Mi, Y. M., Crisfield, M., Davies, G., and Hellweg, H.-B., "Progressive Delamination Using Interface Elements," *Journal of Composite Materials,* Vol. 32, 1998, pp. 1246-1273.

[28] Goyal, V.K., Johnson, E.R., and Dávila, C.G., "Irreversible Constitutive Law for Modeling the Delamination Process Using Interfacial Surface Discontinuities," *Journal of Composite Structures*, Vol. 65, No. 3-4, 2004, pp.289-305.

[29] Chandra, N., Li, H., Shet, C., and Ghonem, H., "Some Issues of Cohesive Zone Models for Metal-ceramic Interfaces," *International Journal of Solids and Structures,* Vol. 39, 2002, pp. 2827-2855.

[30] Falk, M. L., Needleman, A., and Rice, J. R., "A Critical Evaluation of Cohesive Zone Models of Dynamic Fracture," Journal de Physique IV, Vol. 11, No. PR5, 2001, pp. 43-50.

[31] Ortiz, M. and Pandolfi, A., "Finite-Deformation Irreversible Cohesive Element for Three-dimensional Crack Propagation Analysis," *International Journal for Numerical Methods in Engineering*, Vol. 44, 1999, pp. 1267-1282.

[32] Turon, A., Camanho, P. P., Costa, J., and Dávila, C. G., "A Damage Model for The Simulation of Delamination in Advanced Composites Under Variable-mode Loading," *Mechanics of Materials,* Vol. 38, No. 11, 2006, pp. 1072-1089.

[33] Allix, O., and Ladevéze, P., "Interlaminar Interface Modelling for the Prediction of Delamination," *Composite Structures,* Vol. 22, 1992, pp. 235-242.

[34] Schellekens, J., and de Borst, R., "Free Edge Delamination in Carbon Epoxy Laminates a Novel Numerical/experimental Approach," *Composite Structures*, Vol. 28, 1993, pp. 357-373.

[35] Cui, W., and Wisnom, M., "A Combined Stress Based and Fracture Mechanics Based Model for Predicting Delamination in Composites," *Journal of Composite Materials,* Vol. 24, 1993, pp.

467-474.

[36] Song, S., and Waas, A., "Mixed-mode Failure in Laminated Composites Using an Energy Approach," *AIAA Journal*, Vol. 33, 1995, pp. 739-745.

[37] Allix, O., and Corigliano, A. "Geometrical and Interfacial Nonlinearities in the Analysis of Delamination in Composites," *International Journal of Solids and Structures*, Vol. 36, 1999, pp. 2189-2216.

[38] Goyal, V. K., Johnson, E. R., Jaunky, N., and Ambur, D., "Intralaminar and Interlaminar Progressive Failure Analyses of Composite Panels with Circular Cutouts," *Journal of Composite Structures*, Vol 64, No. 1, 2004, pp. 91-105.

[39] Schellekens, J., and de Borst, R., "On the Numerical Integration of Interface Elements," *International Journal for Numerical Methods in Engineering*, Vol. 36, 1993, pp. 43-66.

[40] Goncalves, J. M., de Moura, de Castro, P. M. S. T., and Marques, A., "Interface Element Including Point-to-surface Constraints for Three-dimensional Problems with Damage Propagation," *Engineering Computations*, Vol. 17, No.1, 2000, pp. 28-47.

[41] De Borst, R., and Rots, J., "Occurrence of Spurious Mechanisms in Computations of Strain Softening Solids," Engineering Computations, Vol. 6, 1989, pp.272-280.

[42] Chen, J., Crisfield, M. A., Kinloch, A. J., Busso, E. P., Matthews, F. L., and Qiu, Y., "Predicting Progressive Delamination of Composite Material Specimens Via Interface Elements," *Mechanics of Composite Materials and Structures*, Vol. 6,1999, pp. 301-317.

[43] Chang, F-K, and Lessard, L. B., "Damage Tolerance of Laminated Composites Containing an Open Hole and Subjected to Compressive Loadings: Part I - Analysis," *Journal of Composite Materials*, Vol. 25, 1991, pp. 2-43.

[44] Ladeveze, P., and Le Dantec, E., "Damage Modeling of the Elementary Ply for Laminated Composites," *Composites Science and Technology*, Vol. 43, 1992, pp. 257-267.

[45] Maimi, P., Camanho, P. P., Mayugo, J. A., and Dávila, C. G., "A Continuum Damage Model For Composite Laminates. Part I: Constitutive Model," *Mechanics of Materials*, 2007.

[46] Hassan, N.M., and Batra, R. C., "Modeling Damage in Polymeric Composites," *Journal Composites: Part B*, Vol.39, 2008, pp. 66-82.

[47] Abaqus/Standard, V6.13-3, is a trademark of ABAQUS, Inc.

[48] Hyer, W. M., Stress Analysis of Fiber Reinforces Composite Materials, 1st ed., McGraw-Hill Science/Engineering/Math, New York, 1997.

[49] MATLAB software, V.R2011b, is a trademark of MATLAB, Inc.

[50] Whitney, J. M., Structural Analysis of Laminated Anisotropic Plates, Technomic, 1987, pp. 59-61.

[51] Chang, F. K., Lessard, L. B., and Tang, J. M., "Compression response of laminated composites containing an open hole laminates," *Journal of Composite Materials*, Vol. 19, 1988, No. 4, pp. 46-51.

[52] Chang, F. K., and Lessard, L. B., "Damage tolerance of laminated composites containing an open hole and subjected to compressive loadings: part II - Experiment," *Journal of Composite Materials*, Vol. 25, 1991, pp. 44-64.

[53] Yamada, S. E., and Sun, C. T. "Analysis of Laminate Strength and its Distribution," *Journal of Composite Materials*, Vol. 12, 1978, pp. 275-284.

[54] Tan, S.C. and Nuismer, P.J.,"A Theory for Progressive Matrix Cracking in Composite Laminates," *Journal of Composite Materials*, Vol. 23, No. 10, 1989, pp. 1029-1047.

[55] Tan, S.C., "A Progressive Failure Model for Composite Laminates Containing Openings," *Journal of Composite Materials,* Vol. 25, 1991, No. 5, 1991, pp. 556-577.

[56] Tan, S.C. and Perez, J., "Progressive Failure of Laminated Composites with a Hole Under Compressive Loading," *Journal of Reinforced Plastics and Composites*, Vol. 12, No.10, 1993, pp. 1043-1057.

[57] Satyanarayana, A. and Przekop, A.,"Predicting Failure Progression and failure loads in Composite Open-Hole Tension Coupons," NASA/CR-216700, May. 2010.

[58] Lo, D.C., Coats, T. W., Harris, C. E., and Allen, D. H., "Progressive Damage Analysis of Laminated Composite (PDALC)-A Computational Model Implemented in the NASA COMET Finite Element Code", NASA/CR-4724, Nov. 1996.

[59] Sleight, D.W., "Progressive Failure Analysis Methodology for Laminated Composite Structures," NASA/TP-209107, Mar. 1999.

[60] Las, V., and Zemcik, R., "Progressive Damage of Unidirectional Composite Panels," *Journal of Composite Materials*, Vol. 42, 2008, pp.25-44.

[61] Shahid, I., and Chang, F.-K., "An Accumulative Damage Model for Tensile and Shear Failures of Laminated Composite Plates," Journal of Composite Materials, Vol. 29, 1995, pp. 926-981.

[62] Knight, N.F., "User-Defined Material Model for Progressive Failure Analysis," NASA/CR-214526, Dec. 2006.

[63] Hoskin, B.C., and Baker, A.A., Editors, 1986, "Composite Materials for Aircraft Structures", AIAA Education Series, American Institute of Aeronautics and Astronautics, TL699.C57C66, ISBN 0-930403-11-8, pp. 106 and 107.

[64] Marsh, G., "Composites Lift Off in Primary Aero-structures," *Reinforced Plastics*, Vol. 48,

No. 4, 2004, pp. 22-27.

[65] Washizu, K. Variational Methods in Elasticity and Plasticity. Pergamon Press, 3rd Ed. 1982.

[66] Pagano, N.J., "Exact Solutions for Rectangular Bidirectional Composites and Sandwich Plates," *Journal of Composite Materials*, Vol. 4, 1969, pp. 20-34.

[67] Reissner, E.,"On a Mixed Variational Theorem and on Shear Deformable Plate Theory," *International Journal of Numerical Methods in Engineering*, Vol. 23, No. 2, 1986, pp. 193-198.

[68] Pagano N.J.(Ed.). *Interlaminar Response of Composite Materials*. Elsevier, 1989.

[69] Czichon, S., Zimmermann, K., Middendorf, P., Vogler, M. and Rolfes, R, "Three-dimensional stres1s and progressive failure analysis of ultra-thick laminates and experimental validation," *Composite Structures*, No. 93, 2011, pp. 1394-1403.

[70] Nguyen, B.N. "Three-dimensional Modeling of Damage in Laminated Composites Containing a Central Hole," *Journal of Composite Materials*, 1997, 31, pp. 1672-1693.

[71] Camanho, P.P., and Matthews, F.L.,"A Progressive Damage Model for Mechanically Fastened Joints in Composite Laminates", *Journal of Composite Materials*, 1999, 23, pp. 2248-2249.

[72] Renard, J., Favre, J.P., and Jeggy, T., "Influence of Transverse Cracking on Ply Behavior: Introduction of a Characteristic Damage Variable," *Composite Science and Technology*, Vol. 45, 1995, pp. 29-37.

[73] Kermanidis, T., Labeas, G., Tserpes, K. I., and Pantelakis, S., "Finite Element Modelling of Damage Accumulation in Bolted Composite Joints Under Incremental Tensile Loading," European Congress on Computational Method in Applied Sciences and Engineering ECCOMAS 2000, Barcelona, 11-14 September 2000.

[74] Tserpes, K. I., Labeas, G., Papanikos, P., and Kermanidis, T.,"Strength Prediction of Bolted Joints in Graphite/epoxy Composite Laminates", *Composites: Part B*, 2002, 33, pp. 521 -529.

[75] Riccio, A., and Scaramuzzino, F., "Influence of Damage Onset and Propagation on the Tensile Structural Behaviour of Protruding Composite Joints," 4th GRACM Congress on Computation Mechanics GRACM, 2002, Patras, 27-29, 2002.

[76] Shokrieh, M.M., and Lessard, L.H., "Effects of Material Nonlinearity on the Three-dimensional Stress State of Pin-loaded Composite Laminates," *Journal of Composite Materials*, Vol. 30, No. 7, 1996, pp. 839-861.

[77] Wang, D., and Wen, W., "Three-Dimensional Progressive Damage Analysis of Composite Laminates Containing a Central hole Subjected to Compressive Loading," *International Conference on Mechanical Engineering and Material Science*, Yangzhou, China, Dec 16-18, 2012.

[78] Donadon, M.V., Iannucci, L., Falzon, B.G., Hodgkinson, J.M., and de Almeida, S.F.M.,"A progressive failure model for composite laminates subjected to low velocity impact damage," *Computers and Structures*, Vol. 86, no. 11-12,2008, pp. 1232-1252.

[79] Donadon, M.V., De Almeida, S.F.M., Arbelo, M.A., and de Faria, R.,"A Three-Dimensional Ply Failure Model for Composite Structures," *International Journal of Aerospace Engineering*, 2009.

[80] Ryan, S., "Hypervelocity Impact Induced Disturbances on Composite Sandwich Panel Spacecraft Structures," School of Aerospace, Mechanical and Manufacturing Engineering Science, RMIT University, Melbourne, Australia, 2007.

[81] Hassan, N.M., and Batra, R.C., “Response of Fiber Reinforced Composites to Underwater Explosive Loads”, *Composites B*, **38**, 448-458, 2007.

[82] Batra, R.C., Gopinath, G., and Zheng, J.Q., ”Damage and Failure in Low Energy Impact of Fiber-Reinforced Polymeric Composite Laminates,” *Composite Structures*, Vol. 94, 2012, pp. 540-547.

[83] Batra, R.C., and Xiao, J., “Analysis of Post-buckling and Delamination in Laminated Composite St. Venant-Kirchhoff Beams using CZM and Layerwise TSNDT”, *Composite Structures*, vol. 105, 2013, pp. 369-384.

[84] Hinton, M. J., and A. S. Kaddour. "The background to the second world-wide failure exercise," *Journal of Composite Materials*, vol. 46, No. 19-20, 2012, pp. 2283-2294.

[85] Kaddour, A.S., and Hinton, M.J., "Maturity of 3D Failure Criteria for Fiber-reinforced Composites: Comparison between Theories and Experiments: Part B of WWFE-II," *Journal of Composite Materials*, vol. 47, No. 6-7, 2013, pp. 925-966.

[86] Pinho, S.T., Vyas, G.M., and Robinson P., "Material and Structural Response of Polymer-Matrix Fibre-reinforced Composites: Part B," *Journal of Composite Materials*, Vol. 47, No. 4-7, 2013, pp. 679-696.

[87] Carrere, N., Laurin, F., and Maire, J-F., "Micromechanical Based Hybrid Mesoscopic 3D Approach for Non-linear Progressive Failure Analysis of Composite Structures," *Journal of Composite Materials*, Vol. 46, 2012, pp. 2389-2415.

[88] Puck, A., Festigkeitsanalyse von Fase-Matrix Laminate," Carl Hansa Verlag, 1996.

[89] Deuschle, H. M. and Kroeplin, B., "Finite Element Implementation of Puck's Failure Theory for Fiber-reinforced Composites under Three-dimensional Stress", *Journal of Composite*

Materials, Vol. 46, No. 19, 2012, pp. 2458-2513.

[90] Deuschle, H. M. and Puck, A., "Application of the Puck Failure Theory for Fiber-reinforced Composites Under Three-dimensional Stress: Comparison with Experimental Results", *Journal of Composite Materials*, Vol. 47, No. 6, 2013, pp. 827-846.

[91] Deuschle, H.M., "3D Failure Analysis of UD Fiber Reinforced Composite: Puck's theory within FEA," Department of Aerospace Engineering, Universitat Stuttgart, Stuttgart, Germany, 2010.

[92] Dunlap., R.A., "The Golden Ratio and Fibonacci Numbers", World Scientific, London, 1997, pp.12-15.

[93] Kaddour, A.S., and Hinton, M.J., "Input Data for Test Cases Used in Benchmarking Triaxial Failure Theories of Composites," *Journal of Composite Materials*, Vol.46, No. 20, 2012, pp. 2295-2312.